HIGH RESOLUTION SONAR DF SYSTEM

by

T. A. Rafik, BSc., MSc

A Doctoral Thesis Submitted in Partial Fulfilment of the Requirements for the Award of Doctor of Philosophy of the Lougborough University of Technology

July 1992

Supervisor: Professor J. W. R. Griffiths
Department of Electronic and Electrical Engineering

CONTENTS

CHAPTER THREE

SIMULATION OF SOME HIGH RESOLUTION DF ALGORITHMS ON A TRANSPUTER

CHAPTER FOUR

DESIGN, CONSTRUCTION AND TEST OF A HIGH RESOLUTION SONAR DF SYSTEM

CHAPTER FIVE

PRACTICAL IMPLEMENTATION OF HIGH RESOLUTION ALGORITHMS IN THE WATER TANK AT LOUGHBOROUGH UNIVERSITY

CHAPTER SIX

HIGH RESOLUTION SONAR DF SYSTEM RESULTS OF FOREMARK TRIALS

CHAPTER SEVEN

IMPLEMENTATION OF HIGH RESOLUTION ALGORITHMS IN AN AIR ACOUSTIC SYSTEM

CHAPTER EIGHT

CONCLUSIONS AND SUGGESTIONS FOR FUTURE WORK

SUMMARY

One of the fundamental problems of sonar systems is the determination of the bearings of underwater sources/targets. The classical solution to this problem, the 'Conventional Beamformer', uses the outputs from the individual sensors of an acoustic array to form a beam which is swept across the search sector. The resolution of this method is limited by the beamwidth and narrowing this beam to enhance the resolution may have some practical problems , especially in low frequency sonar, because of the physical size of the array needed.

During the past two decades an enormous amount of work has been done to develop new algorithms for resolution enhancements beyond that of the Conventional Beamformer. However, most of these methods have been based on computer simulations and very little has been published on the practical implementation of these algorithms. One of the main reasons for this has been the lack of hardware that can handle the relatively heavy computational load of these algorithms. However, there have been great advances in semiconductor and computer technologies in the last few years which have led to the availability of more powerful computational and storage devices. These devices have opened the door to the possibility of implementing these high resolution Direction Finding (DF) algorithms in real sonar systems.

The work presented in this thesis describes a practical implementation of some of the high resolution DF algorithms in a simple sonar system that has been designed and built for this purpose. The system is based on transputers as a state-of-art computer technology.

After addressing the problem of estimating the direction of arrivals and reviewing some of the well known high resolution DF algorithms, the thesis presents a simulation of some high resolution DF algorithms on a transputer using OCCAM-2 programming language and studies the computational load of these algorithms. This is followed by details of the design and construction of a transputer-based high resolution sonar DF system. Initially, experimental work was carried out in a large water tank at Loughborough University and then the system was thoroughly tested at a nearby reservoir. The experimental results are reported.

The final part of the thesis presents the results of implementing high resolution DF algorithms on air sonar system. This system is similar to the underwater system mentioned above except that it uses a 15 element air acoustic array.

ACKNOWLEDGMENTS

I would like to express my sincere gratitude to my supervisor, Prof. J.W.R. Griffiths, for all his help, encouragement and support throughout the research. His sympathy and support during the difficult days will never be forgotten by my family and me. Even during his serious illness, his encouragement and support never weakened. My family and I are praying every day for him for a speedy and full recovery.

Also, I would like to thank Mr. W. Wood (Research Assistant) and Mr. A.D. Goodson (Senior Experimental Officer) for their help in conducting the experiments at Foremark reservoir and to Mr. LiBin (Academic visitor from North Western Polytechnical University - China) for his help with the air acoustic work.

My thanks also go to Mr. K. Jeffrey (Academic visitor from the University of Saskatchewan - Canada) for reading the thesis and for his useful comments.

I must also thank Mrs. S. Clarson, all my colleagues in the Sonar and Signal Processing Research Group and all the technicians at the Electronic and Electrical Engineering Department - Loughborough University of Technology for all their help.

Finally, I would like to thank my family for their support and encouragement.

LIST OF SYMBOLS

Chapter 1

BWFN	Half beamwidth between first nulls nearest to the main lobe.
CBF	Conventional beamformer.
dB	Decibels.
DF	Direction Finding.
ESPRIT	Estimation of Signal Parameters via Rotational Invariance Techniques.
Hz	Cycle per second.
IMP	Incremental Multi-Parameter.
MEM	Maximum Entropy Method.
MUSIC	MUltiple SIgnal Classification.
m	Metre.
MODE	Method of Direction Estimation.
WSF	Weighted Subspace Fitting.

Chapter 2

θ	Angle of arrival.
σ^2	Noise variance.
$\cdot^*$	Complex conjugate.
λ_i	The ith eigenvalue.
λ	Wave length.
α	Parameter used in forming the DF spectrum of Byrne and Steels method.
A	Array Manifold.
arg	Argument.
$\vec{a}(\theta)$	Steering vector.
c	Acoustic velocity.
D	Data Matrix.

d	The element spacing.
$\vec{d}$	A vector used to represent the noise or signal subspace.
E	Expectation Operator.
^{H}	Hermitian transpose.
I	Identity matrix.
KT	Kumarson and Tuft Method.
K	Non-negative constant.
M	Number of wavefronts arriving at the array.
MNM	Minimum Norm Method.
N	Number of array elements.
$\vec{n}$	Noise vector.
P	Number of snapshots.
$P_{CBF}(\theta)$	Angular spectrum of the CBF.
$P_{capon}(\theta)$	Angular spectrum of Capon's method.
$P_{MEM}(\theta)$	Angular spectrum of the maximum entropy method.
$P_{JD}(\theta)$	DF spectrum of Johnson and Degraff method.
$P_{Pisarenko}(\theta)$	Angular spectrum of Pisarenko method.
Q_m	Eigenvector associated with the minimum eigenvalue.
R	Spatial covariance matrix.
$\hat{R}$	The estimate of the covariance matrix.
R^{-1}	The inverse of the covariance matrix.
R_s	Signal subspace.
R_N	Noise subspace.
SNR	Signal-to-Noise Ratio
Tr	Trace of a matrix.
^{T}	Transpose.
U_i	The ith eigenvector.
$\vec{W}$	Weight vector.
$\vec{W}_{opt}$	Optimum Weight vector.
y	The output of the delay-and-sum operation.

Chapter 3

BBC	British Broadcast Corporation.
CPU	Central Processing Unit.
kHz	Kilohertz.
KByte	Kilo Byte.
MHz	Megahertz.
MIPS	Million instructions per second.
MByte	Mega Byte.
PC	Personal Computer.
sec	Second.

Chapter 4

μf	Microfarad.
A/D	Analogue to digital convertor.
cm	Centimetre.
D/A	Digital to analogue convertor.
EOC	End of conversion.
f_c	Nyquist sampling frequency.
f_o	Centre frequency.
GND	Ground.
I&Q	In-phase and Quadrature components.
LSB	Least Significant Bit.
LUT	Loughborough University of Technology.
ms	Millisecond.
MSB	Most Significant Bit.
RAM	Random Access Memory.
ROM	Read Only Memory.
Sonar	Sound Navigation and Ranging.
S/H	Sample and hold.
V	Volts.
VCO	Voltage Controlled Oscillator.

V_{P-P} Peak to peak voltage.

V_{dc} Direct current voltage.

Chapter 5

α Coefficient of absorption (dB/m).

η Transducer efficiency.

ρ Fluid density.

μPa Micro-Pascal.

A Area of a circular transducer.

DI Directivity Index.

H Water depth.

I_r Intensity of reflection.

I_i Incident Intensity.

I_0 The Intensity of sound at a reference point located 1m from the source.

I_1 The Intensity of sound at a distant point.

I The Sound Intensity.

NL Noise Level.

P Power.

P_{ele} Electrical power.

p Pressure.

R_{eq} Equivalent resistance of the array.

R Range (in metre).

SL Source Level.

TL Transmission Loss.

TS Target Strength.

V_t Transmit voltage.

V_r Receive Voltage.

W Watt.

Chapter 7

$D(\theta)$	Beam pattern of a linear array with omnidirectional elements.
$J_1(\pi\mu)$	First order Bessel function of $(\pi\mu)$.
$P(\theta)$	Beam pattern of a linear array with directional elements.
$S(\theta)$	Beam pattern of single element.

CHAPTER ONE

INTRODUCTION

1.1 INTRODUCTION TO ARRAY SIGNAL PROCESSING [ref. 1]:

Sensor array processing deals with the processing of signals carried by propagating wave phenomena. The received signal is obtained by means of an array of sensors located at different points in space in the field of interest. The aim of array processing is to extract useful characteristics of the received signal field (e.g., the estimation of the direction from which the signals arrive).

The measurement of the field by an array offers two basic improvements over the signal processing capabilities of a single sensor. The first is the determination of the bearing of the source(s). Bearing information cannot be obtained with a single sensor, whereas an array offers some bearing resolving capability. The second improvement is the increase in the signal to noise ratio. If the noise field is uncorrelated at each sensor location with respect to all other locations the signal to noise ratio in the array output is increased by a factor equal to the number of elements comprising the array. This factor decreases when the noise

field is correlated at the sensor location. The measure of improvement in the signal to noise ratio is the array gain (the ratio of the signal to noise ratio at the array output to that obtained with a single sensor).

The sources of energy responsible for illuminating the array may assume a variety of different forms. They may be non-coherent (i.e., independent of each other) or coherently related to each other. Equally, as seen from the location of the array, the radiation may be from diffused media and therefore distributed in nature, or it may be from isolated sources of finite angular extent.

The array itself can have a variety of different geometries depending on the application of interest. The most commonly used configuration is the rectilinear array, in which the sensors (all of the common type) are uniformly spaced along a straight line. Another common configuration is a planar array, in which the sensors form a rectangular grid or lie on concentric circles.

There are many applications of array signal processing which can be found in seismology, sonar, radar, astronomy and tomography. In exploration seismology, array processing is used to unravel the physical characteristics of a limited region of the interior of the earth. In this case, a shot (e.g., stick of dynamite) is used as a source of acoustic energy that applies an impulse to the earth and the signals received by a number of geophones, placed in certain locations, are recorded. The resultant geophone outputs are due to signals reflected, diffracted or refracted back to the earth surface from the original source of disturbance.

In passive (listening only) sonar, the received signal is externally generated, and the primary requirement of array processing is to estimate both the temporal and spatial structure of the received signal field. The array sensors consist of sound pressure-sensing electro-mechanical transducers known as hydrophones, which are immersed in the underwater medium.

In active sonar, an acoustic signal is transmitted to illuminate the area to be investigated and the reflected signals from the targets are detected by the receiving hydrophones. These signals are then processed in various ways to accomplish the purpose for which the sonar system is intended.

In radar array processing, a transmitting antenna is used to illuminate the environment surrounding the radar site, and a receiving array of antenna elements is used to receive the radar returns caused by reflections from targets located in the path of the propagating electromagnetic wave. Here again, the array signal processing is used to estimate the wavenumber power spectrum of the received signal, with emphasis on spatial resolution.

In radio astronomy, the interest is in radio emission from celestial sources. The emission, depending on the radiation mechanism and the state of the emitting region, shows broad continuum spectral features, narrow band, or absorption line structure. The arrays used here consist of hundreds of antenna elements and extend from hundreds of metres to thousands of kilometres. The requirement is to use array processing for image reconstruction of radio sources, with emphasis on resolution and dynamic range of the reconstructed image.

In tomography, array processing is used to obtain a cross-sectional image of objects from either transmission or reflection data. In most cases, the object is illuminated from many different directions either sequentially or simultaneously, and the image is reconstructed from data collected either in transmission or reflection. The most spectacular success of tomography has been in medical imaging with X-rays. There is also active interest today in extending tomographic imaging to ultra-sound and microwaves for use in medical imaging, seismic exploration, and non-destructive testing.

1.2 ARRAY SIGNAL PROCESSING AND RESOLUTION:

One of the fundamental problems of array signal processing is the determination of bearings of sources/targets. The classical solution to this problem, the 'Conventional Beamformer', uses the outputs from the individual sensors of the array to form a beam. This beam has a pattern which contains a main lobe in the centre and minor side-lobes on each side. Between the lobes are nulls in the direction of zero response. The width of the main lobe is inversely proportional to the frequency of operation and to the size of the array.

The main lobe can normally be steered, either mechanically by physically rotating the array, or electrically by delaying the individual signals from the array sensors (or adjusting their phases in a narrow band system) which effectively rotates the direction of maximum response to some desired direction.

The resolution of an array may be defined as equal to half the beam width between first nulls nearest to the main lobe (BWFN) [ref.2]. The BWFN is approximately equal to the half power beam width. The array can only resolve sources if they are separated by at least a half power beam width.

Narrowing the beam-width to enhance the resolution of the Conventional Beam Former (CBF) has some practical problems especially in sonar where the frequency of operation is relatively low. For example, at 100Hz a sonar array of 150m is required for a resolution of only 6 degrees. In addition, increasing the size of the array increases the near field region which adds another limitation to the system.

From the above, it can be seen that the lack of resolution is the main limitation of the Conventional Beamformer. In addition, the relatively high side-lobes in the beampattern causes more problems. For rectilinear array (set of equally spaced sensors in a straight line), the first side-lobe is only about 13dB below the main lobe. Thus, a strong interference arriving from a direction corresponding to one of these side-lobes might easily cause an output which is greater than the signal coming from the direction to which the main beam is pointed. This results in ambiguity in determining the direction of the signal. Nevertheless, the conventional beamformer is relatively simple to implement, is fairly robust for small array errors and hence is in widespread use in practical sonar systems.

During the last two decades, considerable effort has been devoted to array processing in order to obtain higher resolving power and better rejection of the side-lobes. Several methods have been suggested and were investigated during the late sixties. Examples of these are Capon's method and the Maximum Entropy Method (MEM). Different extensions to these methods were proposed later.

In the early seventies a new approach to the problem of direction finding has been suggested which is based on the eigenvalues and eigenvectors of the covariance matrix of the received signals. This has led to the development of a number of closely related techniques which have demonstrated excellent performance in resolving close sources (or targets). The geometric relationships between the spatial source vectors and the eigenvectors of the covariance matrix obtained from the output of the array sensors is the key to all these techniques. An example of these techniques is MUSIC (MUltiple SIgnal Classification) which is probably the most well known eigenvector method.

All the methods mentioned above need to generate a so-called array manifold (a matrix that contains all the signal direction vectors) which is used for the steering over the observed space. This makes the computation and memory requirements of these methods remarkably high. Recently, a new algorithm has been proposed which does not need to generate the array manifold. It is called the ESPRIT algorithm (Estimation of Signal Parameters via Rotational Invariance Technique) and it is creating considerable interest. It is also based on eigen-decomposition of the covariance matrix but it uses an array consisting of sensor doublets which is grouped into two sub-arrays.

Other new algorithms were also proposed in the last few years which tackled the problems of correlated sources or computation complexity. Examples of these are the CLOSEST, the MODE (Method Of Direction Estimation), the IMP (Incremental Multi-Parameter) and the WSF (Weighted Subspace Fitting).

The development of new high resolution direction finding techniques is continuing and every day new publications appear either to enhance the performance of the existing algorithms or to proposed new ideas.

1.3 REASONS FOR AND AIMS OF RESEARCH:

Although an enormous amount of work has been done to develop new high resolution direction finding algorithms and much has been published on computer simulations, there has been very little done on the practical implementations of these algorithms in real time systems. The main reason for this is the considerable amount of computation involved in these algorithms and the relatively large

memory they require. However, with the continuing advance of semiconductors and computer technologies, it is now becoming possible to implement these algorithms in real time for some specific applications. One such possible application is a sonar system where the relatively slow speed of operation of underwater vehicles allows more time for processing.

Therefore, the main objectives of this project were first to design and build a simple sonar system using transputers, which is the state-of-art computer technology, to implement various direction finding algorithms. The second objective was to evaluate the performance of high resolution direction finding algorithms in practical sonar environment.

The project commenced with a feasibility study where some high resolution direction finding algorithms were simulated on a transputer using OCCAM-2 programming language. In this study, measurements of computation times for each algorithm were made. The results of this study were encouraging enough to go ahead with designing and building a high resolution practical sonar system.

The second stage of this project was to design and build a 10 channel sonar digital receiver capable of implementing the high resolution direction finding algorithms. The system used a BBC microcomputer as a front end data acquisition processor, a T414 transputer to carry out the integer calculations and a T800 floating point transputer to carry out the floating point calculations.

The system was tested first in the department water tank where the environment is well controlled. The aim of this test was to resolve two sources placed within the beam-width of a 10 element receiving array working at 40 kHz using some of the high resolution direction finding algorithms. Other tests, which resolved two passive targets using active sonar principles were also carried out.

A move to a more realistic and less controlled environment has been made by testing the system in a local reservoir to resolve two sources placed at about 9m from a 10 element receiving array.

Initially, it was intended to test the system in the reservoir using active sonar. All the preparations for this test were made which included the mechanism for mounting the targets, carrying-out extensive tests to investigate the reverberation conditions and signal levels, re-engineering the system to reduce the electronic

noise and to offer better matching between the receiving channels and extending the number of channels to 16 to increase the directionality and the signal to noise ratio. Unfortunately, however, these tests were suspended due to construction work at Foremark reservoir tower.

The project was resumed, however, using air acoustics where the system instead of resolving underwater targets, was used to resolve two sources/objects in open air using a 15 element air acoustic array which was designed and built for this purpose.

1.4 ORGANISATION OF CHAPTERS:

CHAPTER 2 of this thesis describes the modelling of signals coming from the far field onto a linear array. This model is then used as a basis to describe and discuss the well known methods for estimating the directions-of-arrival. It emphasizes the eigenvalue and eigenvector methods as they are believed to show better performance.

CHAPTER 3 introduces the transputer and its programming language OCCAM-2. Then it describes the simulation programs in OCCAM-2 used to implement some high resolution direction finding algorithms on a single transputer. The results of these simulations are then presented together with the computation times required to perform each algorithm. The distributions of the computation times over the main steps for each algorithm are also presented. The chapters also discusses the possibilities for introducing concurrency in the implementation of the high resolution algorithms.

In CHAPTER 4, a description of the hardware design of a simple sonar system is presented. It also describes the preliminary tests and the alignment of the system.

CHAPTER 5 presents the results of testing different high resolution algorithms in the department tank. This includes the passive and active sonar tests.

CHAPTER 6 describes the experiments carried out at Foremark reservoir to resolve two sources and shows the results of these experiments.

CHAPTER 7 describes the design and testing of a 15 element air acoustic array. It also shows the results of implementing some high resolution Direction Finding algorithms to resolve two sources/targets in open air.

Finally, CHAPTER 8 summarizes the discussions and conclusions of this project and gives some suggestions for future work.

CHAPTER TWO

REVIEW OF CURRENT DIRECTION FINDING ALGORITHMS

2.1 INTRODUCTION:

In the last two decades or so, a large number of high resolution direction finding algorithms have been published. Excellent reviews of these algorithms already exist and can be found in references 3-13. Therefore the main aim of this chapter is not to give a comprehensive survey of all available methods but to concentrate on a few of the best known algorithms especially in the field of eigen-analysis.

Although the main advantages and disadvantages of these methods are mentioned in this chapter, no attempt is made to directly compare them at this stage as this requires a large number of results, both practically and by computer simulations, which will be carried out for selected algorithms in the following chapters.

In this chapter the receiving array is assumed to be a rectilinear array. This assumption simplifies the mathematics and makes the understanding of the principles of the methods much easier. Some of the high resolution methods described in this chapter are restricted to this type of array. This restriction is considered as a disadvantage, as will pointed out.

2.2 PROBLEM FORMULATION AND MODELLING:

Consider the diagram in Figure 2.1 and assume one of the signals is coming from a source in the far field of the array with arrival direction θ relative to the normal to the array.
Using the first element as a reference we can represent the voltages on each element of the array due to this signal as:-

$$x_1(t) = s(t)$$

$$x_2(t) = s(t-\alpha)$$

$$x_3(t) = s(t-2\alpha)$$

$$\vdots \qquad (2.1)$$

$$x_N(t) = s(t-(N-1)\alpha)$$

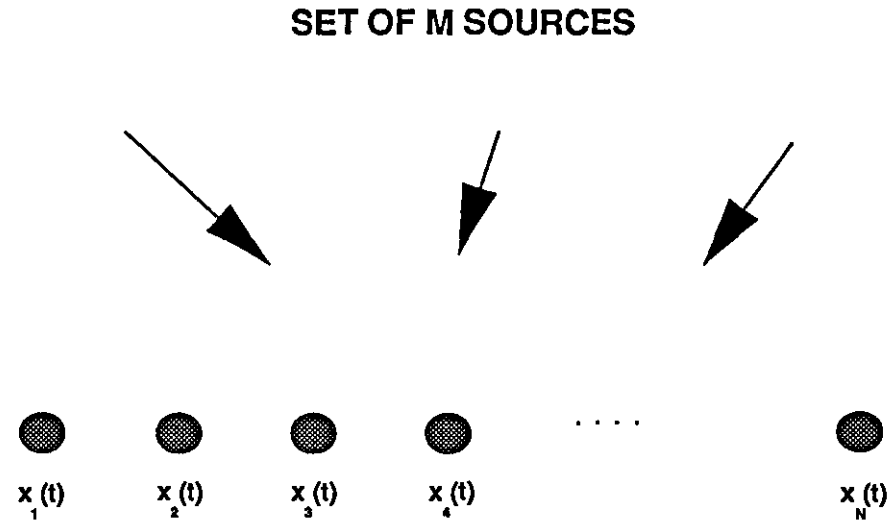

Figure 2.1: The Theoretical Model.

where $$\alpha = \frac{d}{c}\sin(\theta),$$

d = the spacing between elements,
N = the number of elements in the array and
c = the acoustic velocity.

We can represent this set of signals as a vector

$$\vec{x}(t) = \begin{bmatrix} x_1(t) \\ x_2(t) \\ \cdot \\ \cdot \\ x_N(t) \end{bmatrix} \tag{2.2}$$

If we are dealing with narrow band signals, then the time delays can be represented by phase shifts. Thus

$$\vec{x}(t) = \vec{a}(\theta)s(t) \tag{2.3}$$

where

$$\vec{a}(\theta) = \begin{bmatrix} 1 \\ \exp(-j\phi) \\ \exp(-j2\phi) \\ \cdot \\ \cdot \\ \exp(-j(N-1)\phi) \end{bmatrix} \quad \text{and}$$

$$\phi = \frac{2\pi d}{\lambda}\sin(\theta)$$

Assuming that there are a set of M sources present then the expression can be extended to

$$\vec{x}(t) = A\vec{s}(t) \tag{2.4}$$

where $A = [\vec{a}(\theta_1), \vec{a}(\theta_2), \ldots, \vec{a}(\theta_M)]$

and $$\vec{s}(t) = \begin{bmatrix} s_1(t) \\ s_2(t) \\ \cdot \\ \cdot \\ s_M(t) \end{bmatrix}$$

The matrix containing the total set of possible direction vectors is known as the array manifold.

$$A = \{\vec{a}(\theta_i) \qquad \theta_i \in \Theta\} \tag{2.5}$$

Normally there is additive noise which can be included as

$$\vec{x}(t) = A\vec{s}(t) + \vec{n}(t) \tag{2.6}$$

where $\vec{n}(t) = [n_1(t), n_2(t), \ldots, n_N(t)]^T$

The vector of element voltages at a particular time is called a snapshot. A number of such snapshots can be taken and a data matrix D can be formed which contains the set of snapshots.

$$D = [\vec{x}(1), \vec{x}(2), \ldots, \vec{x}(P)] \tag{2.7}$$

where P is the number of snapshots.

The covariance matrix is defined as

$$R = E[\vec{x}\vec{x}^H]$$

$$= A(\theta)SA^H(\theta) + \sigma^2 I \tag{2.8}$$

where $S = E[\vec{s}(t)\vec{s}^H(t)]$ and it is assumed that the noise voltages on each element are independent and have zero mean.

An estimate of the covariance matrix can be made from the P snapshots

$$\hat{R} = \frac{1}{P}\sum_{t=1}^{P}[\vec{x}(t)\vec{x}^{H}(t)]$$

$$= \frac{1}{P}[DD^{H}]. \qquad (2.9)$$

2.3 CONVENTIONAL BEAMFORMER:

Conventional beamforming (CBF) employs a procedure known as delay-and-sum processing in an attempt to steer a beam in a particular direction. The concept is based on the physics of wave propagation phenomenon whereby sensors at different locations with respect to the incoming plane wave receive (nearly) the same signal, but with different time delays with respect to some reference due to the different propagation path lengths. If delays are inserted at each of the sensors to exactly compensate for the propagation and differential receiver delay, and the outputs of the delay elements summed to form a scalar output, the signal waveforms will add constructively while the noise in each sensor, being uncorrelated from sensor to sensor, will add incoherently. Unfortunately, as is well known, such simple beamformer also produce unwanted outputs from signals arriving from directions other than the desired direction (sidelobes leakage).

Figure (2.2) illustrates the implementation of the CBF. The outputs of the individual elements are weighted to form a common output, y [ref.13]:

$$y = \vec{w}^{T}\vec{x} \qquad (2.10)$$

where

$$\vec{w}^{T} = [w_1, w_2, \ldots, w_N] \qquad (2.11)$$

is the weighting vector.

The power output is given by:

$$P_{CBF} = E[y^* y]$$

$$= E[\vec{w}^T \vec{x}\vec{x}^H \vec{w}^*]$$

$$= \vec{w}^T R \vec{w}^* \qquad (2.12)$$

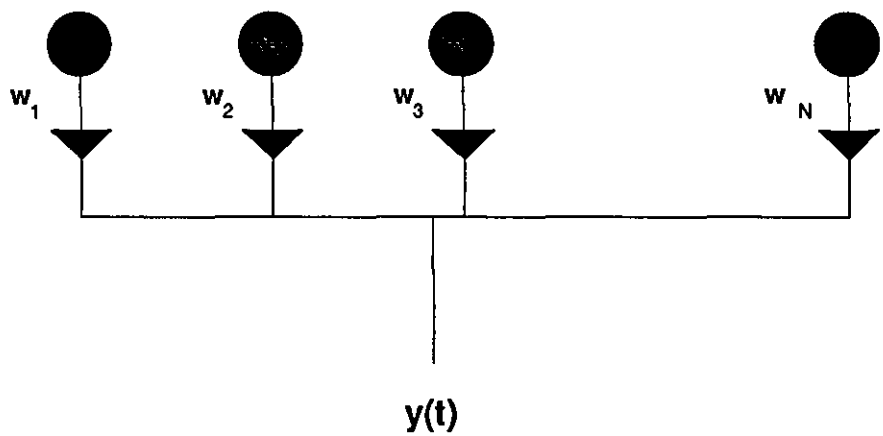

Figure 2.2: The Conventional Beamforming.

The spatial power spectrum of the CBF can be formed by replacing the weighting vector, $\vec{w}$, in equation 2.12 with $\vec{a}^*(\theta)$ and scan the region of $\theta - space$ in which sources may be present, i.e:

$$P_{CBF} = \vec{a}^H(\theta)\hat{R}\vec{a}(\theta) \qquad (2.13)$$

where $\hat{R} = \frac{1}{P}\sum_{p=1}^{P} \vec{x}(t)\vec{x}^H(t)$ is the sample covariance matrix of the array data of P snapshots.

A typical curve for the conventional beamformer is shown in figure (2.3). It should be noticed that this is a power response and that the first sidelobes are about 13dB down from the main lobe. The resolution capability of the conventional beamformer is defined as the 3dB beamwidth and this, expressed in radians, is approximately the reciprocal of the length of the array measured in wavelenghs. For the array in the figure (2.3) the length is 4 wavelengths so the beamwidth is approximately 15 degrees.

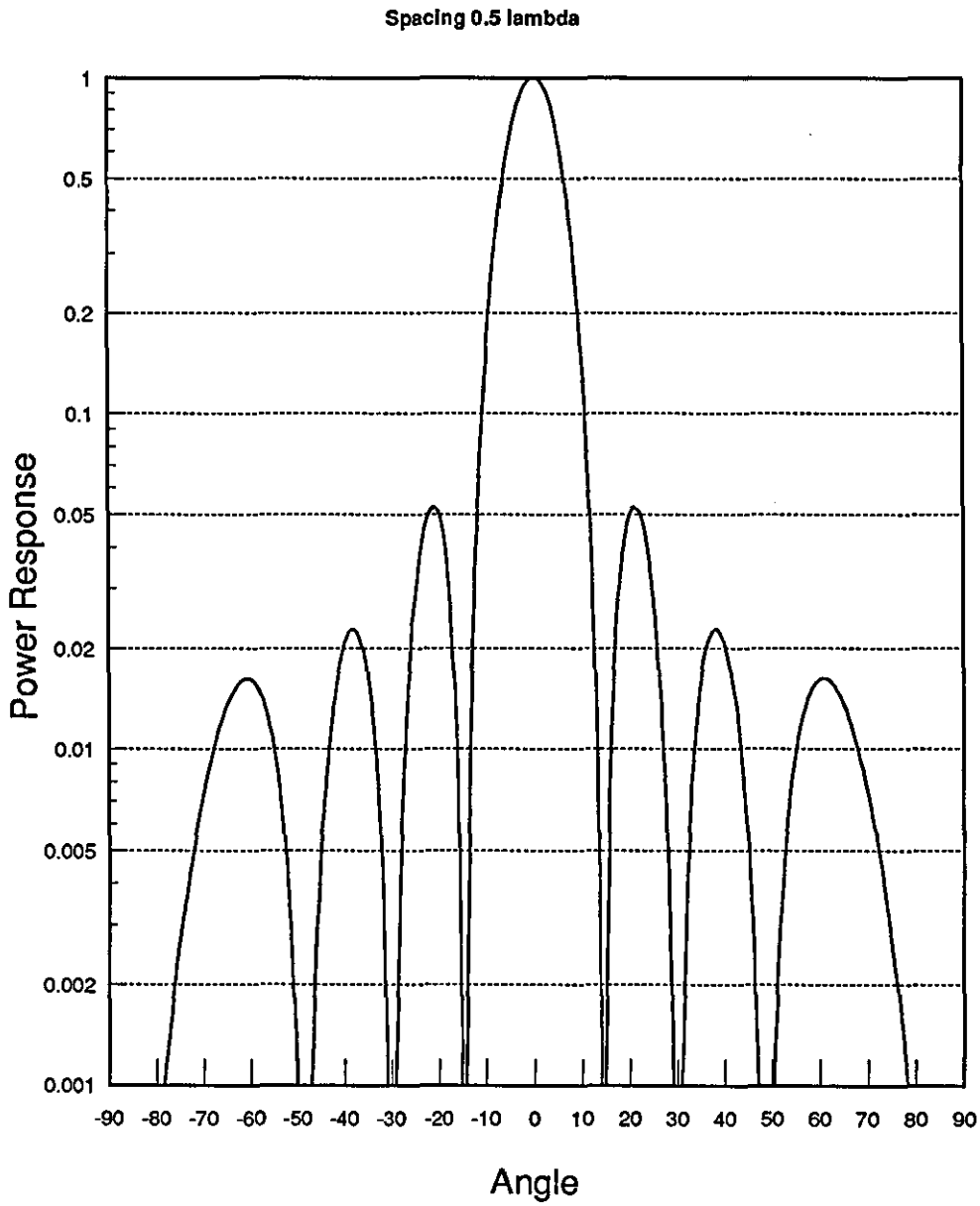

Figure 2.3: Beam pattern of an 8 element array.

In the presence of a single source, if there are no ambiguities, the output power will be maximum at the appropriate θ. If more than one source exists, and they are well separated, the conventional beamformer will still exhibit peaks in close proximity to the true direction of arrivals. However, the method completely fails to resolve sources that are less than approximately one beamwidth in separation.

The poor resolution and the sidelobes leakage are the two main disadvantages of conventional beamforming. However, because it is easy to implement, its computation load is relatively low and its robustness, it is still widely used in practical sonar systems.

2.4 HIGH RESOLUTION AND ADAPTIVE METHODS:

The basic property of an adaptive system is its ability to change its parameters to meet the changing nature of the environment in which it is operating. Thus instead of using the fixed weighting of the conventional beamformer we can adjust the weights to achieve some particular goal. Capon's method described below is a typical example of such a system in which the gain of the array for a given direction is fixed by a constraint while the output power is minimised.

Another major group of methods which are superior to the beamformer in terms of resolution is referred to as high resolution methods and is primarily based on eigen-structure analysis. The MUSIC algorithm is a typical example of these methods.

2.4.1 CAPON'S METHOD:

A different approach to increasing the resolution beyond that of conventional beamformer (delay-and-sum processing) was introduced by Capon in 1969[ref.15]. He argued that the poor resolution of the conventional beamformer method could be attributed to the fact that the output of the delay and sum processor at a given angle depends not only on the power of the source at that angle but also on undesirable contributions from all other sources. To mitigate this effect, he proposed to constrain the gain of the system to signals from a particular direction to unity, and to minimise the total output power subject to this

constraint. This will enhance the ratio of the wanted to unwanted signals. Such a constraint can be implemented by finding an optimum weighting vector $\vec{w}_{opt}$ which minimises the output power of the system subject to a unity gain in the look direction, i.e.,:

minimise

$$\vec{w}_{opt}^{H} R \vec{w}_{opt}$$

subject to

$$\vec{w}_{opt}^{H} \vec{a}(\theta) = 1 \tag{2.14}$$

where $\vec{a}(\theta)$ is a steering vector that 'points' the array in the look direction.

The optimum weighting vector for the above constraint is[ref.13]:

$$\vec{w}_{opt} = \frac{R^{-1}\vec{a}^{H}(\theta)}{\vec{a}^{H} R^{-1} \vec{a}(\theta)} \tag{2.15}$$

and the output power is:

$$P_{CAPON}(\theta) = \frac{1}{\vec{a}(\theta)^{H} R^{-1} \vec{a}(\theta)} \tag{2.16}$$

Capon's method may be viewed as a set of narrowband spatial filters, each of which has the property (by virtue of the optimum control of equation 2.14) of being a matched filter to a single plane wavefront incident upon the array aperture at the appropriate angle.

It is interesting to express Capon's spectrum of equation 2.16 in terms of an eigenvector decomposition of R (refer to 2.4.3). The matrix inverse R^{-1} can be calculated using all of the eigenvector and eigenvalue information, i.e.,:

$$P_{CAPON}(\theta) = \frac{1}{\sum_{i=1}^{N} \frac{1}{\lambda_i} | \vec{a}^{H}(\theta) \vec{U}_i |^2} \tag{2.17}$$

where λ_i is the eigenvalue associated with the eigenvector $\vec{U}_i$.

The result of equation 2.17 may be understood as an attempt to create a filter which is maximally orthogonal to the signal since noise eigenvectors will receive greater weight in the calculation of R^{-1}.

The main advantages of Capon's method are:
1. The adaptive filter used gives improved performance over that obtained from the conventional beamformer in terms of resolution and side-lobes although the available resolution increase is limited by the main-beam nature of the method.
2. The output power is directly referenced to the receiver noise power thus permitting calibration and measurement of relative source strength.
3. The array sensors need not be equally spaced provided that the array manifold is known.
4. The residual background ripple is low and relatively well behaved.

Despite the above advantages, Capon's method has some disadvantages:
1. It fails to resolve correlated sources.
2. The computation task involved in calculating the DF function is relatively high.
3. Ill conditions may arise when calculating the inverse of the covariance matrix.
4. Its resolution is less than some of the other high resolution techniques which are discussed below.

2.4.2 THE MAXIMUM ENTROPY METHOD (MEM):

The Maximum Entropy Method (MEM) is a result of Burg's[ref.16] attempt to derive a procedure for increasing resolution when only a small number of samples of the estimate of the auto-correlation function are available from the observed data. The MEM suggests that the estimated auto-correlation function should be extrapolated (predicted) beyond the data limit range. The principle used for this extrapolation (prediction) process is that the spectral estimate must be the most random or have the maximum entropy of any power spectrum which is consistent with the sample values of the calculated auto-correlation function. It has been shown that the MEM is equivalent to Least Squares Error Linear Prediction (frequently used in speech processing) and auto-regression (commonly used in statistics) [ref.17].

In the MEM method the constraint vector is the unit vector defined below and which fixes the weight of the first element to 1 allowing the other weights to take any value. The effect of this is to minimise the output and provided there are enough elements will place nulls at the position of all strong signals. The inversion of this response gives an estimate of the angular spectrum but the amplitude of the peaks are not directly related to the power of the sources.

The MEM angular spectrum is given by:

$$P_{MEM}(\theta) = \frac{\vec{e}_1^H R^{-1} \vec{e}_1}{|\vec{e}_1^H R^{-1} \vec{a}(\theta)|^2}. \qquad (2.18)$$

where $\vec{e}_1^T = [1 \quad 0 \quad 0 \quad 0 \quad . \quad . \quad . \quad 0]$.

The main advantages of the MEM are:
1. It can be applied to short data records.
2. Its computation load is relatively low.
3. Its resolution is higher than the CBF.

However, it has several disadvantages:
1. Line splitting may occur giving false targets.
2. It is limited to a linear equispaced array.
3. It is prone to spurious direction estimates particularly at low signal to noise ratios.

2.4.3 THE EIGEN-STRUCTURE METHODS:

Eigen-structure techniques are based on a different approach to the parameter estimator problem obtained by exploitation of the geometrical aspects of the underlying signal model. These types of algorithms were pioneered first by Pisarenko[ref.18] in 1973 when he proposed an eigen-structure technique for the harmonic retrieval problem that could be applied to the source localization problem only for rectilinear arrays. However, it was not until 1977, when Schmidt[ref. 19 and 20] developed the MUSIC (MUltiple SIgnal Classification)

algorithm, that a full appreciation of the geometrical aspects of the deterministic signal in additive noise parameter estimation problem was obtained. These techniques were further extended by many authors.

Before describing these methods in full, the eigenvector decomposition of the covariance matrix will be examined [ref. 21].

The eigenvectors of a matrix R are defined by the property

$$\overrightarrow{RU}_i = \lambda_i \overrightarrow{U}_i \qquad i = 1,2,\ldots,N \tag{2.19}$$

where λ_i is the eigenvalue associated with the eigenvector $\overrightarrow{U}_i$.

If R is Hermitian i.e., it has conjugate symmetry, then the eigenvectors form an orthogonal set.

The covariance matrix, or the estimate of it obtained from the measured data, can be decomposed into a number of matrices each of which is an outer product of one of the eigenvectors of the covariance matrix. This is rather similar to the way in which we decompose a time series waveform into a series of sine-waves using Fourier Analysis. Thus

$$R = \sum \lambda_i \overrightarrow{U}_i \overrightarrow{U}_i^H \tag{2.20}$$

We can express this in matrix form viz:

$$RU = U\Lambda \tag{2.21}$$

where U is a matrix whose columns are the eigenvectors and Λ is a diagonal matrix of eigenvalues.

If there is no noise R is singular ($M<N$) and there are only M non-zero eigenvalues. Hence

$$R = \sum_{i=1}^{M} \lambda_i \overrightarrow{U}_i \overrightarrow{U}_i^H \tag{2.22}$$

On the other hand, if there are no signals then all the eigenvalues are equal, since

$$R = \sigma^2 I$$

$$= \sum_{i=1}^{N} \sigma^2 \vec{U}_i \vec{U}_i^H \tag{2.23}$$

When we have both signal and noise then

$$R = \sum_{i=1}^{M} (\sigma^2 + \lambda_i) \vec{U}_i \vec{U}_i^H + \sum_{i=M+1}^{N} \sigma^2 \vec{U}_i \vec{U}_i^H$$

$$= R_s + R_N \tag{2.24}$$

where R_S is known as the signal subspace and

R_N is known as the noise subspace.

It is obvious these two subspaces are orthogonal.

From our earlier analysis we can express the covariance matrix as:

$$R = \sum_{i=1}^{M} s_i \vec{a}(\theta_i) \vec{a}^H(\theta_i) s_i^H + \sigma^2 I \tag{2.25}$$

thus

$$\sum_{i=1}^{M} s_i \vec{a}(\theta_i) \vec{a}^H(\theta_i) s_i^H = R - \sigma^2 I \tag{2.26}$$

This is a matrix of rank M and hence will have only M non-zero eigenvalues. Therefore

$$\sum_{i=1}^{M} s_i \vec{a}(\theta_i) \vec{a}^H(\theta_i) s_i^H = \sum \lambda_i \vec{U}_i \vec{U}_i^H \tag{2.27}$$

Hence the signal direction vectors are contained in the signal subspace and hence are orthogonal to the noise eigenvectors. That is:

$$\vec{a}(\theta)_i . U_j = 0 \qquad i = 1 \quad to \quad M$$

$$j = M+1 \quad to \quad N \tag{2.28}$$

This provides the basis for a number of very powerful techniques for determining the directions of the signals. The first technique suggested by Pisarenko made use of the eigenvector associated with the smallest eigenvalue on the basis that this is very unlikely to be other than due to noise. This vector was then used to find the zeros of the polynomial *D(z)* given by:

$$D(z) = \sum_{m=0}^{N-1} \vec{U}_{m+1} z^{-m} \tag{2.29}$$

These zeros occur at $z = \exp(j\omega_m), m = 1,2,..,M$ and from which ω_m can be found.

The angular spectrum of Pisarenko method is:

$$P_{Pisarenko}(\theta) = \left[\vec{a}^H(\theta)\vec{U}_{\min}\vec{U}^H_{\min}\vec{a}(\theta)\right]^{-1} \tag{2.30}$$

where $\vec{U}_{\min}$ is the eigenvector associated with the minimum eigenvalue.

Because the minimum eigenvector is orthogonal both to the signal and also to any other noise related eigenvalues, the result may contain spurious noise generated peaks in positions unrelated to the signal directions.

In the late seventies, many methods were proposed to increase the robustness of Pisarenko method by making use of all the noise eigenvectors for estimating the noise subspace. Among these methods is the MUSIC (MUltiple SIgnal Classification) of Schmidt which is probably the most well known eigenvector method. In the following, some of these methods are presented.

2.4.3.1 The Multiple Signal Classification Method (MUSIC):

The MUSIC algorithm uses the uniformly weighted average of all the noise eigenvectors and provides an asymptotically unbiased estimate of many important parameters of multiple wavefronts arriving at an array of sensors. These parameters include the number of incident wavefronts, direction of arrival, strength and cross correlation among the directional wavefronts polarization and strength of noise interference.

The orthogonal relationship in equation 2.28 is used to form the following spectrum:

$$P_{Music}(\theta) = \frac{1}{\vec{a}(\theta)^H U_N U_N^H \vec{a}(\theta)} \tag{2.31}$$

or

$$P_{Music}(\theta) = \frac{1}{|\vec{a}(\theta) U_N^H|^2}$$

$$= \frac{1}{|\sum_{j=M+1}^{N} \vec{a}(\theta)\vec{U}_j^H|^2} \tag{2.32}$$

The reciprocal nature of the spectra in equation 2.32 and the result derived in equation 2.28 give a theoretically infinite resolution. This does not occur in the sampled case but it is still possible to obtain superior resolution compared with other non-eigenvector techniques.

The form of the denominator in equation 2.32 makes it important that the number of signals M is chosen accurately. There are different techniques available for choosing M most of which require a subjective threshold to be set. The effect of improperly setting the threshold on the performance was studied by Johnson [ref. 22]. He stated that, in the case of high SNR, overestimated signal order does not appear to be a significant problem while underestimated signal order results in a significant decrease in spectral resolution. In low SNR cases the selection of signal order is more critical. Over-estimation produces peaks which cannot be discriminated from the signal sources without prior knowledge. Under-estimation suffers the same penalties as incurred in the high SNR cases.

Simulations show that the MUSIC method produces very good resolution, especially for small numbers of data vectors (e.g. of the order of the number of the array elements). The scan pattern is very stable with low sidelobes.

The main disadvantages of the MUSIC method are the large amount of computation it requires to estimate the angular spectrum and its failure to resolve correlated sources. Other disadvantages are the need to estimate the number of signals and that the maxima do not depict relative strength of the arriving signals.

Many publications related to the MUSIC algorithm have appeared in the last few years. Nickel[ref. 23] studied the relation between MUSIC and Capon's method and he concluded that the MUSIC method can be interpreted as a Capon-type method, but one which uses the covariance matrix (computed with the eigenvectors) which corresponds to infinite signal/noise ratio. This explains the superior resolution of the MUSIC pattern compared to that of the Capon's method. Other publications analyzed the performance of the MUSIC algorithm in the presence of sensor perturbations [ref. 24] or system errors [ref. 25] which cause differences between the array manifold used by MUSIC and the true array manifold.

Reference 26 and reference 27 describe the adaptive implementation of the MUSIC algorithm which, instead of starting from scratch for calculating each new direction of arrival, these methods use the previously estimated signal subspace as a good approximation to the new one.

Many authors have advocated the use of a beamforming preprocessor to facilitate application of high resolution direction finding algorithms. The benefits cited include reduced computation, improved performance in environments that include spatially coloured noise, and enhanced resolution. Reference 28 presented an analysis of the beamspace version of the MUSIC algorithm and showed that the resolution threshold of the MUSIC algorithm is proportional to the dimension of the noise subspace; therefore the threshold can be reduced substantially by utilizing an appropriate beamformer to reduce the dimension of the noise subspace.

As has been mentioned earlier, the performance of the MUSIC algorithm fails drastically when the signals to be resolved are correlated. Correlated emitters can occur in practice for several reasons, most notably due to multiple propagation paths, man-made interference sources, and when the observation time is limited. Recently, some work has been carried out to deal with this problem. One promising solution has been to use a technique called 'Spatial Smoothing' which removes the source correlations by averaging over the results of a set of subarrays. This Spatial Smoothing can be implemented either by physically moving the array[ref. 29] or by using a fixed array with regular linear structure and composed of identically matched sensors[ref. 30].

The performance of the MUSIC algorithm to resolve correlated sources using Spatial Smoothing has been studied by many authors [ref. 31, 32 and 33]. Reference 33 studied a more general and realistic case of resolving three sources, two of them are correlated while the other is not correlated with the first two.

2.4.3.2 Johnson and DeGraaf Method:

As mentioned earlier, one of the main problems with MUSIC is that knowledge of the number of sources present is required. If an eigenvector belonging to the signal subspace is included in the summation in equation 2.32, so that the number of sources present is underestimated, there will not be peaks in the DF function corresponding to positions of all the sources since the source subspace eigenvectors are not orthogonal to the source direction vectors. Conversely, if not all the noise eigenvectors are included in the summation, so that the number of sources present is overestimated, there may be values of θ not corresponding to a true source for which the direction vector is orthogonal to the reduced set of noise eigenvectors. Spurious peaks in the DF function will then be seen.

Johnson and DeGraaf[ref.34] suggested a method similar to MUSIC in the way that they both divide the eigenvector space into signal subspace and noise subspace and then use the eigenvectors from the noise subspace only to estimate the desired parameters of the incident signals. However, their method is different from MUSIC in that it weights the noise eigenvectors in inverse proportion to their eigenvalues in an attempt to reduce the consequences of improperly setting the number of sources. The angular spectrum of Johnson and DeGraaf method is expressed as:

$$P_{JD}(\theta) = \frac{1}{\sum_{j=M+1}^{N} \lambda_j^{-1} \left| \vec{a}(\theta)^H \vec{U}_j \right|^2} \qquad (2.33)$$

This unequal value weighting gives more emphasis to the smaller eigenvectors which are thought to be more likely associated with noise eigenvalues. This reduces the sensitivity to estimate the number of sources and depicts a smoother

background in the spectrum than MUSIC. However, these improvements are obtained at the expense of array gain. Another disadvantage of this method is that it is sensitive to ill-conditioning.

2.4.3.3 The Minimum Norm Method (MNM):

This method, sometimes referred to as the KT method, was proposed by Kumaresan and Tufts[ref.35]. It is similar to MUSIC except that it uses a single vector ($\vec{d}$) orthogonal to the signal subspace, generated either from the signal subspace or from the noise subspace, to calculate the angular spectra. One attractive feature of this algorithm is that the time consumed to calculate the angular spectrum is less than in MUSIC.

Let E_s be the matrix that contains signal subspace eigenvectors,

$$E_s = [\vec{U}_1, \quad \vec{U}_2, \quad ., \quad ., \quad \vec{U}_M] \tag{2.34}$$

and E_N the matrix that contains the noise subspace eigenvectors,

$$E_N = [\vec{U}_{M+1}, \quad \vec{U}_{M+2}, \quad ., \quad ., \quad \vec{U}_N] \tag{2.35}$$

Now partition E_s and E_N as follows:

$$E_s = \frac{g^T}{E_s'} \qquad and \tag{2.36}$$

$$E_N = \frac{h^T}{E_N'} \tag{2.37}$$

where g and h have the first elements of the signal and the noise subspace eigenvectors respectively, and E_s' and E_N' have the same elements as E_s and E_N respectively with the first row deleted.

Since $\vec{d}$ to be in the subspace E_N, $\vec{d}$ will be orthogonal to the columns of E_s. The first element of $\vec{d}$ is forced to be unity. The rest of the coefficients $[d_2, d_3, ., ., d_N]$ can be found by:

$$\vec{d} = \frac{1}{-E_s' g^* / (1 - g^H g)} \tag{2.38}$$

$\vec{d}$ can also be obtained from the noise subspace eigenvectors due to the orthogonality of the signal and noise subspaces. The expression of d in terms of the noise subspace eigenvectors is:

$$\vec{d} = \frac{1}{-E_N' h^* / h h^H} \tag{2.39}$$

The DF function of the MNM method is:

$$P_{MNM} = \frac{1}{|\vec{a}^H(\theta)\vec{d}|^2} \tag{2.40}$$

which will exhibit large peaks in the signal directions.

The effect of using a single noise subspace vector or a single signal subspace vector to describe the orthogonality between the noise subspace and the source direction vectors is to produce a more peaky DF function than the MUSIC algorithm, in which averaging over the whole subspace reduces the effect of any single root close to the unit circle.

2.4.3.4 Byrne and Steel's Method:

Byrne and Steel's method[ref.36] is considered as a reweighting extension of Capon's method since it also uses all the eigenvectors, both in the noise subspace and the signal subspace, but provides improved performance by introducing two modifying parameters into the expression for spectrum estimation to reweight the eigenvectors:

$$P_{BS} = \frac{1}{\sum_{i=1}^{N} \frac{\lambda_i^{K-1}}{\left(\lambda_i^2+\alpha^2\right)^K} |\vec{a}^H(\theta)\vec{U}_i|^2} \tag{2.41}$$

where α should be chosen greater than the eigenvalues of unstable eigenvectors and smaller than the smallest signal eigenvalues; K is an nonnegative integer, the bigger its value the more emphasis is placed on the eigenvectors with eigenvalues near α. An appropriate choice of these two parameters ensures a more stable null structure in the estimated spectrum because they decrease the weighting for signal eigenvectors which degrade the resolution and the smallest eigenvector which tends to be unstable. It follows from equation 2.41 and equation 2.17 that Capon's method is a special case of Byrne and Steel's method when $K = 0$. In the case of partially correlated signals, most nonlinear methods fail to perform properly either by failing to resolve the signals or by the presence of a bias in the estimated signal directions. With respect to these two problems, Byrne and Steel's method makes an improvement when the values of K are sufficiently large. This method can be used in the presence of correlated arrival and phase errors, but the computational burden is heavier than that of the MUSIC or Johnson and Degraaf's method.

2.4.3.5 The ESPRIT Algorithm:

One of the problems encountered with the MUSIC algorithm is that it requires full knowledge of the array manifold, i.e., the gain and phase patterns of the sensors and the geometry of the array. The array must be precisely calibrated, a process that is expensive, requires large amounts of data storage, and is often very difficult. In addition, a computationally expensive search of the array manifold is required to determine the MUSIC spectrum from which the angles of arrival are estimated.

The ESPRIT (Estimation of Signal Parameters via Rotational Invariance Techniques) algorithm is a new technique which reduces the practical problems encountered with MUSIC such as computational load, storage, and finite-sample bias[ref.37 and 38]. In particular, the array manifold need not be known and the search procedure is replaced by an eigenvalue problem. The estimates obtained

with ESPRIT appear to be unbiased for finite data lengths. Simulation results suggest that this algorithm is more robust with respect to array perturbation than MUSIC, which is highly sensitive to inaccurate modelling of the array manifold.

In the ESPRIT algorithm, the array is assumed to compromise a number of doublets which can be obtained by moving an arbitrary array by a fixed amount. It is not necessary to know the array manifold, only the vector through which it is moved and the assumption that the array manifold of the two arrays are identical except for the factor due to this movement. This simplifies the calculation and produces some very good results without knowledge of the manifold. The detailed derivation of this algorithm is presented in references 37 and 38.

Reference 39 compares the performance of the ESPRIT algorithm with the MUSIC algorithm and reference 40 extends ESPRIT to wideband signals. Reference 41 simulates the ESPRIT algorithm on a transputer using OCCAM and studies the performances of this algorithm on different simulated data.

More recent advances in the ESPRIT algorithm have been made by its original authors in the form of Total Least Square ESPRIT (TLS-ESPRIT)[ref.42].

2.4.3.6 The WSF (Weighted Subspace Fitting) Algorithm:

The signal subspace methods are all based on the observation that if the signals are non-coherent the true steering matrix $A(\theta)$, will span the signal subspace (E_s). A natural exploitation of this fact is to try to fit a space spanned by the steering matrix to the estimated signal subspace in a Least-Squares (LS) sense. Since the eigenvectors in $\hat{E}_s$ correspond to different eigenvalues, it is natural to introduce a weighting of these eigenvectors. This *Weighted Subspace Fitting* method can be formulated as:

$$\hat{\theta} = arg \quad \min_{\theta,T} \| \hat{E}_s W^{1/2} - A(\theta) T \|_F^2 \qquad (2.42)$$

where W is a M x M Hermitian positive definite weighting matrix and T is any complex M x M matrix. The symbol $\|.\|_F$ represents Frobenius norm.

By minimising equation 2.42 analytically with respect to T, the following equivalent problem is obtained:

$$\hat{\theta} = arg \quad \min_{\theta} Tr\{P_A(\theta)\hat{E}_s W \hat{E}_s^H\} \tag{2.43}$$

The matrix $P_A(\theta) = A(A^H A)^{-1} A^H$ is the orthogonal projection onto the range space of $A(\theta)$.

This concept of subspace fitting was proposed by Viberg [ref. 43 and 44] and it is now receiving more attention because it shows excellent performance.

2.4.4 OTHER HIGH RESOLUTION DF METHODS:

A number of other high resolution methods have been published recently offering some advantages when compared to the MUSIC algorithm which now is often taken as a standard of performance.

One of these new methods is the CLOSEST algorithm [ref. 45]. This is useful when it is desired to use high resolution methods to separate a group of sources in a cluster. The method selects one (or a group) of the noise sub-space vectors which are closest in some sense to the desired direction and because of this provides superior resolution to the MUSIC algorithm without introducing bias.

Another new technique, called the IMP (Incremental Multi-Parameter)[ref.46], uses the information preserved in the conventional beamformer as a basic processing component. The first step of the algorithm assumes that there is only one signal present and uses the beamformer to find the best estimate of its position. The subsequent stages of the algorithm use modified beam scan which projects the data into a subspace orthogonal to that spanned by the steering vectors which corresponds to the latest estimates of signal angles of arrivals. If the resulting estimate is flat with respect to θ or has no significant peak, the algorithm terminates. If sufficient residual power exists in the modified beamformer output, the principle peak with respect to θ is taken as the initial estimate of the location of the next signal.

Recently, a new eigenanalysis-based method called MODE (Method Of Direction Estimation) has been published[ref.47]. The authors of this algorithm claim that their algorithm performs better than MUSIC especially in situations where the sources are highly correlated.

Finally, it is evident from this chapter that this area of science is very active and many researchers are working very hard to enhance and develop high resolution direction finding algorithms and time will tell which prove to have long term advantages.

CHAPTER THREE

SIMULATION OF SOME HIGH RESOLUTION DF ALGORITHMS ON A TRANSPUTER

3.1 INTRODUCTION:

It has been shown in chapter 2 that an enormous amount of work has been done to develop new high resolution DF algorithms which provide resolution enhancement beyond that of a conventional beamformer. However, most of these algorithms have been based on computer simulations and very little has been published on the practical implementation of these algorithms. Main reasons for this lack of practical implementation are the extensive computation involved in these algorithms and the huge memory they require.

On the other hand there have been great advances in semiconductors and computer technologies in the last few years which have led to the availability of more powerful computational and storage devices. An example of such devices is the transputer. These devices have opened the doors for the possibility of implementing high resolution DF algorithms in real time.

This chapter discusses the feasibility of implementing some high resolution DF algorithms in real time using transputers as a state-of-the-art computer technology. Four main algorithms were considered. These are:

1. Capon's Method.
2. Maximum Entropy Method.
3. MUSIC.
4. MNM.

The discussion is based on the results of speed measurements of these algorithms when simulated on a single transputer using the OCCAM-2 programming language. This chapter also studies the distribution of the computational load of these algorithms over their main computational steps.

The chapter ends by discussing the possibilities of increasing the speed of processing by introducing parallelism, pipelining, and systolic arrays.
The results presented in this chapter have been published in ref. 48 and 49.

3.2 THE TRANSPUTER AND OCCAM:

The transputer was designed by the Bristol-based company, Inmos, as a programmable component for building parallel systems [ref. 50]. The name is an amalgamation of 'transistor' and 'computer', since the transputer is both a computer on a chip and a silicon component like transistor.

Figure 3.1 shows the block diagram of a typical transputer chip. What differentiates the transputer from conventional microprocessors is that, as well as processor and memory, the single chip also contains four bidirectional communication links which provide connections to other transputers. These communication links allow transputer networks of various sizes and topologies to be constructed as shown in figure 3.2. No additional components are required to interconnect transputers on the same board [ref. 50].

Table 3.1 shows the main members of the transputer family and summarises their specifications [ref. 51].

The latest addition to the transputer family is the T9000 which provides a balance between the computation and communication facilities of the transputer. It provides high performance computation as well as high throughput communication [ref. 52].

TABLE 3.1
TRANSPUTER FAMILY

	TRANSPUTER TYPE				
	T225	**T400***	**T425**	**T805****	**T801*****
Bus Architecture	16bit	32bit	32bit	32bit	32
MIPS (Peak)	30	20	30	30	30
ON-CHIP SRAM	4K	2K	4K	4K	4K
No. of Serial Link	4	2	4	4	4
Speed of Serial Link (MBITS/sec)	5,10,20	5,10,20	5,10,20	5,10,20	5,10,20
CPU Speed (MHz)	20,25,30	20	20,25,30	20,25,30	20,25,30
Package	68 pin PLCC,PGA and 100 pin PQFP	84 pin PLCC,PGA and 100 pin QFP	84 pin PLCC,PGA and 100 pin QFP	84 pin PLCC,PGA and 100 pin QFP	100 pin PGA

* Low cost Transputer.

** Includes On-Chip IEEE754 Floating Point Unit.

*** Includes On-Chip IEEE754 Floating Point Unit and demultiplexed address and data bus.

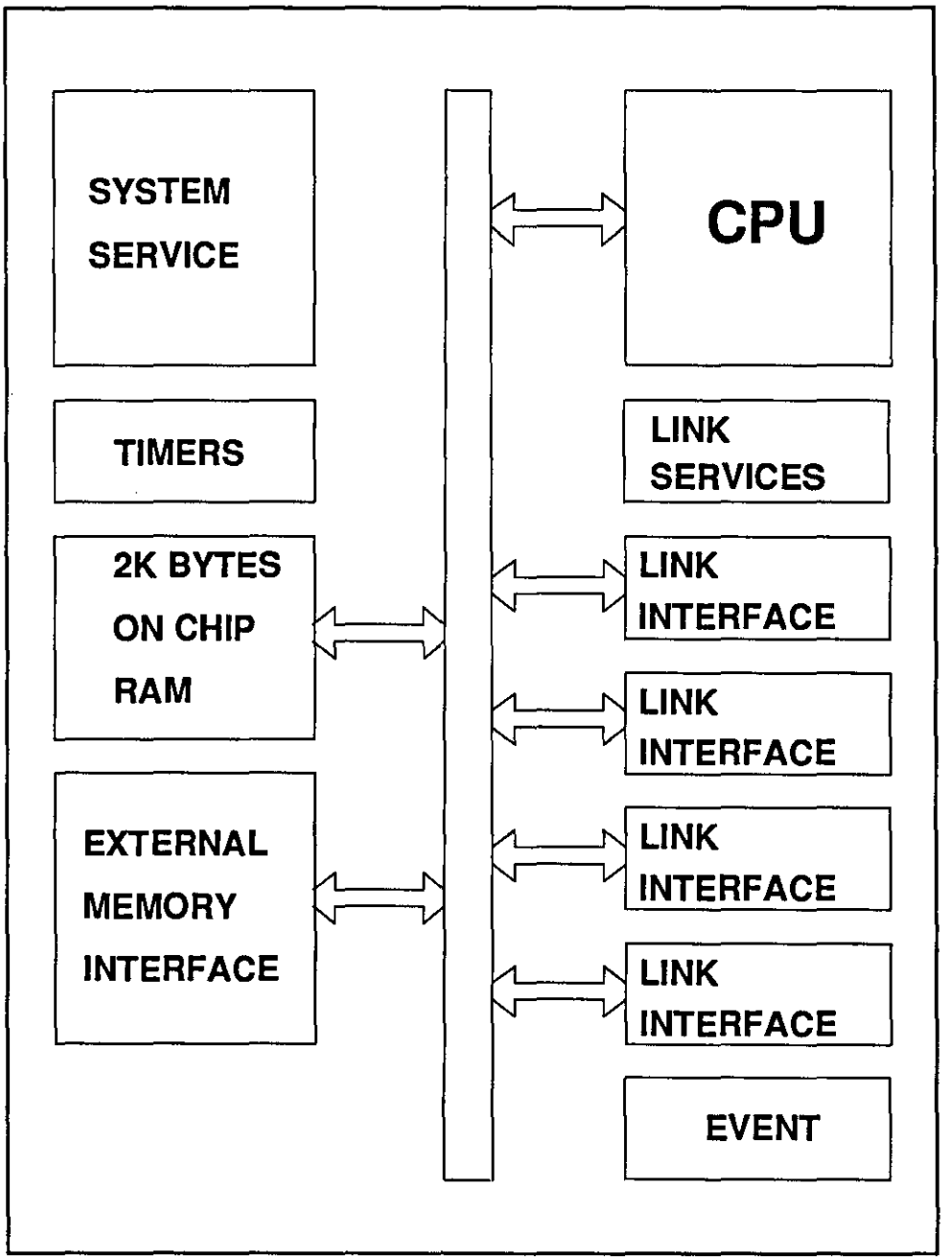

Figure 3.1: The Generic Transputer Architecture.

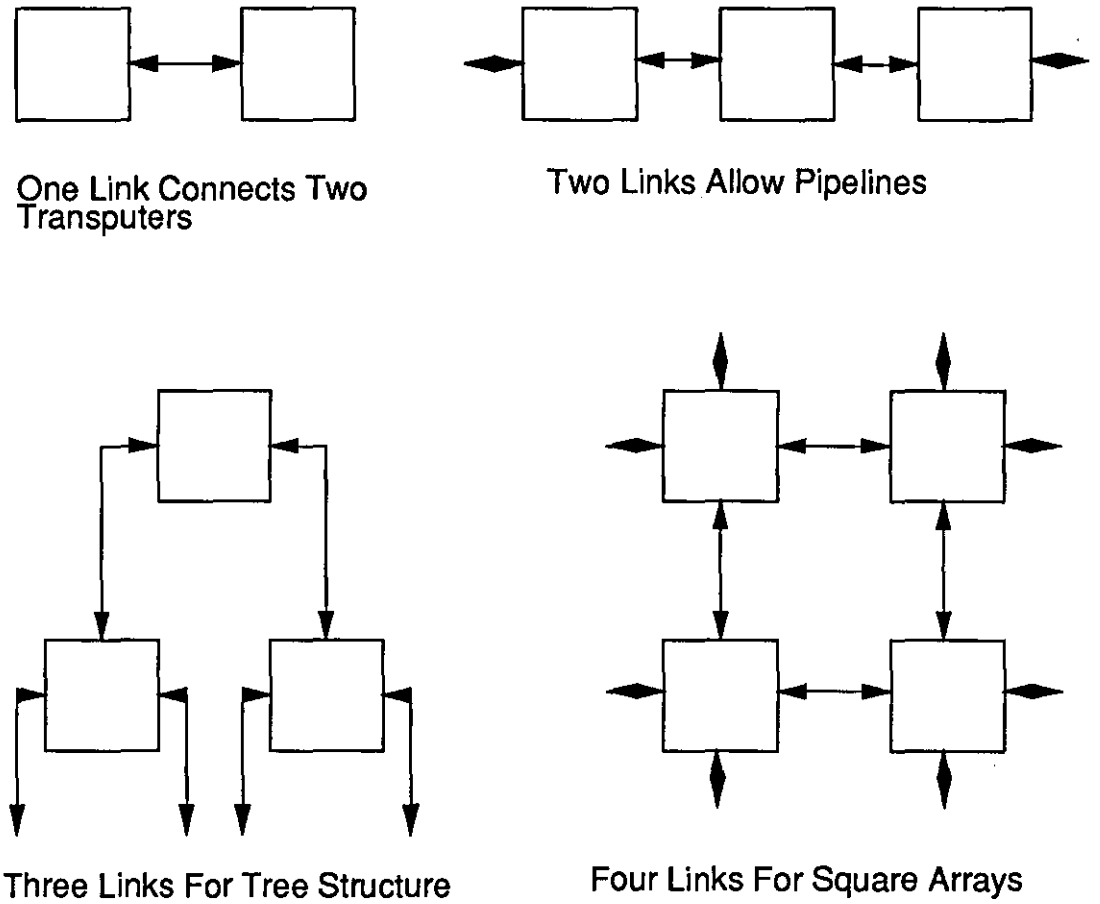

Figure 3.2: Different Transputers Networks.

The transputer family also includes some supporting devices like the 'Link Adapter' and the 'Programmable Link Switch' [ref. 51 and 53]. The Link Adapter is used to communicate with the outside world. It is a peripheral chip which converts the Inmos serial communication link to parallel bus and visa versa (i.e., it is a serial to parallel and parallel to serial converter).
The Programmable Link Switch is a 32 way cross bar switch.

The natural language for programming transputers is OCCAM, which views a program as a collection of concurrent processes communicating with each other through channels [ref. 54 and 55]. Communication is synchronised; if a channel is used for input in one process, and output in another, communication only takes place when both processes are ready.

An OCCAM program may be executed by a network of transputers, with the inter-processor links corresponding to OCCAM channels, but equally, the same program may be executed virtually unchanged by a single transputer, in which case the OCCAM channels connect to memory locations as shown in figure 3.3.

Conventional languages, such as Fortran and C, augmented by subroutine calls to carry out message passing, are also supported. When implemented on multi-transputer systems, these alien languages are embedded in an OCCAM harness which actually accomplishes the communications.

Various systems for developing and executing OCCAM programs are available. Probably the most common is the Inmos IMS B004 which is a plug-in card for the IBM PC (or compatibles). This card, together with a Transputer Development System (IMS D700D), provides an integrated environment for the development and execution of OCCAM programs. OCCAM development systems are also available for other computer systems like VAXes, Sun and Macs, and specialised transputer equipment such as Meiko's Computing Surface.

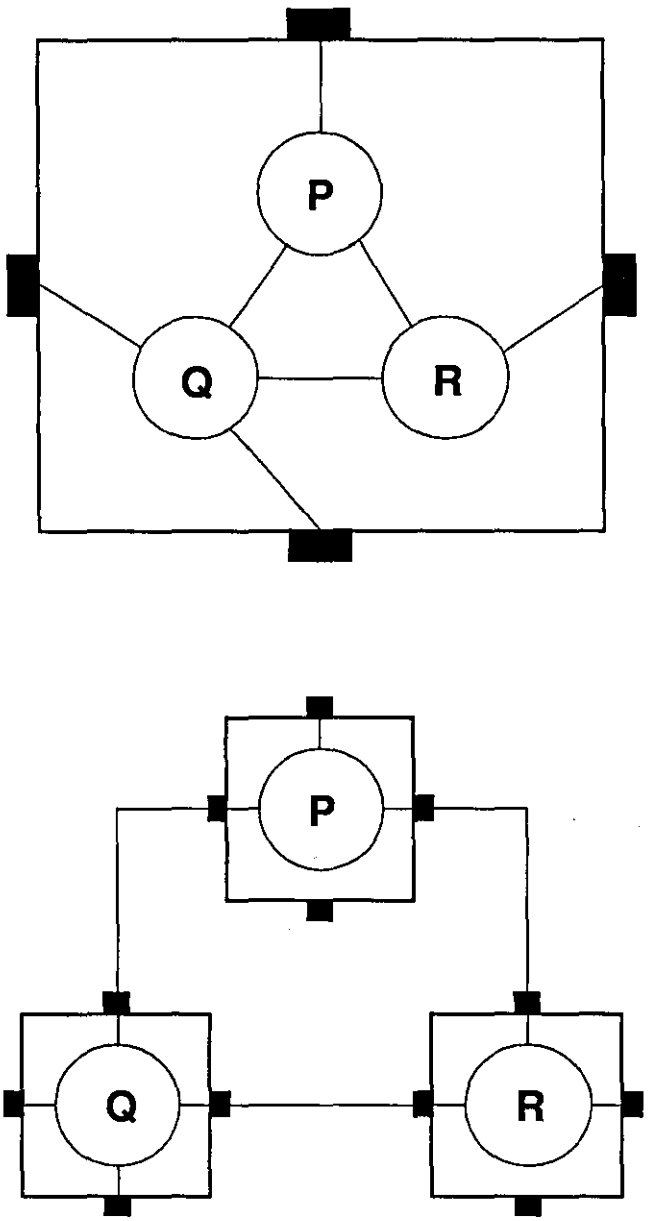

Figure 3.3: OCCAM Programming Model.

3.3 IMPLEMENTATION OF SOME HIGH RESOLUTION TECHNIQUES ON A TRANSPUTER:

Some of the high resolution algorithms discussed in the previous chapter were tested on single T414 and T800 transputers respectively. These tests were carried out for two simulated uncorrelated source signals, 20dB each, pointed 5 ° and 0 ° off normal, that are corrupted with additive noise. The number of snapshots was considered to be 10.

The receiving array was assumed to be a linear array with 10 elements spaced by $\lambda/2$. The simulation model is shown in figure 3.5.

Noise samples were generated using an internally available random number generator. This random number generator was also used to generate random phases for the source signals.

The array manifold was calculated for the array parameters mentioned above and stored in a look-up table. The search sector was a 60° arc that started at -30° and ended at 30°. The search was carried out in one degree incremental steps.

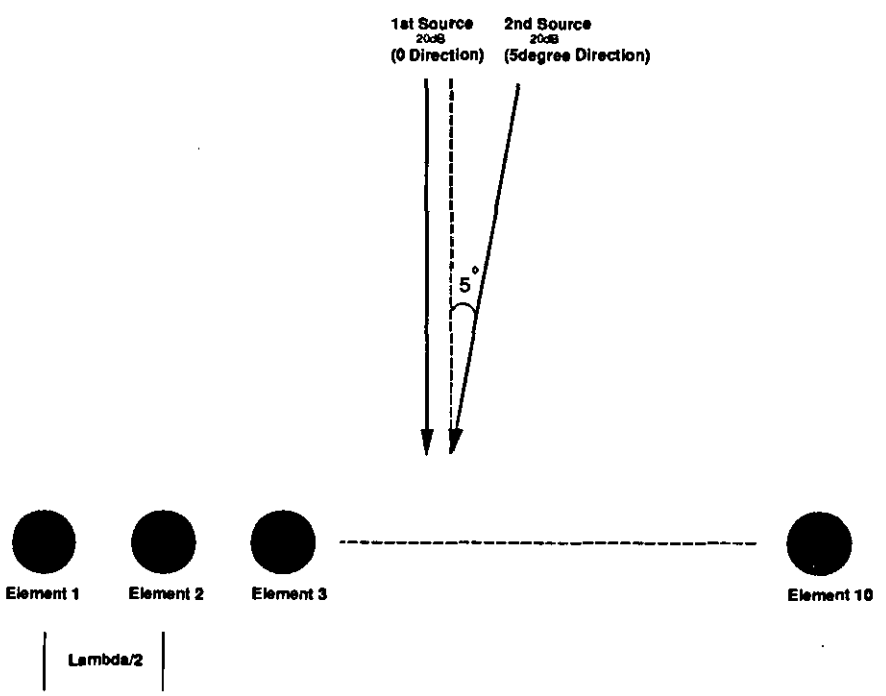

Figure 3.5: The Simulation Model.

3.4 SOME ELEMENTARY PROCEDURES WRITTEN IN OCCAM:

As has been said earlier, an OCCAM program consists of a number of processes communicating with each other by named channels. When running this program on a single transputer, the transputer shares its time between these processes and channel communication is implemented by moving data within memory. The program can also be run on a network of transputers. In this case the communication between the processes is implemented directly by transputer links.

Before describing the simulation programs, it is convenient to first introduce some of the elementary procedures that are shared by all or some of the algorithms.

3.4.1 THE COVARIANCE MATRIX PROCESS (C.M):

This process is shared by all algorithms. Its purpose is to calculate the covariance matrix of a complex data matrix using equation 2.9. Its input parameters are:

VALUE INT N	This parameter defines the number of columns of the data matrix which corresponds to the number of elements of the receiving array.
VALUE INT P	This parameter defines the number of rows of the data matrix which corresponds to the number of the snapshots.
[ ][ ] VALUE REAL32 XR	This parameter feeds the process with [N][P] data values which represent the real part of the data.
[ ][ ] VALUE REAL32 XI	This parameter feeds the process with [N][P] data values which represent the imaginary part of the data.

The output parameters of the process are:

[ ][ ] REAL32 XXR	This output parameter gives the [N][N] values of the real part of the covariance matrix.

[ ][ ] REAL32 XXI — This output parameter gives the [N][N] values of the imaginary part of the covariance matrix.

The syntax of this process is:

C.M(VAL INT N, VAL INT P, VAL REAL32 [][]XR, VAL REAL32 [][]XI, XXR, XXI)

3.4.2 THE MATRIX INVERSE PROCESS (M.I) [ref. 56]:

This procedure is used by Capon's method and the MEM method. Its purpose is to calculate the inverse of a complex matrix. Its input parameters are:

VALUE INT N — This parameter defines the dimension of the input matrix.

[ ][ ] VALUE REAL32 XXR — This parameter feeds the process with [N][N] data values which represent the real part of the input matrix.

[ ][ ] VALUE REAL32 XXI — This parameter feeds the process with [N][N] data values which represent the imaginary part of the input matrix.

The output parameters of the process are:

[ ][ ] REAL32 Z — This output parameter gives the [N][N] values of the real part of the matrix inverse.

[ ][ ] REAL32 W — This output parameter gives the [N][N] values of the imaginary part of the matrix inverse.

The syntax of this process is:

M.I(VAL INT N, VAL REAL32 [][]XXR, VAL REAL32 [][]XXI,[][]Z,[][]W)

3.4.3 THE EIGENVALUES AND EIGENVECTORS PROCESS (EIGEN) [ref. 56]:

The purpose of this process is to calculate the eigenvalues and eigenvectors of a Hermetain matrix. This procedure is used by MUSIC and MNM methods. Its input parameters are:

VALUE INT N	This parameter defines the dimension of the input matrix.
[ ][ ] VALUE REAL32 XXR	This parameter feeds the process with [N][N] data values which represent the real part of the input matrix.
[ ][ ] VALUE REAL32 XXI	This parameter feeds the process with [N][N] data values which represent the imaginary part of the input matrix.

The output parameters of the process are:

[ ] REAL32 D	This output parameter gives the [N] eigenvalues of the input matrix.
[ ][ ] REAL32 Z	This output parameter gives the [N][N] values of the real part of the eigenvectors of the input matrix.
[ ][ ] REAL32 W	This output parameter gives the [N][N] values of the imaginary part of the eigenvectors of the input matrix.

The syntax of this process is:

EIGEN(VAL INT N, VAL REAL32 [][]XXR, VAL REAL32 [][]XXI,[]D,[][] Z,[][] W)

3.5 DESCRIPTION OF THE SIMULATION PROGRAMS AND THE RESULTS:

The four main high resolution DF algorithms mentioned earlier in this chapter were simulated and tested on a single T414 and T800 transputer. The purpose of these tests was to study the computation times of these algorithms when implemented on a single transputer.

All the algorithms were tested for the same data set and measurements of the time required by each algorithm to resolve the two sources were recorded. Also, the distribution of the computation time over the main steps of each algorithm were recorded. The computation time was counted from the start of the covariance matrix calculations until the end of calculating the angular spectrum.

In the following, a description of the simulation programs are presented together with the results of these simulations.

3.5.1 Capon Method:

The Capon simulation program starts by calculating the array manifold for the receiving array (according to the parameters mentioned in section 3.3) and storing them in a look-up table. The program then generates the signals received by each element of the receiving array (with additive noise) and this was repeated for the number of snapshots to form the data matrix.

The covariance matrix of the generated data is then calculated using the predefined C.M process mentioned in section 3.4.1. The program sets a timer to measure the time required to do this calculation. The generation of the array manifold, the generation of the array signals and the calculation of the covariance matrix are common to all methods to be tested.

The next step in Capon's method is to calculate the inverse of the covariance matrix using the predefined M.I process described in section 3.4.2. Another timer is set to measure the time required to execute this process.

The angular spectrum of Capon's method is then calculated by setting the starting angle of the sector to be searched, reading the value of the steering vector which corresponds to this angle from the look-up table and then calculating the value of the DF function at that angle using equation 2.17. The search angle is then incremented by one degree and the calculation of the DF function is repeated until all the sector has been searched. A third timer is set to measure the time required to form the angular spectrum. The resulting spectrum is then displayed.

The total computation time of Capon's method was found to be 2.443 seconds. This includes the formation of the covariance matrix, the inversion of the covariance matrix and the calculation of the angular spectrum. Table 3.2 shows the distribution of the computation time over the main steps of Capon's method.

As it can be seen from this table, most of the computation time is spent in the calculation of the power spectrum (80%).

Table 3.2
Distribution of the computation load of Capon's method

	Time (sec.)	% of Total Time
Formation of covariance Matrix	0.164	7%
Inversion of covariance Matrix	0.313	13%
Calculating The Power Spectrum	1.966	80%
Total Computation Time	2.443	

3.5.2 The MEM Method:

The simulation program for the MEM method is similar to that of Capon's method except that the calculation of the angular spectrum is much simpler.

The MEM method was found to be the fastest high resolution algorithm among the four tested. It takes only 0.686 sec. This is 3.7 times faster than Capon's method. Table 3.3 shows the distribution of the computation time of this method. The main computation load of the MEM is the inversion of the covariance matrix which takes 48% of the total computation time.

Table 3.3
Distribution of Computation Load of The MEM Method

	Time (sec.)	%of Total Time
Formation of covariance Matrix	0.164	25%
Inversion of Covariance Matrix	0.313	48%
Calculation The DF Function	0.209	27%
Total Computation Time	0.686	

3.5.3 The MUSIC Method:

After calculating the covarince matrix, the MUSIC simulation program calculates the eigenvalues and eigenvectors of the covariance matrix using the predefined process 'EIGEN'. The number of sources is then calculated by setting a threshold on the eigenvalues. According to the number of sources, the eigenvectors are split into noise and signal eigenvectors respectively. The program then calculates the angular spectrum using the MUSIC DF function formula shown in 2.38.

Although the MUSIC algorithm shows superb resolution, its computation time is relatively high (2.493 sec.). Table 3.4 shows the distribution of the computation load over the main steps of this method.

Table 3.4
Distribution of Computation Load of The MUSIC Algorithm

	Time (sec.)	%of Total Time
Formation of covariance Matrix	0.164	7%
Calculating The Eigenvectors	0.9	36%
Calculating The DF Function	1.429	57%
Total Computation Time	2.493	

The main computation load of the MUSIC algorithm is the calculation of the DF function which takes 57% of the total computation time. This is because MUSIC uses all the noise subspace eigenvectors to calculate the DF function.

3.5.4 The MNM Method:

The MNM simulation program is similar to that of MUSIC except that it calculates a d-vector which represents all the noise (or signal) eigenvectors before generating the angular spectrum. This reduces the time to form the angular spectrum which is the dominant computation load in MUSIC.

The computation time of the MNM method was found to be about half that of the MUSIC algorithm (1.287 sec). Table 3.5 shows the distribution of the computation time for this algorithm. The main computation load of the MNM method is the calculation of the eigenvectors which takes 70% of the total computation time.

Table 3.5
Distribution of Computation Load of The MNM Algorithm

	Time (sec.)	%of Total Time
Formation of covariance Matrix	0.164	13%
Calculating The Eigenvectors	0.9	71%
Calculating The DF Function	0.223	16%
Total Time	1.287	

The results shown in tables 3.1-3.4 are summarized in pie charts and shown in figure 3.10.

The above tests were also carried out for T800 transputer. The results are summarised in figure 3.11.

3.6 CONCURRENCY:

The real strength of the transputer/OCCAM architecture is its ability to support concurrency. This unique ability allows the computing power of a single transputer to be easily multiplied by using several transputers concurrently.

Concurrency may take different forms such as parallelism, pipelining and systolic arrays. In the following, a description of the different types of concurrency is introduced with the discussion of the possibilities of introducing them in the implementation of the high resolution DF algorithms.

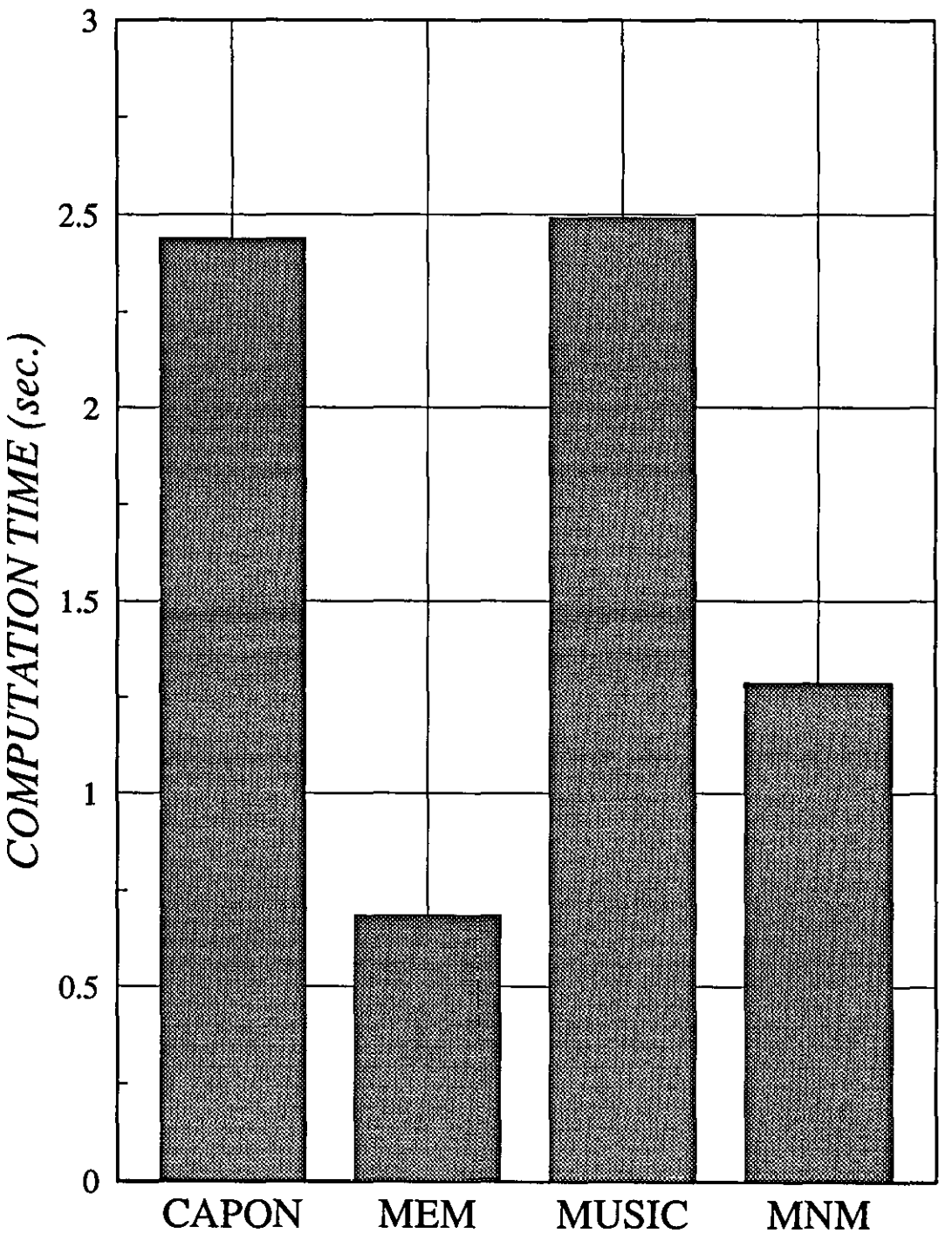

Figure 3.6: Comparison of Computation Times of Different High Resolution Algorithms.

Distribution of Computation Load
Over The Main Steps of DF Algorithms.

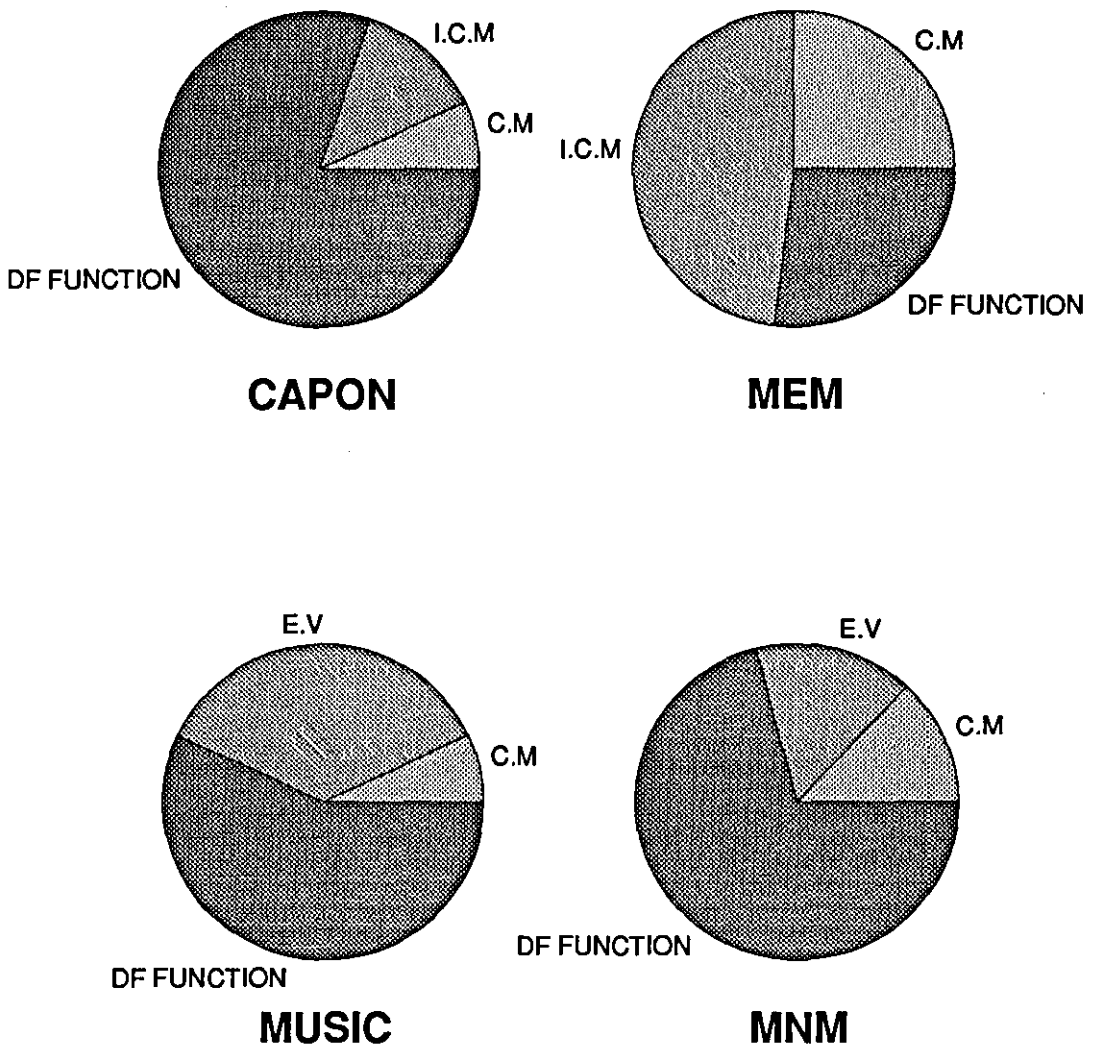

Figure 3.7: Distribution of Computation Loads Over The Main Steps of Different High Resolution Algorithms.

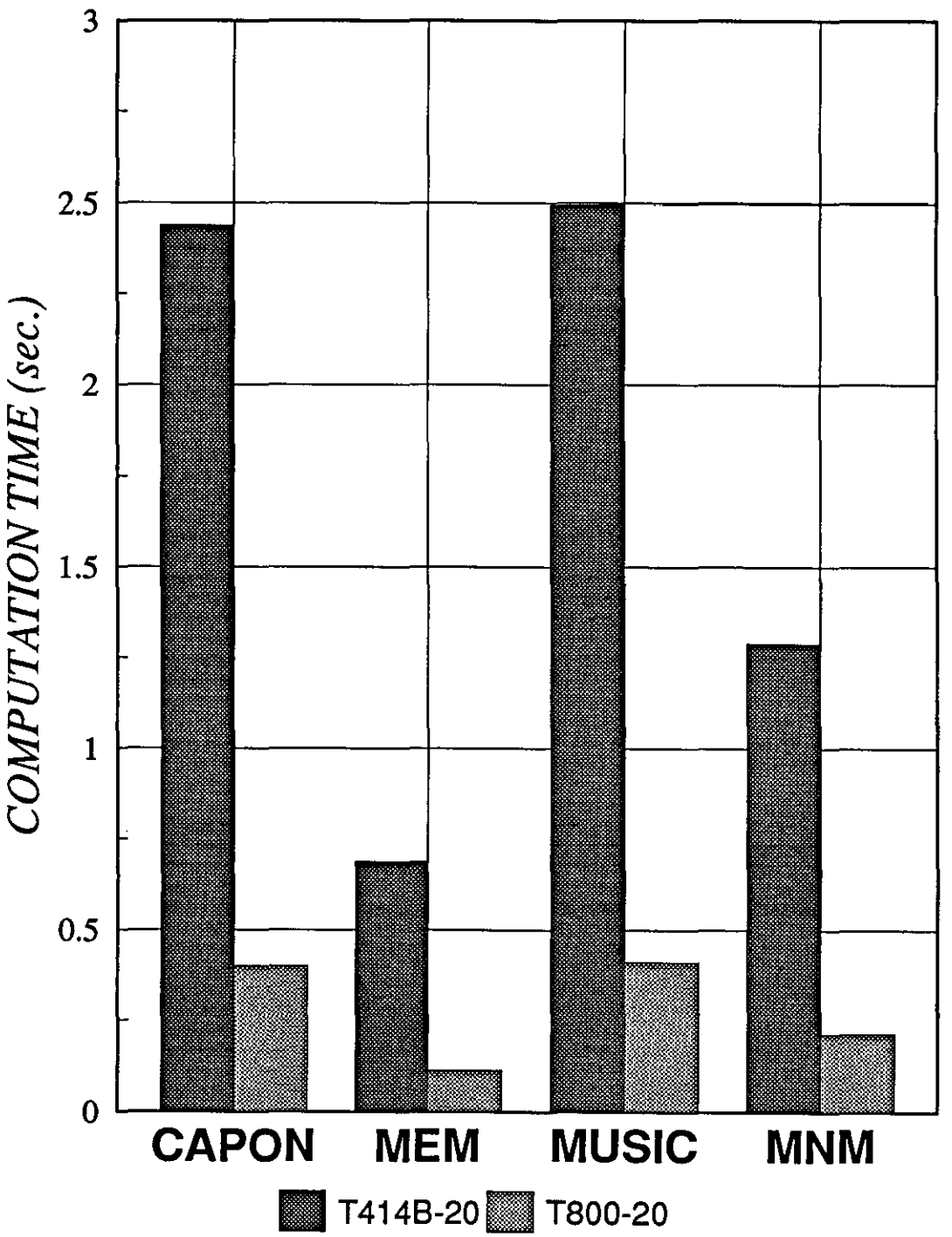

Figure 3.8: Computation Times of Different High Resolution Algorithms Using The T-800 Transputer.

3.6.1 The Parallelism:

If a program consists of many data items which can be processed independently then this program can be split into many processes running in parallel on a network of transputers thus decreasing the processing time by a factor proportional to the number of transputers used. However it is not always possible to split a program into many independent processes.

In the case of the high resolution algorithms, it seems there are limited possibilities to introduce parallelism as the nature of the algorithms is sequentially data dependent. Parallelism may only be introduced in the calculations of the angular spectrum where the sector to be searched is divided into small subsectors and then divide the process of calculating the angular spectrum into many processes each work for certain subsector and run on a separate transputer. This is particularly fits the MUSIC algorithm where the computation of the angular spectrum is the main computation load of this algorithm.

3.6.2 The Pipelining:

As has been said before, there are some problems that can only be solved sequentially. For example consider a program consisting of processes A,B and C. All data input into the program must first be processed by A. The last operation within A is to pass on iterim results to B. B is dependent on the preprocessed data from A, and C has a similar dependency on data from B. Suppose that these three processes are located on three interconnected processors. As A, B and C can only run sequentially, the final results of the program, which are produced by C would be obtained no more quickly by running on three processors than on one (assuming the interprocessor communication overhead to be negligible compared to the execution time of A, B and C). However, if each process is implemented in such a way that it would accept a new set of data as soon as it had passed on its iterim results to the next process, then A, B and C would then be a pipeline. Implementing this pipeline on three processors would increase the data throughput by a factor of three (assuming A,B and C are of equal computation time) compared with a single processor implementation. It should be remembered that the response time, from initiating the run to receiving

the first set of results will be the same. This can be visualised in terms of a car production line. There will be some delay from the line starting up to the first car being driven out of the factory but, from then on, finished cars are produced at a high rate. This technique is an effective way of distributing OCCAM programs across processors in order to share the load and increase throughput. In the case of the high resolution algorithms, where the nature of calculations are mostly sequential, this technique can be very useful to increase throughput.

Another technique similar to pipelining, known as spacelining, is used when the items arrive faster than a single processing element can process them. In this technique there are several processing elements operating in parallel, a distributor which distributes data to each processing element in turn and a collector which collects the results as they are produced. This is again very useful and applicable technique to speed up the processing of the high resolution algorithms.

3.6.3 The Systolic and Wavefront Arrays:

Systolic processors are a new class of pipelined array architectures. It is a network of processors which rhythmically compute and pass data through the system. Every processor pumps data in and out regularly , each time performing some short computation, so that a regular flow of data is kept up in the network [ref. 57].

The main features of systolic arrays are:

a. *Synchrony:* The data are rhythmically computed (timed by a global clock) and passed through the network.

b. *Modularity and Regularity:* The array consists of modular processing units with homogeneous interconnections. Moreover, the computing network may be extended indefinitely.

c. *Spatial Locality and Temporal Locality:* The array manifests a locally communicative interconnection structure, i.e., spatial locality. There is at least one unit time delay allotted so that signal transactions from one node to the next can be completed, i.e., temporal locality.

d. *Pipelinability:* The systolic array exhibits a linear rate pipelinability (pipelining rate is the reciprocal of the time interval between two successive input data).

The major factors of adopting systolic arrays for special purpose signal processing architectures are: simple and regular design, concurrency and communication, and balancing computation with I/O [ref. 57].

One of the main disadvantages of systolic arrays is that it is controlled by global timing reference "beats". From a hardware prospective, this global synchronisataion incurs problems of clock skew, fault tolerance and peak power. From a software perspective, severe requirements are imposed on compiler design in order to synchronise the activities in a systolic array [ref. 57].

A simple solution to the above problems is to exploit the principle of data flow computation for array processors. This leads to the design of the wavefront array processors.

By the virtue of the data driven approach in wavefront array processing, instructions cannot be executed until their operands have become available. In this approach the arrival of data from neighbouring processors will be interpreted as a change of state and will initiate some action. Thus it eliminates the need for global control and global synchronization.

Most of the high resolution DF algorithms are dominated by matrix algebraic operations which are very computing extensive. Fortunately, however, most of these operations posses common properties such as regularity, recursiveness and locality which are very useful for systolic array design.

The structure of transputer, with its communication links, makes it ideal for implementing the wavefront and systolic arrays. In the Sonar Research Group at Loughborough University, a study has been carried out to implement high resolution DF algorithms on systolic arrays using transputers [ref. 58 and 59]. Many other related studies have also been published [ref. 60 and 61].

3.7 PROPOSED SYSTOLIC ARRAYS FOR IMPLEMENTING HIGH RESOLUTION ALGORITHMS [Ref. 58]:

It was shown in the last section that the most convenient way of introducing concurrency in the implementation of high resolution algorithms is by using systolic arrays.

In this section, a description of proposed systolic array architectures that can be used in the implementation of high resolution algorithms are presented. It starts with the QR decomposition as it is a key tool in implementing matrix operations on systolic arrays.

3.7.1 QR Decomposition

A data matrix X can be decomposed as a multiplication of an $P \times N$ orthogonal matrix Q and an $N \times N$ upper triangular R, i.e.,

$$X = QR$$

where $\quad QQ^H = I, \quad Q^T Q^* = I.$

The covariance matrix defined in equation 2.9 can be written now as (we eliminated 1/P for simplicity):

$$\begin{aligned} R &= X^T X^* \\ &= (QR_R)^T (QR_R)^* \\ &= R_R^T Q^T Q^* R_R^* = R_R^T R_R^*. \end{aligned}$$

The systolic implementation of QR decomposition has been discussed by many authors (ref. 57 and 59). The standard architecture based on Givens plane rotations is shown in figure 3.9. The n cells of the 1st row in the array annihilate 1st column entries of the matrix, (n-1) cells of the 2nd row annihilate 2nd column, and so on. At 1st iteration, 1st row of A enters the systolic array. At 2nd iteration, a Givens rotation, G(2,1), between rows 2nd and 1st, is performed. At 3rd iteration, two Givens rotations, G(3,1) and G(3,2), are performed in 1st row cells

and 2nd row cells concurrently. At 4th iteration and on, 4 Givens rotations are performed in parallelism. After m iterations, the all operations in QR decomposition are completed.

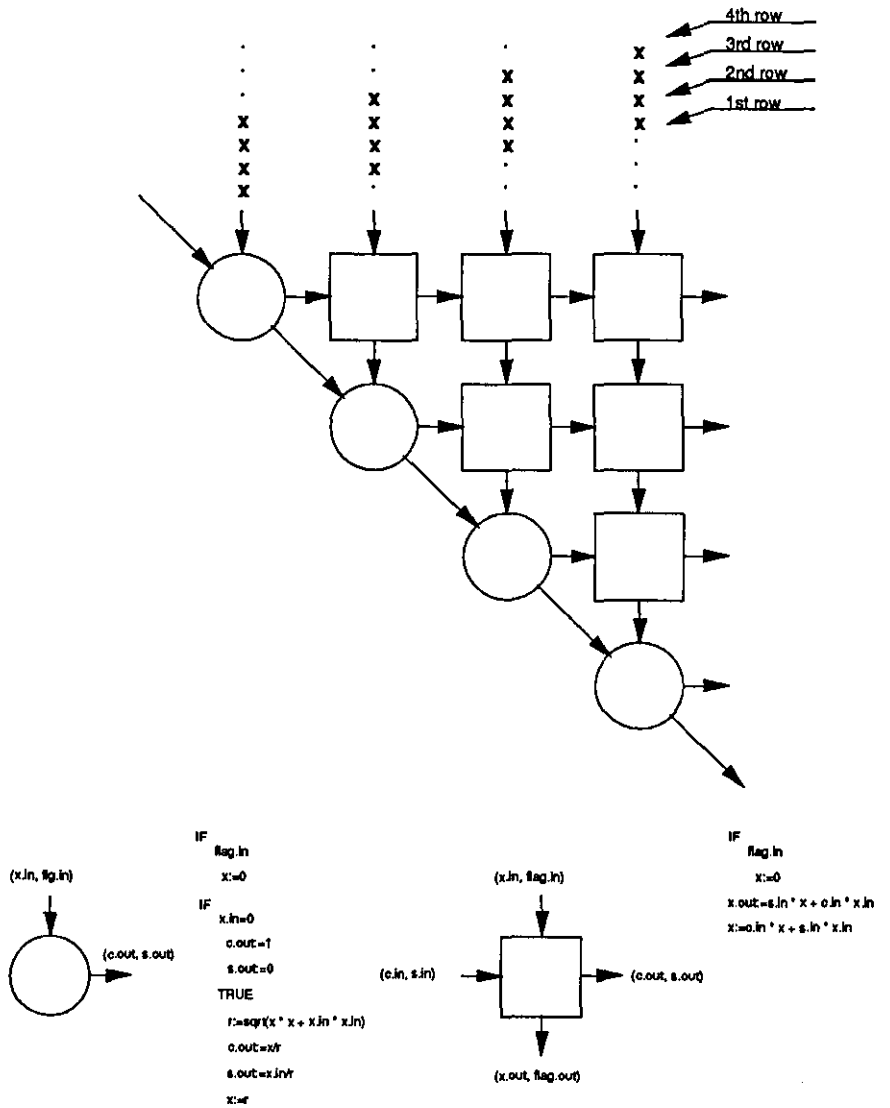

Figure 3.9: Systolic Array for QR decomposition.

3.7.2 Implementation of CBF on Systolic Array

Using the QR decomposition, equation 2.13 can be rewritten as:

$$P_{CBF} = \vec{a}^{H}(\theta)\hat{R}\vec{a}(\theta)$$

$$= \vec{a}^{H}(\theta)R_R^T R_R^{*}\vec{a}(\theta)$$

$$= [R_R^{*}\vec{a}(\theta)]^{H}[R_R^{*}\vec{a}(\theta)]$$

Figure 3.10 shows the systolic implementation of the CBF. The direction vector $a(\theta)$ input from the top of the array, the triangular matrix R is stored in the systolic array. The spectrum can be derived from the bottom of the array.

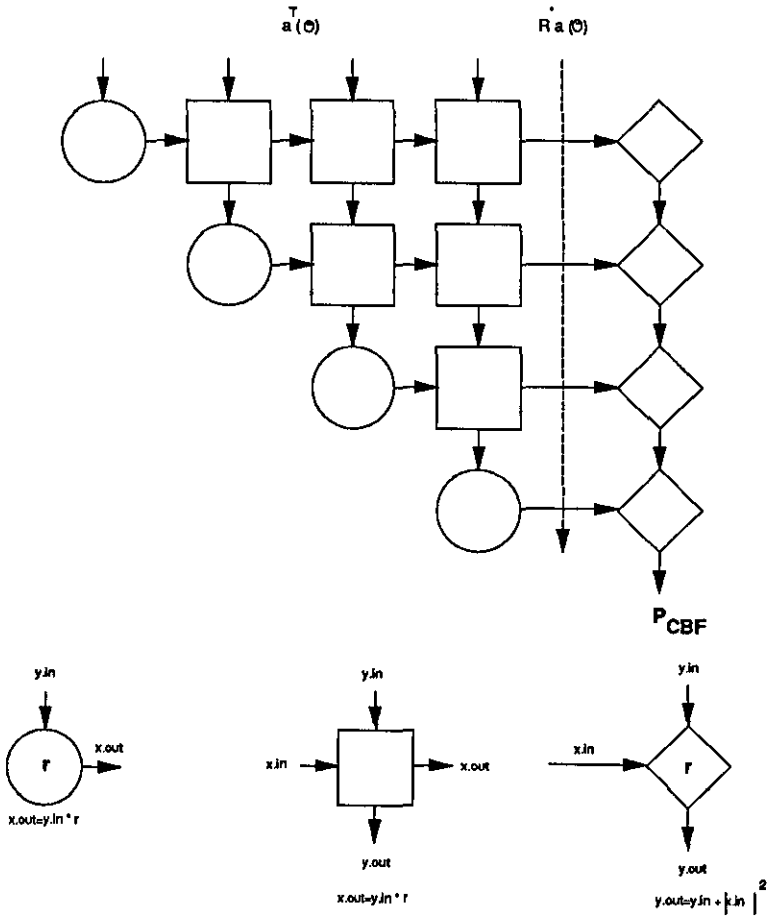

Figure 3.10: Systolic Array for CBF.

3.7.3 Implementation of Capon's Method on Systolic Array

Equation 2.16 can be rewritten as:

$$P_{Capon} = \frac{1}{\vec{a}^H(\theta)\hat{R}^{-1}\vec{a}(\theta)}$$

$$= \frac{1}{\vec{a}^H(\theta)(R_R^T R_R^*)^{-1}\vec{a}(\theta)}$$

$$= \frac{1}{[(R_R^T)^{-1}\vec{a}(\theta)]^H[(R_R^T)^{-1}\vec{a}(\theta))]}$$

Figure 3.11 shows the systolic implementation of Capon's method on systolic array. The direction vector enters the array from the top of the array and the triangular matrix R is stored in the systolic array.

3.7.4 Implementation of MEM Method on Systolic Array

In this method the inversion of the covariance matrix (R^{-1}) must be calculated.

The systolic array shown in figure 3.12 performs the inversion of the triangular matrix R in an updating way. Then the first row of R^{-1} is computed to produce the spectrum.

3.7.5 Implementation of MUSIC on Systolic Array

In MUSIC algorithm we need to calculate the eigenvalues and eigenvectors.

QR decomposition can be used to solve eigenvalue problem using singular value decomposition. The algorithm starts with matrix $A_0 = Q_0R_0$ and then reverse the two factors $A_1 = R_0Q_0$. This new matrix is similar to the original one since $Q_0^{-1}A_0Q_0 = Q_0^{-1}Q_0R_0Q_0 = A_1$, and the process continues with no change in the eigenvalues

$A_k = Q_kR_k \quad and\ then \quad A_{k+1} = R_kQ_k.$

This easily generates to A_k

$$A_k = (Q_0Q_1 \cdots Q_{k-1})^{-1}A_0(Q_0Q_1 \cdots Q_{k-1})$$

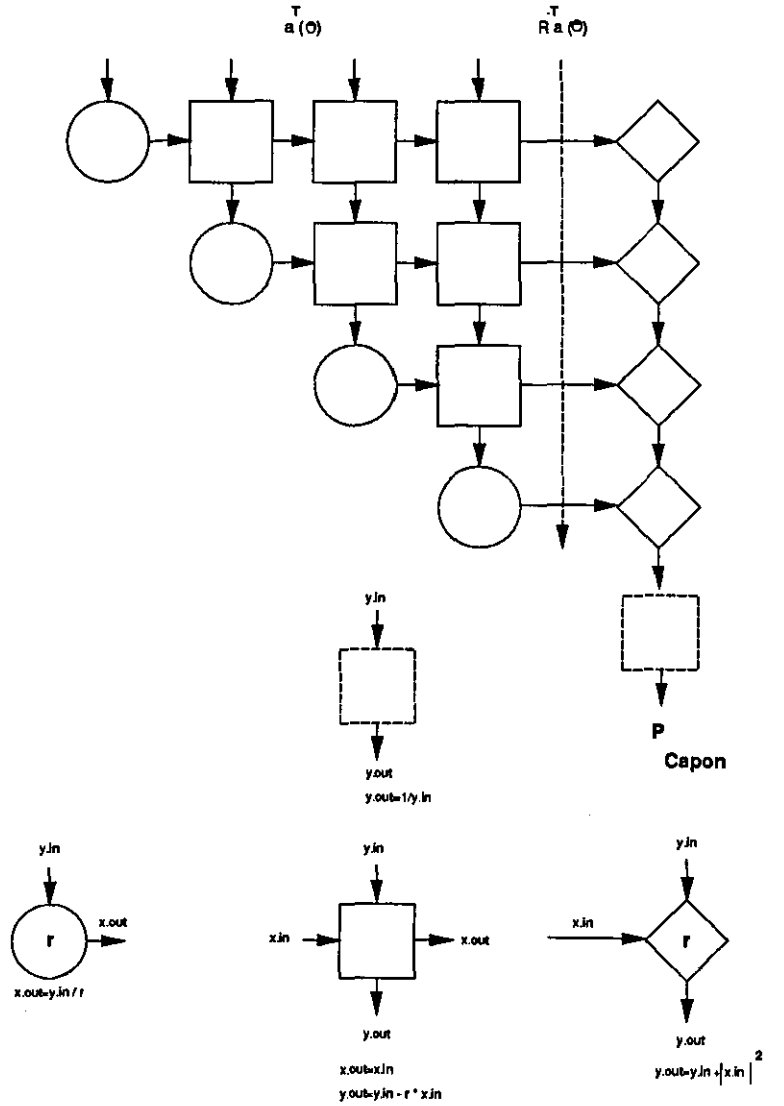

Figure 3.11: Systolic Array for Capon's Method.

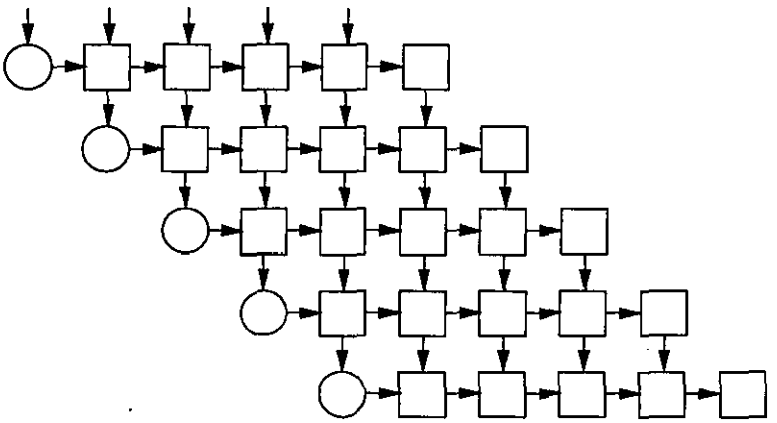

Figure 3.12: Systolic Array for MEM.

and $\lim_{k \to \infty} A_k$ is upper triangular and eigenvalues of A are diagonal entries of $A_k (k \to \infty)$.

The SVD can be implemented on an array of M/2 linearly connected processors as shown on the top of figure 3.13. From the results of the SVD, the spectrum of the MUSIC algorithm can be calculated using the systolic array shown in figure 3.13. The direction vector $\vec{a}(\theta)$ flow into the systolic array from the top and the spectrum can be extracted from the bottom.

3.7.6 Implementation of MNM on Systolic Array

After calculating the d-vector, the computation of the spectrum is rather simple. The systolic array architecture for MNM is shown in figure 3.14

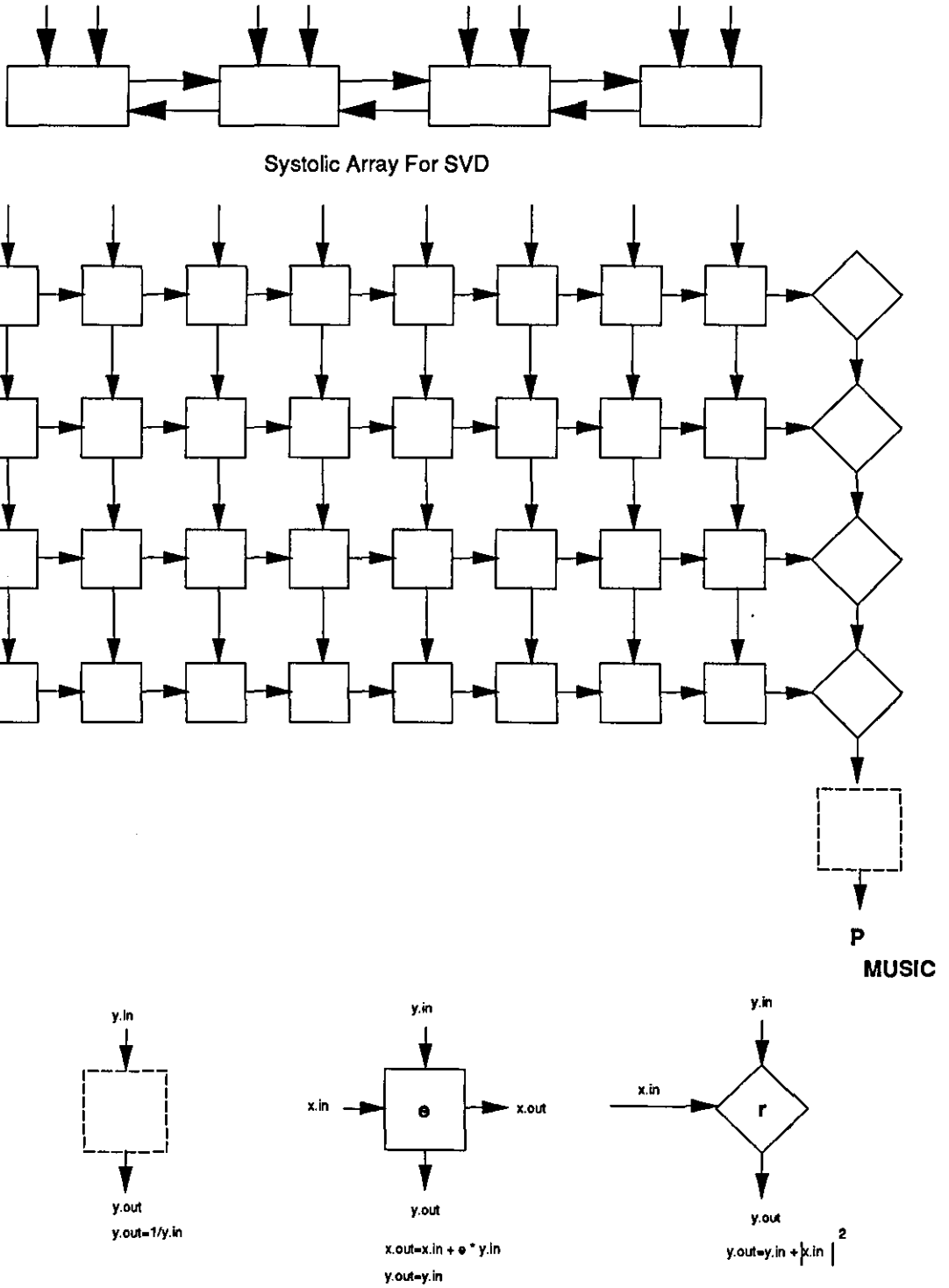

Figure 3.13: Systolic Array for MUSIC.

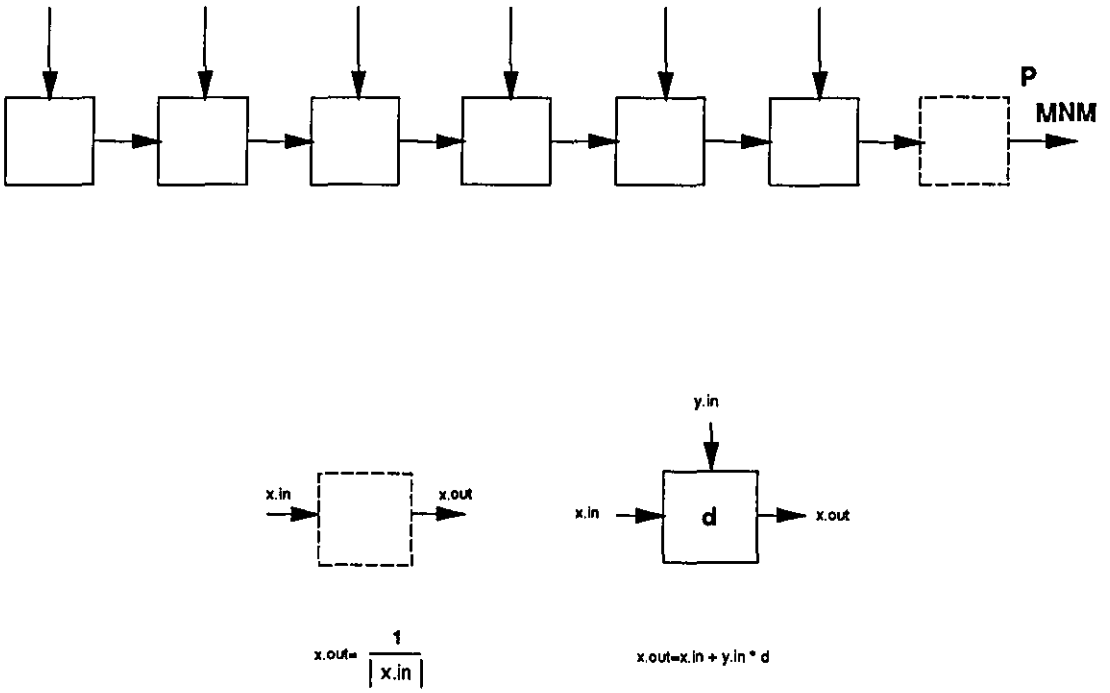

Figure 3.14: Systolic Array for MNM.

CHAPTER FOUR

DESIGN, CONSTRUCTION AND TEST OF A HIGH RESOLUTION SONAR DF SYSTEM

4.1 INTRODUCTION:

The simulation results presented in chapter 3 showed that the computation times of the high resolution algorithms, when implemented on a single transputer, were quite encouraging especially for sonar systems, where the speed of the underwater vehicles is relatively slow, allowing more time to carry out the data processing. In addition, there are great possibilities for increasing the speed of processing significantly by introducing the techniques of concurrency processing mentioned in the last chapter.

Therefore it was decided to design and build a simple sonar system, based on transputers, that could implement the high resolution DF algorithms to resolve closely separated underwater targets/sources. The system was to be designed to work in the department water tank as well as in a nearby reservoir.

This chapter discusses the design, construction and testing of the system. The proposed design was published in ref. 62.

4.2 SELECTION OF THE DESIGN PARAMETERS:

Before designing the system it was necessary to specify its parameters. In this section, a brief discussion of the main system parameters is presented.

4.2.1 The Frequency of Operation:

The system was intended to be used in the department tank (with a maximum range of about 9 metres), as well as at a nearby reservoir (with a range of several tens of metres). This placed restrictions on the frequency of operation. High frequencies might have been suitable for the tank room, but would not have been appropriate for the longer ranges involved at the reservoir because of the high attenuation. On the other hand, low frequencies would be more suitable for higher ranges but would not be practical for use in the tank room because of the limited physical size of the water tank and the reverberation problems inherent in such an environment. Therefore, it was necessary to reach a compromise in selecting an appropriate frequency.

The above considerations indicated that operation somewhere between 20 and 100 kHz would be in order, and finally it was the availability of a 15 element array working at about 40 kHz, which led to this being the chosen frequency.

4.2.2 The Number of Receiving Channels:

The 40kHz array that we decided to use consists of 15 piston elements. The diameter of these elements is 0.0365m (which is equal to λ at 40kHz) and the full array length is about 0.6m. Therefore the length of the near field zone is about 9.8m.

Since the length of the water tank at LUT is only 9m, the use of the whole 15 elements of the array would have involved near field problems. Therefore it was decided to only use ten elements from the array, which corresponds to a near field of 3.75m approximately. This also allowed selection of the best-matched ten elements of the array.

In Mark II, the number of channels was extended to 15 to make use of all elements in the array.

4.2.3 The Sampling Frequency and Memory Requirement:

Signals of the type found in sonar applications are, in many cases, band limited. A naive application of the Nyquist criterion would indicate a sampling rate much higher than that actually required [ref. 63]. Figure 4.1 shows the spectrum of a typical ultrasonic signal, with a centre frequency of f_0 and a bandwidth B. The minimum sampling frequency using the Nyquist criterion is f_s, where

$$f_s = 2(f_0 + B/2)$$

$$= 2f_0 + B. \qquad (4.1)$$

If this signal was translated to baseband, however, two quadrature channels would be required, but the sampling rate on each one would only be f_s', where

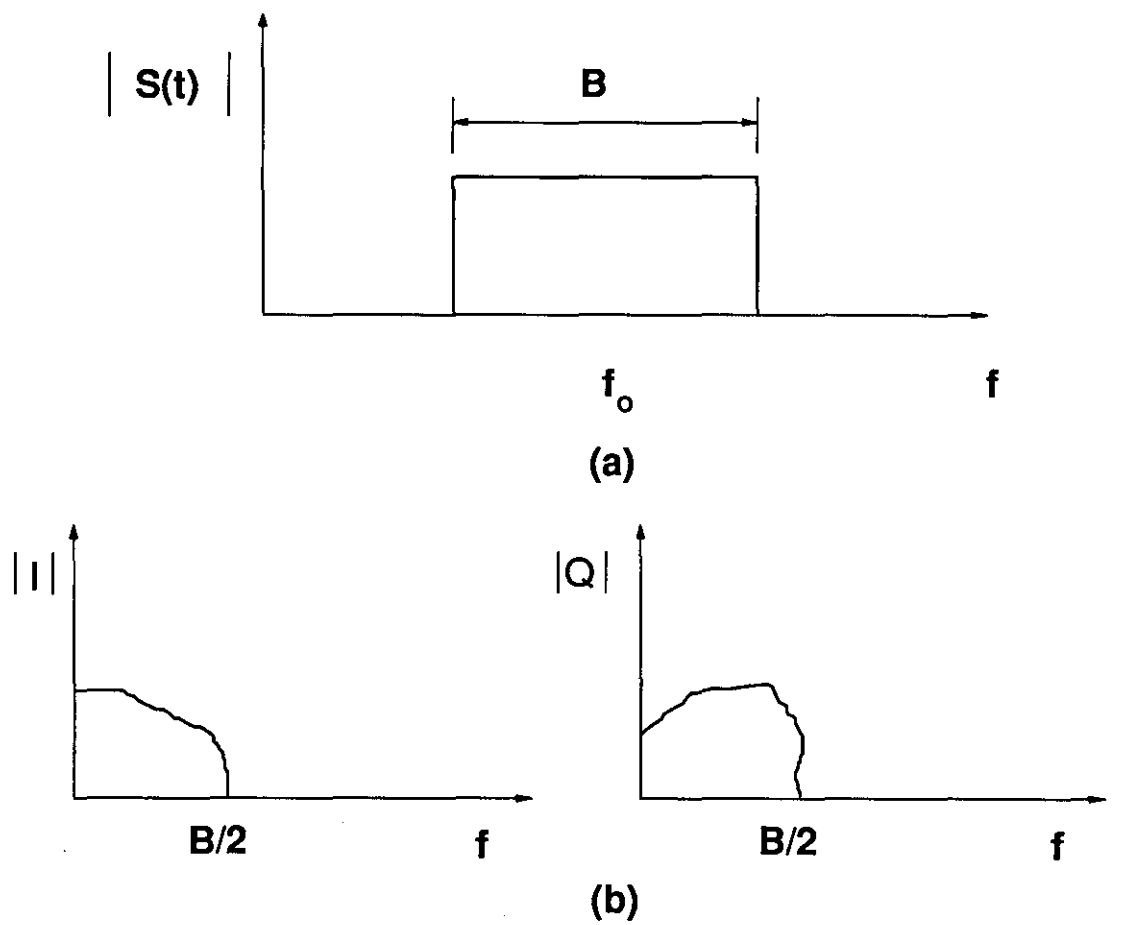

Figure 4.1: The Spectrum of a Typical Ultrasonic Signal.

$$f_s' = 2(B/2)$$

$$= B \tag{4.2}$$

This is a sampling rate reduction of η_r, where

$$\eta_r = (f_s'/f_s)$$

$$= Y/(2+Y) \tag{4.3}$$

and Y is the relative bandwidth and is equal to $Y = B/f_0$.

In ultrasonic systems, for example, Y=0.1 and $\eta_r = 0.05$, a significant reduction.

Figure 4.2 illustrates how the quadrature components I(t) and Q(t) can be obtained from a received signal [ref. 63].

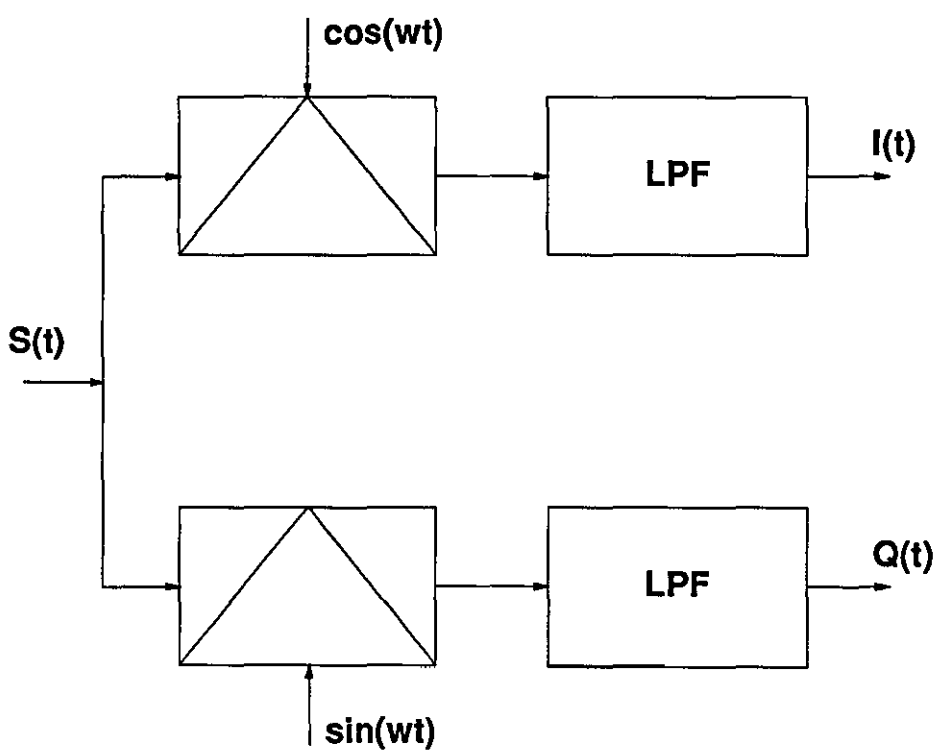

Figure 4.2: Obtaining The Quadrature Components From a Received Signal.

This sampling rate reduction also has an impact on the data storage requirement of the system. The amount of digital data storage required is the product of the data acquisition time and the sampling rate. Hence the data storage reduction factor using baseband signals is η_q, where

$$\eta_q = \frac{2f_s'T}{f_sT}$$

$$= 2\eta_r = \frac{2Y}{(2+Y)} \qquad (4.4)$$

and where T is the time length of the data sample, and the factor 2 reflects the requirement for the two quadrature channels. Using the typical case numbers from the example above, $\eta_q = 0.1$.

To collect data from a maximum range R with an array of N transducers requires a data receive time of approximate length $2R/c$ (where c is the acoustic velocity in the medium, and assuming a single frequency system). Hence the total data storage is Q, where

$$Q = 2f_s'TN \qquad or$$

$$Q = \frac{4BNR}{c} \qquad (4.5)$$

The total data storage requirement is therefore proportional to the number of array elements, the bandwidth and the maximum range of interest.

It was decided to use the I & Q sampling technique for the high resolution sonar system because it enabled the use of a much lower sampling frequency. This in turn, allowed the use of cheaper A/D convertors (as their cost increases significantly with speed). It also reduced the data storage requirement.

The sampling frequency was chosen to be 12.5 kHz and the memory assigned for data storage was chosen to be 1MBit (refer to sections 4.4.3.6 and 4.4.5).

4.2.4 The Pulse Length Consideration:

Careful consideration of the pulse length is very important when designing a sonar system. The shorter the pulse, the more accurate the range information on the target. Conversely, the longer the pulse, the greater the detection capability [ref.64].

The minimum pulse length depends on the Q-factor of the elements in the array and the sampling frequency. The maximum pulse length is dependant on the amount of time available before the arrival of interfering signals caused by reflections from the water boundaries and other bodies. As the tank room and reservoir are two widely different experimental environments, it was decided to build into the pulse generator circuit the ability to vary the pulse length, and the final system allows the generation of pulses up to a maximum of 255 cycles long (which is equivalent to 6.375 ms at 40 kHz).

4.3 GENERAL DESCRIPTION OF THE SYSTEM:

The overall layout of the system is shown in figure 4.3. It consists of two parts: data acquisition and data processing.

The data acquisition part makes use of ten elements out of a fifteen element array with each element connected to an individual A/D receiver board. These boards extract the In-phase and Quadrature components (I & Q) of the signal picked up by each element, and convert them to 12 bit digital forms. The SINE and COSINE reference signals, and all the control signals required for data conversion and multiplexing, are generated by the "Reference and Signal Generator Board" (section 4.4.4) under the control of a BBC microcomputer. The output data from each board is conveyed over a 12 bit bus to a memory buffer. The size of the memory that is available limits the range of the system. This memory is shared between the data acquisition part and the data processing part.

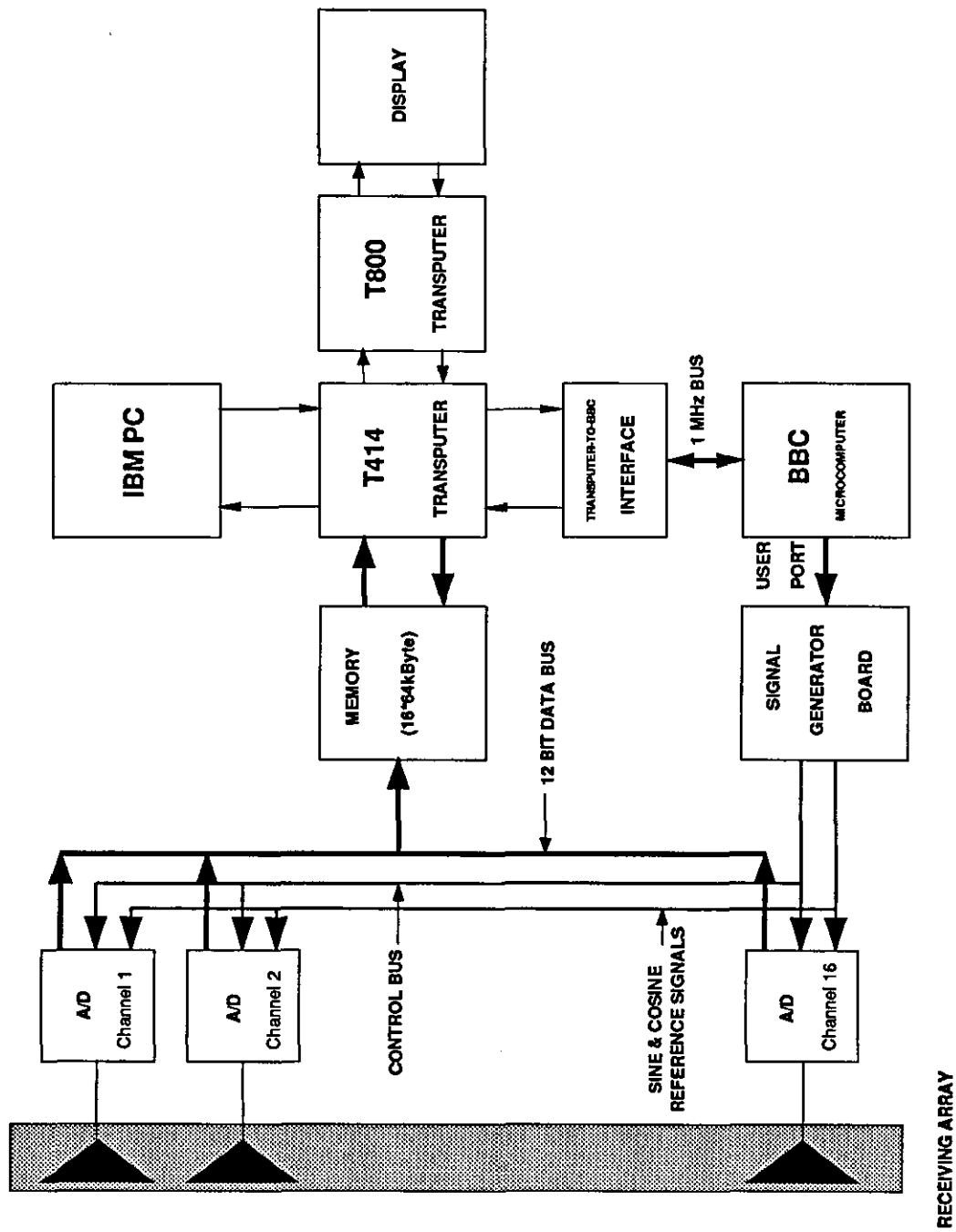

Figure 4.3: The Layout of The High Resolution Sonar DF System.

The data processing part can either be a single transputer or a network of transputers. In the data acquisition phase, the A/D boards access the shared memory to store the collected data samples. After acquiring a certain number of samples, the BBC indicates to the transputer that a data set is ready and waiting to be moved from the buffer memory to the transputer for processing. The transputer then gains access to the memory and starts moving the collected data to another part of its RAM memory in order to free the shared memory as quickly as possible for the data acquisition part to collect a new data set. When the transputer finishes reading the data it sends an 'End of Reading' signal to the BBC to transmit a new pulse and start a new cycle.

After firing a certain number of pulses (snapshots), the master transputer (T414) starts calculating the covariance matrix and passes the results to the slave T800 transputer for further processing. When the T800 finishes the calculation, it sends the resulting angular spectrum to a display system (e.g., frame-store). The system can easily be expanded by adding more transputers and/or digital signal processors.

In the system Mark II, the control of the whole system was by the master transputer using a link adapter and the BBC microcomputer was retained only to display the angular spectrums.

The concept of using shared or switchable transputer memory was also exploited in another sonar project at LUT - Sonar Research Group. This project is concerned with generating different types of sonar signals [ref. 65 and 66]. In this case the process is reversed; the transputer calculates the individual values of a set of waveforms and stores them in 16 switchable RAM memories (one for each channel). The transputer then isolates itself from these memories using tristate buffers. An external address generator circuit gains access and control over the shared RAMs and starts clocking the data out from these memories to their respective D/A converter, low pass filter, power amplifier and finally to the staves of transducer array.

4.4 DETAILED DESCRIPTION OF THE SYSTEM HARDWARE:

Figure 4.4 shows a photograph of the High Resolution Sonar System. The system consists of a PC, a BBC microcomputer, a 6U rack (which hosts the main system boards) and the 16-channel preamplifiers box. The 6U rack contains the following boards:

a. The T414 Master Transputer Board.
b. The T800 Transputer Board.
c. The Receiver A/D Boards.
d. The Signal and References Generator Board.
e. The Memory Board.
f. The Transputer-BBC Interface Board.

Figure 4.4: The High Resolution Sonar DF System.

These boards are plugged into the rack with its self contained dc power supply. To reduce noise pick up, the rack is enclosed in a metal case. At the back of this case there is a 34 way female connector to connect the receiving array to the system (through the 16-channel preamplifiers box if needed). At the front, the following connectors are used to connect the different parts of the system:

a. The PC-Transputer connector: this is a 4-way INMOS connector which connects the Transputer Interface Board hosted by the PC to the master transputer board.

b. The USER PORT connector: this is a 20-way connector that carries 8 data lines, 2 control signals and GND. It is used to connect the BBC USER PORT to the Signal and References Generator Board.

c. The 1MHz bus connector: this is 34 way connector which connects the BBC 1MHz bus to the Transputer-BBC Interface Board.

d. The transputer memory connector: this connector is used to connect the master transputer data, address and memory select lines to the shared memory placed on the memory board.

e. A miniature BNC connector: which provides the transmitted pulse signal from the Signal and References Generator Board.

f. An INMOS serial connector: this is a 4-line connector which connects LINK 2 of the Master Transputer Board to the Transputer-BBC Interface Board.

In the following, a detailed description of the system hardware is presented. The 16-channel preamplifiers box is discussed first, followed by a description of each of the boards in the system.

4.4.1 The 16-Channel Preamplifiers:

The preamplifiers are used to amplify the signals received by the array sensors. One preamplifier is needed for each sensor. Since the output of the preamplifier is to be converted to 12 bit digital signal, a dynamic range of minimum 72 dB is required. After considering many preamplifier chips, it was decided to use the Raytheon RC/RM4227 precision monolithic dual operational amplifier.

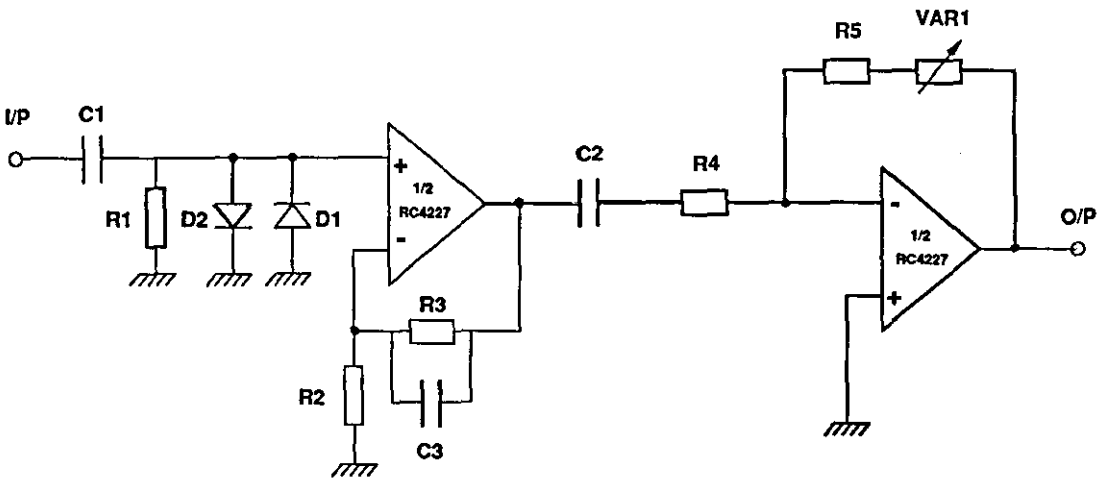

Figure 4.5: Circuit Diagram of The Preamplifier.

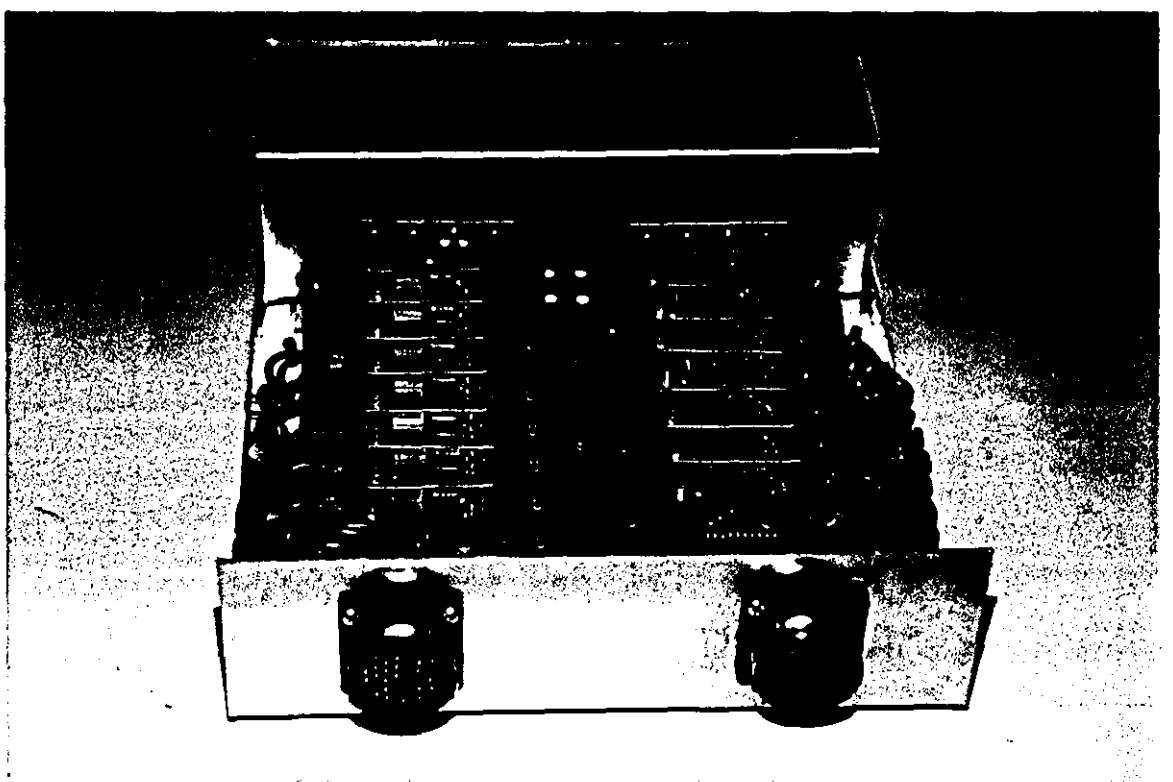

Figure 4.6: The 16-Channel Preamplifiers.

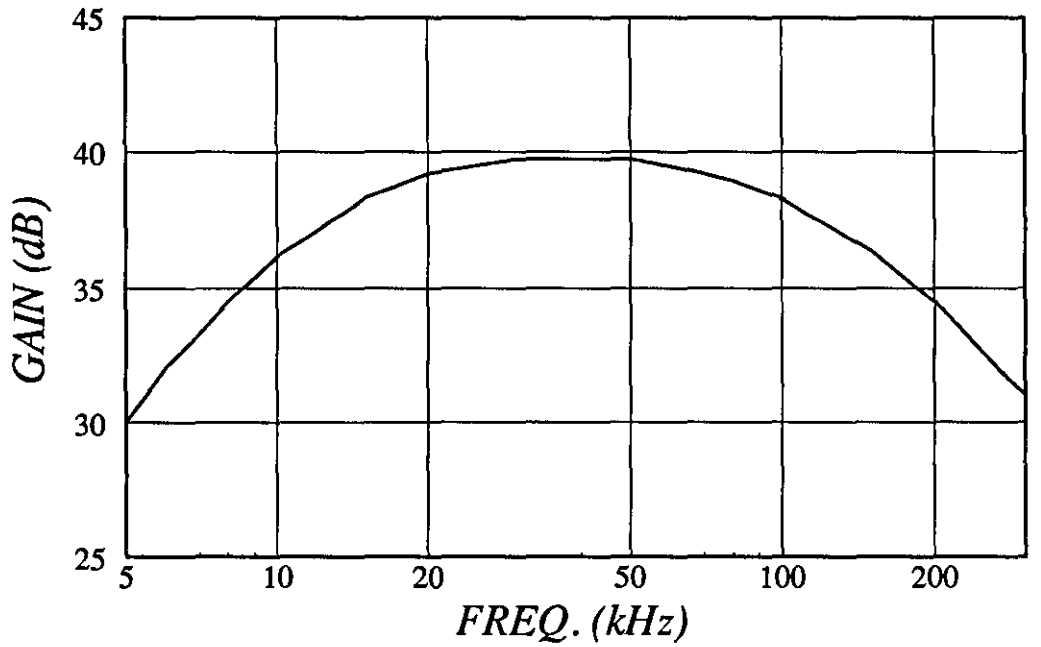

Figure 4.7: Frequency Response of The Preamplifier.

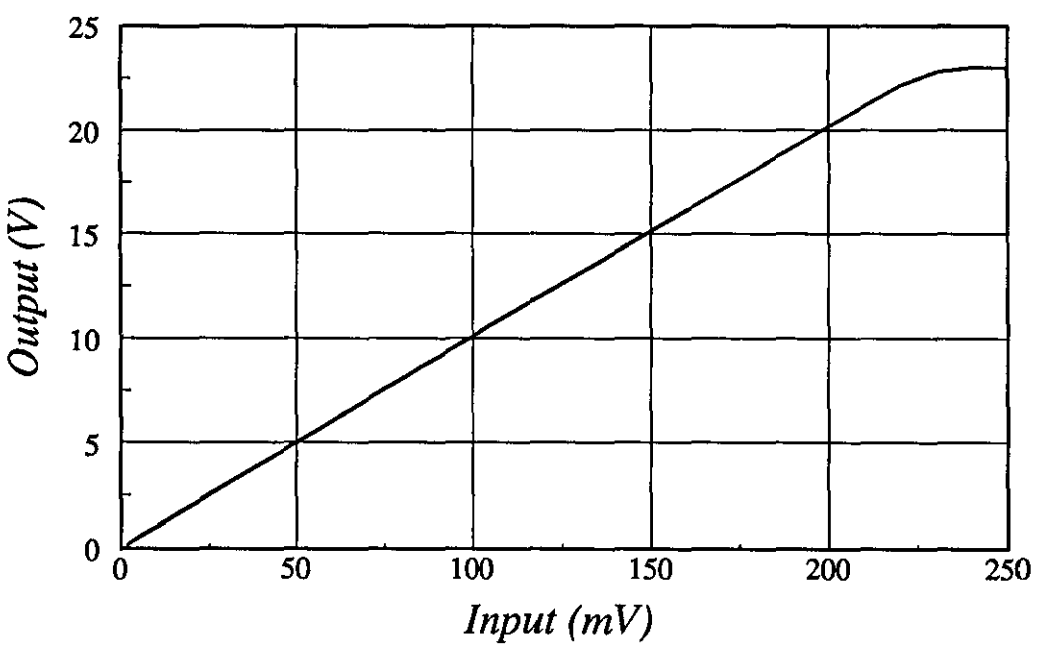

Figure 4.8: Input-Output Relation of The Preamplifier.

The circuit diagram of the preamplifier is shown in figure 4.5. It contains two stages. The first is a non-inverting amplifier with a fixed gain of 20 dB and the second is an inverting amplifier with a variable gain of 13-23 dB, i.e., the total gain of the preamplifier is in the range of 33-43 dB.

The input impedance of the amplifier is determined by R_1 (56k). The two diodes D_1 and D_2 are used to protect the amplifier from high input voltages.

The frequency response of the amplifier is mainly controlled by three RC networks. R_1C_1 and R_4C_2 controls the low cutoff frequency which was chosen to be 10kHz. The other RC network, R_3C_3, controls the high frequency cutoff. This was selected to be 120kHz.

A printed circuit board for the above amplifier was carefully designed for low noise. Sixteen of these boards were built and mounted on a mother board by special connectors and enclosed in a metal box. The box also contained a screened dc supply powered from the mains. The dc output from this power supply was double regulated before being applied to the mother board; the first set of regulators were ∓15V and the other set of regulators were ∓ 12V. This double regulation was desirable to ensure stable and low noise supply voltages. The dc rails were also decoupled by two capacitors at each preamplifier board to reduce any RF pick-up.

The box was fitted with two 35 way multipole connectors; a female for the input and a male for the output. Figure 4.6 shows a photograph of this box.

Figure 4.7 shows the frequency response of the preamplifier and figure 4.8 shows a plot of the input-output relation. The dynamic range of the preamplifier was found to be about 80dB and the noise performance was satisfactory.

4.4.2 The Master Transputer Board:

The master transputer board is responsible for pre-processing the raw data collected by the data capture part of the system and passing the intermediate results to the other transputer (or transputer network) for further processing. It is also responsible for sending the final processed results to the BBC

microcomputer for display. The pre-processing of the raw data includes forming an (N X P) complex data matrix (where N is the number of elements and P is the number of snapshots). It also includes calculating the covariance matrix and passing it to the other transputer (or transputers) for further processing.

The master transputer controls the data capture process indirectly through the BBC microcomputer. The BBC and the master transputer board communicate through the Transputer-BBC Interface Board (see section 4.6).

In the initial tests of the system only one transputer board was used and this did all the processing. Later on, another T800 transputer board was added to the system to handle the heavy floating point arithmetic (e.g., calculation of matrix inverse, eigenvalues and eigenvectors and the angular spectrum). No major changes were needed to the software to accommodate the additional T800 transputer because of the structure of OCCAM programs as discussed in chapter 3.

Since most conventional applications of transputers use the serial links to communicate with the outside world, it was very difficult to find a commercial transputer board that allows access to the transputer data and address busses in the way needed by our design. However, we found one transputer board which was custom designed for the UNISON project [ref. 67] at Loughborough University which assigns 64K X 32 bit of its memory to optional PROMs memory and the sockets for these PROMs do carry the necessary data and address lines. Therefore it was decided to use this board and assign the buffer memory, which is shared between the data capture system and the transputer, to the same memory slot that had been assigned to the PROMs in the memory map of the UNISON transputer board. This memory was physically placed on another board called the 'Memory Board' (section 4.4.5), so we used a ribbon cable to convey the necessary signals from the transputer board to the memory board. This ribbon cable has special connectors that can be plugged into the PROMs i.c. sockets at the transputer end and another edge connector at the memory board end (figure 4.9). Besides the necessary data and address lines, the ribbon cable carries the 'ROM SELECT' signal which is an address coded signal that

enables this part of the memory when it is addressed. The address of this memory starts at $380000 and the OCCAM command 'PLACE' was used in the software to tell the transputer where to look for the collected data, i.e.,

PLACE x AT $380000:

where x was defined early in the program as an INT32 variable of size 64K.

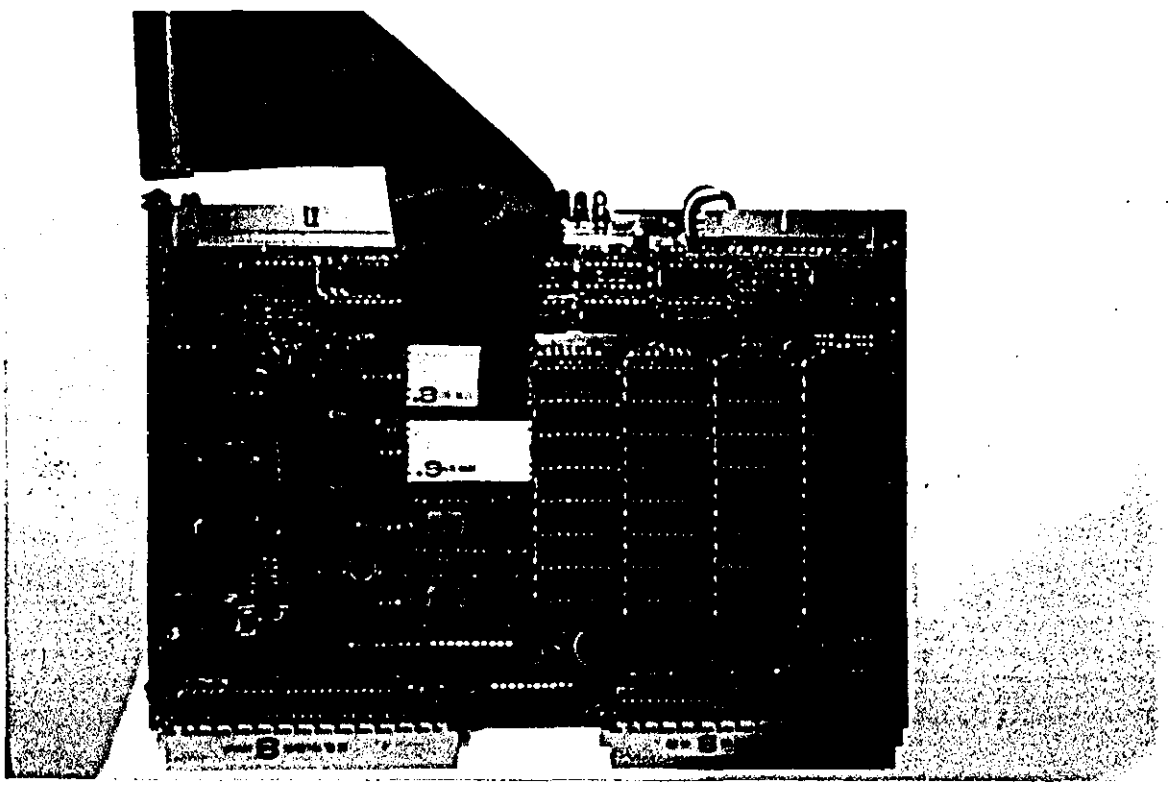

Figure 4.9: The UNISON Transputer Board.

The UNISON Transputer Board is a four-layer pcb board and contains a T414 transputer chip which can be replaced by a T800 without requiring any hardware changes. It also contains 1 MByte of RAM that can be upgraded to 4 MByte. The board has an edge connector at the front of the board which carries the four transputer communication links, 'RESET', 'ERROR' and the 'DOWN LOAD' signals. LINK 1 of the master transputer was used to communicate with the PC and LINK 2 was used to communicate with the BBC. LINK 3 and LINK 4 were available to directly connect the master transputer to other transputers.

The master transputer board is connected to a PC through a link adapter interface board hosted by a PC. This allows the user to develop OCCAM-2 programs on the PC, then down load and run them on the transputer board.

The T800 Transputer Board is similar to the master board except that it uses the T800 floating point transputer.

4.4.3 The Analogue-to-Digital Converter Boards:

The main function of these boards is to convert the analogue signals from the array sensors to digital form. Figure 4.10 shows the block diagram of this board. The I & Q sampling technique discussed in section 4.2.2 was used in which the incoming signal is translated into two baseband channels using Quadrature carriers in the frequency changers and the channels are separately sampled. Each A/D channel included the following main circuits:

a. An on-board preamplifier.
b. Two analogue multipliers to extract the In-phase and the Quadrature components of the incoming signal.
c. Two 4th order low pass filters, one for the I channel and the other for the Q channel, to filter out the high frequency products of the multipliers.
d. Two Sample-and-Hold circuits (one for the I channel and the other for the Q channel).
e. A multiplexer which multiplexes the output of the I & Q channels and feeds them to the A/D convertor.

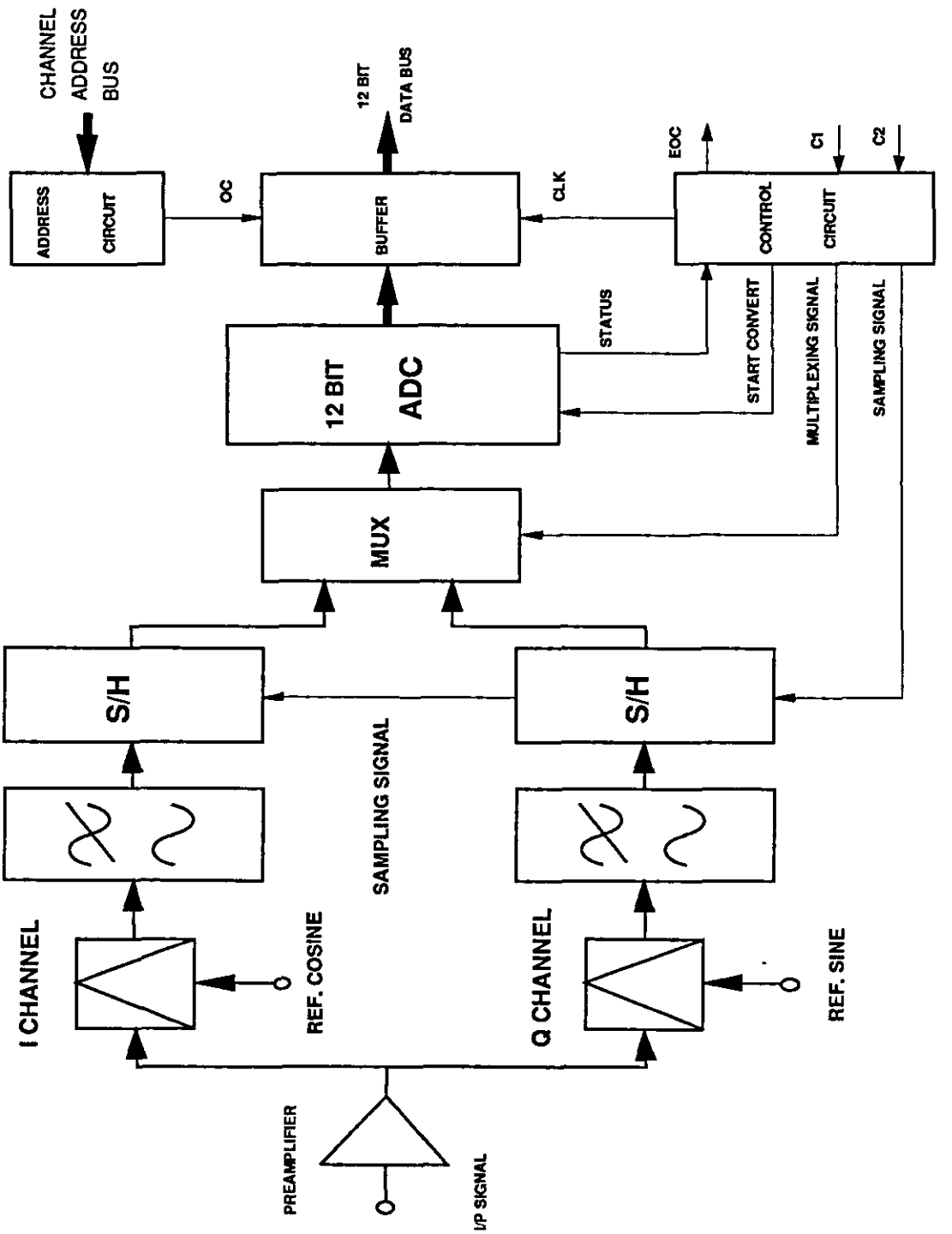

Figure 4.10: Block Diagram of The A/D Board.

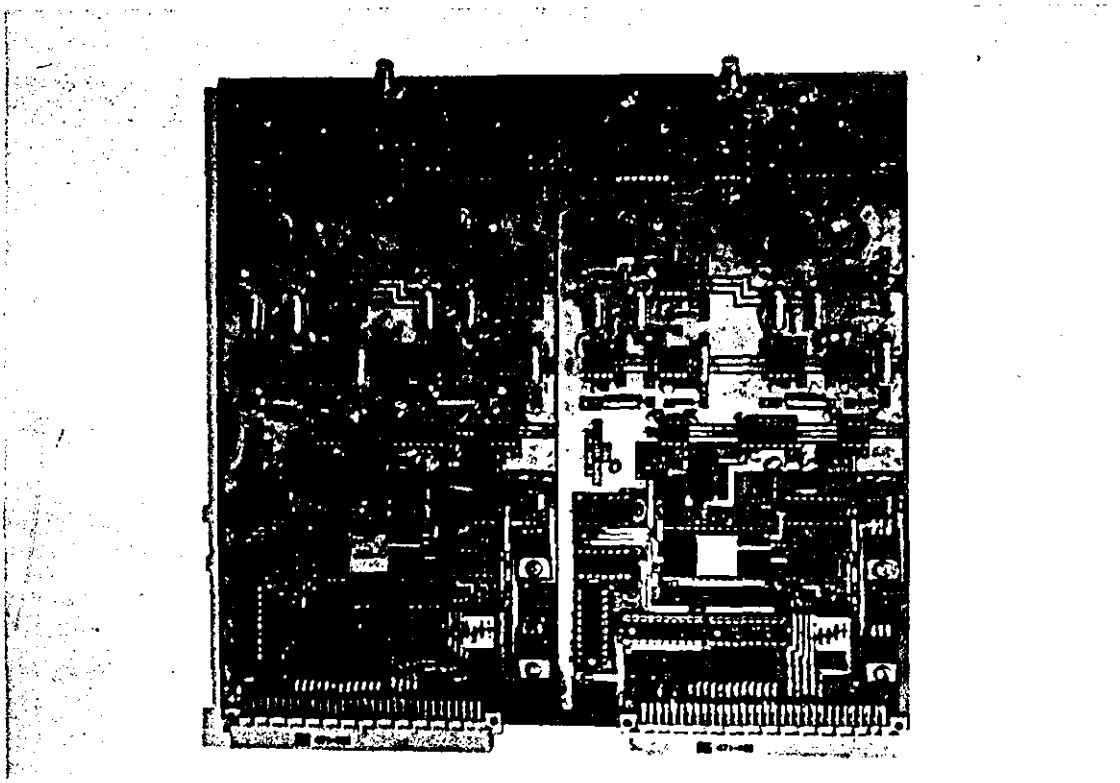

Figure 4.11: The A/D Board.

f. A 12-bit A/D converter.
g. Tri-state buffers.
h. Addressing circuit.
i. +15V and -15V voltage regulators.

A carefully designed printed circuit board with ground plane was made to include two individual channels on one board. These boards were plugged into the same 6U rack that contains the transputer boards. Figure 4.11 shows a photograph of this board.

In the following a detailed description of this board is presented.

4.4.3.1 The On-Board Premplifier:

This is the first stage on the A/D board. Its function is to raise the signal level before its I & Q components are extracted. The OP-37 high speed, low noise operational amplifier was used in an inverting mode with a gain of 27 dB. Figure 4.12 shows the circuit diagram of this amplifier.

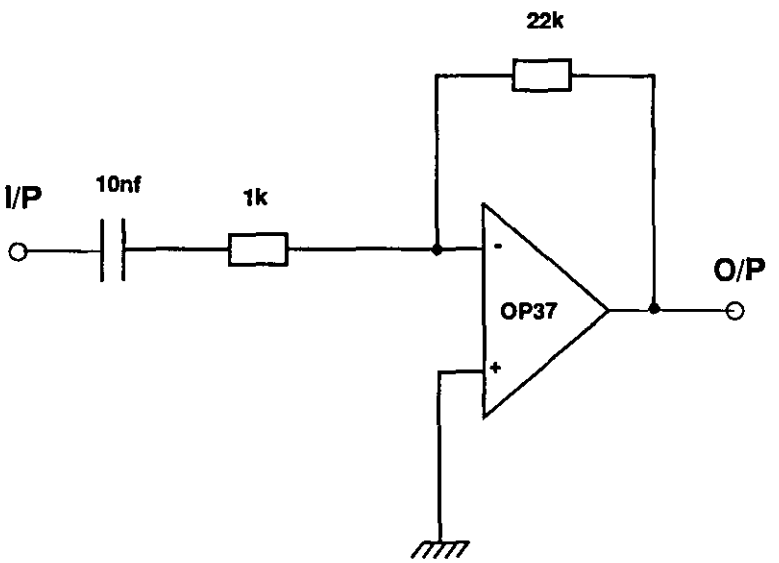

Figure 4.12: Circuit Diagram of The On-board Preamplifier.

4.4.3.2 The Analogue Multiplier:

The output signal from the on-board preamplifier is multiplied by the SINE and COSINE reference signals to extract the In-phase and Quadrature components (I & Q) of the received signal. The sine and cosine reference signals are generated by the "Signal and References Generator Board" (section 4.4.4). Two RS1495 four quadrant multipliers were used [ref. 68]. Figure 4.13 shows the circuit diagram of these multipliers. The multiplier has offset adjustments for both input and output to remove any offset error. The multiplier output was buffered by a low noise high speed operational amplifier (OP-37).

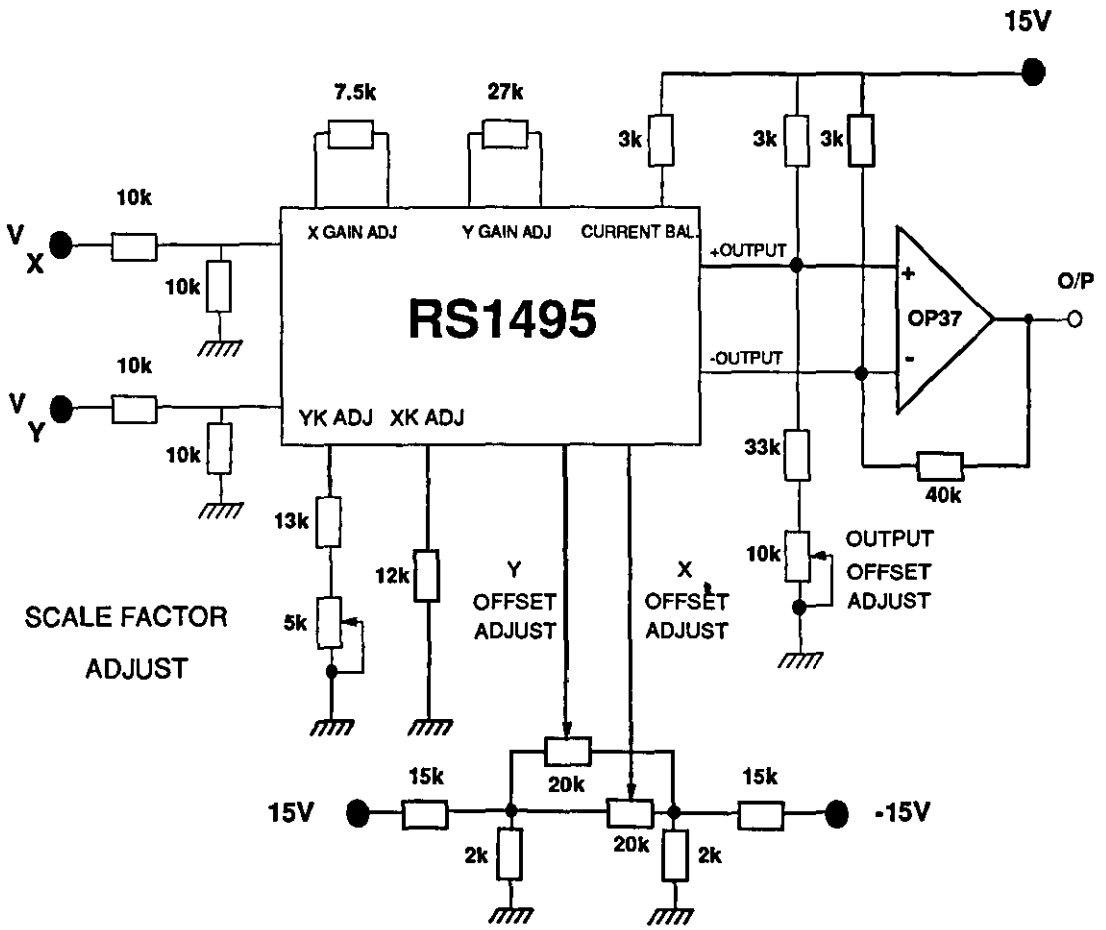

Figure 4.13: Circuit Diagram of The Analogue Multiplier.

4.4.3.3 The Low Pass Filter:

The low pass filter is used to remove the high frequency products of the multiplication. A 4th order Butterworth active filter was chosen which gives -24dB/octave attenuation. The filter was designed for a cut-off frequency of 5 kHz which can easily be changed if necessary.

The design procedure for low pass active filters is presented in ref.(69). Using this procedure, the values of the external components were calculated for the above cut-off frequency.

Figure 4.14 shows the complete circuit diagram of the fourth order Butterworth low pass filter and figure 4.15 shows its frequency response.

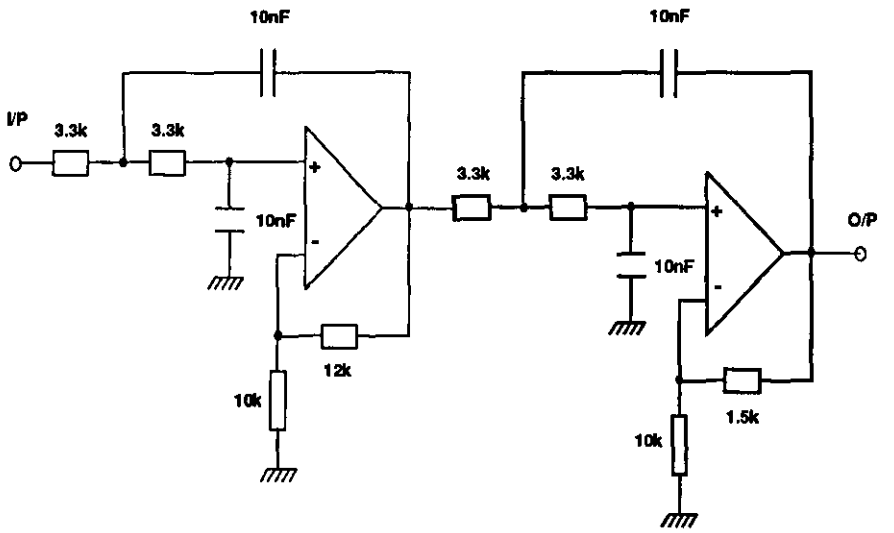

Figure 4.14: Circuit Diagram of The Low Pass Filter.

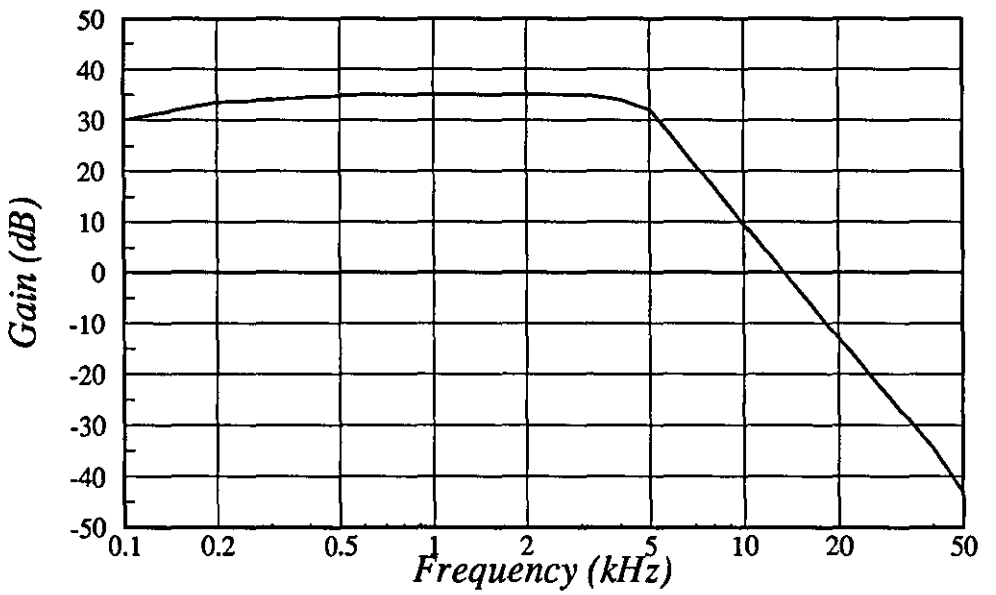

Figure 4.15: Frequency Response of The Low Pass Filter.

4.4.3.4 The Sample and Hold (S&H) Amplifiers:

The A/D convertor requires that the input amplitude be held constant during the conversion cycle. Therefore it was necessary to use a Sample and Hold device to hold the present value of the signal just before the beginning of the conversion and keep it constant until the conversion is finished. Two LF398 S&H devices were used to sample and hold the I and Q signal components simultaneously. The Sample and Hold control signal ($S/\overline{H}$) was generated from the master control signal C2 and the End of Conversion signal (EOC) of the D/A convertor using a D-type positive edge triggered flip flop (see figure 4.16).

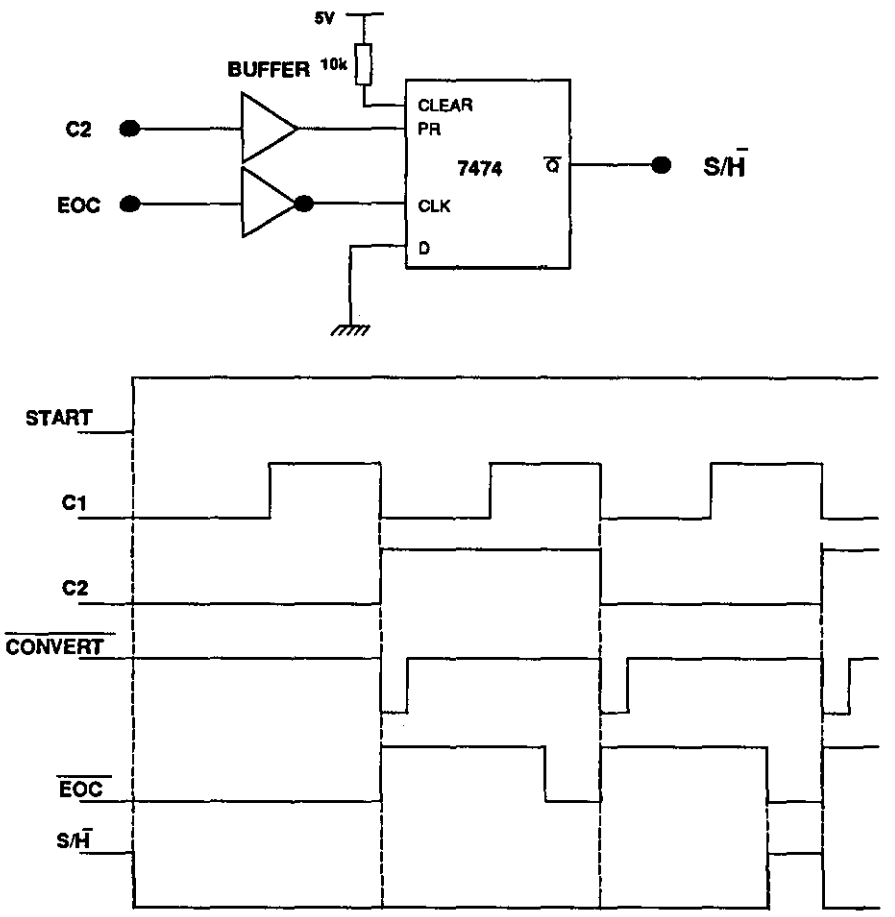

Figure 4.16: Control and Timing Signals.

4.4.3.5 The Analogue Multiplexer:

An analogue switch was used to multiplex the output of the two S&H devices, which hold the I and Q values of the input signal, to the 12 bit A/D convertor. The multiplexing signal is generated from the master control signal C2 (see figure 4.16).

4.4.3.6 The Analogue-to-Digital Convertor:

There are many factors to be considered when selecting the type of A/D convertor to be used. The main factors are the resolution, speed and cost.

After considering these factors, it was decided to use the AD574 12 bit 25 microsecond A/D convertor. Since the conversion time of this device is less than half the minimum sampling period, only one chip is needed to convert both the I&Q signals using the analogue multiplexer mentioned above.

Figure 4.17 shows the circuit diagram of the A/D convertor [ref. 70]. The A/D convertor is configured for a 12 bit data bus by wiring the DATA MODE SELECT (pin 2) high and A0 (pin 4) low. The input analogue signal level is selected to be $\mp$ 10 volts by applying the analogue signal to pin 14. The digital output of the A/D convertor is interfaced to the 12 bit data bus via two 8 bit tristate latches. The conversion is initiated when the $READ/\overline{CONVERT}$ signal, generated from a monostable triggered by C1, goes low. Once the conversion is initiated, the STATUS signal (pin28) goes high and it remains high as long as the conversion is taking place. When the conversion is finished, The STATUS signal goes low and the converted data becomes valid on the output data pins. The falling edge of the STATUS signal is used to latch this data to the tristate buffers and to generate the 'End of Conversion' (EOC) signal. The data stays in these buffers until the memory board reads it.

4.4.3.7 The Addressing Circuitry:

After each analogue to digital data conversion is completed, the memory board starts reading the converted data from each A/D board sequentially. Since this

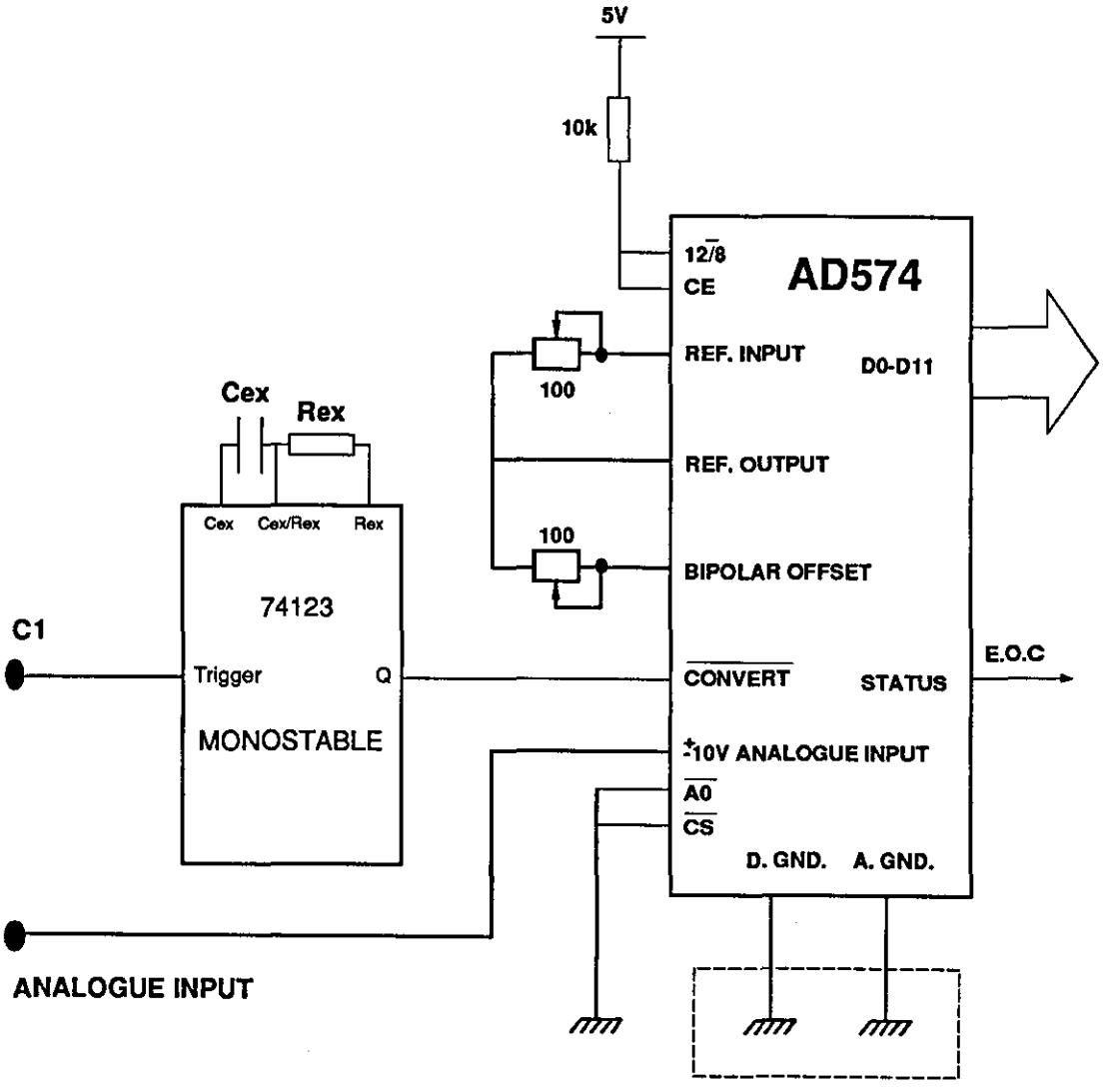

Figure 4.17: Circuit Diagram of The ADC.

data is conveyed over a common 12 bit data bus to the memory board, it was necessary to put an addressing circuit on each A/D board to enable the memory board reading data from one selected A/D board at a time.

The addresses for the A/D boards are generated by a 4-bit binary counter on the memory board and initiated by the EOC signal. The four bit output from the this counter is sent to all A/D receiver boards over the address bus.

On each of the A/D boards, there is an addressing circuit which is basically four dip-switches and a 4-bit binary comparator. The address of each board is set with the 4 dip-switches. The 4-bit binary comparator is used to compare the board address and the instantaneous address on the address bus. When the two addresses are matched, a strobe signal is generated to latch the 12 bit data from the tristate buffers to the data bus and then to the memory board.

4.4.4 The Signal and References Generator Board:

The main function of this board is to generate the transmitted pulse and the SINE and COSINE reference signals. It also generates the C1 and C2 control signals. Figure 4.18 shows the block diagram of this board.

The discrete digital samples of one cycle of each of the transmitted pulse signal, the SINE and the COSINE reference signals are stored in three individual PROMs respectively. Each cycle is represented by 32 samples 8 bit wide. The digital data output of each PROM is connected to an 8 bit digital to analogue convertor D/A and the analogue current output of each of the D/A's is converted to voltage using the OP-37 operational amplifier to give an output of $\mp$ 10 volts. To ensure that the analogue outputs of the D/A convertors stay at 0V level when their respective PROMs are not selected (tristate), the MSB of the 8 bit data input to the D/A was pulled up while the remaining 7 LSB were pulled down.

The addresses for all three PROMs are generated by 5-bit binary counter driven from a master voltage controlled oscillator (VCO). The frequency of this oscillator determines the frequency of the output analogue signals. The MSB of the memory address counter is cascaded to another eight bit binary counter, driven by the same master clock, to count the number of cycles in the transmitted pulse.

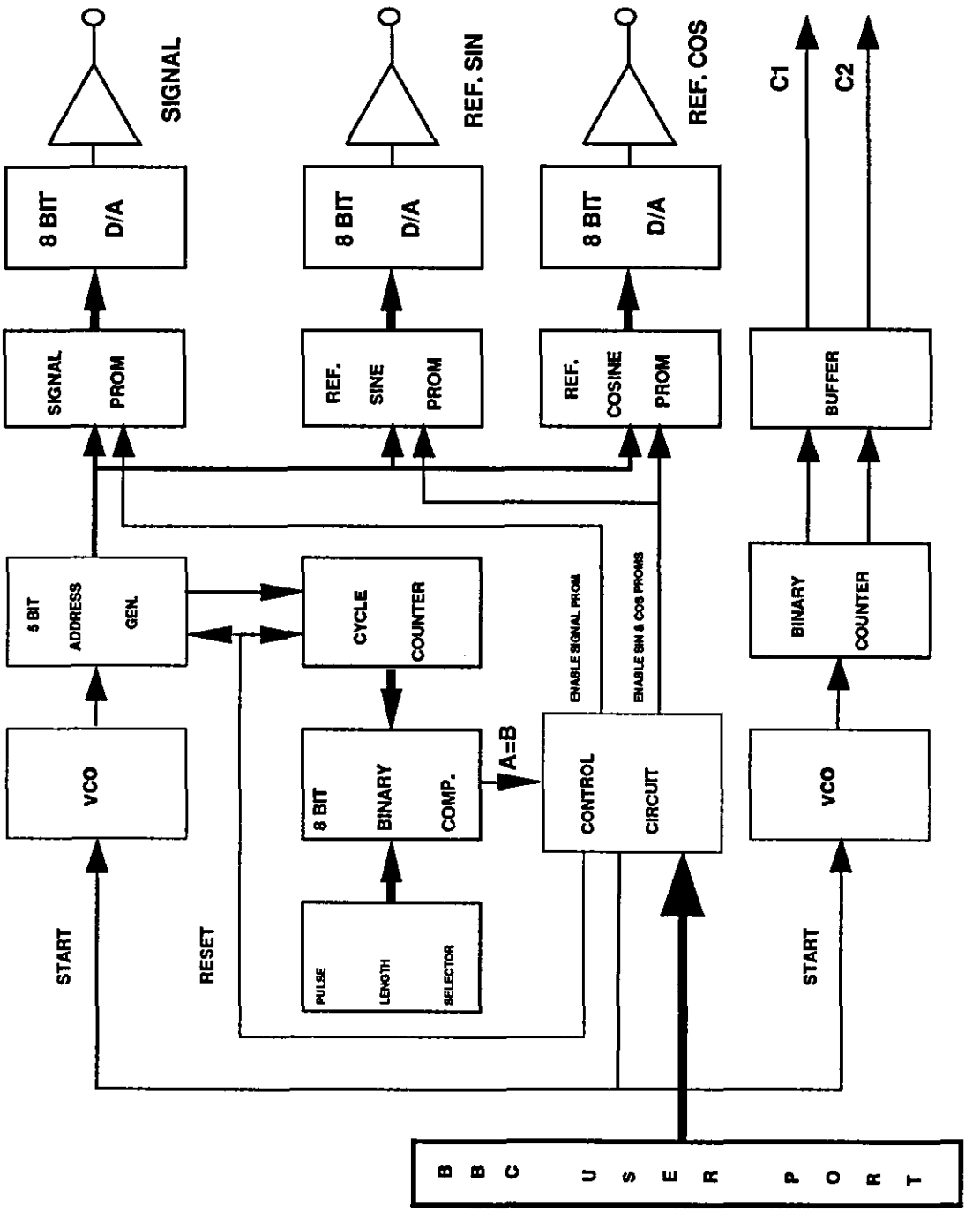

Figure 4.18: Block Diagram of The Signal and References Generator Board.

The output of this cycle counter is connected to an eight bit binary comparator which compares the number of counted cycles with the preset value selected by 8 dip-switches.

At the beginning of the data capture phase, the BBC microcomputer sends a START signal from the user port to this board. This signal initiates the clock generator after resetting all the counters. It is also used to enable the Transmitted Pulse PROM and disables the reference SINE and COSINE PROMS. As a result, the digital samples of the transmitted pulse start reading out of the PROM to the D/A convertor and then to the outside world.

When the number of the generated cycles of the transmitted pulse equates the required number of cycles preselected by the dip-switches, the 8-bit comparator disables the Transmitted Pulse PROM and enables the SINE and COSINE PROMs. This leads to the generation of the SINE and COSINE reference signals immediately after the end of the transmitted pulse and this continues till the end of the data capture phase.

As mentioned earlier, this board also generates the two main control signals C1 and C2. The generation of these signals is also initiated by the START signal and their frequencies are controlled by a separate VCO.

4.4.5 The Memory Board:

This board is used to store the digital values of the I & Q components of the received echoes before being processed by the transputer. Each echo sample consists of a 12 bit I component and a 12 bit Q component. The memory size required for 10 channels and a maximum sampling frequency of 20kHz is 400 X 12 bits per one millisecond (which corresponds to 1.5m in range). If a maximum range of 90m is assumed, then the memory size required is:

$$\text{Min. } Memory \quad Size = [400 \times 12] \times \frac{90}{1.5}$$

$$= 24K \times 12Bits$$

The memory size used in the system was 64K X 16 bit.

As mentioned earlier, this memory is shared between the data capture part of the system and the master transputer board where it occupies the slot assigned originally to the PROM memories. The size of this slot is 64K X 32 bit. In the data capture phase, this memory is isolated from the transputer address and data busses by tristate buffers. The End-of-Conversion (EOC) signals from the A/D convertor boards are used to initiate two address counters; one, which is 4 bit, to generate the channel addresses and the other, which is 16 bit, to generate the memory addresses. The channel address generator resets itself with every EOC while the memory address carries on counting until the memory is full (address FFFF). This is detected by a simple logic circuit and generates the MEMORY FULL control signal which isolates the memory from the data capture unit and connects it to the transputer data and address busses. It is also used to signal to the transputer that the data is ready for processing. The transputer will then start reading the data and copying it to another part of its memory in order to free the shared memory for a new data set.

Figure 4.19 shows the block diagram of the memory board. It contains one 64Kx16 bit CMOS high speed static RAM (HMS41664) [ref. 71]. In the WRITE mode, the local 16 bit address generator generates the memory addresses while the data is read from the selected A/D convertor channel through edge connectors at the back of the board. The clock pulse that drives the address counter is also used as the memory WRITE STROBE signal (after introducing an appropriate delay). The NOT CHIP ENABLE and the OUTPUT ENABLE pins are both connected to GND.

The channel address generator on the board generates the 10 different channel addresses and sends them across a 4-bit address bus to all the A/D convertor boards. When this address matches the address of the respective channel, the 12 bit digital data is transferred from the tristate buffers of that channel to the data bus and then to the memory board.

In the READ mode, the address and data busses of the transputer are connected to their respective pins by enabling tristate buffers using the ROM select signal from the transputer. The R/notW pin of the memory chip is held high during the read cycle.

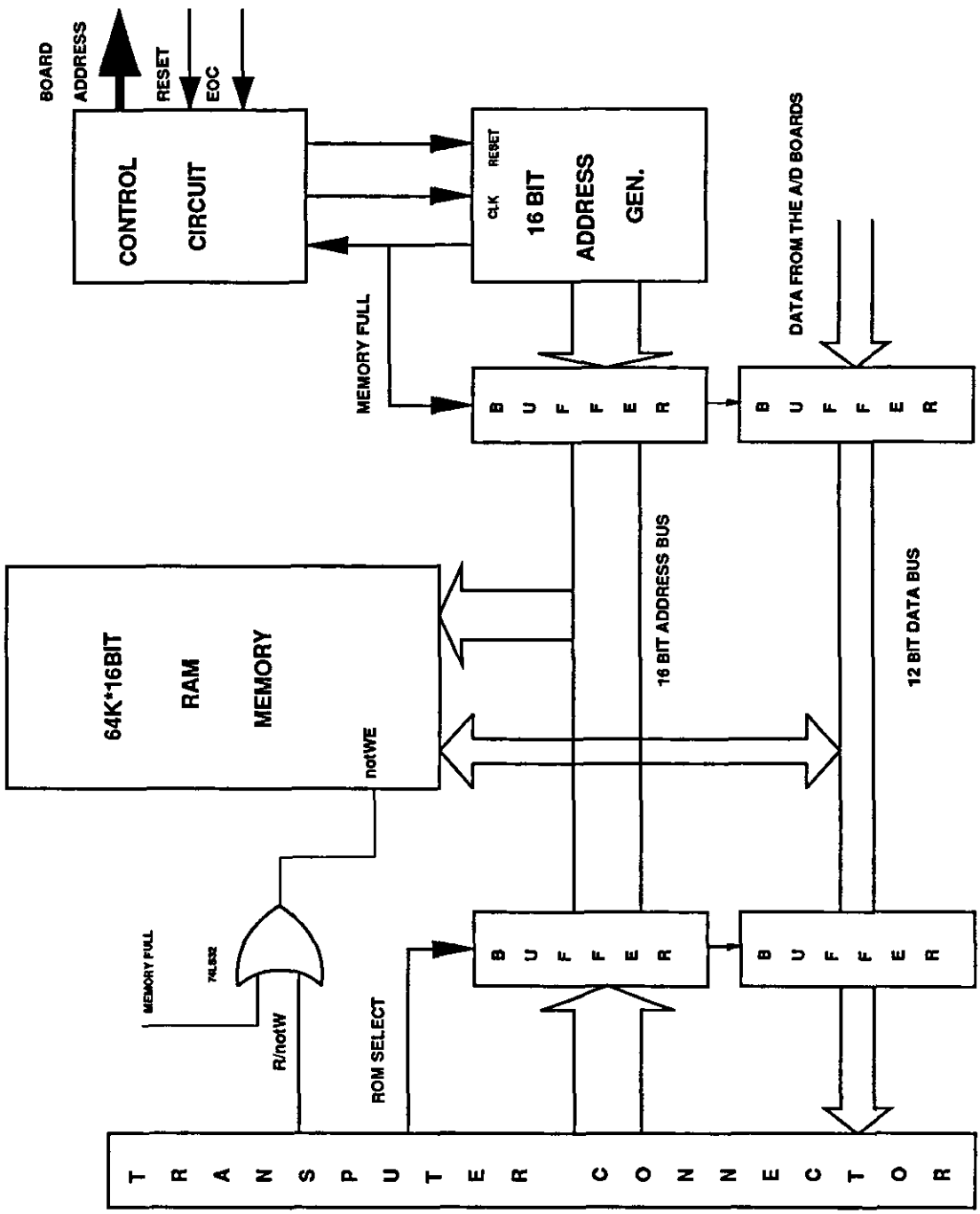

Figure 4.19: Circuit Diagram of The Memory Board.

4.4.6 TRANSPUTER-BBC Interface:

This interface, which uses the CO11 link adapter, allows data communications between the 1 MHz bus on the BBC side and the serial INMOS link on the transputer side. Its purpose in the High Resolution Sonar System is to convey control signals between the master processor, the T414 transputer, and the slave BBC front end microcomputer. It is also used to transfer the angular spectrum results from the transputer to the BBC for display.

4.4.6.1 The 1MHz Bus:

There are basically two routes to communicate with the BBC. One of these is the 6522 USER port. The problem with the USER port is that there are only 8 I/O lines with few control signals. For more complex peripherals, direct access to the 6502 address and data buses are required. This interface is provided by the 1MHz bus [ref 71].

Physically, the 1MHz bus interface is a 34 pin connector mounted at the front edge of the main BBC microcomputer circuit board. A buffered data bus and the lower 8 bits of the address bus are connected to this connector together with a series of useful control signals.

The standard use of the 1MHz bus allows up to 64K bytes of paged memory to be addressed as well as 255 direct memory mapped devices (plus the paging register). To add on hardware interface to the 1MHZ bus, the 'Not page &FC' (NPGFC) signal together with the lower 8 address lines are decoded to select the add on circuit.

Figure 4.20 shows the 1MHz bus connector. The detailed specification for the signals on this connector can be found in ref. 72. However, for convenience a brief review of the signals that are used by the Transputer-BBC interface is presented below:

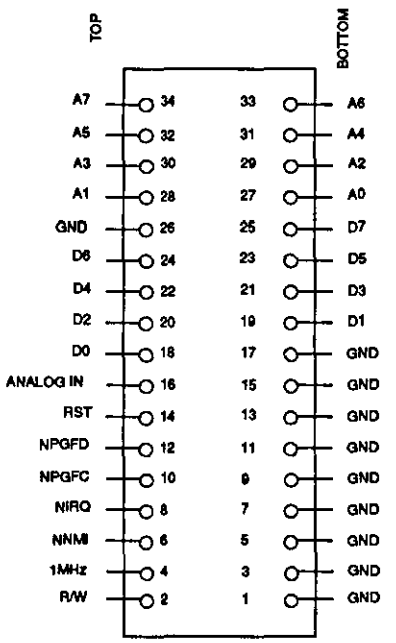

Figure 4.20: The 1MHz Bus.

R/NOT W	This is the READ-NOT-WRITE signal from the 6502 CPU.
1MHz	This is the 1MHz system timing clock.
NPGFC (NOT PAGE FC)	This signal is derived from the 6502 address bus. It goes low whenever page &FC is written to or read from.
D0-D7	This is a bidirectional 8 bit data bus which is connected via a 74LS245 buffer to the CPU. The direction of the data transfer is controlled by the R/NOT W signal.
A0-A7	These are connected directly to the lower 8 bit CPU address lines via a 74LS244 buffer which is always enabled.

All the 1MHz peripherals are clocked by a 1 MHz, 50% duty cycle clock to allow chips like 6522 VIAs to use their internal timing elements correctly. The system 6502 CPU is usually operates at 2 MHz. So if the CPU wishes to access any device on the 1MHz bus it needs to be slowed down. Unfortunately this slowing

down process creates glitches which may cause spurious pulses to occur on the various chip select pins leading to possible malfunction of some devices. To remove these glitches, a standard clean-up circuit shown in figure 4.21 is used. The operation of this circuit is described in details in ref. 72.

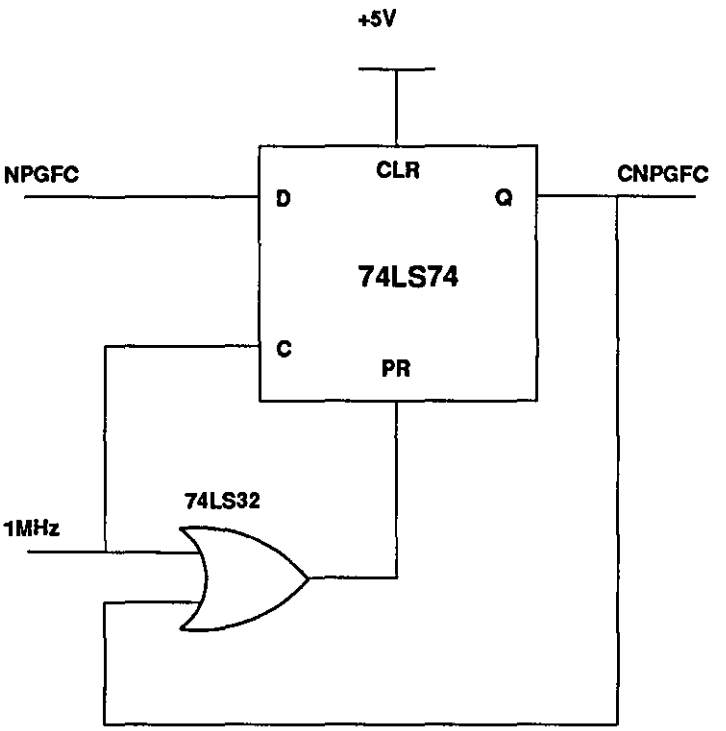

Figure 4.21: The Clean-Up Circuit.

4.4.6.2 The INMOS Serial Link:

The transputer uses a DMA block transfer mechanism to transfer messages between memory and other transputer products via the INMOS serial links. The link interfaces and the processor all operate concurrentlly, allowing processing to continue while data is being transferred on all of the links. These point to point communication links simplify system design and allow transputer networks of arbitrary size and topology to be constructed [ref. 51].

To provide synchronised communication, each message must be acknowledged. Consequently, a link requires at least one signal wire in each direction. Each message is transmitted as a sequence of single byte communications, requiring only the presence of a single byte buffer in the receiving transputer to ensure that no information is lost. Each byte is transmitted as a start bit followed by a one bit followed by the eight data bits followed by a stop bit. After transmitting a data byte, the sender waits until an acknowledgment is received; this consists of a start bit followed by a zero bit. The acknowledge signal signifies both that a process was able to receive the acknowledge byte, and that the receiving link is able to receive another byte. The sending link reschedules the sending process only after the acknowledgment for the final byte of the message has been received.

Data bytes and acknowledge signals are multiplexed down each signal line. An acknowledge signal can be transmitted as soon as reception of a data byte starts (if there is room to buffer another one). Consequently transmission may be continuous, with no delays between data bytes.

In general, there are three methods of communication between the transputer and peripherals as shown in figure 4.22. The first method employs a peripheral control transputer (e.g for graphics or discs), in which the transputer chip connects directly to the peripheral concerned. The interface to the peripheral is implemented by special purpose hardware within the transputer. The application software in the transputer is implemented as an OCCAM process, and controls the interface via OCCAM channels linking the processor to the special purpose hardware.

The second method is by employing link adapters. These devices convert between a link and a specialized interface. The link adapter is connected to the link of an appropriate transputer, which contains the application designer's peripheral device handler implemented as an OCCAM process.

The third method is by memory mapping the peripheral onto the memory bus of the transputer. The peripheral is controlled by memory accesses as a result of PORT inputs and outputs. The application designer's peripheral device handler provides a standard OCCAM channel interface to the rest of application.

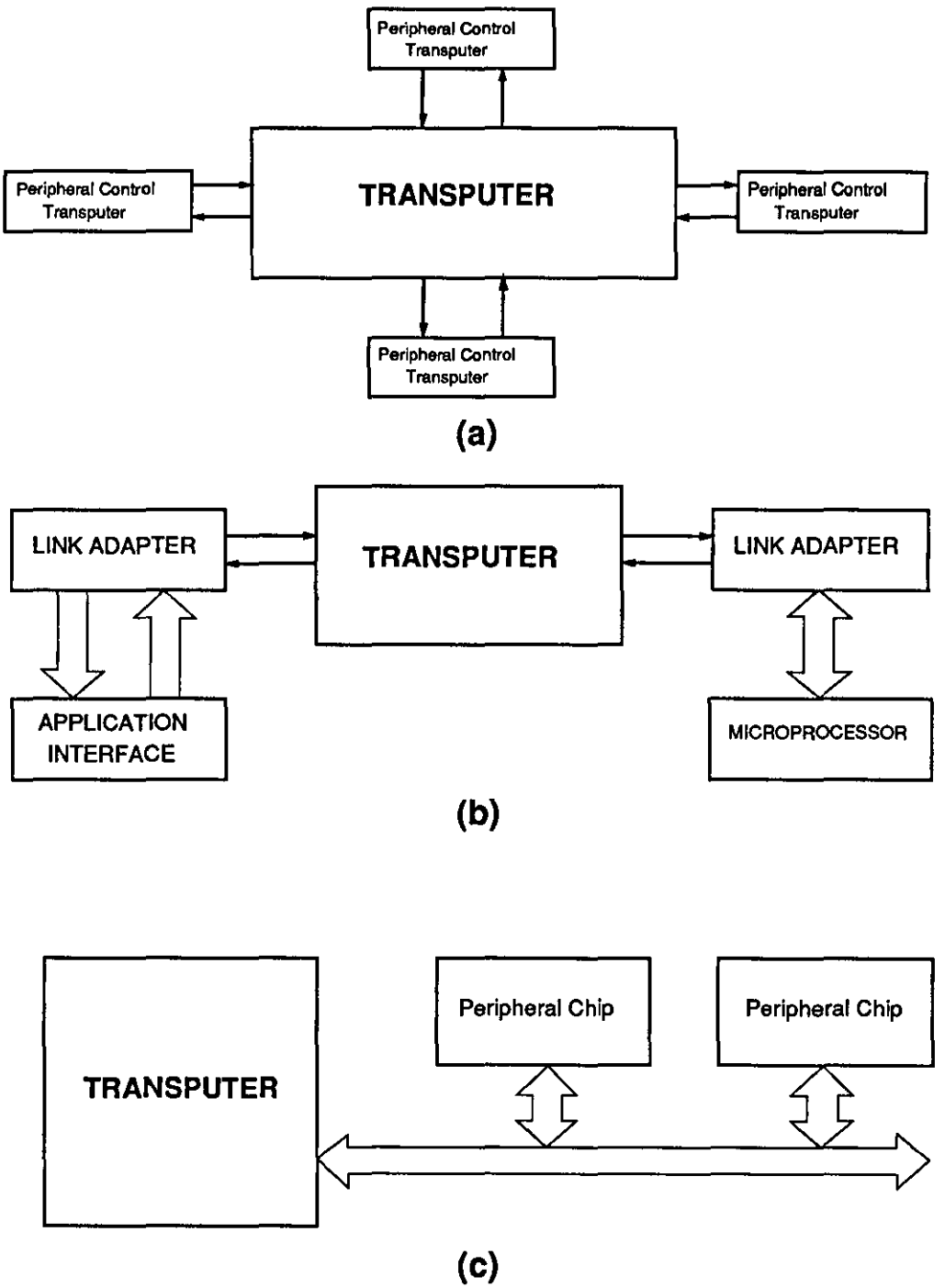

Figure 4.22: Methods of Communications Between The Transputer and Peripherals.

4.4.6.3 The IMS CO11 Link Adapter:

The most convenient way to interface the BBC microcomputer to the transputer is by implementing the second method which is based on using a link adapter. The IMS CO11 link adapter provides full duplex transputer link communication with standard microprocessor and sub-system architectures, by converting bidirectional serial link data into parallel data streams.

The link adapter can be operated in one of two modes (figure 4.23). In mode 1 the IMS CO11 converts between a link and two independent fully handshake byte-wide interfaces, one input and one output. It can be used by a peripheral device to communicate with a transputer, an INMOS peripheral processor or another link adapter, or it can provide programmable input and output pins for a transputer. More details about using this mode can be found in ref. 51.

In mode 2 the IMS CO11 provides an interface between an INMOS serial link and a microprocessor system bus. Status and data registers for both input and output ports can be accessed across the byte-wide bidirectional interface. Two interrupt outputs are provided, one to indicate input data available and one for output buffer empty. The signal summary for mode 2 is:

D0-D7 Bi-directional data bus. The bus is high impedance unless the link adapter chip is selected and the RnotW line is high. The bus is used by the microprocessor to access status and data registers.

notCS The link adapter chip is selected when notCS is low.

RnotW This signal, in conjunction with the notCS, selects the link adapter registers for the read or write mode. When RnotW is high, the contents of an address register appear on the data bus D0-D7. When RnotW is low the data on D0-D7 is written into the addressed register. The state of the RnotW is latched into the link adapter by notCS going low.

RS0-RS1 One of four registers is selected by RS0-RS1. A register is addressed by setting up RS0-RS1 and then taking notCS low; the state of RnotW when notCS goes low determines whether the

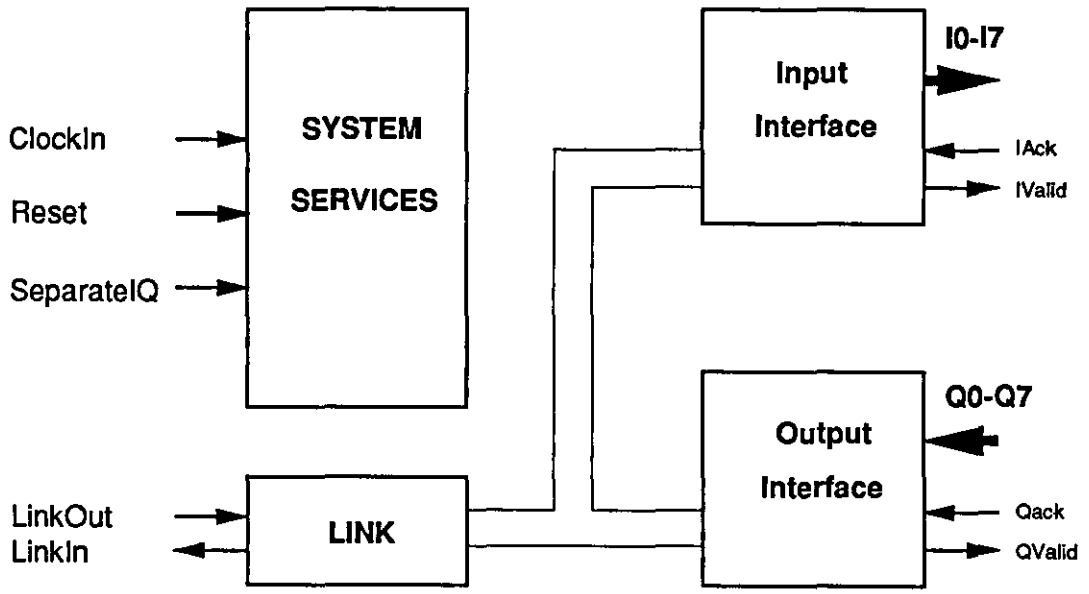

MODE 1

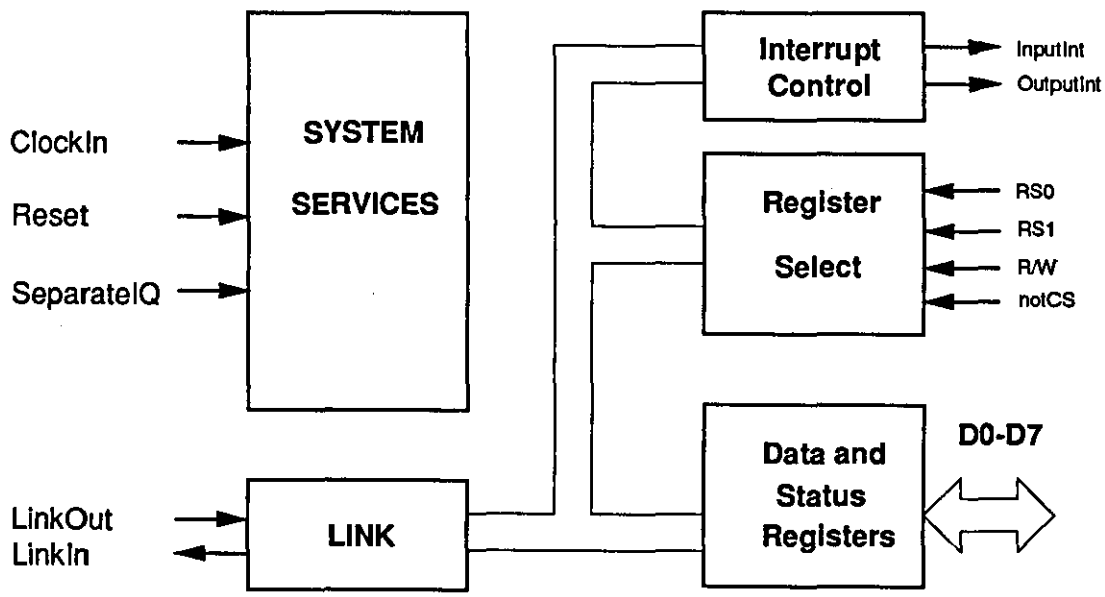

MODE 2

Figure 4.23: Modes of Operation of The Link Adapter.

register will be read or written. The state of RS0-RS1 is latched into the link adapter by notCS going low. The register set comprises a read-only data input register, a write-only data output register and a read/write status register for each. Table 4.1 below shows how to select each of these registers.

Table 4.1

RS1	RS0	RnotW	REGISTER
0	0	1	Read Data
0	0	0	Invalid
0	1	1	Invalid
0	1	0	Write Data
1	0	1	Read Input Status
1	0	0	Write Input Status
1	1	1	Read Output Status
1	1	0	Write Output Status

In the following a brief definition of these four registers is presented:

Input Data Register: This register holds the last data packet received from the serial link.

Input Status Register: This register contains the data present flag and the interrupt enable control bit for Input Interrupt. The data present flag is set to indicate that the data in the data input buffer is valid. It is reset low only when the data input buffer is read or by reset. When writing to this register the data present bit must be written as zero.

	Output Data Register:	Data written to this link adapter register is transmitted out of the serial link as a data packet. Data should only be written to this register when the output ready bit in the output status register is high, otherwise data already being transmitted may be corrupted.
	Output Status Register:	This register contains the output ready flag and the interrupt control bit for Output Interrupt. The output ready flag is set to indicate that the data output buffer is empty. It is reset low only when data is written to the data output buffer and it is set high by reset.
SeparateIQ	This must be wired to GND to select mode 2.	
LinkSpeed	Determines the speed of the links. If wired to GND link speed is 10 Mbits/sec, if wired to VCC speed is 20 Mbits/sec.	
LinkIn	INMOS serial link input.	
LinkOUT	INMOS serial link output.	
Reset	Reset link adapter.	

4.4.6.4 Description of The Interface Hardware:

Figure 4.24 shows the block diagram of the Transputer-BBC interface. As mentioned earlier, the heart of this interface is the IMS CO11 link adapter. The CO11 is configured to mode 2 and to a link speed of 10 Mbits/sec by wiring the SeperateIQ and the LinkSpeed pins to GND. A simple reset circuit is used to reset the link adapter automatically when it is powered on. It also allows manual resetting by a push switch.

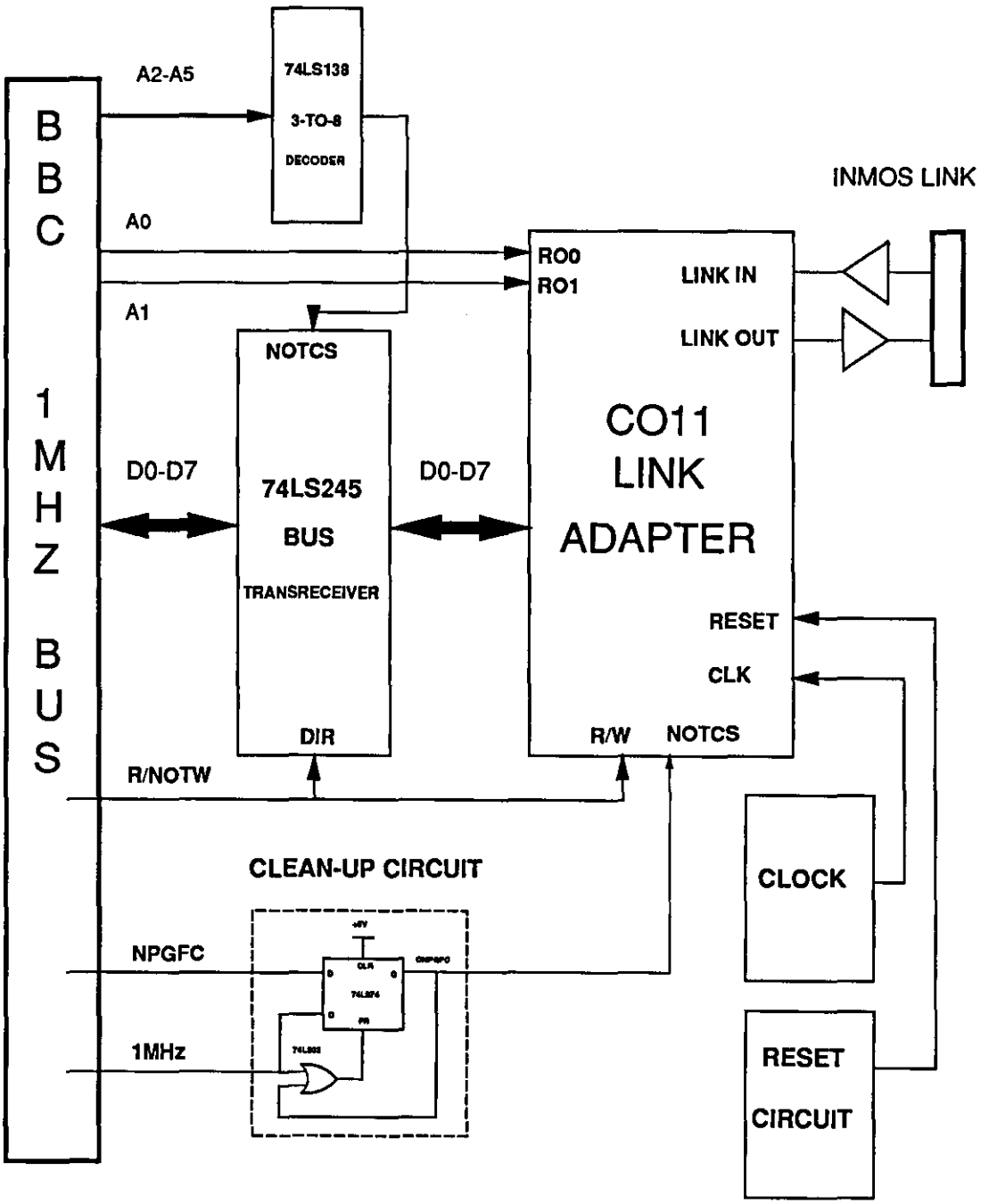

Figure 4.24: Block Diagram of The Transputer-BBC Interface.

At the transputer end, the LinkIN and LinkOut signals are connected to their respective LinkIn and LinkOut of the link adapter via buffers.

At the BBC end, the 1 MHz clock and the NPGFC signals from the 1MHz bus are used to generate a clean NPGFC signal (CNPGFC) using the standard cleaning circuit mentioned earlier. This CNPGFC is used to enable the link adapter.

The data lines D0-D7 from the 1MHz bus are connected to their respective data lines of the link adapter via a bidirectional tristate buffer (74LS245). The direction of this buffer is determined by the R/notW signal from the BBC. This R/notW signal is also connected to the respective RnotWrite input of the link adapter. The BBC address lines A0 and A1 are connected to RS0 and RS1 pins of the link adapter respectively via a buffer. These signals, together with the RnotW signal are used to select either data or status registers for read or write as shown in table 4.1.

Address lines A3-A5 are decoded to set the board address using a 3-to-8 lines decoder (74LS138).

4.4.6.5 Description of The Interface Software:

a. Transferring Data From Transputer to BBC:

To transfer data from the transputer to the BBC, an OCCAM output channel should be declared. The TYPE of this channel determines the type of data that is going through. It can be assigned to carry BYTE, INT16 or INT32 type data. It can also be declared to carry single data, array data or multidimensional data. Typical declaration statements are:

```
CHAN OF BYTE outlink:
CHAN OF INT16 outlink:
CHAN OF [N][N]INT outlink:
```

Since the transputer uses DMA data block transfer to communicate with the outside world, a memory should be assigned for each input or output channel. A PLACE command is used for this purpose and its syntax is:

PLACE outlink AT 1:

An output is indicated in OCCAM by the symbol !. For example:

outlink! x

where the value of x is transmitted on the channel named outlink.
On the BBC side, a program should be written to read the data sent by the transputer. The program starts by defining the type of data that the BBC is going to receive and the size of this data. Then the program will enter a loop to read the contents of the status register to see if there is any data available in the link adapter buffer. When data is available, the BBC will read it from the output data register. If the data is INT16, then the BBC will read two successive bytes to re-construct the number sent by the transputer. Likewise, if the data is INT32, then the BBC will read four successive bytes to reconstruct the number. This process will continue until all the data packet has been read.

b. Transferring Data From BBC to Transputer:

To send data from the BBC to the transputer, the BBC first checks the status register to see whether the transputer is ready to receive the data. Then the BBC starts sending the data byte by byte.

On the transputer side, an input channel must be declared for the input data. The declaration specifies the type of data that the channel is to carry (BYTE, INT16, INT or array data). For example:
CHAN OF BYTE inlink:
CHAN OF INT16 inlink:

Again the PLACE command is used to assign a certain part of transputer memory to accommodate the incoming data from the input channel as shown below:
PLACE inlink AT 2:

The OCCAM symbol for reading data from an input channel is (?). For example, the command for reading the value of a variable named x from the input channel named inlink is:
inlink? x.

4.5 TEST OF THE SYSTEM:

In the previous section, the design of the high resolution DF system was discussed. The system was then constructed and programmed, and a series of tests carried out to examine its performance. The purpose of this section is to present and discuss the results of these tests.

The section begins with a description of the calibration procedures, measuring the system dynamic range and testing the system with a simulated echo pulse. Then it presents the results of a series of tests carried out in the tank room to measure the phase and amplitude across a ten element 40 kHz acoustic array using a signal transmitted from a single source. These tests were carried out on two different arrays. The section then examines the results of these tests and discusses the possible causes of some errors that were apparent and the ways to correct them.

Finally, the system was used to implement the Conventional Beamformer Method (CBF) using a single source and the resulting beam patterns were compared with their respective patterns obtained by using the LUT computer controlled Beam-plotting system [ref. 73 and 74].

4.5.1 System Configuration and Calibration:

The system was designed and built to work around a frequency of 40 kHz. The frequency of operation is controlled by a multiturn pot on the "Reference and Signal Generator Board". The resonant frequencies of the transducers are clustered around 40 kHz and they range from 37-41 kHz [ref. 75]. Therefore the pot was trimmed to get the best possible signal from the transducers.

Figure 4.25a shows a trace of the START signal and the transmitted pulse while figure 4.25b shows the reference SINE and COSINE signals which start immediately after the end of the transmitted pulse.

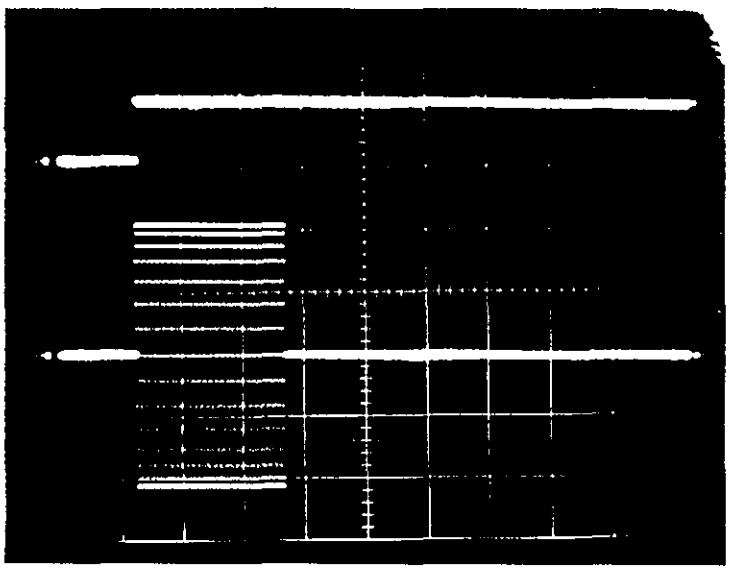

(a)

TOP TRACE: The START Pulse.
BOTTOM TRACE: The Transmit Pulse.

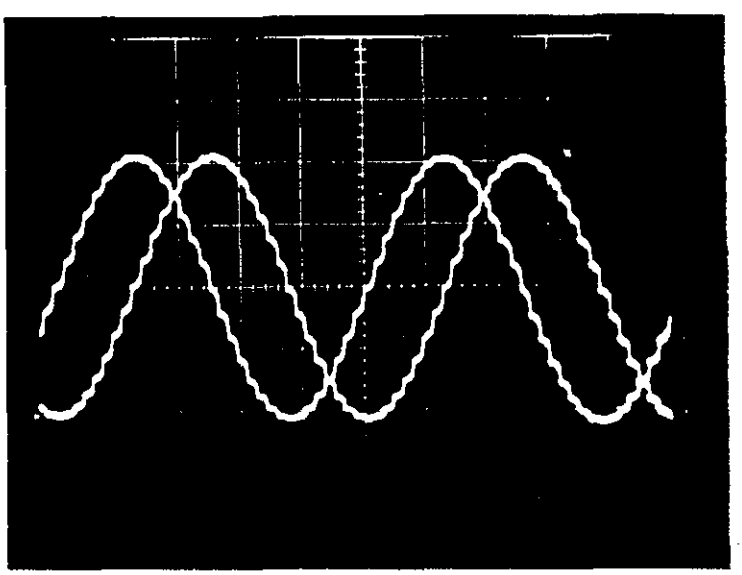

(b)

The Reference SINE and COSINE Signals.

Figure 4.25

The pulse length is selected by setting the number of cycles in the pulse using eight dip-switches on the "Reference and Signal Generator Board". This gives a selection of maximum 255 cycles per pulse (which is equivalent to 6.375 msec at 40 kHz). For these measurements, the pulse length was chosen to be 32 cycles/pulse.

The sampling frequency is controlled by the frequency of the C1 control signal. The frequency of this signal is set by a multiturn pot on the Reference and Signal Generator board. The conversion time for one sample is 25 μsec [ref. 70]. A short time is needed after that to read the converted data from the A/D boards (around 5μsec). Therefore a minimum of 60 μsec is required to convert both the I & Q samples. This means that the maximum sampling frequency of the system is 16.6 kHz. However, in practice it was noticed that some of the A/D chips take more than 25 μsec to finish the conversion. Therefore a sampling frequency of 12.5 kHz was chosen.

Figure 4.26a shows a trace of C1 and C2 control signals, figure 4.26b shows a trace of $\overline{START\ \ CONVERT}$ and $\overline{E.O.C}$ and figure 4.26c shows a trace $SAMPLE/\overline{HOLD}$ and $\overline{E.O.C}$ signals.

Each of the ten A/D boards contains two multiplier circuits. Within the monolithic multiplier, transistor base-emitter junctions are typically matched within 1 mV and resistors are typically matched within 2%. Even with this careful matching, output error can occur. This output error comprises X-input offset voltage, Y-input offset voltage, and output offset voltage. These errors were adjusted to zero using the following procedure:

1. X input Offset

(a) A sinewave signal of 1 kHz, 5 V_{p-p} was connected to the 'Y' input.

(b) The 'X' input was connected to ground.

(c) The X offset potentiometer 'P_2' was adjusted for an ac null at the output.

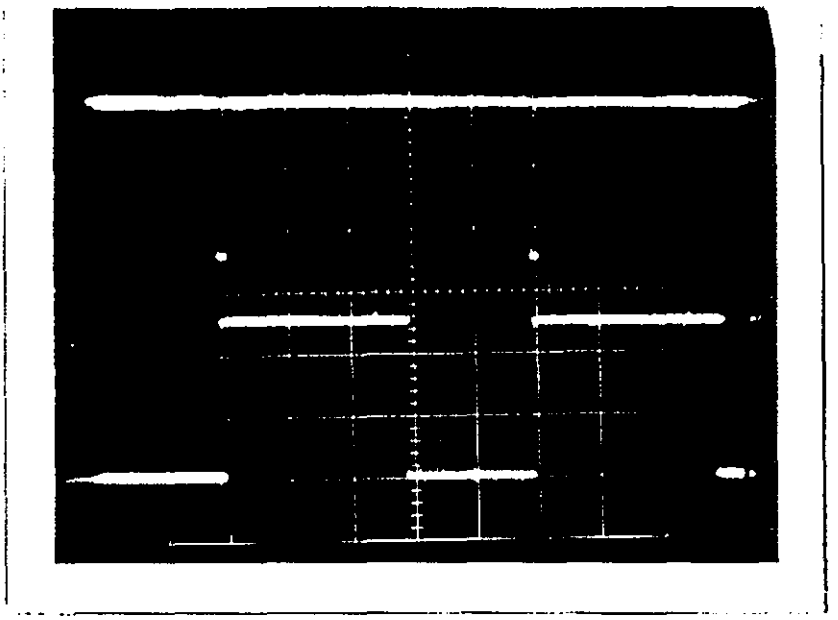

(a)

TOP TRACE: The START CONVERT Pulse.

BOTTOM TRACE: The END OF CONVERSION Pulse.

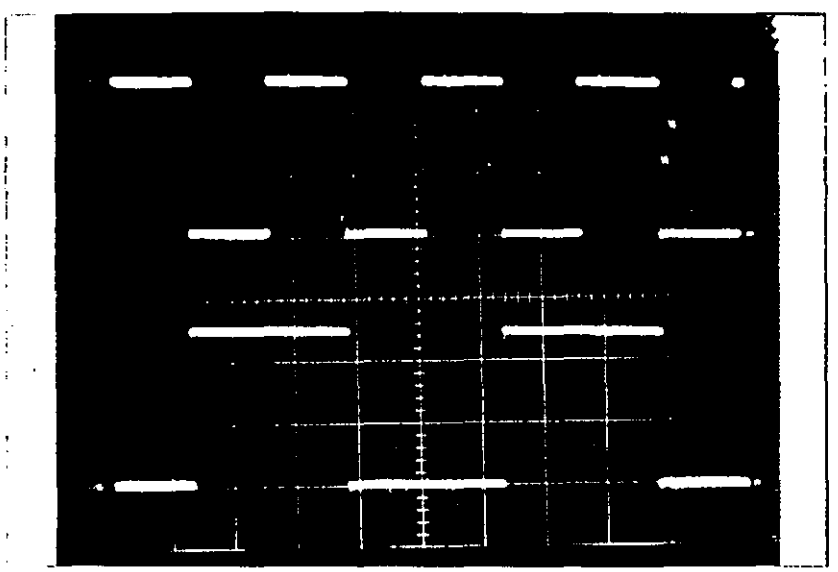

(b)

TOP TRACE: The Control Signal C1.

BOTTOM TRACE: The Control Signal C2.

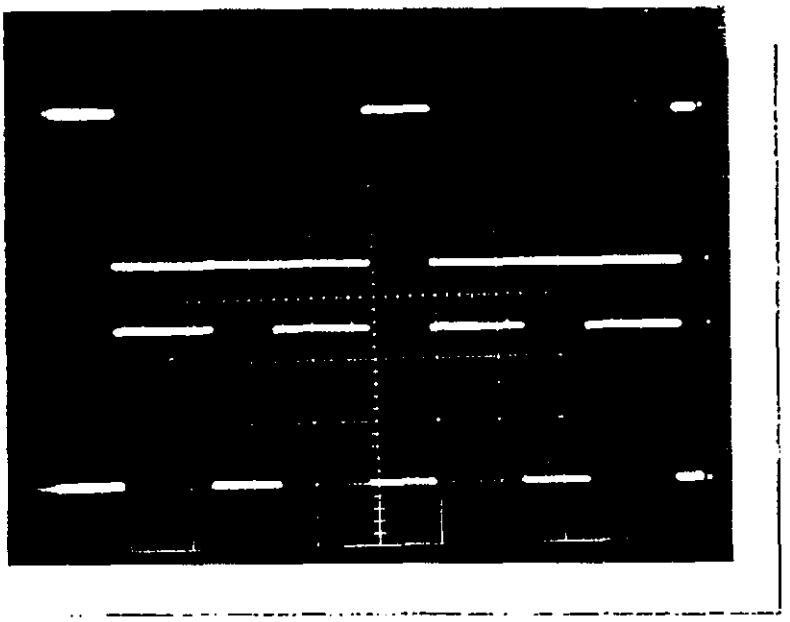

(c)

TOP TRACE: The SAMPLE/$\overline{\text{HOLD}}$ Signal.

BOTTOM TRACE: The $\overline{\text{END OF CONVERSION}}$ Signal.

Figure 4.26

2. Y input Offset

(a) A sinewave signal of 1 kHz, 5 V_{p-p} was connected to the 'X' input.

(b) The 'Y' input was connected to ground.

(c) The Y offset potentiometer 'P_1' was adjusted for an ac null at the output.

3. Output Offset

(a) The 'X' and 'Y' inputs were connected to ground.

(b) The output offset potentiometer, P_4, was adjusted until the output voltage was zero volt dc.

4. Scale Factor

(a) The 'X' and 'Y' inputs were connected to +10 V_{dc}.

(b) The scale factor potentiometer, P_3, was adjusted to achieve +10.00V at the output.

The above steps were repeated as necessary.
All the potentiometers used for adjusting the multipliers were multiturn with a low temperature coefficient.

Each multiplier circuit is followed by a low pass filter to remove the high frequency products of multiplication. A fourth order Butterworth filter is used for this purpose. However, these filters introduce some phase shifts which might vary from filter to filter due to tolerances of the external components (especially the capacitors). These differences in phase shifts can cause some errors in reading the phases of the incoming signals. Therefore it was very important to match all the external components needed to build the filters used by the system.

The 12 bit A/D circuit of each of the A/D boards was calibrated by applying a signal, which was 1/2 LSB above negative full scale, and trimming R1 to give the first transition (0000 0000 0000 to 0000 0000 0001). Then a signal which was 1/2 below positive full scale was applied and R2 was trimmed to give the last transition (1111 1111 1110 to 1111 1111 1111).

4.5.2 Measuring The System Dynamic Range:

The A/D boards convert the received analogue signals to 12 bit digital form. This provides a resolution of one part in 4096. However, to achieve this resolution in practice, the dynamic range of the system must be at least 72 dB. Since the maximum output of the system is ± 10V, the noise level in the system must be kept below 5mV. The main sources of noise were:

a. Power supply ripple.
b. Noise leaked from the digital circuitry.
c. Electromagnetic radiation.

To reduce the noise from these sources, the following measures were taken:

a. Use of on-board power supply regulators which have a ripple rejection factor of -60 dB.

b. Use of separate grounds for analogue and digital circuitry.
c. Use of ground planes.
d. The DC supplies were decoupled at each ic by 0.1 μf capacitors.

The measured input-output characteristics of the A/D boards showed that the obtainable dynamic range is about 70dB. It is possible to improve this figure by providing better shielding around the A/D circuitry.

4.5.3 Testing The System With a Simulated Pulse:

A circuit was built to generate a delayed version of the transmitted pulse. The amount of delay is selected by five dip switches which set the starting value of the counter that drives the signal PROM. This pulse was fed directly to all A/D boards and measurements of I&Qs were made. These measurements were repeated for different delays. Figure 4.27 shows a plot of these measurements. Also, during this test, the deviation of the measured values from board to board was found to be within 3%.

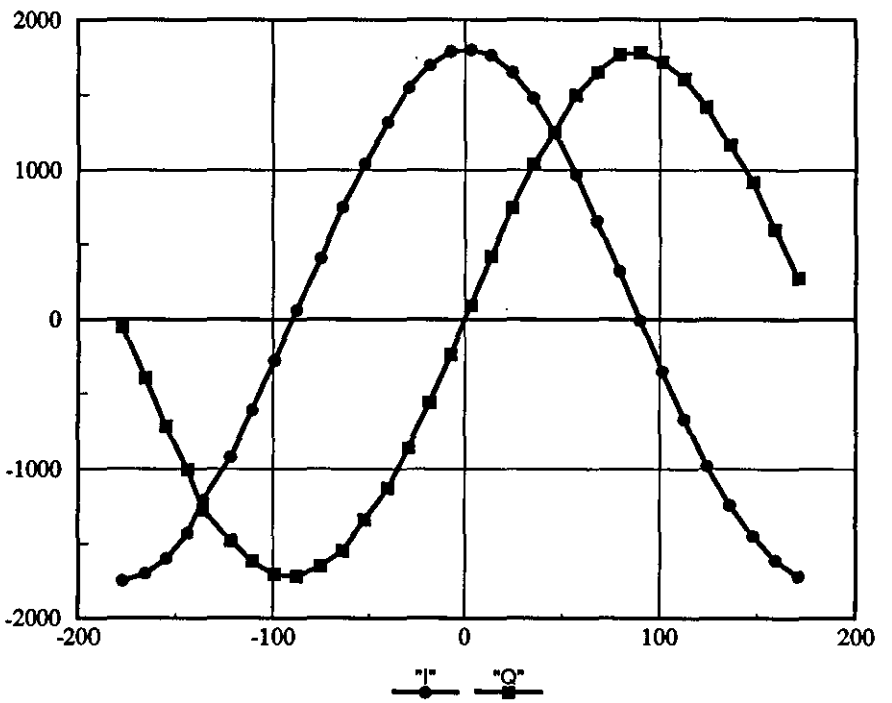

Figure 4.27: Plot of Measured I & Q.

4.5.4 Testing The System With a Real Pulse:

After passing the above test, the system was connected to the 40 kHz, 15 element acoustic array. The first ten elements were used. The array was mounted on a pan and tilt unit and deployed in the water tank at LUT. The signal was transmitted from an array of 4 elements connected in parallel and mounted vertically on a wooden post about 270 cm in front of the receiving array. The wooden post was attached to a mobile trolley. Figure 4.28 shows the experimental set-up used for this test.

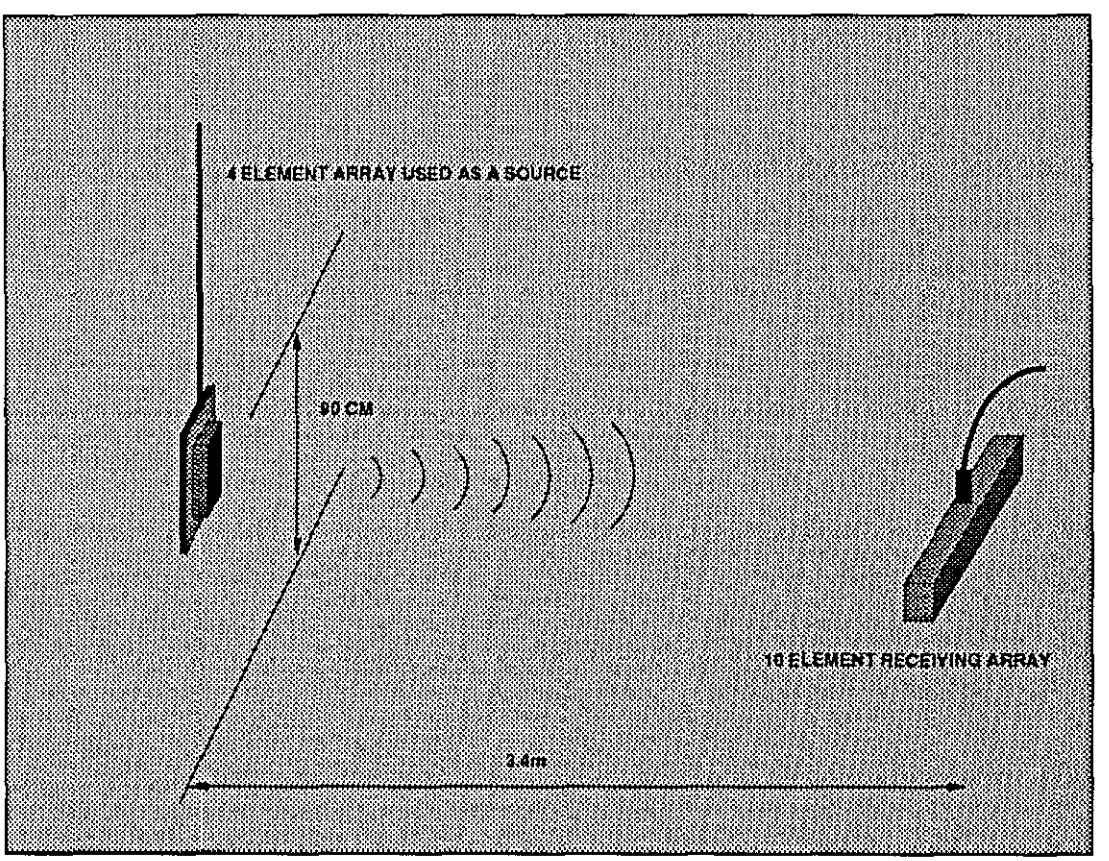

Figure 4.28: System Set-Up.

4.5.5 Implementing The Conventional Beamformer to Measure the Array Beam Pattern:

The last test carried out was to implement the Conventional Beamformer (CBF) method and use that as a measure of the array beam pattern. In this test a source was placed in the zero direction at a distance from the receiving array, transmitting in the direction of the receiving array, and the High Resolution DF system was used to measure the angular spectrum. Different combinations of array elements were tried and these were compared with their respective beam patterns measured by the traditional method of steering the array physically and recording the array response at each angle. Figures 4-39 to 4-44 shows the results of this test.

4.6 DISCUSSION:

a. The old array

It can be seen from figure 4.31 that the phase errors associated with this array range from +12.8 to -12.8 degrees. These errors result from a combination of electronic and acoustic factors. Electronic errors may be caused by the multiplier circuits (which may have up to 5 degrees phase difference between channels X and Y) and the slight mismatch between the filter circuits. Acoustic errors may be caused by the mechanical misalignments of the transducers in the array. Unfortunately the positions of the elements within the nylon body of the array could not be measured exactly, and so there are no figures available for the mechanical misalignment.

Although these errors are significant, they can be corrected in software because they are consistent.

b. The new array:

The observed error figures for this array are much better than those for the old array. However, there are relatively large errors on element 5 (+11.2 degrees) and element 7 (-8.2 degrees). Other elements look quite good. Again these errors

might be caused electronically or acoustically. The phase errors due to the mechanical mismatch (as listed in ref. 75) were compared with the observed practical phase errors and it was found that there is little correlation between them.

The extensive tests carried out on this array showed that these errors are consistent which means that they can be eliminated by software.

After the extensive tests carried out on the system, the final conclusions are:

1. The system is working in a satisfactory manner.
2. There are some phase errors (which might be caused electronically or acoustically) which can be eliminated by software.

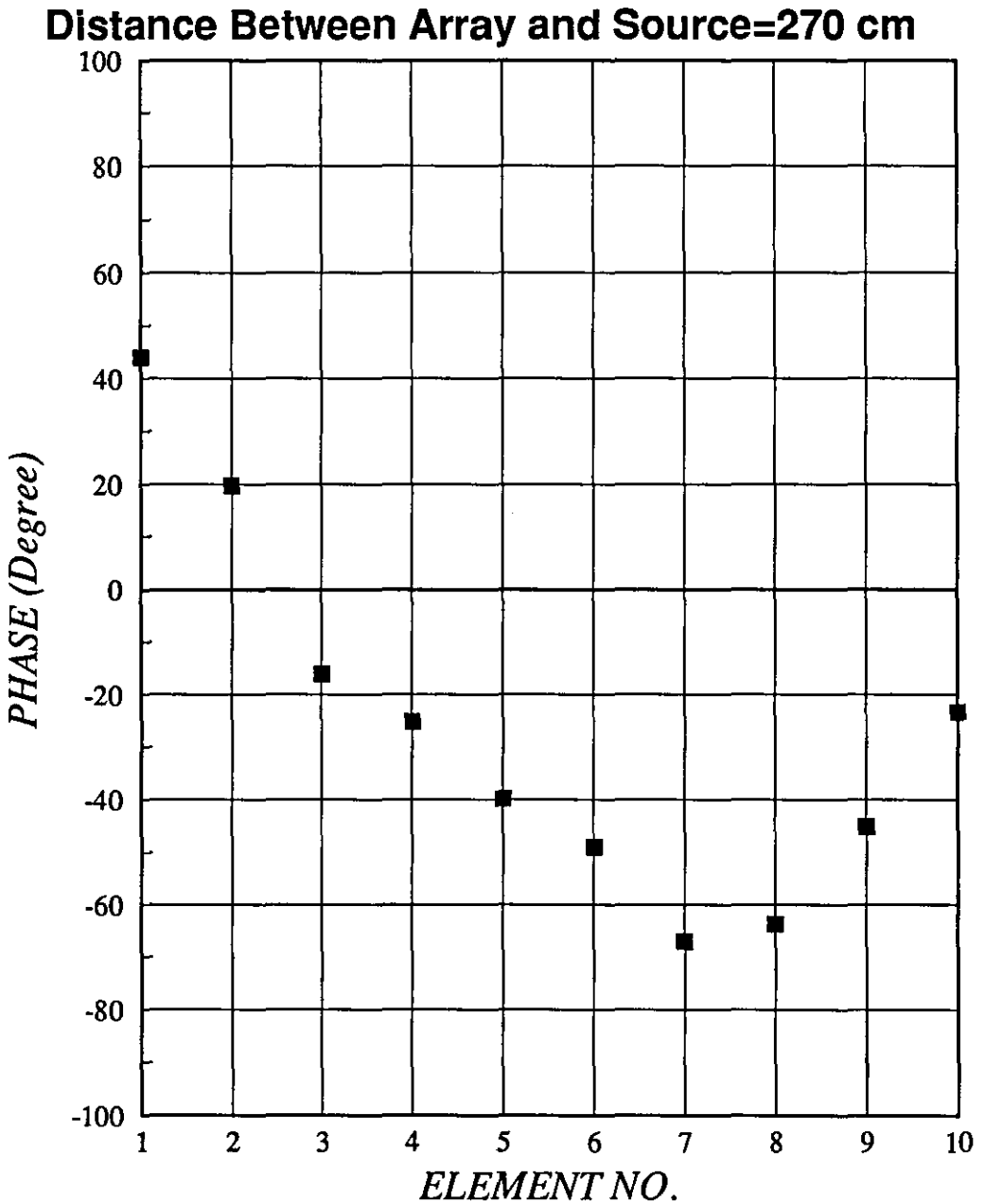

Figure 4.29: Phases across The Old Array.

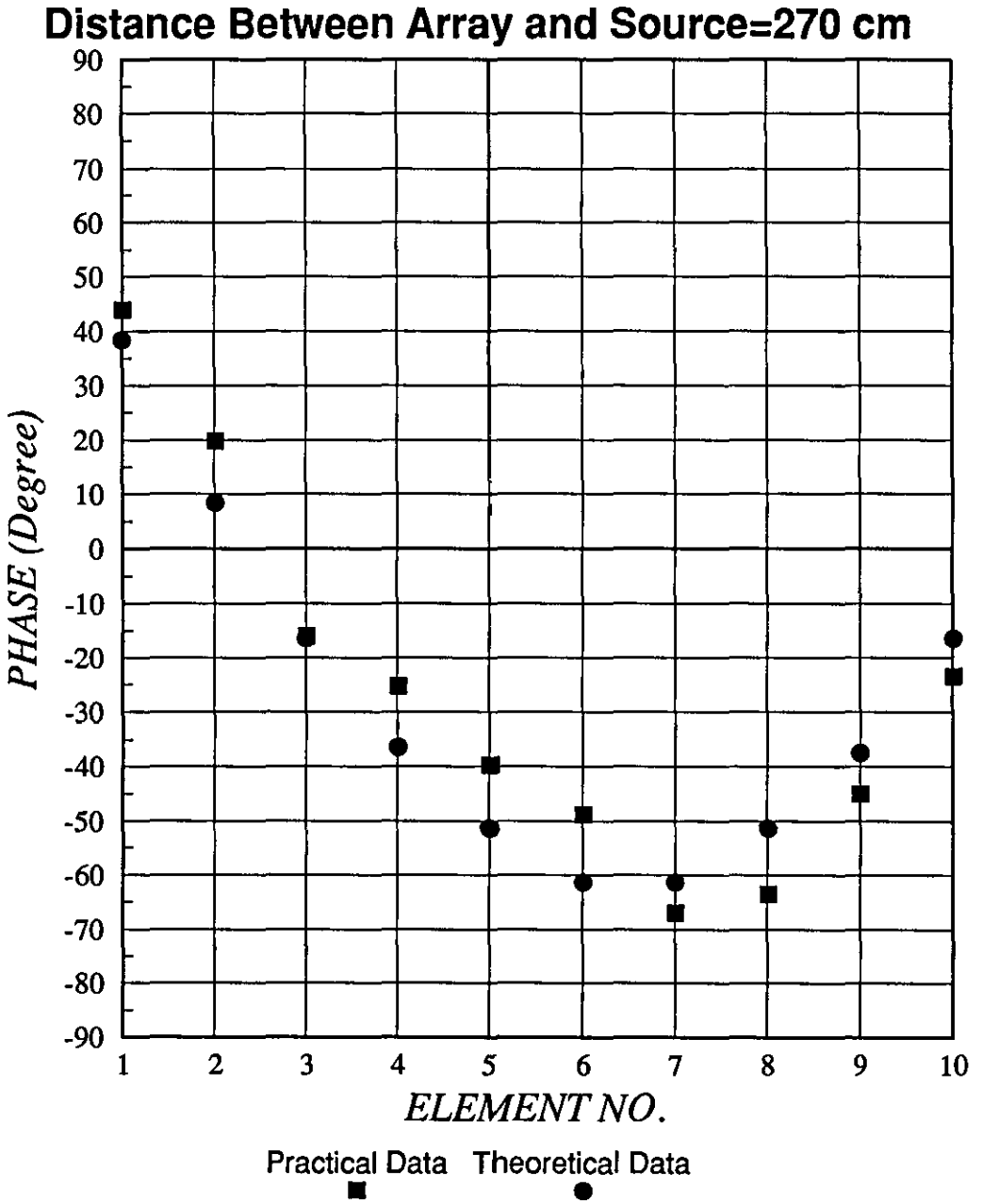

Figure 4.30: Comparison Between Practical and Theoretical Results For The Old Array.

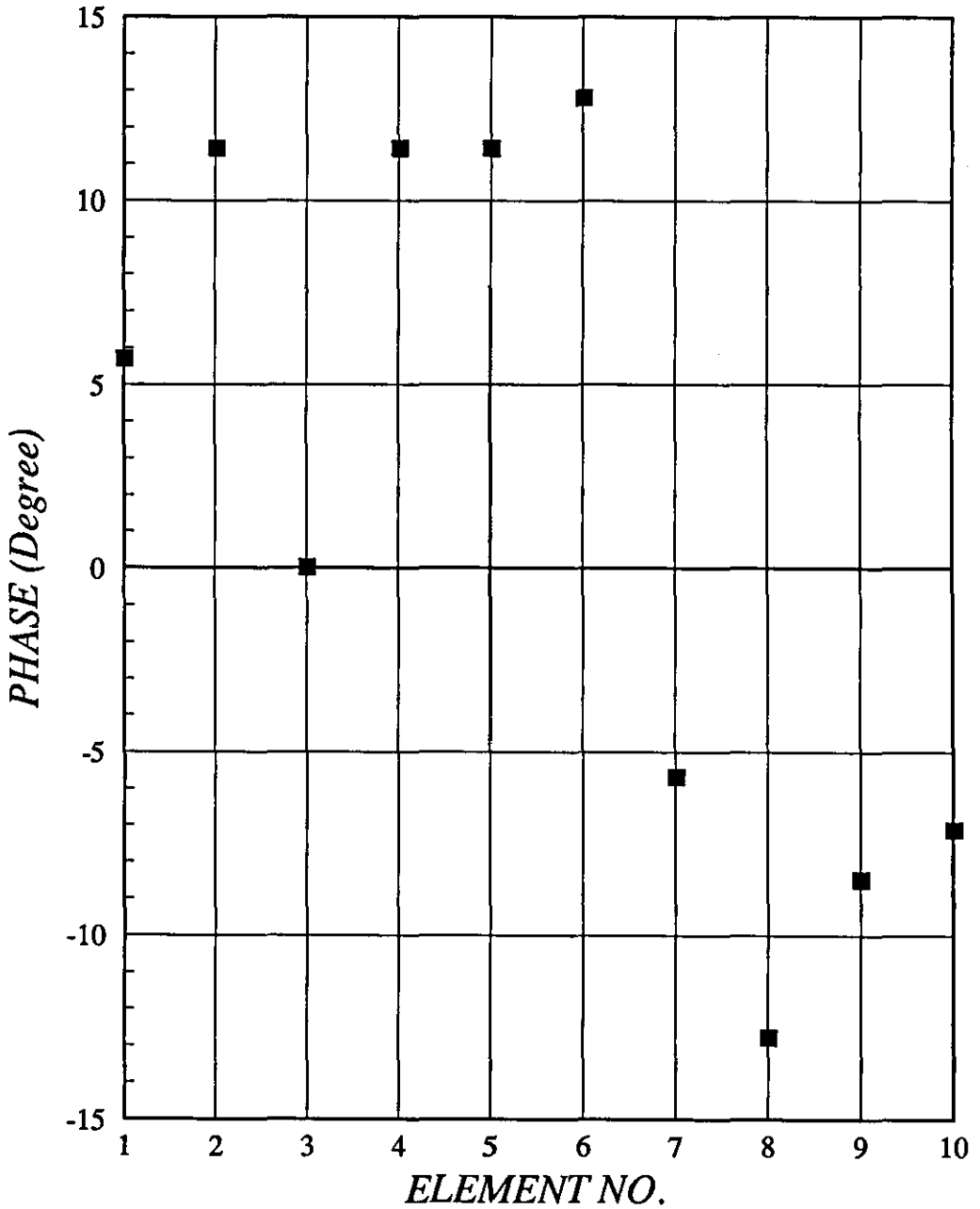

Figure 4.31: Phase Error For The Old Array.

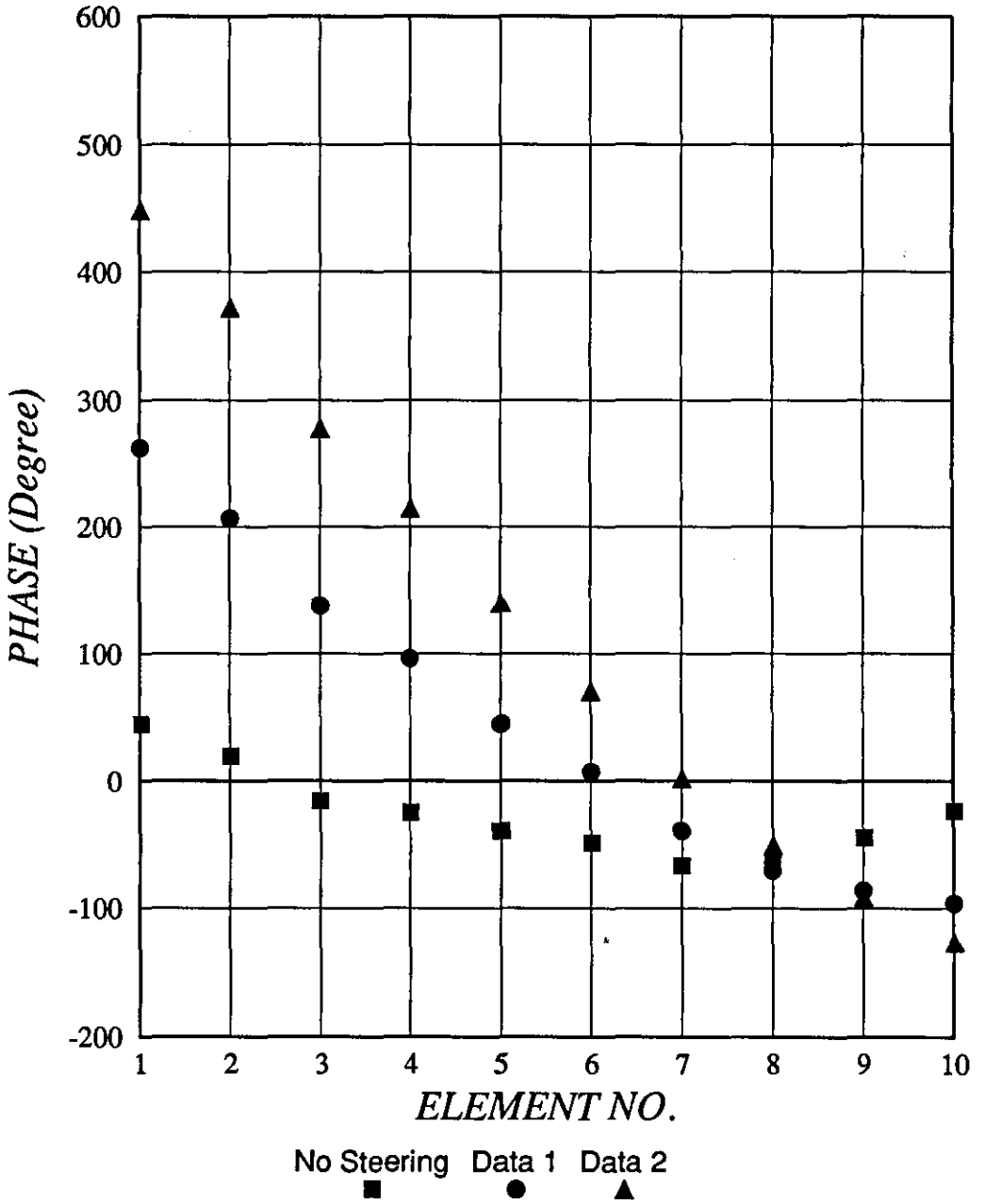

Figure 4.32: Phases Across The Old Array When Steered To The Right.

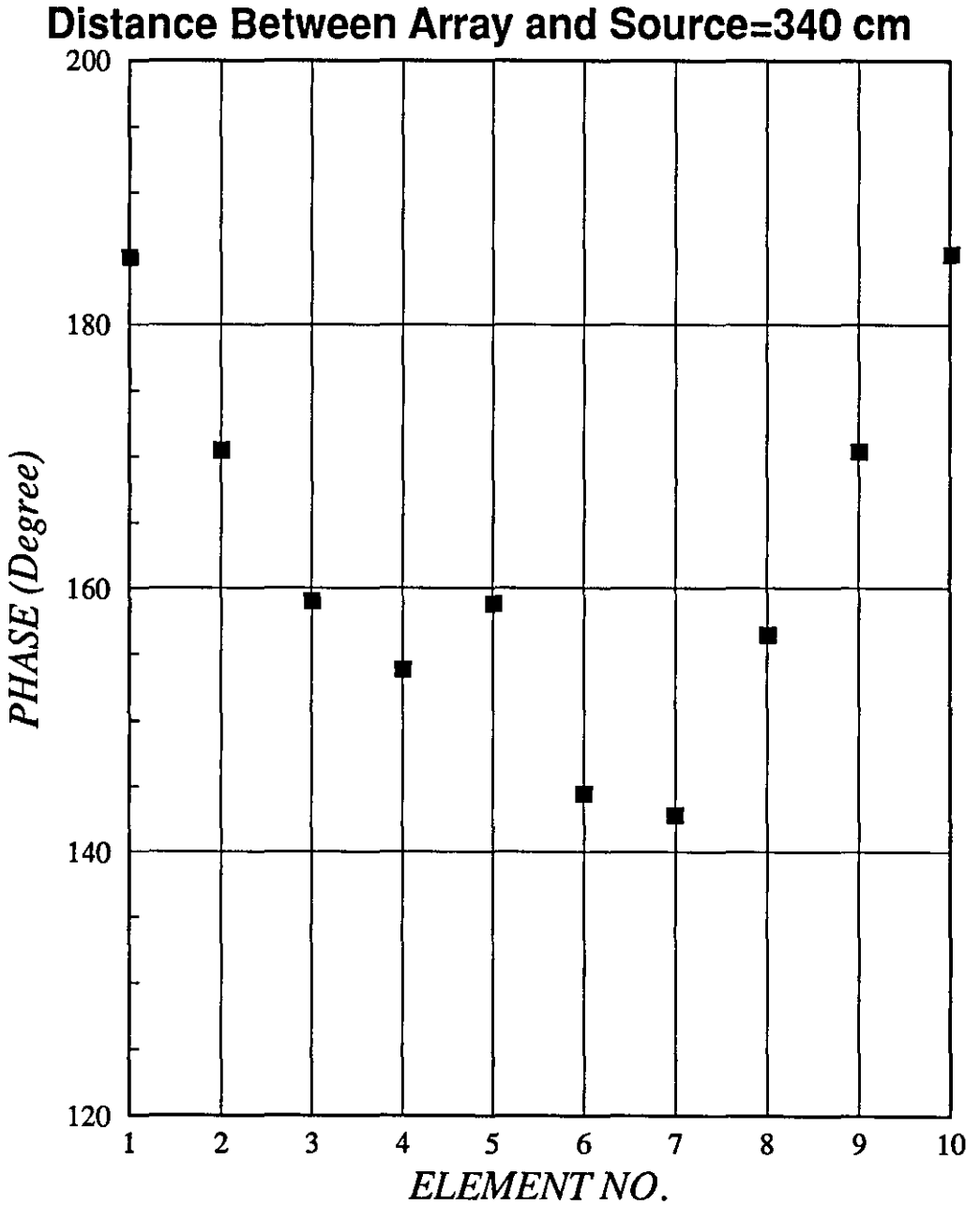

Figure 4.33: Phases Across The New Array.

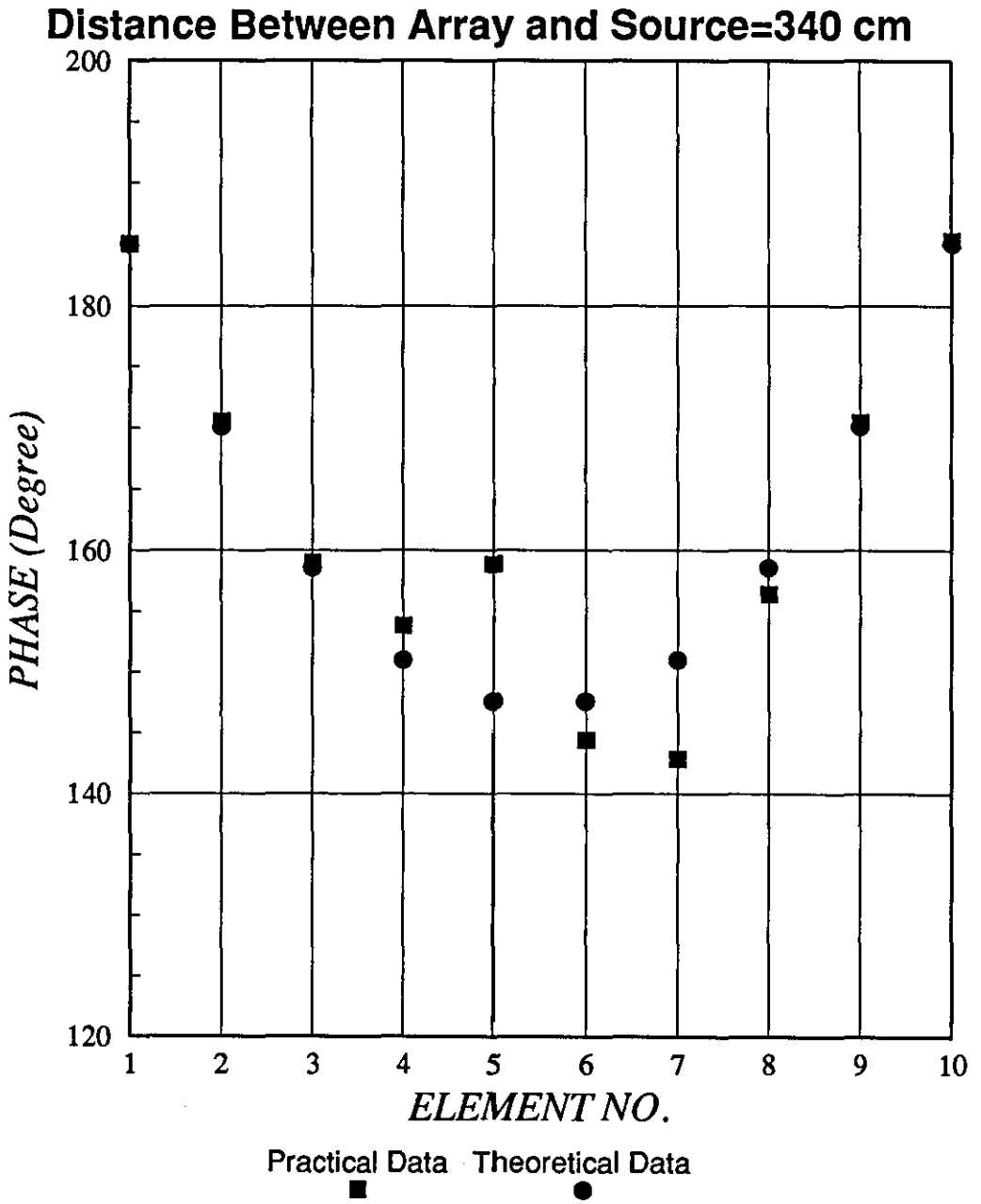

Figure 4.34: Comparison Between Practical and Theoretical Results For The New Array.

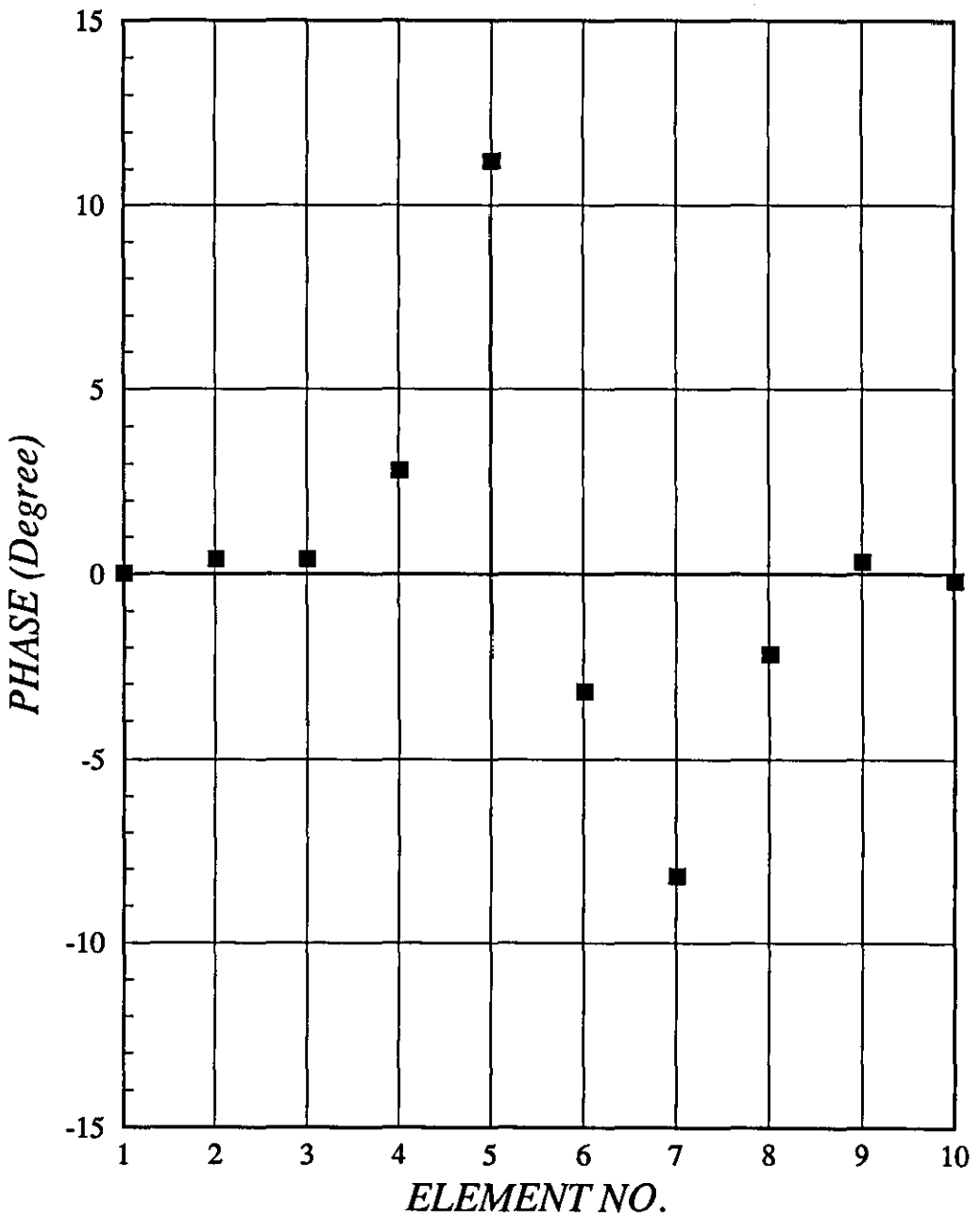

Figure 4.35: Phase Error For The New Array.

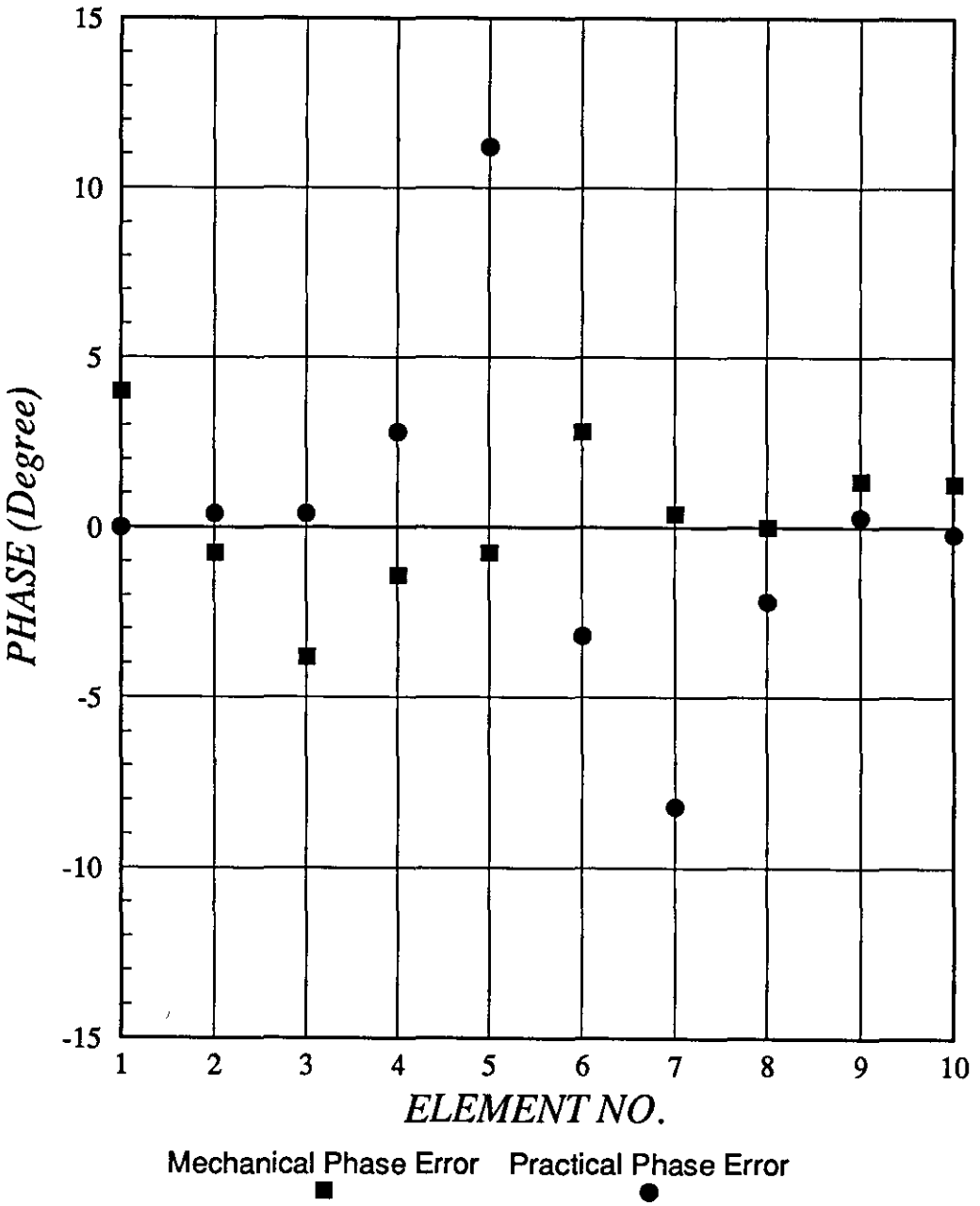

Figure 4.36: Comparison Between Practical Phase Errors and Mechanical Phase Errors For The New Array.

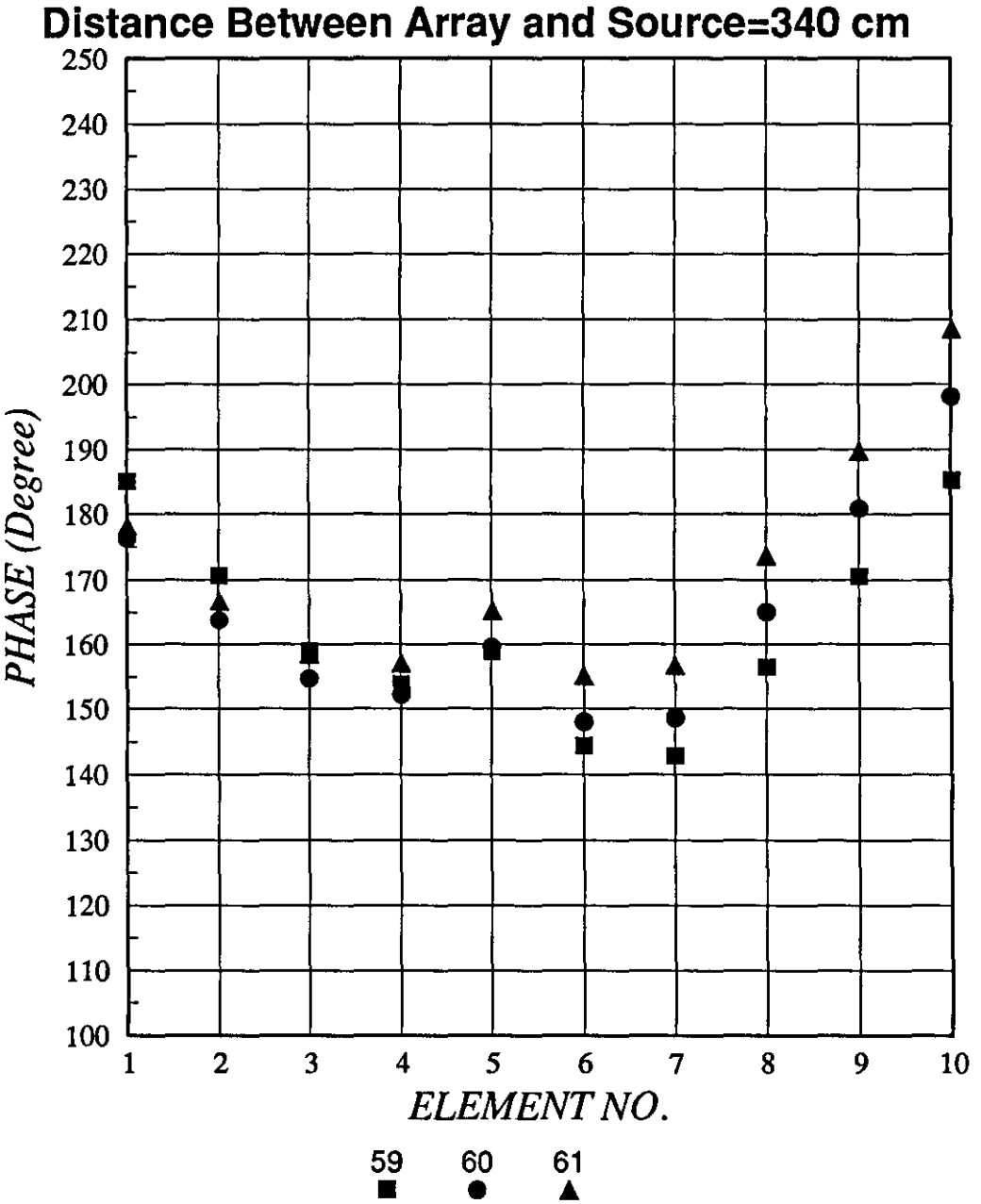

Figure 4.37: Phases Across The New Array As The Source Moved To The Left.

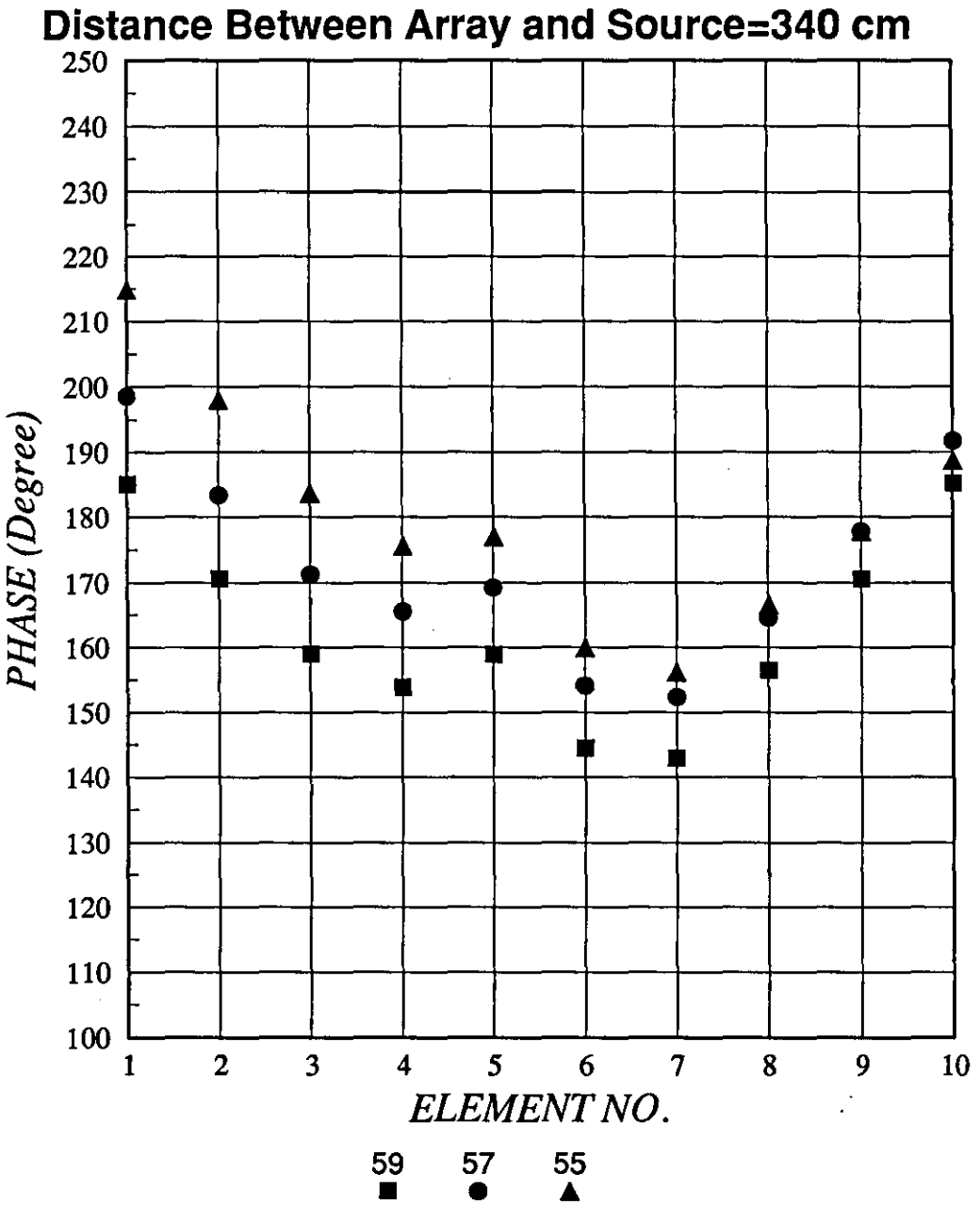

Figure 4.38: Phases Across The New Array As The Source Moved To The Right.

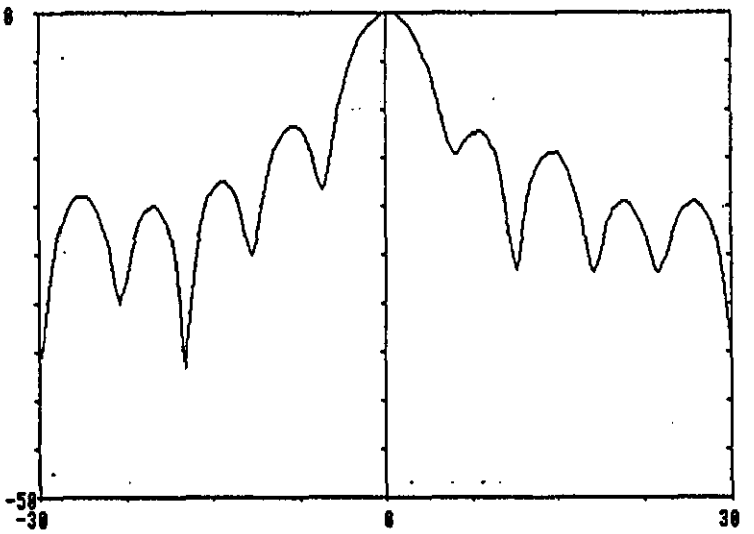

High Resolution System

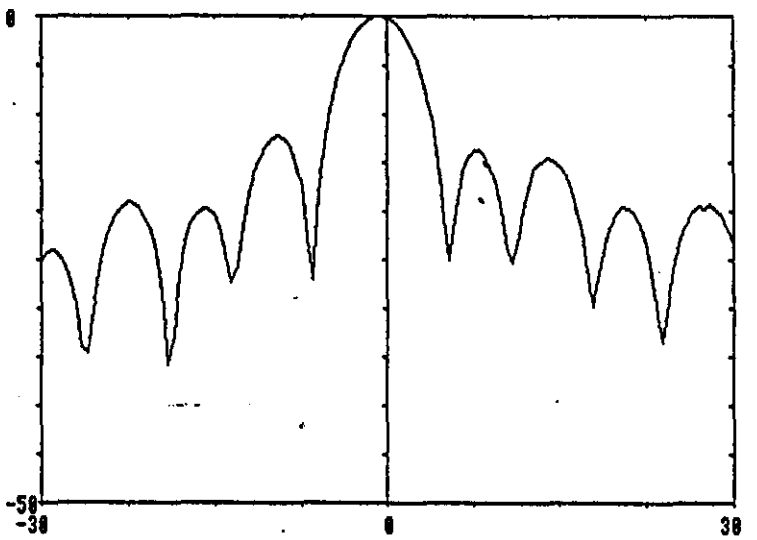

Beam-Plotter

Figure 4.39: Conventional Beamforming For Elements 1-10.

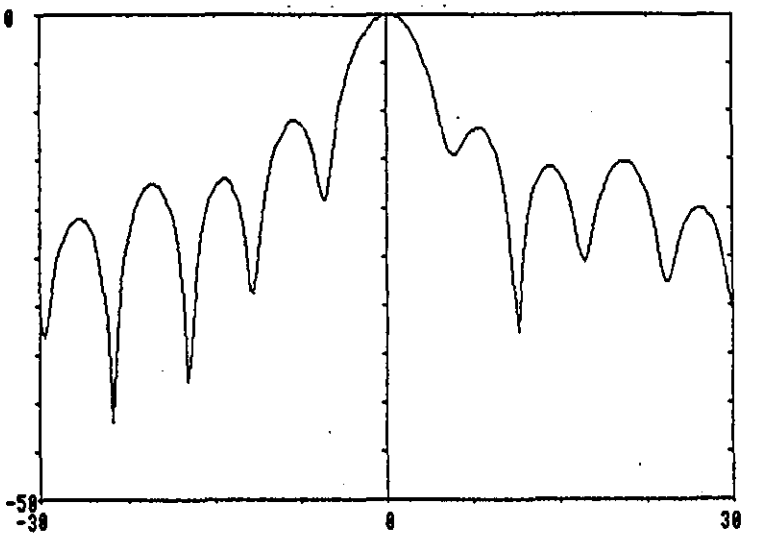

High Resolution System

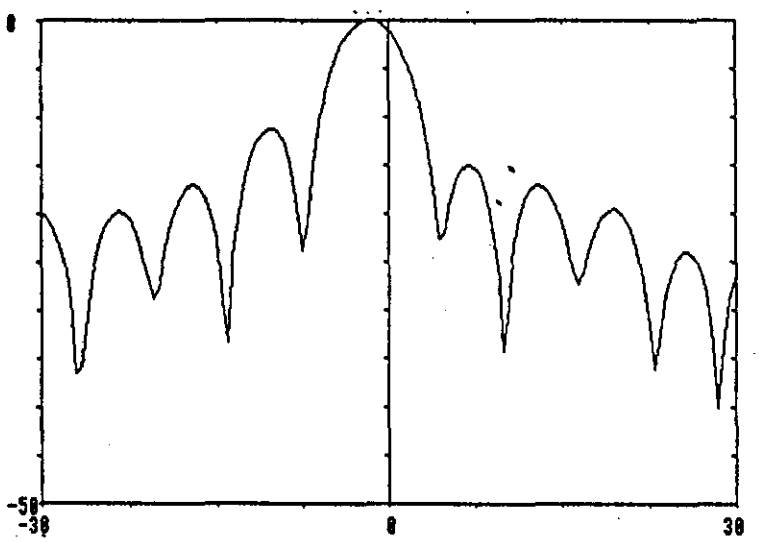

Beam-Plotter

Figure 4.40: Conventional Beamforming For Elements 2-11.

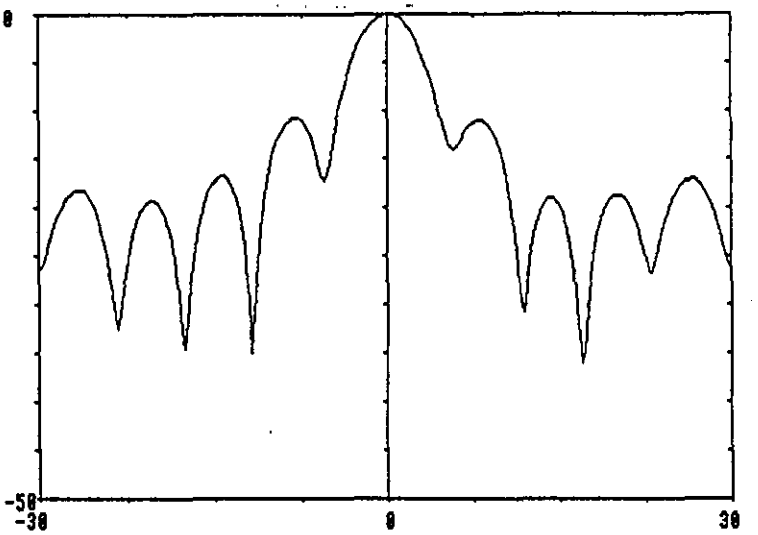

High Resolution System

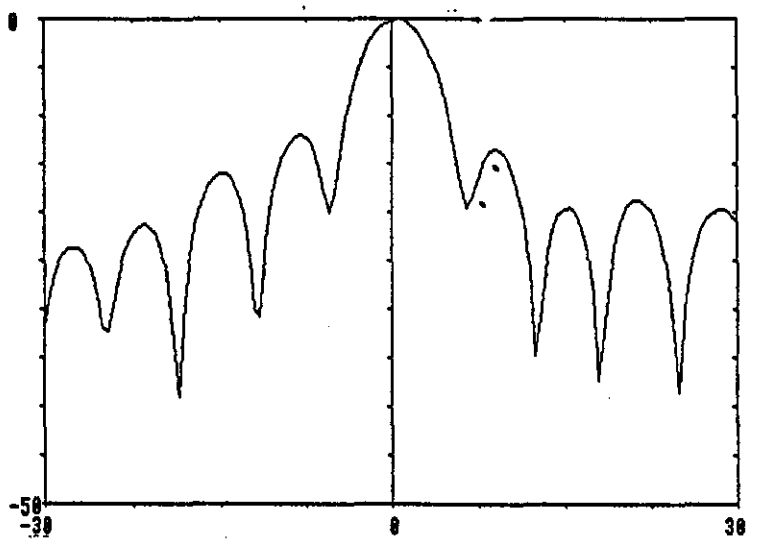

Beam-Plotter

Figure 4.41: Conventional Beamforming For Elements 3-12.

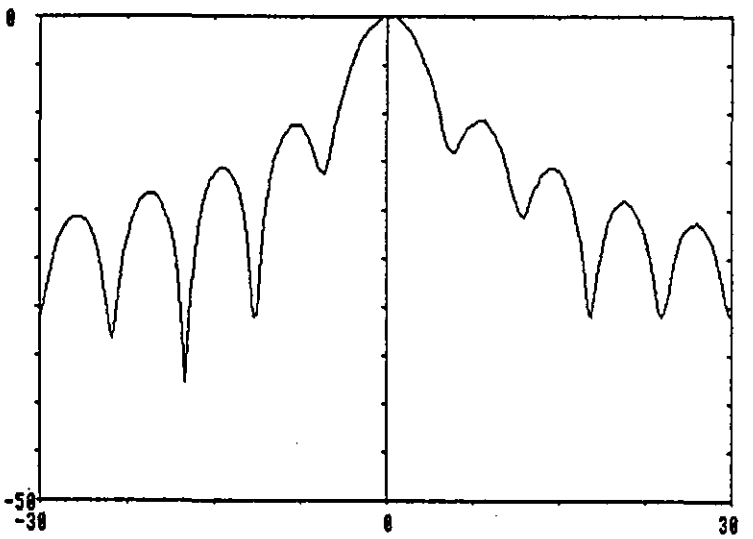

High Resolution System

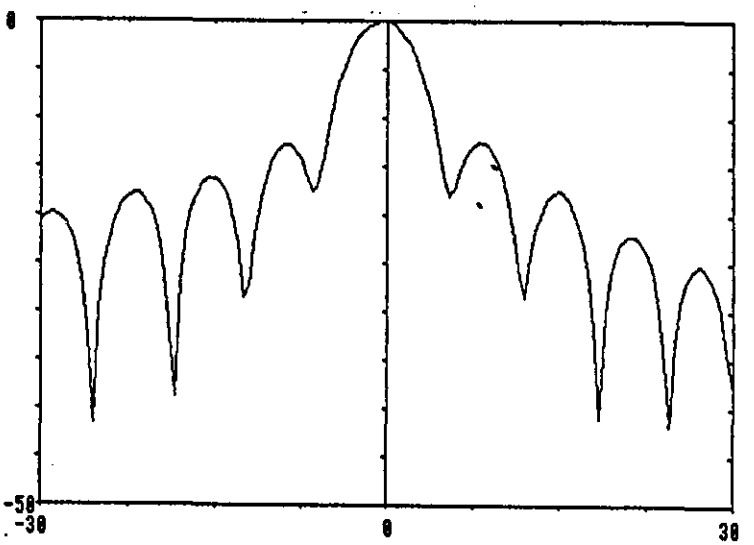

Beam-Plotter

Figure 4.42: Conventional Beamforming For Elements 4-13.

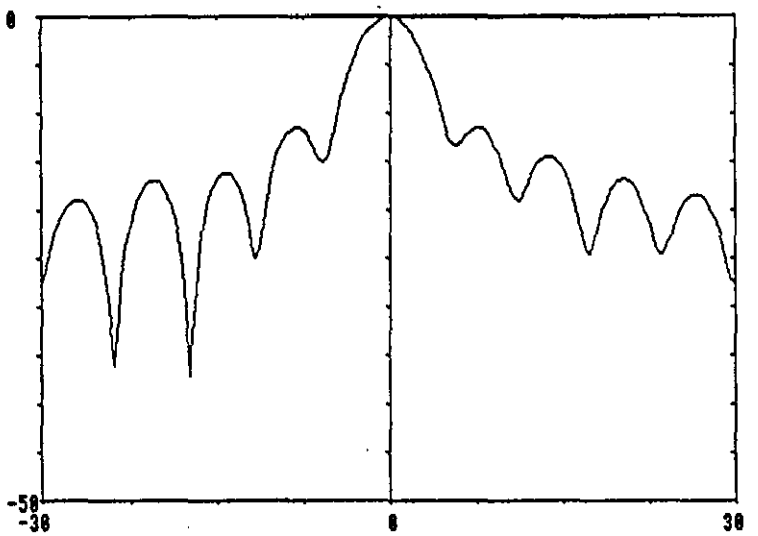

High Resolution System

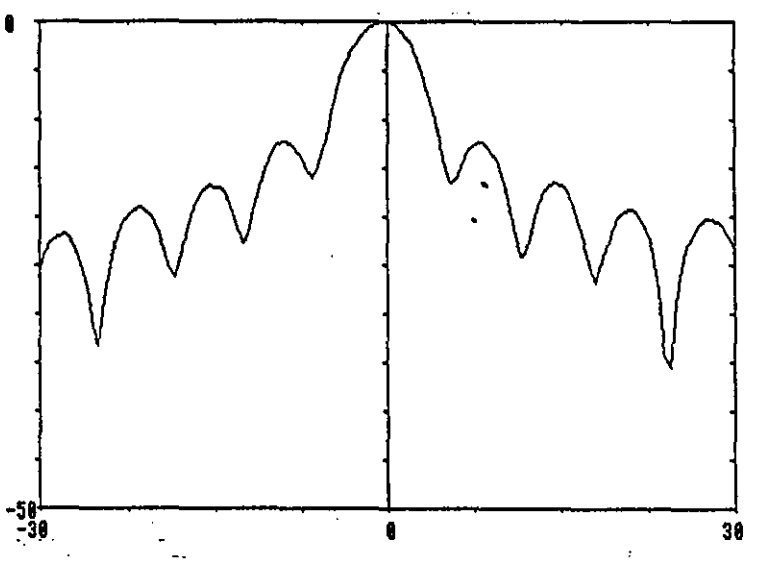

Beam-Plotter

Figure 4.43: Conventional Beamforming For Elements 5-14.

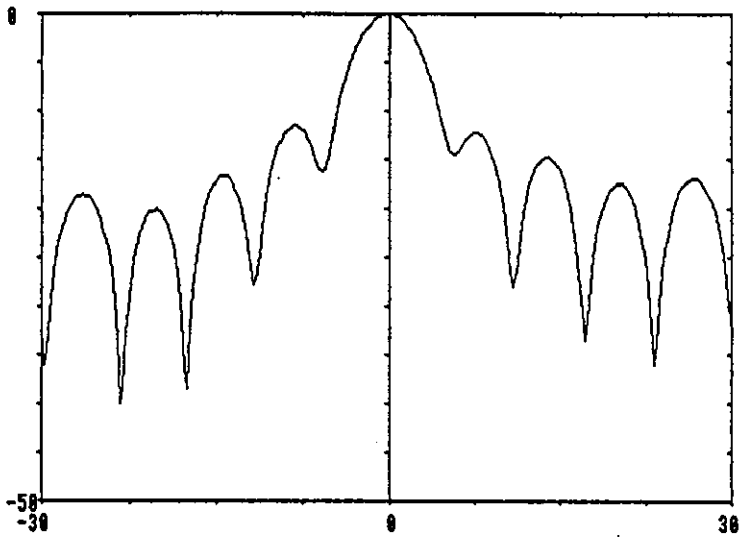

High Resolution System

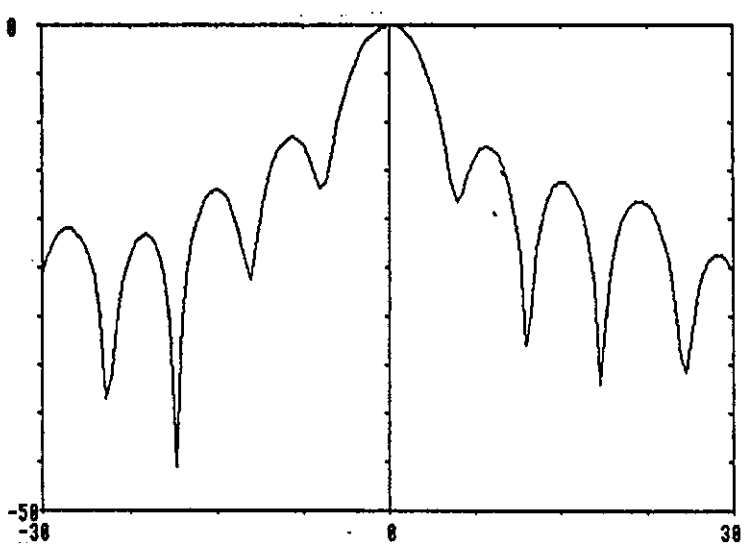

Beam-Plotter

Figure 4.44: Conventional Beamforming For Elements 6-15.

CHAPTER FIVE

PRACTICAL IMPLEMENTATION OF HIGH RESOLUTION ALGORITHMS IN THE WATER TANK AT LOUGHBOROUGH UNIVERSITY

5.1 INTRODUCTION:

The results of the initial tests of the High Resolution Sonar DF System, presented in the previous chapter, gave enough confidence to move on and carry out the practical implementation of the high resolution algorithms. Initially, it was decided to do some tests in the water tank at Loughborough University where the experimental environment is relatively controllable. The purpose of these experiments was to resolve two closely separated sources/targets using high resolution algorithms. The following high resolution methods were tested and compared to Conventional Beamforming:

1. Capon's Method.
2. MEM.
3. MUSIC.
4. MNM

Two sets of tests were carried out; one with two sources impinging on the receiving array (passive sonar) and the other with two passive targets illuminated by a pulse sent by the system (active sonar).

This chapter presents the details of these tests and their results which have been published in ref.(76).

5.2 DESCRIPTION OF THE DEPARTMENTAL WATER TANK:

The "Ultrasonics and Fluid Flow" laboratory (known as the 'Tank Room') is situated on the ground floor of the Department of Electronics and Electrical Engineering at Loughborough University of Technology. Its most prominent feature is a large water tank measuring 9m long x 5m wide x 2m deep and holds approximately 20,000 gallons of water. The walls and floor are smooth and flat and are built from concrete that has been covered in plaster and gloss painted. No attempt has been made to give the tank an acoustic lining.

The tank is flanked on three sides by benches with ample mains power protected by 'Earth Leakage Contact Breakers'.

Above the tank, at one end, are a pair of steel rails upon which are three carriages holding triangular steel towers. Equipment can be attached to the base of these towers, lowered to the correct depth and moved through the water parallel to the end wall.

Spanning the opposite end is a fixed gantry with a small moveable platform. This allows easy access to the steel tower when the transducers are being tested by the automatic beam pattern measurement system.

Finally, there is a large movable gantry that can be pushed into any position along the length of the tank between the steel rails and fixed gantry already discussed. This movable gantry contains a platform that can move across the tank, giving access to virtually any position within the tank.

The main limiting factor on work in the tank is the time delay between the arrival of the start of the desired signal, and that of any unwanted reflections. In general the most important of these reflections come from the water surface and from the floor of the tank. The dimensions involved are such that the maximum differential delay possible is only about 0.3 to 0.6 milliseconds. As a result, the minimum practical working frequency is about 10kHz.

5.3 THE SONAR EQUATION [Ref. 77, 78 and 79]:

Before going into the details of the experiments it is necessary to mention one of the fundamental problems in underwater acoustics; that is the detection of the wanted signal against unwanted background.

The wanted signal is the acoustic energy generated or reflected by the target. The unwanted background can be either:

a. Reverberation created by the generated sound within the water media.
b. Noise inherent in the transmission medium (ambient Noise).
   or
c. Noise associated with the equipment used for detection and the platform on which it is mounted (self noise).

Detection of a wanted signal against an unwanted background takes place when:

$$\frac{SIGNAL}{BACKGROUND} \geq Recognition \quad Differential$$

The Recognition Differential, some times called Detection Threshold, is defined as the signal-to-noise ratio necessary for a certain probability of detection. We require to be able to calculate the received signal for a given situation.

The many phenomena and effects peculiar to underwater acoustics produce a variety of quantitative effects which can be conveniently and logically grouped together in a small number of quantities called sonar parameters which, in turn are related by the sonar equations. These equations are the working relationships that tie together the effects of the medium, the target and the equipment.

The relationship of these quantities can be best illustrated by considering a simple active sonar system. We shall first derive an expression for the relationship between the various parameters and then discuss some of the parameters in more details.

A transmitter produces a source level of *SL* decibels reference to a standard distance of 1 m on its axis. When the radiated signal reaches the target, its level will be reduced by the transmission loss, and become *SL-TL*. On reflection or scattering by the target of target strength *TS*, the reflected signal will be

SL-TL+TS at a distance of 1 m from the acoustic centre of the target in the direction towards the source. In travelling back towards the source, the signal is again attenuated by the transmission loss and becomes *SL-2TL+TS.* This is the echo level at the transducer.

If the background is isotropic noise rather than reverberation, then the background noise level can be expressed as *NL.* This level is reduced by the directivity index of the transducer and the relative noise power becomes *NL-DI.* Since the axis of the transducer is pointing in the direction from which the echo is coming, the relative echo power is unaffected by the transducer directivity. The signal-to-noise ratio at the transducer therefore is:

$$SNR = SL - 2TL + TS - (NL - DI) \tag{5.1}$$

Some of these parameters will be discussed in more detail in the following section. Although the calculation for the received signal in a passive sonar case is rather different, it involves many of the same parameters.

5.3.1 The Source Level:

The source level is a measure, in dB reference to 1 micropascal (μPa), of the power flux ($Watt/m^2$) delivered into the water by a source and is always referred to standard range from the presumed acoustic centre of the source. Standard range is usually 1 metre. The acoustic centre is a convenient fiction which provides a starting location for loss calculations. At 1 metre, the acoustic centre is surrounded by a spherical envelope of radius $r=1m$ and area $4\pi r^2 = 12.6m^2$. If the source power output is P watts, and the source radiates equally strongly in all directions, then the source level at standard range is $P/12.6Wm^{-2}$. The relative acoustic level, denoted *SL* and measured in dB ref 1 μPa, is calculated as:

$$SL = 10\log_{10}\left(\frac{P/12.6}{reference \quad wave \quad intensity}\right) \tag{5.2}$$

The reference acoustic wave intensity is calculated from the formula

$$I = p^2/\rho c \tag{5.3}$$

where

p is the pressure,
ρ is the fluid density and
c is propagation velocity of wave.

The factor ρc is called the specific acoustic resistance of the fluid. For sea water, $\rho = 1000 kg/m^3$ and $c = 1500 m/s$, thus for a reference plane wave of rms pressure of $1\mu Pa$, the intensity is

$$I = \frac{(1\times10^{-6})^2}{1.5\times10^{6}}$$

$$= 0.67\times10^{-18} Wm^{-2} \quad ref. \quad to \quad 1\mu Pa. \tag{5.4}$$

Now substitute this value of the reference wave intensity in equation 5.2, we get

$$SL = 10\log_{10}\left(\frac{\mathrm{P}/12.6}{0.67\times10^{-18}}\right)$$

$$= 10\log_{10}\mathrm{P} + 170.8 \quad dB \quad ref. \quad to \quad 1\mu Pa. \tag{5.5}$$

5.3.2 The Directivity Index:

The above calculation of Source Level assumes omnidirectional spreading of sound from its acoustic centre. Often the source possesses some directional properties where more energy is transmitted along a specific direction. This causes the signal strength to increase by an amount referred to as the Directivity Index *(DI).*

The transmitting directivity index of a source is defined as the difference, measured at a point on the axis of the beampattern, between the level of sound generated by the source and the level that would be produced by a nondirectional source radiating the same total amount of acoustic power. If the intensity represented by the directional pattern along its axis is I_D, and if the intensity represented by the nondirectional pattern is I_{Nond}, then the transmitting directivity index is

$$DI = 10\log_{10}\frac{I_D}{I_{Nond}}. \tag{5.6}$$

For a circular source of area *'A'*, the transmitting directivity index is [ref. 80]

$$DI = 10\log_{10}\frac{4\pi A}{\lambda^2}. \tag{5.7}$$

Equation 5.5 for source level can be rewritten to include the directivity of the source, i.e.,

$$SL = 10\log_{10}\mathrm{P} + 170.8 + DI \quad dB \quad ref. \quad to \quad 1\mu Pa. \tag{5.8}$$

5.3.3 The Target Strength:

Target Strength *(TS)* of a reflecting body is usually measured in decibels and is defined as the ratio of the intensity of the sound returned by the target (at a distance of 1m from its acoustic centre in the same direction) to the incident intensity from a distant source. In symbols,

$$TS = 10\log\frac{I_r}{I_i}|_{r=1m} \tag{5.9}$$

where

I_r is the intensity of reflection at 1m and
I_i is the incident intensity.

The meaning of target strength can be shown by computing the target strength of a sphere, large compared to a wavelength, on the assumption that the sphere is an isotropic reflector; that is, it distributes its echo equally in all directions. Let a large, perfect, rigid sphere be insonified by a plane wave of sound of intensity I_i. If the sphere is of radius *'a'*, the power intercepted by it from the incident wave will be $\pi a^2 I_i$. On the assumption that the sphere reflects this power uniformly in all directions, the intensity of the reflected wave at a distant *'r'* metres from the sphere will be the ratio of this power to the area of a sphere of radius *'r'*, or

$$I_r = \frac{\pi a^2 I_i}{4\pi r^2}$$

$$= I_i \frac{a^2}{4r^2} \tag{5.10}$$

where I_i is the intensity of the reflection at range r. At the reference distance of 1metre, the ratio of the reflected intensity I_r to the incident intensity is

$$\frac{I_r}{I_i}|_{r=1m} = \frac{a^2}{4} \tag{5.11}$$

and the target strength of the sphere becomes

$$TS = 10\log_{10}\frac{I_r}{I_i}|_{r=1m}$$

$$= 10\log_{10}\frac{a^2}{4} \tag{5.12}$$

5.3.4 The Transmission Loss:

Transmission loss indicates the amount of weakening of the signal between a reference point and a point at a distance in the water. If I_0 is the intensity of sound at the reference point located 1m from the source and I_1 is the intensity at a distant point, then the transmission loss , *TL*, between the source and the distant point is defined as:

$$TL = 10\log_{10}\frac{I_0}{I_1} \quad dB \tag{5.13}$$

Transmission loss is the sum of two quantities, spreading and attenuation. Spreading loss is the geometrical effect representing the regular weakening of the signal as it spread outwards from the source to occupy a larger and larger

area and varies with the log of the range. Attenuation loss includes the effects due to absorption, scattering and leakages out of the sound channel and varies linearly with range.

5.3.4.1 TRANSMISSION LOSS DUE TO SPREADING

Spherical Spreading:

Consider a small source in a homogeneous, unbounded and lossless medium, as shown on figure 5.1a. The power generated by the source is radiated equally in all directions, so as to be equally distributed over the surface of a sphere surrounding the source. Since there is no loss in medium, the power crossing all such spheres must be the same. The sound intensity, *'I'* at a radial distance *'R'*, from the source, 'S', of power 'P' is:

$$I = \mathrm{P}/4\pi^2 \tag{5.14}$$

If $R_1 = 1m$ and substituting equation 5.14 into equation 5.13 for *I*, the transmission loss at range R_2 is:

$$TL = 10\log_{10}(R_2^2)$$

$$= 20\log_{10}(R_2) \tag{5.15}$$

Cylindrical Spreading:

When the medium is bounded by a parallel upper and lower limits (as the shallow part of the sea is by the surface and bottom), the spreading is no longer spherical as illustrated in figure 5.1b. Beyond a certain range the power radiated by the source is distributed over the surface of the cylinder. The intensity at radial distance *R* from the source is now:

$$I = \frac{\mathrm{P}}{2\pi R H} \tag{5.16}$$

where H is the sea depth.

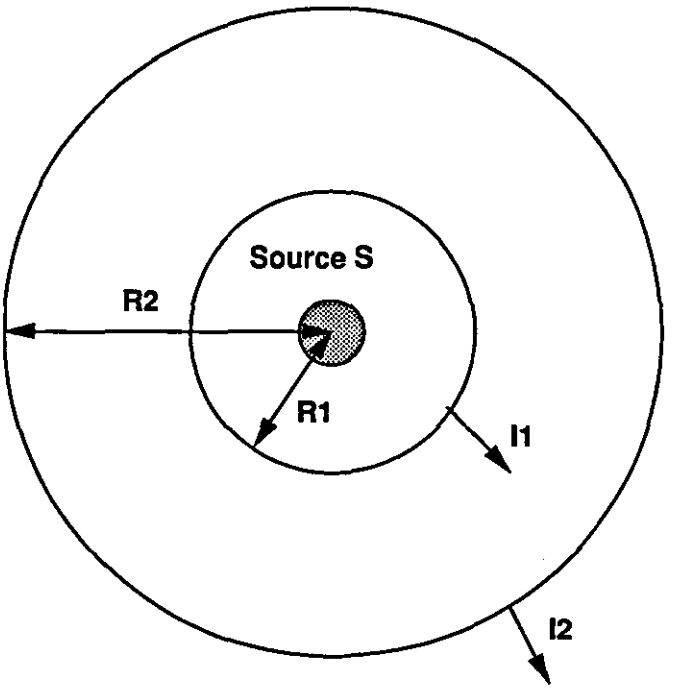

Figure 5-1a: Spherical Spreading in an Unbounded Medium.

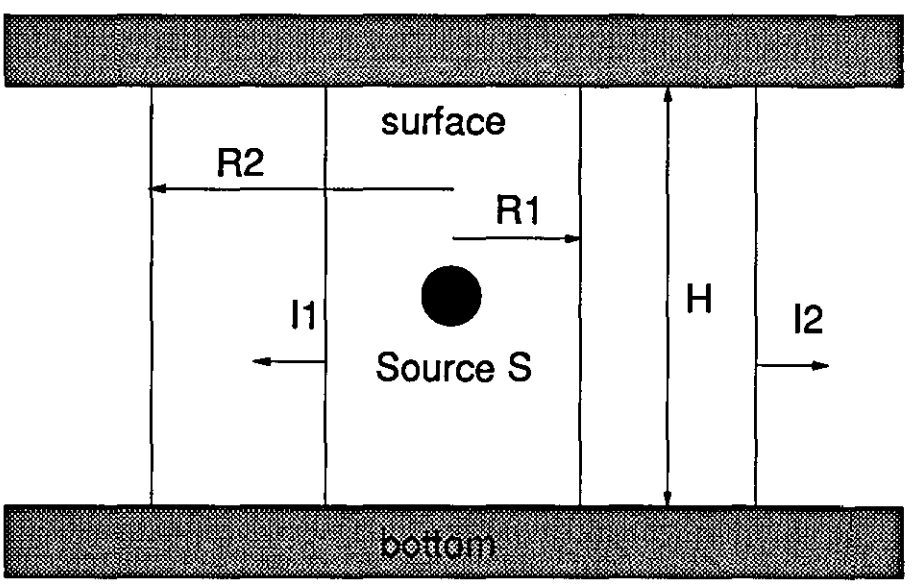

Figure 5-1b: Cylindrical Spreading in Shallow water.

The transmission loss now depends on both *R* and *H*.

5.3.4.2 TRANSMISSION LOSS DUE TO ABSORPTION:

Absorption is the loss in signal energy due to the conversion of acoustic energy into heat as the signal travels through the water. The absorption loss is a function of frequency of the signal, the salinity and depth of water.

Taking into account the absorption loss, the expression for transmission loss with spherical spreading now becomes:

$$TL = 20.\log(R) + \alpha R \qquad (5.17)$$

where α is the coefficient of absorption in dB/m.

5.4 SYSTEM SOFTWARE AND OPERATION:

The system software was split between the transputers and the BBC. The transputer software was written in OCCAM-2 while the BBC software was written in BASIC. The whole system software can be divided into three main parts:

a. Data Collection.
b. Data processing.
c. Results display.

In the following sections detailed descriptions of these parts are presented.

5.4.1 The Data Collection:

This is the first part of the system software. At the beginning of this part, the master transputer displays a message on the PC monitor asking the user to enter some parameters. These parameters include the number of elements, number of snapshots, range, repetition time of the transmitted pulses and the spectrum step angle. These user parameters are used in the subsequent steps of the system software. While entering the user parameters, the BBC is waiting for a command from the master transputer.

When the user finishes entering the parameters, the master transputer will pass some of them to the BBC while it calculates the array manifold (steering vectors). After that, the master transputer will instruct the BBC to start the data collection phase. The BBC will respond by initiating a transmit pulse and will start collecting the data received from the array elements and store them in the buffer memory. After collecting a programmed number of samples, the master transputer takes control over the buffer memory and starts extracting the 'I' and 'Q' values of the respective channels using the user range information. These values will corresponds to single snapshot. This process is repeated for the number of snapshots specified by the user.

5.4.2 The Data Processing:

All the data processing procedures are handled by transputers. The master T414 transputer forms the data matrix and passes it, together with the array manifold, to the T800 transputer for further processing. Depending on the algorithm to be implemented, the T800 processes the data matrix and produces the respective angular spectrums using the processes defined in chapter 3. The resulting angular spectrums are sent back to the master transputer through a pre-specified link channel.

5.4.3 The Result Display:

Before transferring the resulting spectrum to the BBC for display, the master transputer normalizes the data of the spectrum and converts it to INTEGER16 data type. This data type is easier and faster to transfer across the INMOS link than the REAL32 data type.

At the BBC side, the system displays the received spectrum using a simple graphics routine written in BASIC. Then the BBC asks the user whether the user wants to produce a hard copy of the spectrum on the printer or to file the results on a floppy disk. Otherwise the user will be asked to press the RETURN key to start collecting a new data block and generating a new spectrum.

5.5 PASSIVE SONAR TESTS:

In these tests two sources, placed close to each other, were transmitting pulses simultaneously towards the 40kHz receiving array located 4.5m in front of the sources. The purpose of the tests was to try to resolve the two sources using some of the well known high resolution algorithms. The details of these tests are presented below.

5.5.1 The Experimental Set-up:

Figure 5.2 shows the experimental set-up for the passive sonar tests. The 40kHz receiving array was mounted on a motor controlled pan-and-tilt unit which was fixed on one end of a 2m cylindrical post. The other end of the post was attached to a special mechanical holding system that allows moving the post, and its attachments, up and down. This facility helps in positioning the array at the right depth in the water. The post can be locked in the required position by a special key. The whole system was fixed on a moving trolley that can be moved across the tank on two channel rails.

Because of the limited size of the water tank, the signals reflected from the water surface and the tank bottom arrive very early and may mix with the real signal coming directly from the source. To avoid this, we used two 4-element block arrays, mounted vertically, to represent the two sources. These blocks have approximate main beamwidth of 13° and that helps to avoid hitting the surface and bottom. The sidelobes still cause reflected signals but their strength is much less than the direct beam.

The four elements of each block were connected together and fed a signal for transmission. To avoid full correlation between the two sources, an external circuit was added to the system to generate two signals with slightly different frequencies (40kHz and 39kHz), each connected to one of the array blocks. This circuit was driven by the original system pulse. The amplitude of the two generated signals was adjusted to $20V_{P\text{-}P}$. However, because the two blocks have different impedances, the generated signal intensities in the water were different.

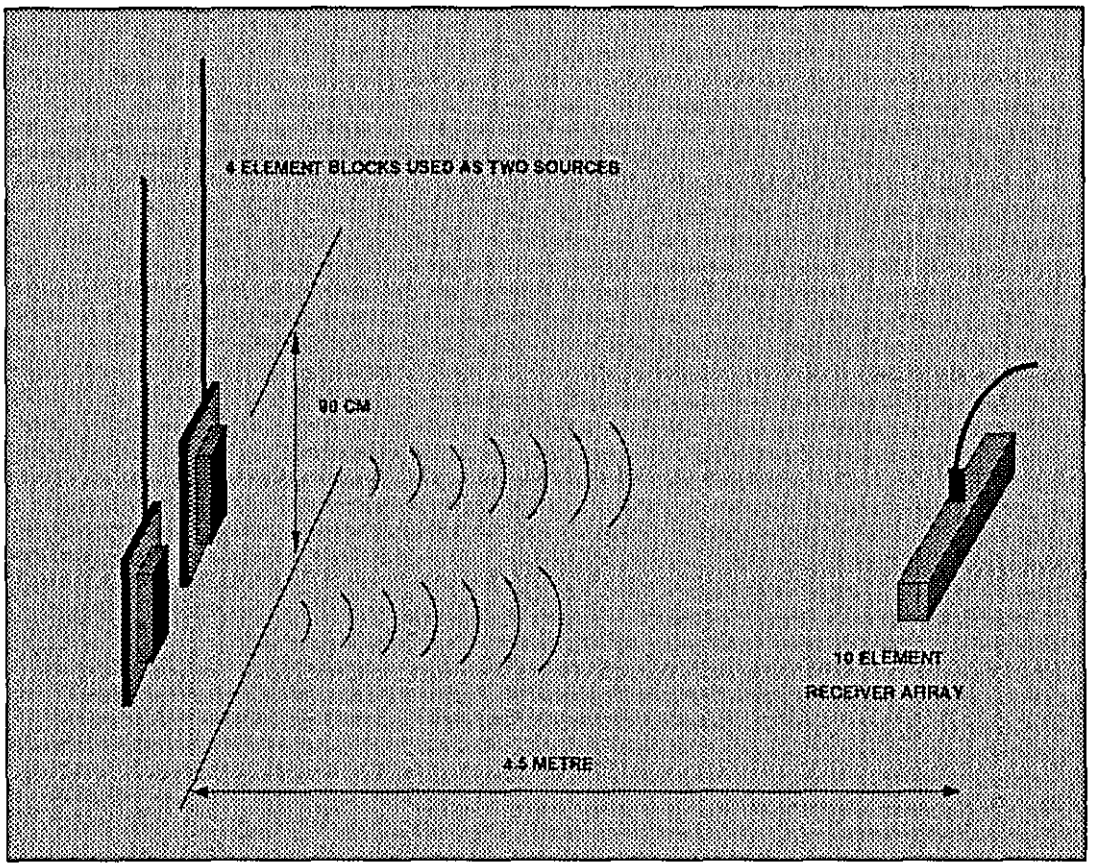

Figure 5-2: The Experimental Set-up For Passive Sonar Tests.

The two blocks were fixed on wooden posts and deployed in the water at a distance of 4.5m from the receiving array. The two posts were held by two separate mechanical holders which allowed the posts to be moved up or down, forward or backward and to the left or to the right. They also allowed rotation of the posts to change transducer orientation. The relative distance between the two posts could therefore be adjusted easily and accurately and it was set so that the two sources were located within the beamwidth of the receiving array. The two mechanical holders were fixed on a moving trolley that could be moved along and across the water tank.

5.5.2 Calculation of The Expected Signal Level:

Before carrying out the experiments it is always very useful to calculate the expected level of the received signal. These calculations helped in deciding whether or not power amplifiers at the transmit side, and/or preamplifiers at the receive side were needed.

Although the sonar equations derived in section 5.3 were discussed for an active system, many of the parameters are applicable for a passive system where the signal travels in one direction only. Therefore equation 5.1 can modified to represent our set-up as:

$$RL = SL - TL \tag{5.18}$$

where *RL* is the received signal level,
SL is the source level and
TL is the transmission loss.

In the following, the calculation of the above parameters in presented.

Source Level

The Source Level defined in equation 5.8 can be rewritten as:

$$SL = 10\log_{10}(P_{ele}.\eta) + 170.8 + DI \quad dB \quad ref. \quad to \quad 1\mu Pa \tag{5.19}$$

where

P_{ele} is the electrical power,

η is the transducer efficiency and

DI is the Directive Index defined by equation 5.7.

For the 40kHz, 4 element transmitting array, the element radius is 0.037m and λ is 0.0375m, therefore the directivity of a single element is

$$DI = 10\log_{10}\frac{4\pi A}{\lambda^2}$$

$$= 10\log_{10}(9.608)$$

$$= 9.826 \quad dB$$

Since there are 4 elements in the array, then

$$DI = 9.826 + 10\log_{10}(4)$$

$$= 15.85 \quad dB.$$

Substitute this value for DI in equation 5.20 we get:

$$SL = 10\log_{10}(P_{ele}\eta) + 170.8 + 15.85$$

$$= 10\log_{10}(P_{ele}\eta) + 186.65.$$

Assume the efficiency is 60% then:

$$SL = 10\log_{10}P_{ele} + 10\log_{10}(0.6) + 186.65$$

$$= 10\log_{10}P_{ele} + 184.43. \qquad (5.20)$$

Now since

$$P_{ele} = V_t^2/R_{eq}$$

where

V_t is the transmitted voltage and

R_{eq} is the equivalent resistance of the array,

then equation 5.21 can written as:

$$SL = 20\log_{10}(V_t) - 10\log_{10}(R_{eq}) + 184.43.$$

The equivalent resistance of the array is 550Ω, therefore

$$SL = 20\log_{10}(V_t) - 10\log_{10}(550) + 184.43$$

$$= 20\log_{10} V_t + 157 \quad dB \quad ref \quad 1\mu Pa. \tag{5.21}$$

Transmission Loss

The Transmission Loss for passive systems (single path) is calculated as (neglecting the absorption loss):

$$TL = 20\log_{10} R$$

where *R* is the distance between the source and the receiver. In our experiments, this distance was set to be 4.5m. Therefore:

$$TL = 20\log_{10}(4.5)$$

$$= 13.06dB.$$

Calculation of the expected level of the received echo:

Substituting the values of *SL* and *TL* in equation 5.19 we get:

$$20\log\left(\frac{V_r}{ReceiverSensitivity}\right) = 20\log V_t + 157 - 13.06$$

$$= 20\log V_t + 143.94$$

or

$$20\log\left(\frac{V_r}{V_t}\right) = 143.97 + ReceiverSensitivity(in\ dB)$$

The receiver sensitivity is -184 dB ref. 1V/μPa [ref. 75], therefore:

$$20\log\left(\frac{V_r}{V_t}\right) = 143.97 - 184$$

$$= -40 \quad dB.$$

For a $20V_{P\text{-}P}$ transmitted voltage, V_r is expected to be $0.2V_{P\text{-}P}$.

This signal level was quite enough and there was no need neither to use a power amplifier on the transmitter nor preamplifiers on the receiver.

5.5.3 RESULTS:

After setting the system up, a series of tests were carried out to resolve two sources placed within the beamwidth of the receiving array and at a distance of 4.5m. Ten elements of the receiving array were used and the number of snapshots considered was also 10.

The sector to be searched was between -25° and +25° with a scanning step angle of one degree. The resulting spectrums were either printed directly from the BBC screen, or stored on data files by the BBC microcomputer and printed later.

The first test carried out was to locate the position of each source individually. This was done by alternatively switching one source off and using the CBF to locate the other source. Figure 5.3 shows the result of this test which indicates that the two sources were located at -14° and -9° directions respectively and separated by 5 degrees. This means that the two sources were separated by less than the beam width of the receiving array which is 5.5 degree.

Figure 5-4 shows the angular spectrum of the CBF when the two sources were switched on. It is clear that the CBF failed to resolve the two sources.

The system was then used to locate the positions of the two sources using four of the most well known high resolution algorithms. Figures 5.5-5.8 show the results of these experiments. Two sets of results are presented for each method.

Figure 5.5 shows the result of using Capon's method. Clearly, the two sources have now been resolved. However, it was noticed that there are two little extra peaks in the spectrum which were fairly consistent. This was looked at and the explanation we came out with was that since these peaks appeared in roughly the mirror image positions of the actual sources, they might be caused by the way that the steering vectors were calculated. The calculations of these vectors assumed that the arrived wave is completely plane which, in our experiment at 4.5m range, was not exactly true.

Figure 5.6 shows the angular spectrum of the MEM method. As was expected, the angular spectrum of this method is not very smooth and it contains many spikes. On the other hand its resolution is obviously better than CBF method and its computation time is much less than Capon's method.

Figure 5.7 shows the angular spectrum of the MUSIC method. The performance of this algorithm was superb and the background of the spectrum is very smooth. However, it was noticed that for some data sets the algorithm failed while Capon's method produced good results. This behaviour, which has also been noticed by other researchers, needs more investigations.

Finally, the results of using the MNM method are presented in figure 5.8. The resolution of this method is very similar to that of the MUSIC algorithm but the background is not as smooth as that of the MUSIC method.

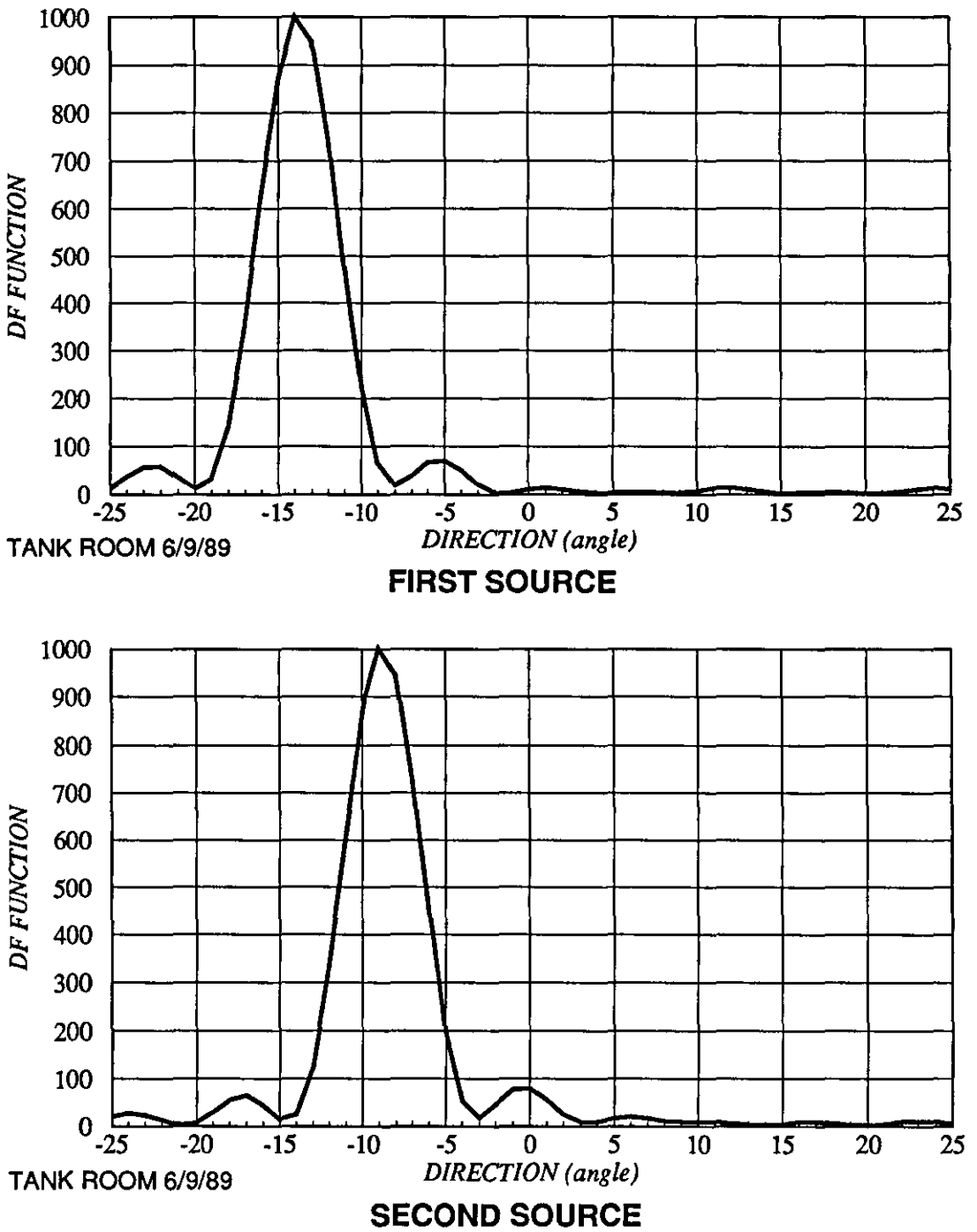

Figure 5-3: Locating The Position of Each Source Individually Using CBF.

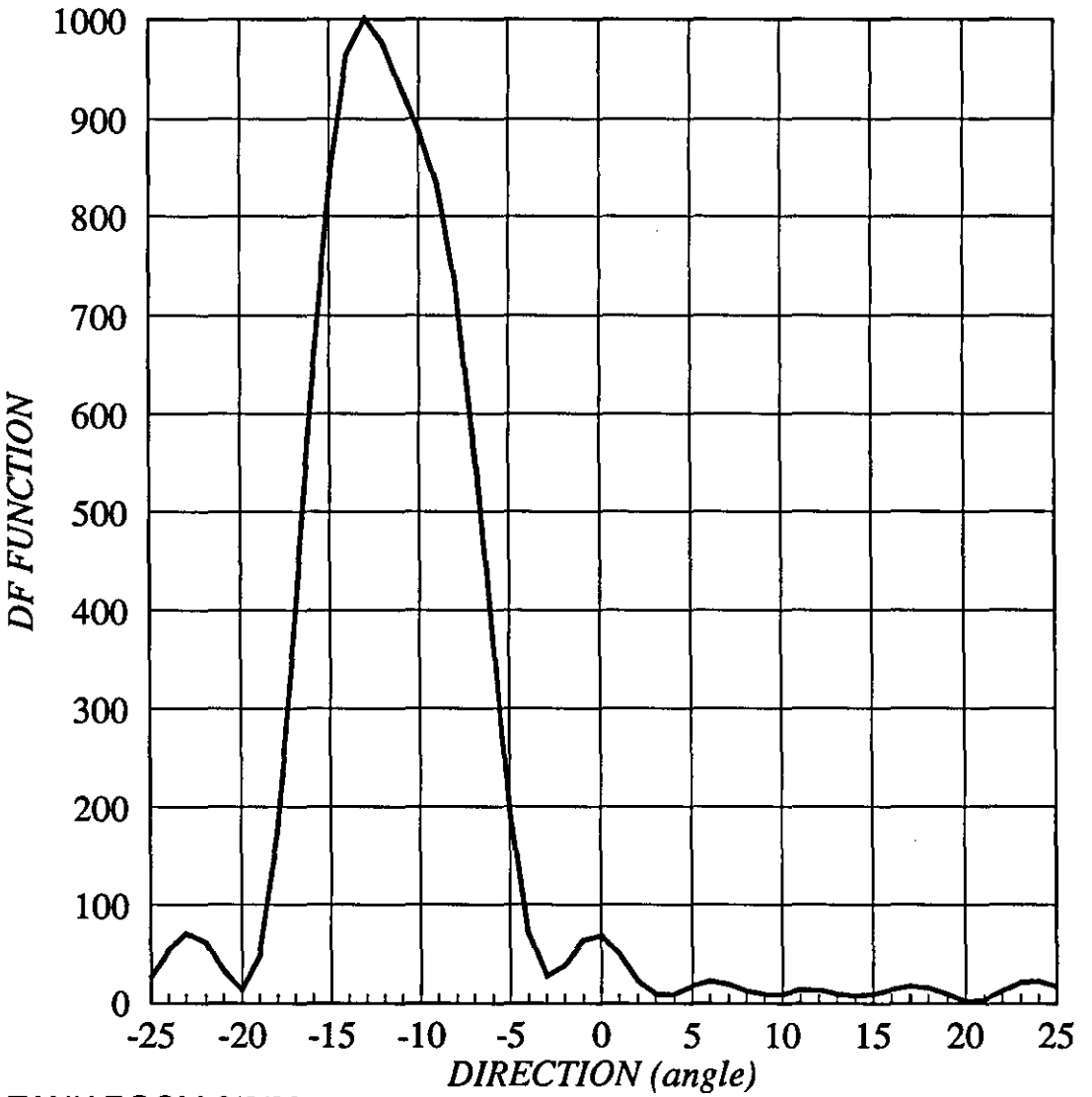

Figure 5-4: Angular Spectrum of CBF For The Two Sources.

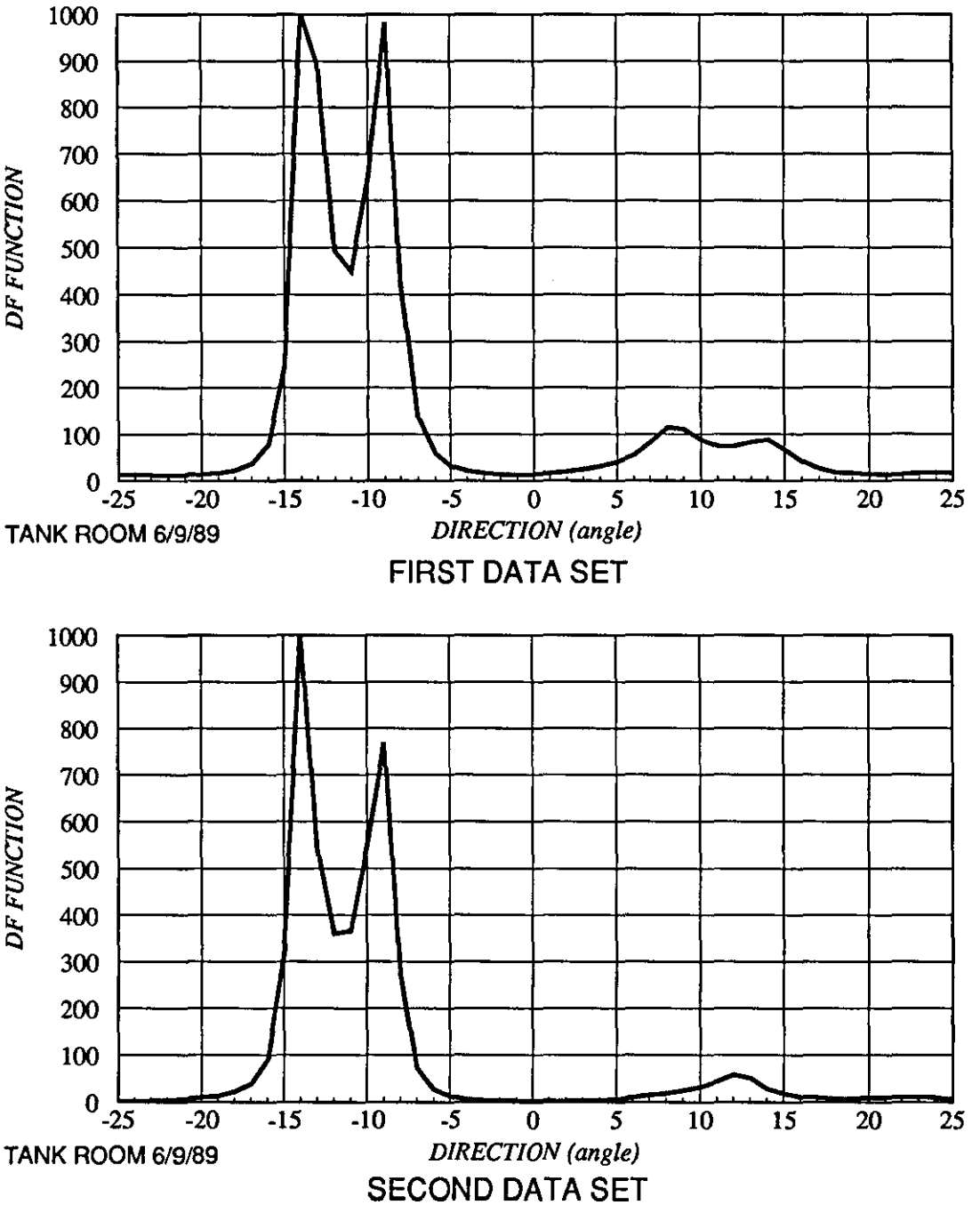

Figure 5-5: Angular Spectrum of Capon's Method.

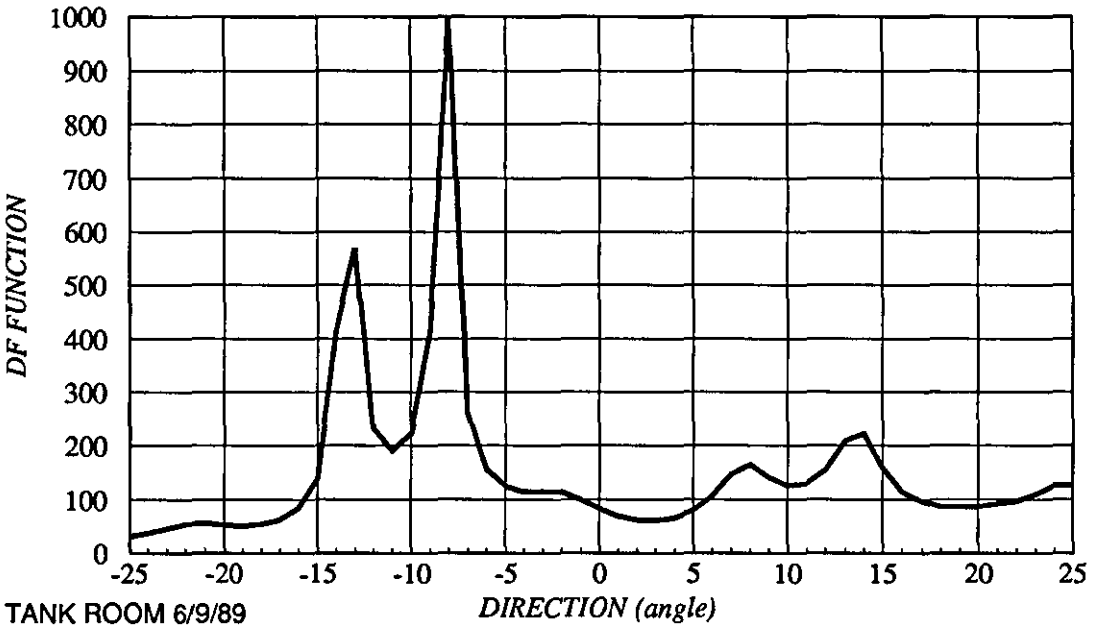

FIRST DATA SET

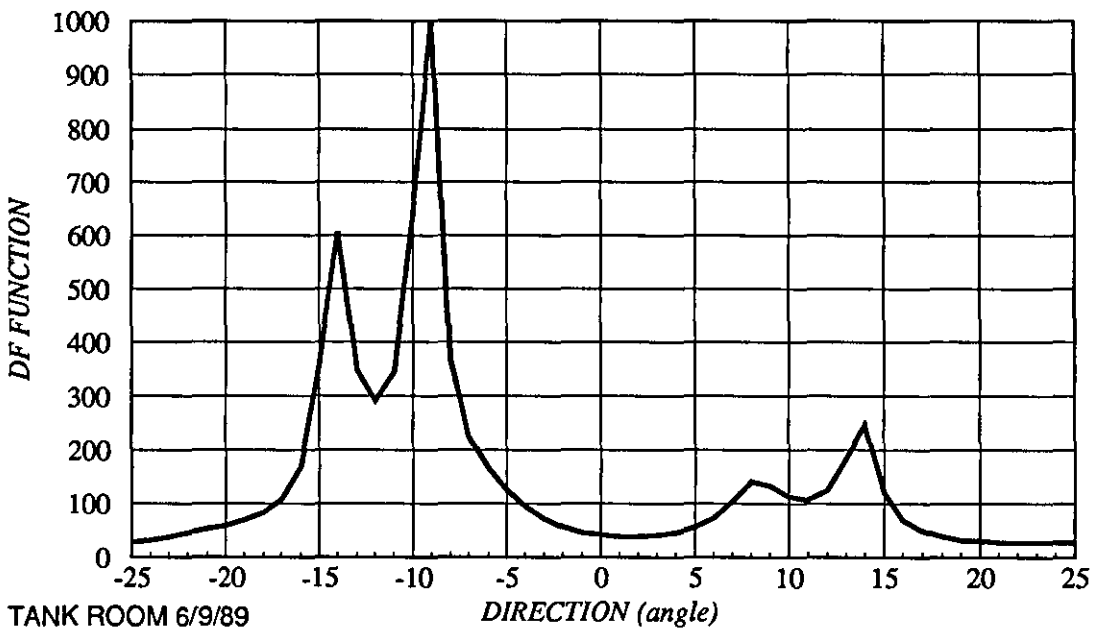

SECOND DATA SET

Figure 5-6: Angular Spectrum of MEM.

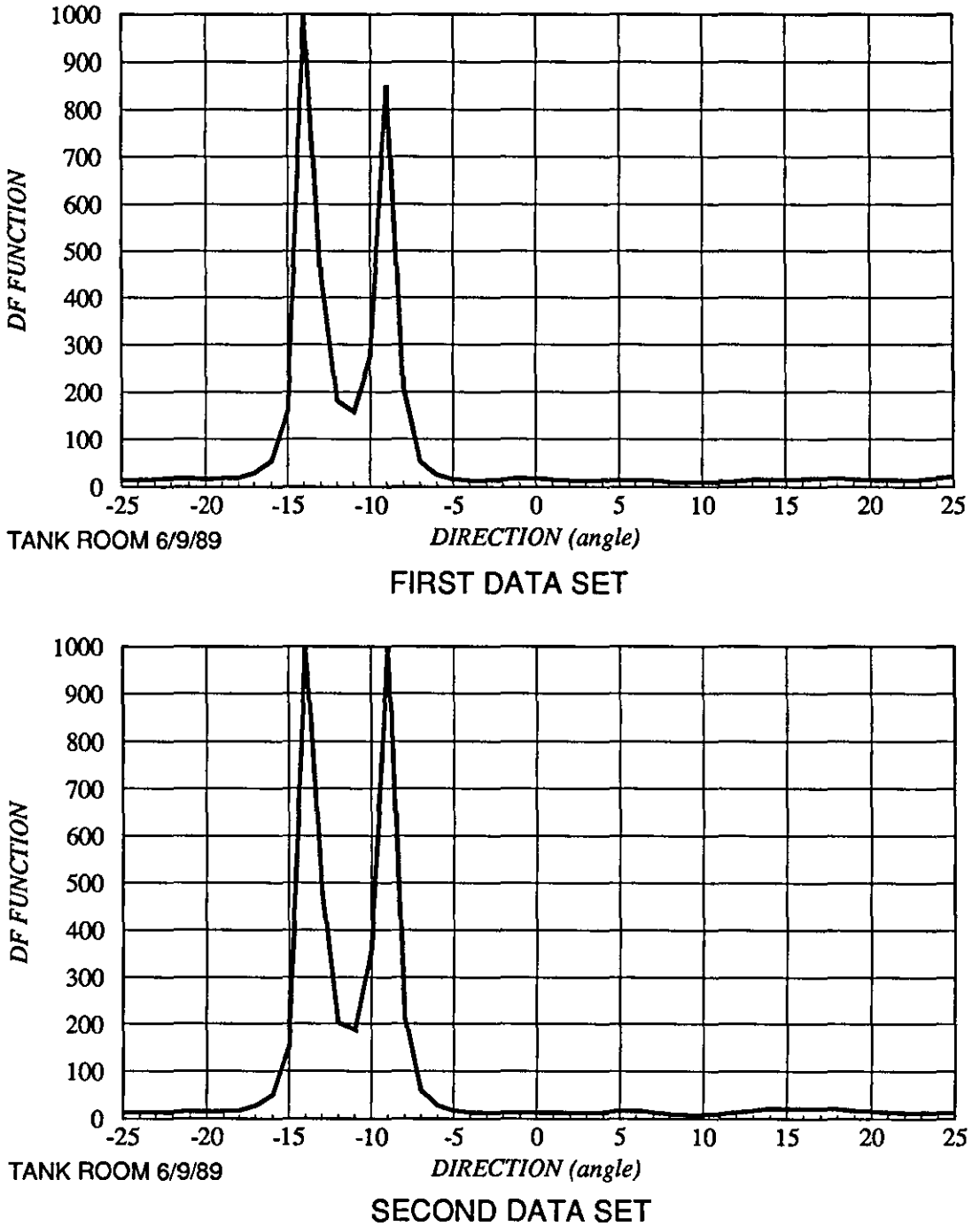

Figure 5-7: Angular Spectrum of MUSIC.

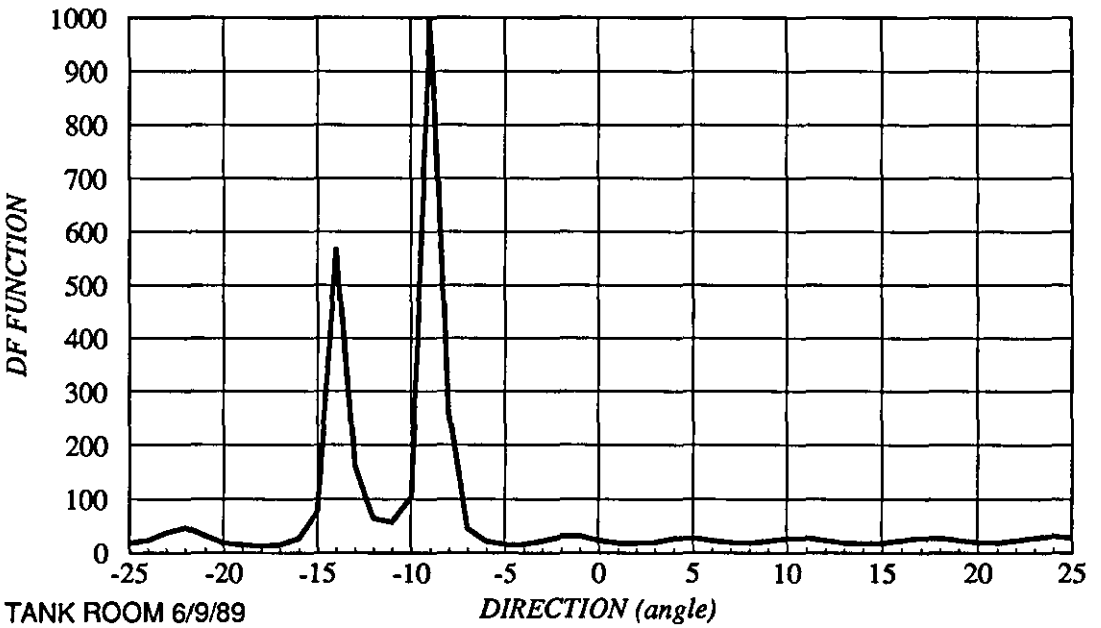

FIRST DATA SET

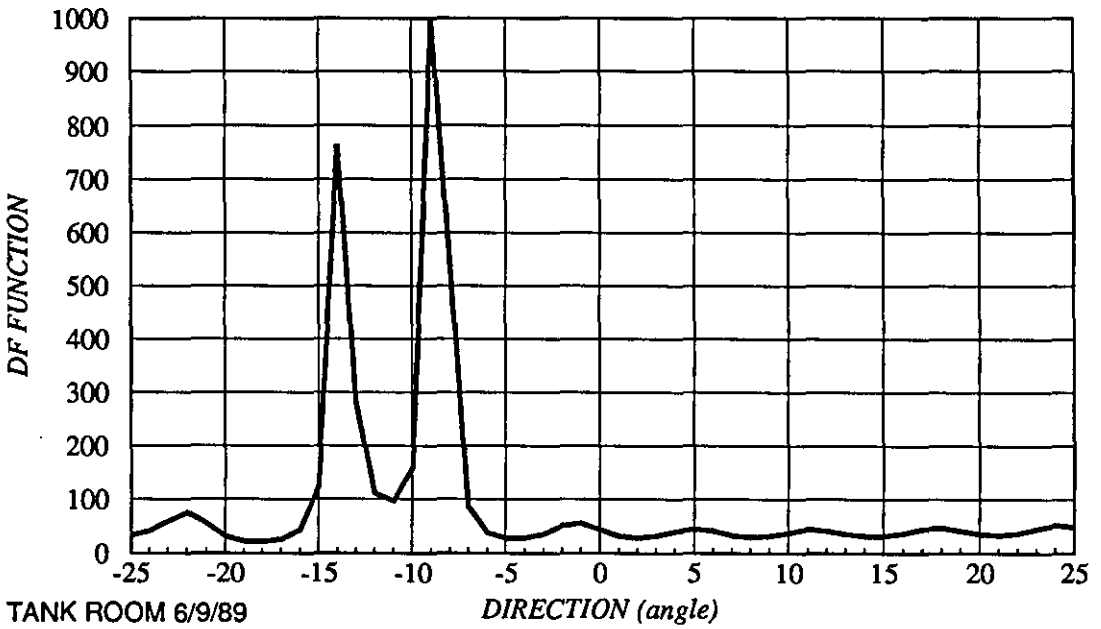

SECOND DATA SET

Figure 5-8: Angular Spectrum of MNM.

5.6 ACTIVE SONAR TESTS:

After carrying out the passive sonar experiments, we moved to a more difficult situation where the two targets to be resolved were passive and they needed an active sonar system to illuminate them. The targets used in these tests were two spheres of diameter 25cm. In the following the details of these tests are presented.

5.6.1 The Experimental Set-up:

Figure 5.9 shows the experimental set-up for the active sonar tests. The 40kHz receiving array was mounted in the same way as that described in the experimental set-up for passive sonar tests. However, another array was used as a transmitter. Initially, a four element array was fixed vertically above the receiving array and used as a transmitter. The four elements of this array were joined together and connected to the output of a power amplifier fed by the transmit pulse generated by the system. This configuration gave a 13° beamwidth which was used to illuminate the targets. However, this was not enough to reduce the effects of reverberation to a satisfactory level and we had to replace the 4-element array with a 15-element array to give a narrower beam, thus reducing the effects of the reverberations. The 15-element array was mounted vertically on a separate triangular tower and deployed in the water next to the receiving array.

The two targets were represented by two 25cm diameter spheres. Each sphere was held by a fin net tied to a heavy metal sheet which rested on the bottom of the tank. A long rope was tied to each metal sheet by a small hook. These ropes enabled pulling the metal sheets and moving the targets to the required positions.

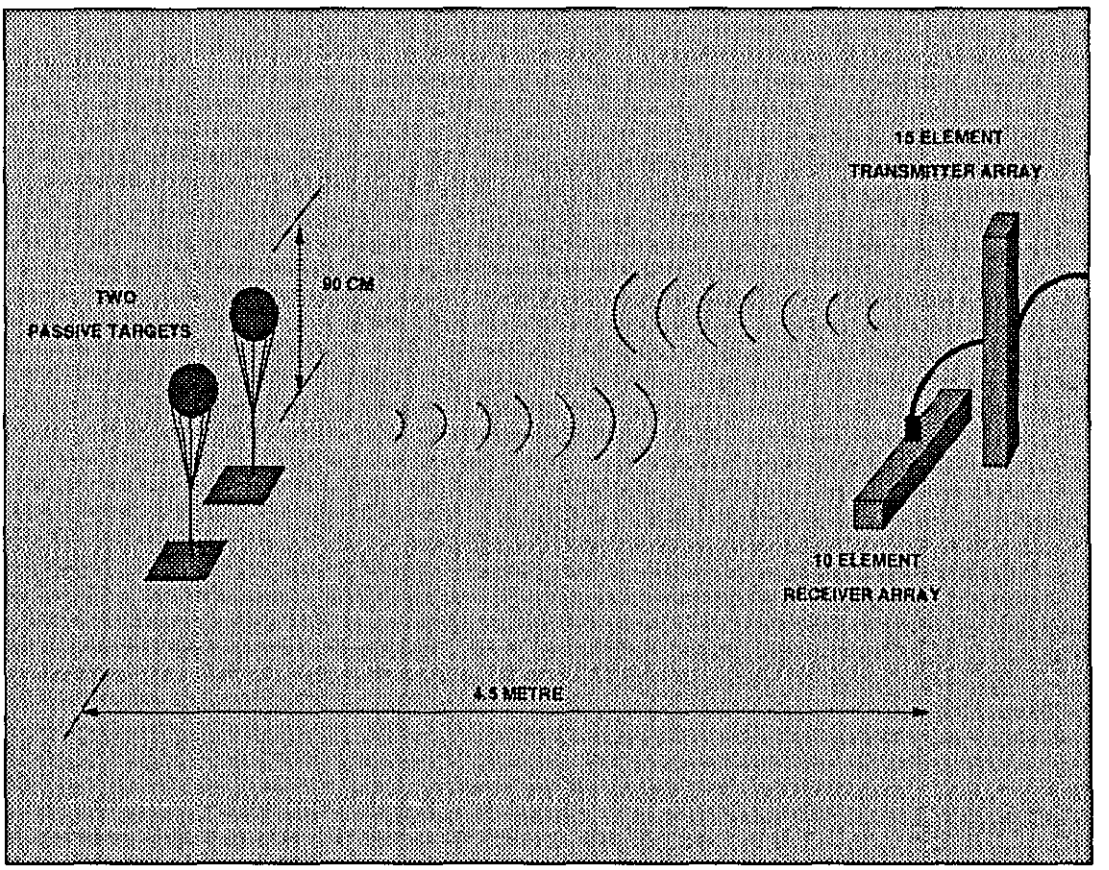

Figure 5-9: The Experimental Set-up For Active Sonar Tests.

5.6.2 Calculation of The Expected Signal Level:

As before, the expected level of the received signal was calculated before starting the experiments. The sonar equation that represents the active sonar set-up was described in equation 5.1. The parameters of this equation are calculated below:

Source Level

The Directivity Index, defined in equation 5.7, can be recalculated for the 15 element array as:

$$DI = 9.826 + 10\log_{10}(15)$$

$$= 21.59 \quad dB.$$

Substituting this value for *DI* in equation 5.20 we get:

$$SL = 10\log_{10}(P_{ele}.\eta) + 192.39 \quad dB \quad ref. \quad to \quad 1\mu Pa.$$

Assume the efficiency is 60%, then;

$$SL = 10\log_{10}(P_{ele}) - 190.17 \quad dB \quad ref. \quad to \quad 1\mu Pa$$

or

$$SL = 20\log_{10}(V_t) - 10\log_{10}(R_{eq}) + 190.17.$$

The equivalent resistance of the 15 element array is 133Ω, therefore

$$SL = 20\log_{10}(V_t) - 10\log_{10}(133) + 190.17$$

$$= 20\log_{10}(V_t) + 168.93 \quad dB \quad ref. \quad to \quad 1\mu Pa.$$

Transmission Loss:

The Transmission Loss for active systems is double that of passive systems because of the double path of transmission, therefore:

$$TL = 40\log R.$$

In these experiments, the range was set to 4.5m. Therefore:

$$TL = 40\log 4.5$$

$$= 26.13dB.$$

Target Strength:

The Target Strength of a sphere of diameter 25cm is:

$$TS = 10\log\frac{a^2}{4}$$

$$= -24.08dB.$$

Calculation of Sonar Equation:

Substituting the values of SL, TL and TS in equation 5.1 we get:

$$20\log\left(\frac{V_r}{Receiver Sensitivity}\right) = 20\log V_t + 168.93 - 26.13 - 24.08$$

$$= 20\log V_t + 118.72$$

or

$$20\log\left(\frac{V_r}{V_t}\right) = 118.72 + Receiver Sensitivity (in\ dB).$$

The receiver sensitivity is -184 dB ref 1V/μPa, therefore:

$$20\log\left(\frac{V_r}{V_t}\right) = 118.72 - 184$$

$$= -65.28dB$$

A power amplifier with a maximum output of 180 V_{P-P} was used at the transmit side. At the receive side, V_r was expected to be 0.05 V.

5.6.3 RESULTS:

The first test carried out was to move a single target across the sector to different positions and to detect its location by the CBF. Figure 5-10 shows six sets of results which corresponds to six locations of single passive target.

The next test was to position two passive targets and to try to locate them using the high resolution algorithms. In these tests the CBF (shown as dotted plot in the spectrum) was also calculated for each high resolution spectrum.

Figure 5.11 shows the result of using Capon's method. The first two sets of results showed that the two targets were separated by about 6degree and in these cases the CBF showed some signs of resolving the two targets. On the other hand, Capon's method resolved the two targets very clearly although it produced, in the first data set, a small peak at direction -6°. This might have been caused by some reflected signals.

In the other two data sets, the two targets were brought closer to each other and the results of these tests showed that the CBF completely failed to resolve the two targets while Capon's method was still able to resolve them very clearly.

Figure 5.12 shows the angular spectrum of the MEM method for two sets of data. As in the results of the passive tests, the angular spectrum of this method was spiky although it did resolve the two targets while the CBF failed completely.

Figure 5.13 shows the angular spectrum of MUSIC method for two sets of data. Again, the CBF failed to resolve the two targets while MUSIC succeeded. There are some differences in the positions of the two targets between the two data sets which may have been caused by slight movements of the spheres.

Finally, the results of using the MNM method are presented in figure 5.14 for two data sets. The resolution of this method was high and very similar to the MUSIC. Like the other high resolution algorithms, the MNM resolved the two targets while the CBF failed.

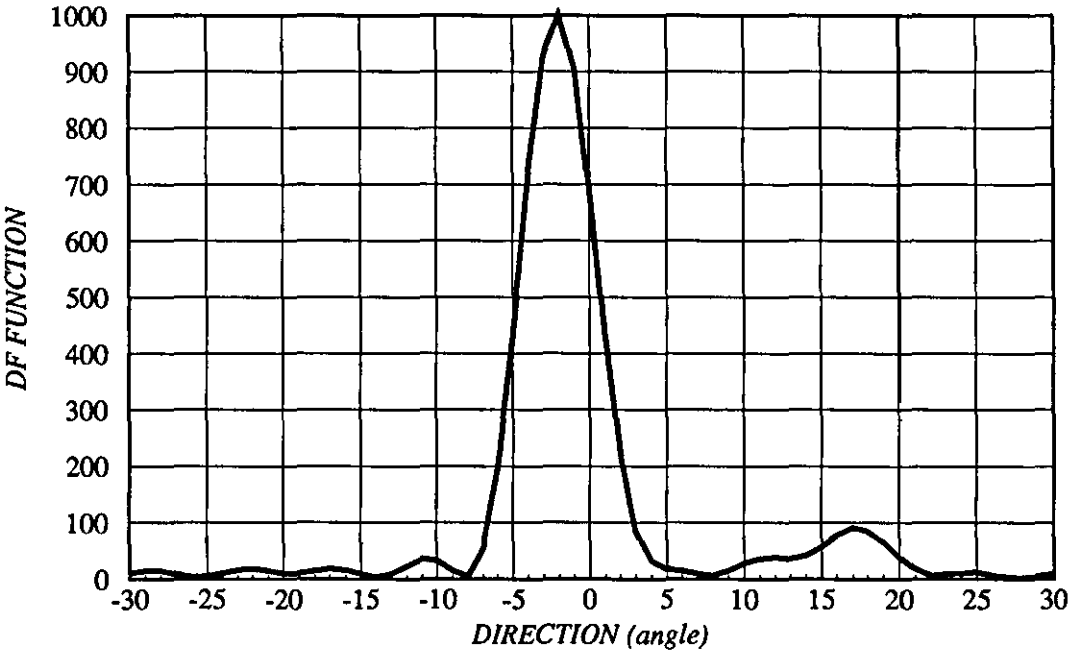

Position 1

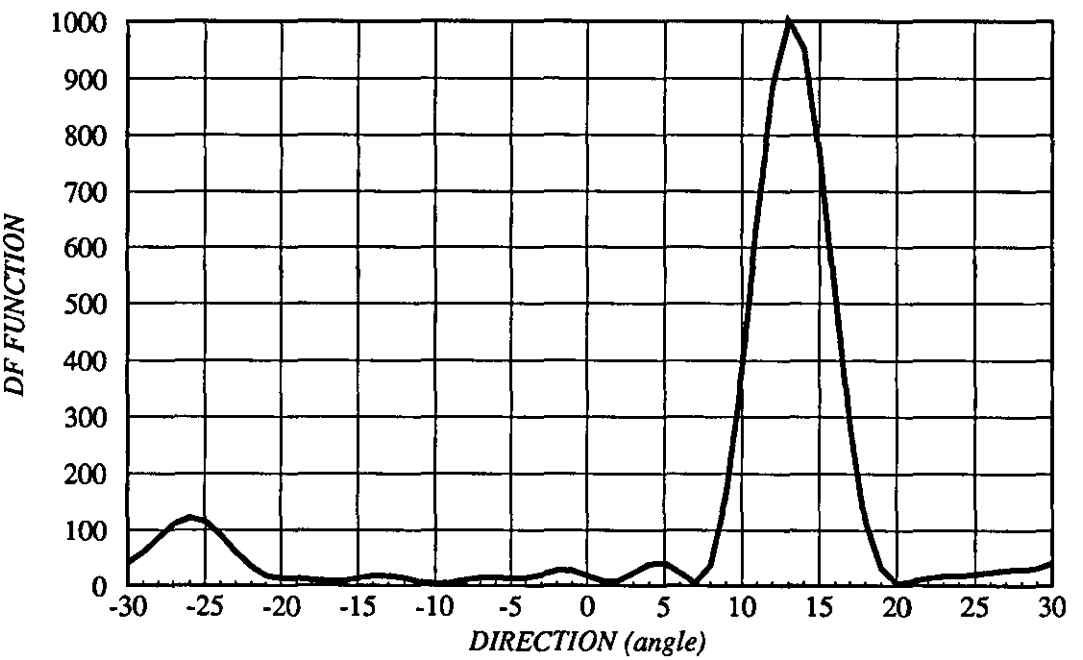

Position 2

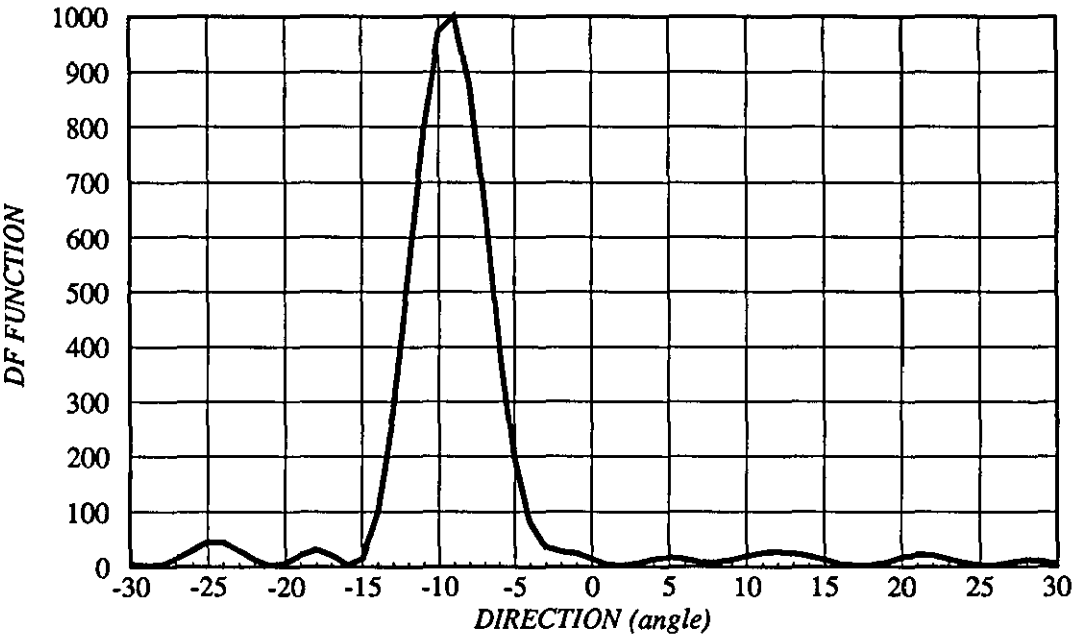

Position 3

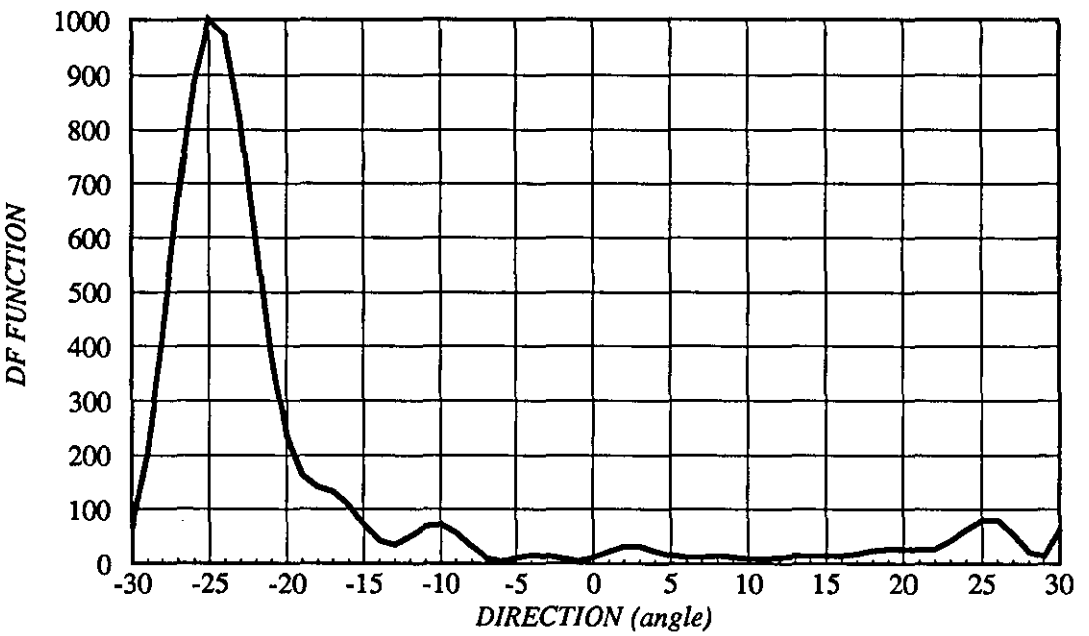

Position 4

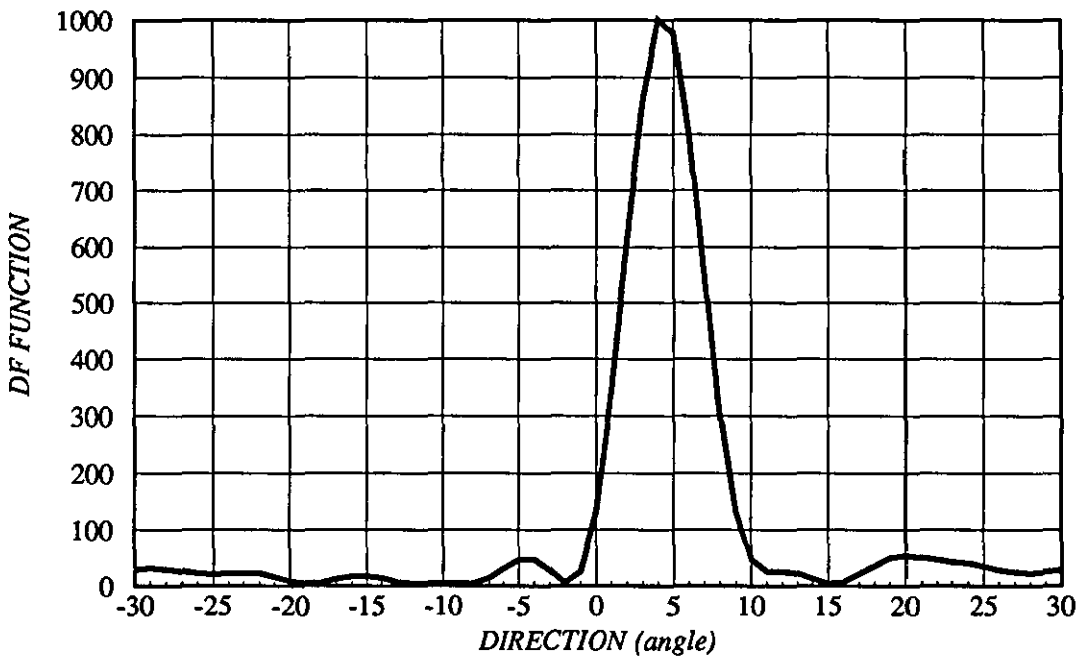

Position 5

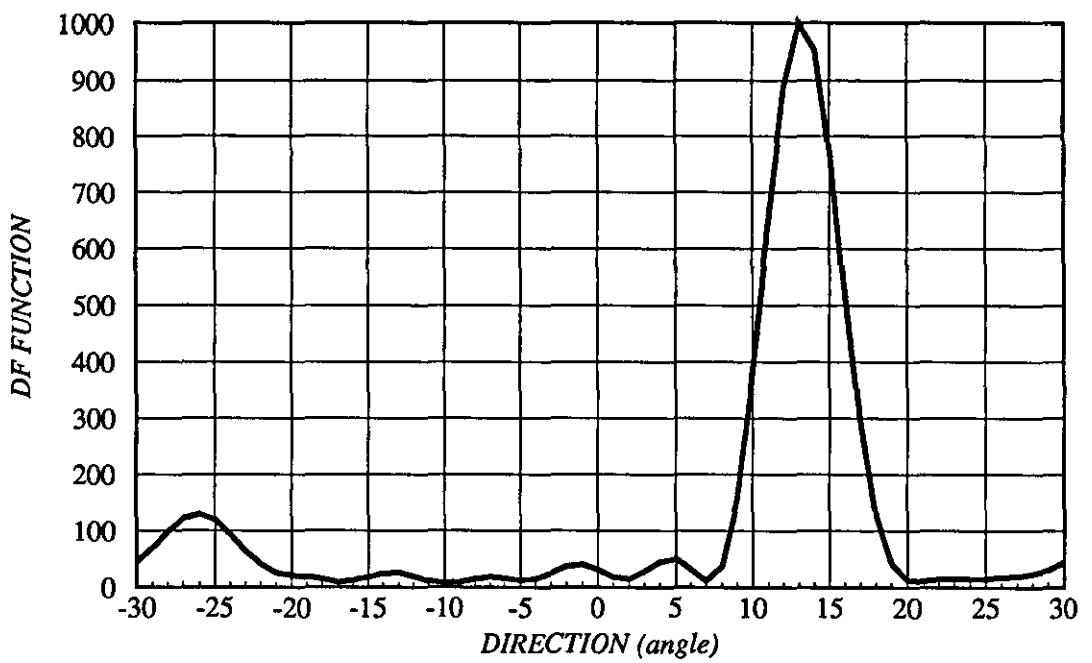

Position 6

Figure 5-10: Moving One Passive Target Across The Sector.

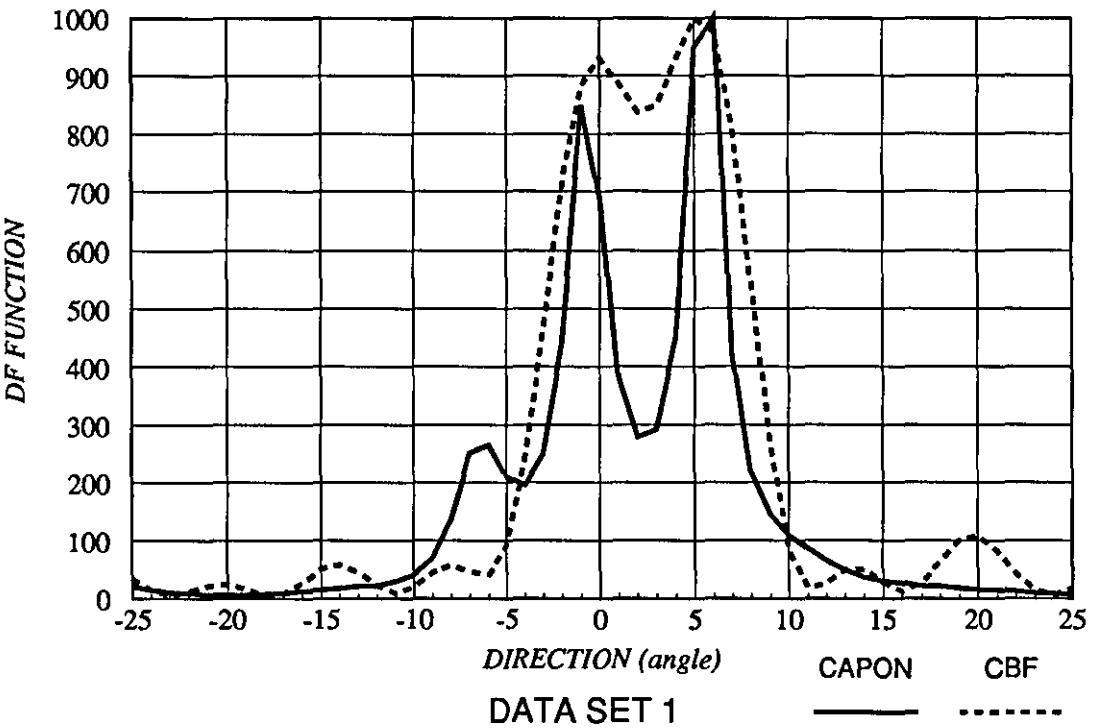
1000
900
800
700
600
500
400
300
200
100
0
DF FUNCTION
-25 -20 -15 -10 -5 0 5 10 15 20 25
DIRECTION (angle)
CAPON
CBF
DATA SET 1

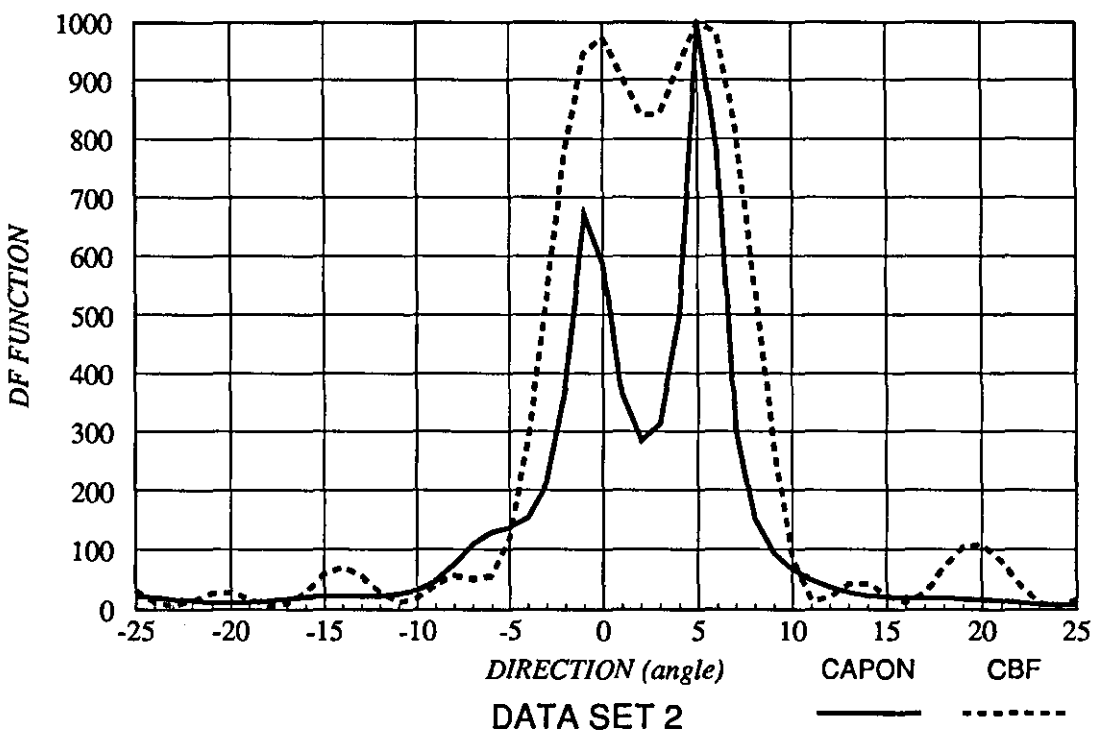
1000
900
800
700
600
500
400
300
200
100
0
DF FUNCTION
-25 -20 -15 -10 -5 0 5 10 15 20 25
DIRECTION (angle)
CAPON
CBF
DATA SET 2

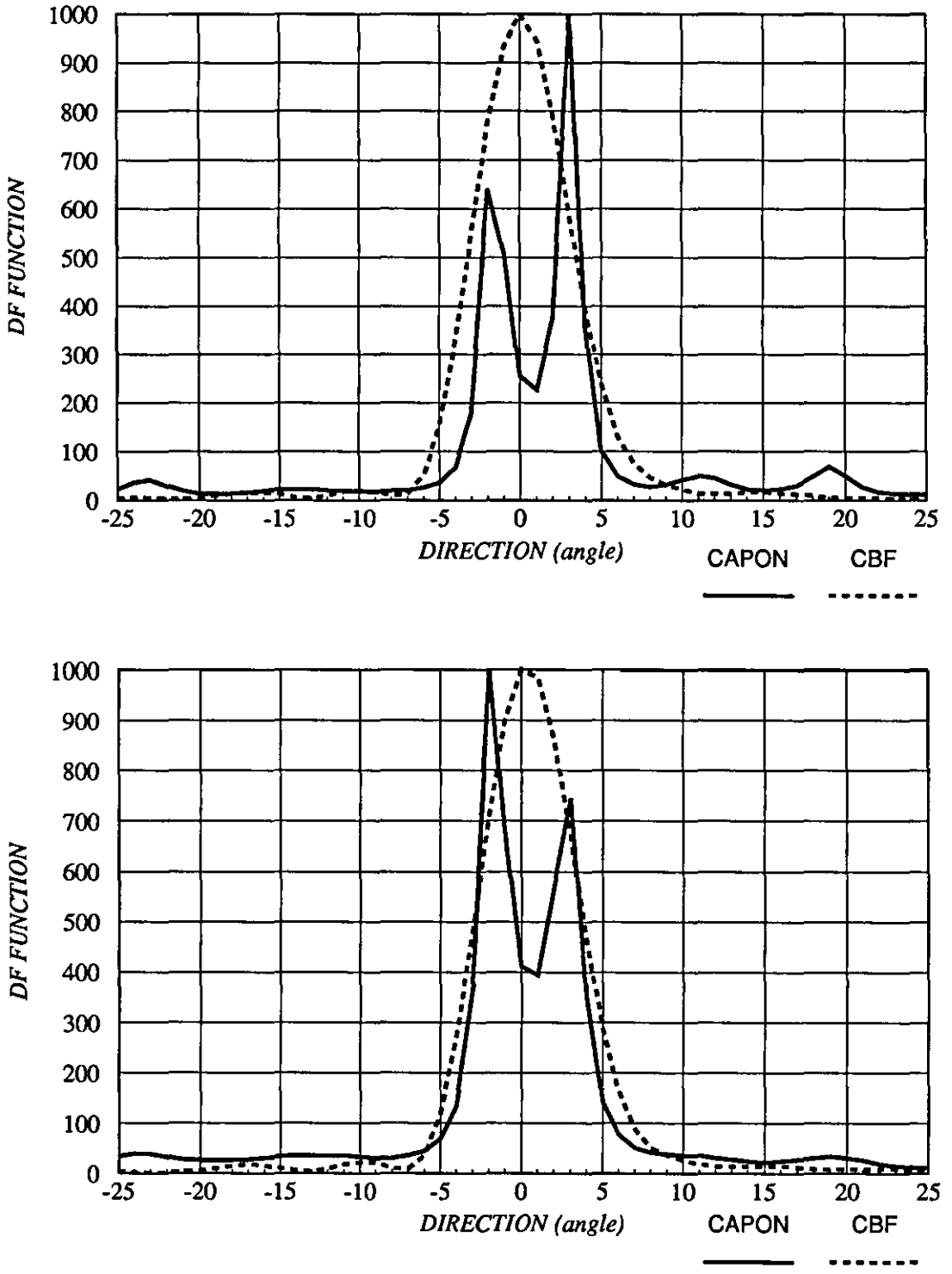

Figure 5-11: Angular Spectrum of Capon's Method.

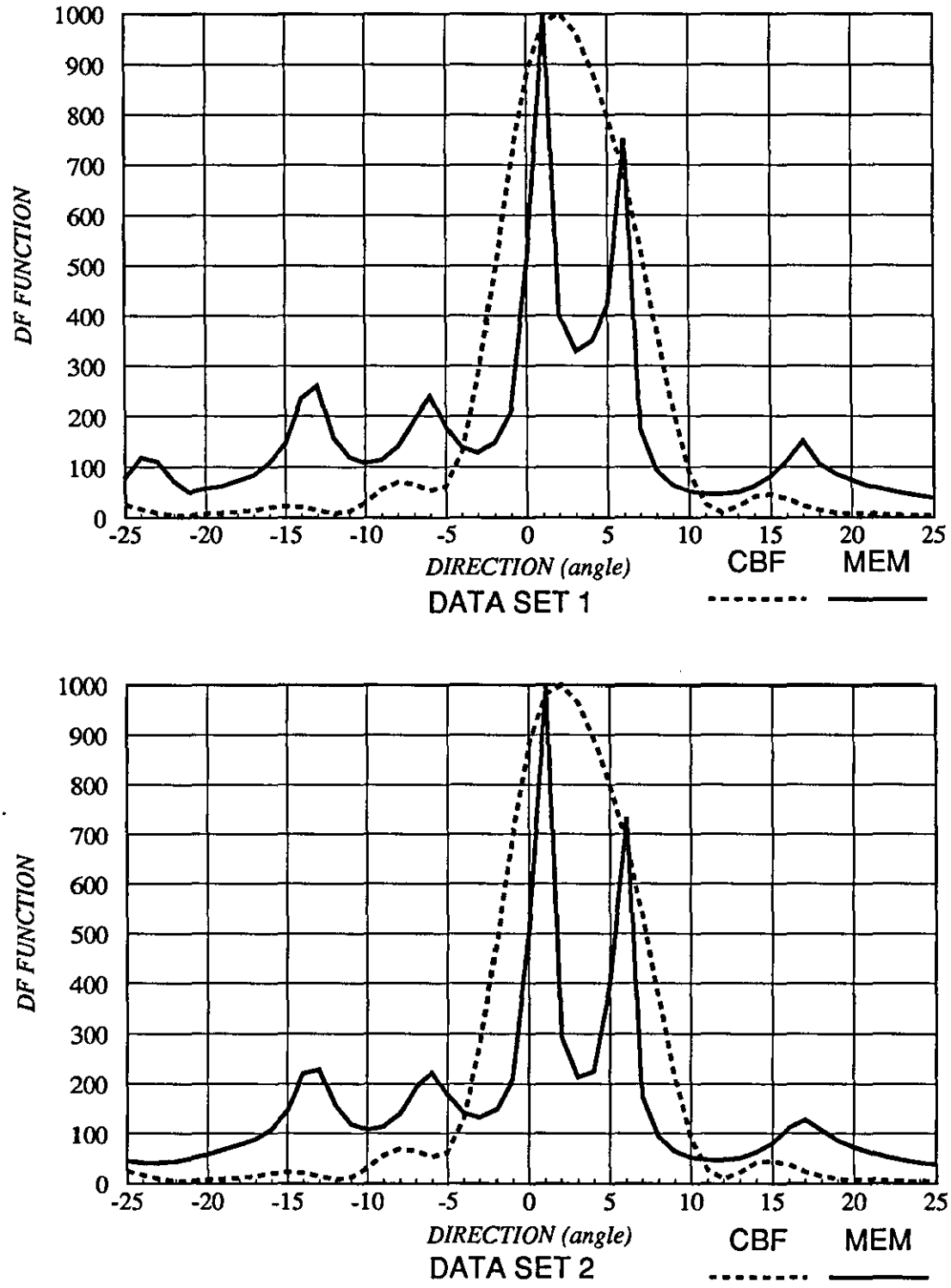

Figure 5-12: Angular Spectrum of MEM.

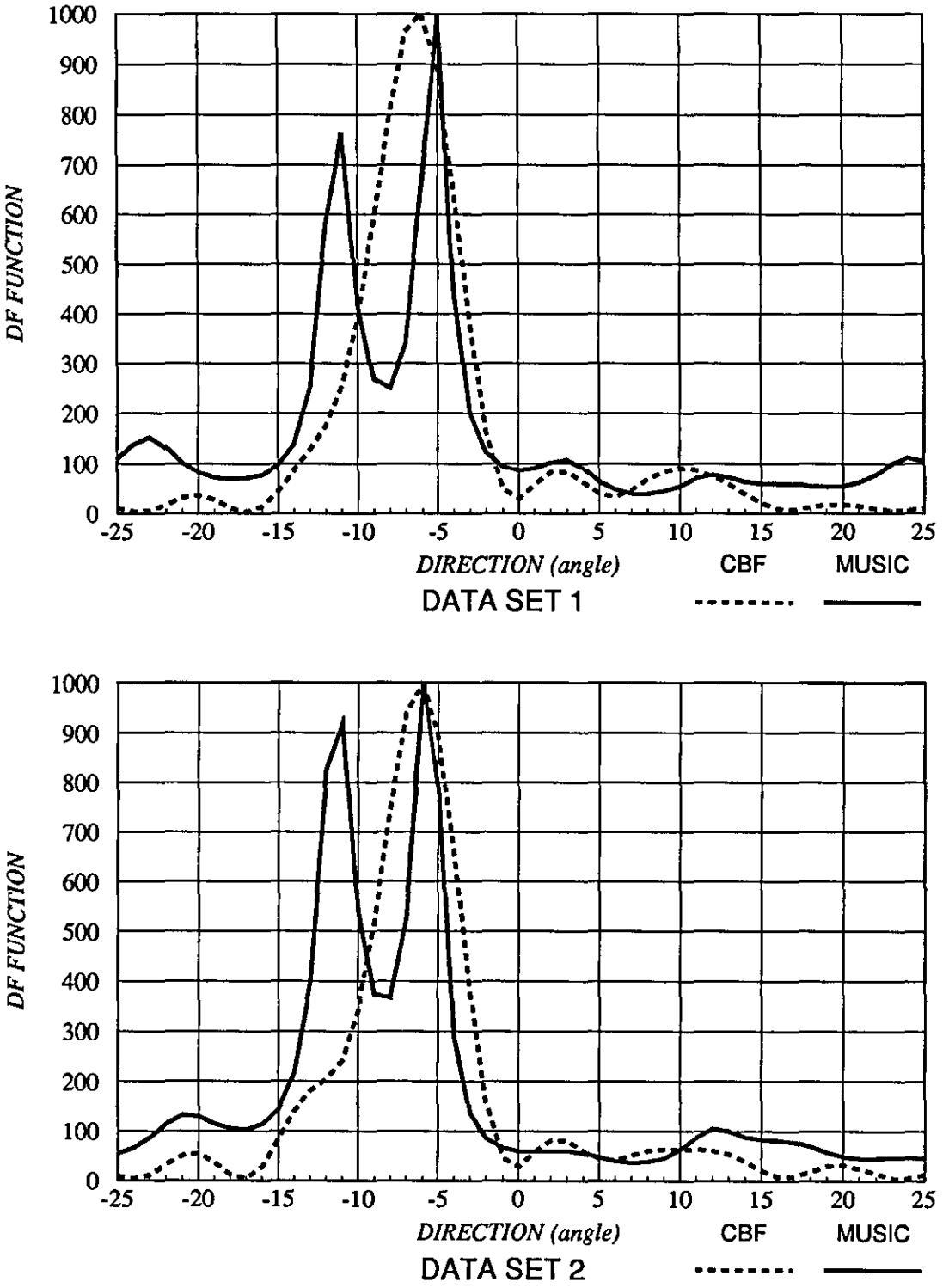

Figure 5-13: Angular Spectrum of MUSIC.

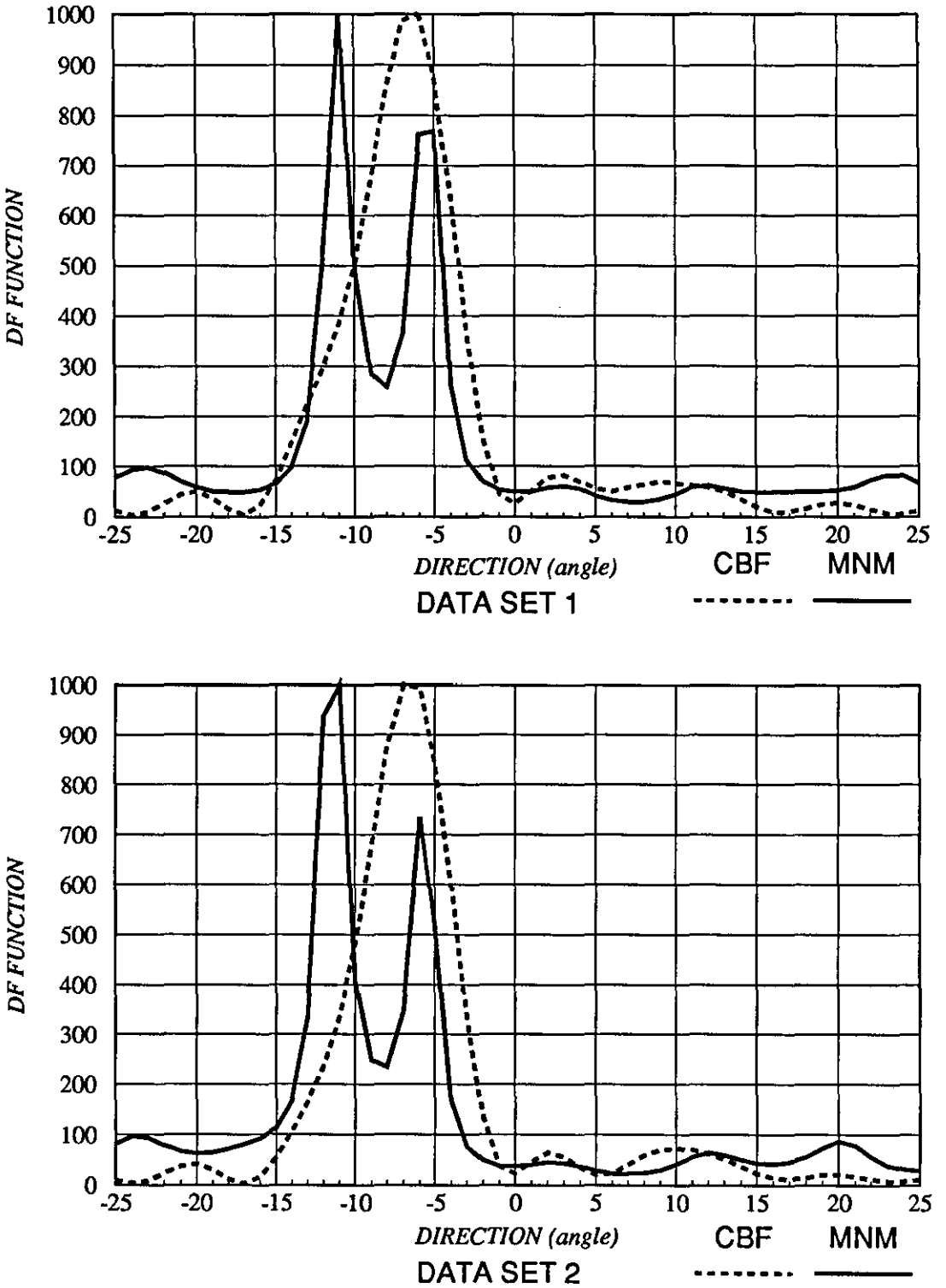

Figure 5-14: Angular Spectrum of MNM.

CHAPTER SIX

HIGH RESOLUTION SONAR DF SYSTEM RESULTS OF FOREMARK TRIALS

1. INTRODUCTION:

In the last chapter, the results of implementing high resolution DF algorithms on a transputer-based sonar system were presented. These results were obtained from tests carried out in the water tank at LUT. The limiting factor associated with these tests was the relatively small size of the tank which caused severe problems with reverberation. Also, it was necessary to work very close to the near field of the array, and complex calculations were required to remove the effects due to this closeness. However, the results obtained from these experiments demonstrated that the system was functioning and provided sufficient confidence to continue the work in a more realistic environment.

In order to carry out practical tests under more realistic conditions, it was decided to move the system to a large nearby reservoir (Foremark). Although the problem of reverberation was reduced, other difficulties arose. These can be summarized as follows:

a. The echo or signal level was reduced due to the increased ranges used, and it was necessary to make use of power amplifier and/or preamplifiers.

b. The reservoir is liable to adverse weather conditions. In particular, high winds and waves caused movements of the targets/sources.

In this chapter, the results of some experiments carried out at Foremark reservoir to test the performance of the high resolution DF sonar system are presented.

The results presented in this chapter have been published in ref.[81] and [82].

6.2 GENERAL DESCRIPTION OF FOREMARK RESERVOIR - DERBYSHIRE [Ref. 83 and 84]:

This large capacity reservoir (11×10^9 *Litres*), completed in 1977, functions as a pumped storage reservoir for Leicestershire's water supply. The original valley contours were widened during the construction of the dam and the final water depth exceeds 30 metres when full. Working from the draw-off tower a deep water path extends for over 1 kilometre with a depth exceeding 20 metres. The very wide valley has necessitated a long curved dam wall and a very large sector of water is available to work in. Equipment can be transported by vehicle to the narrow roadway on the dam wall, and transferred to the tower using trolleys to manhandle the equipment across a foot bridge (figure 6.1).

6.3 PASSIVE SONAR TESTS:

The main objective of these tests was to study the performance of some high resolution algorithms in resolving two underwater hydrophone sources placed at a distance of 9 metres from a receiving array. The tests included varying some parameters to study their effects on the performance of the algorithms. These parameters were:

a. The distance between the two sources.
b. The signal/noise ratio of the two sources.
c. The number of snapshots.

In the following section a detailed description of these tests with their results are presented.

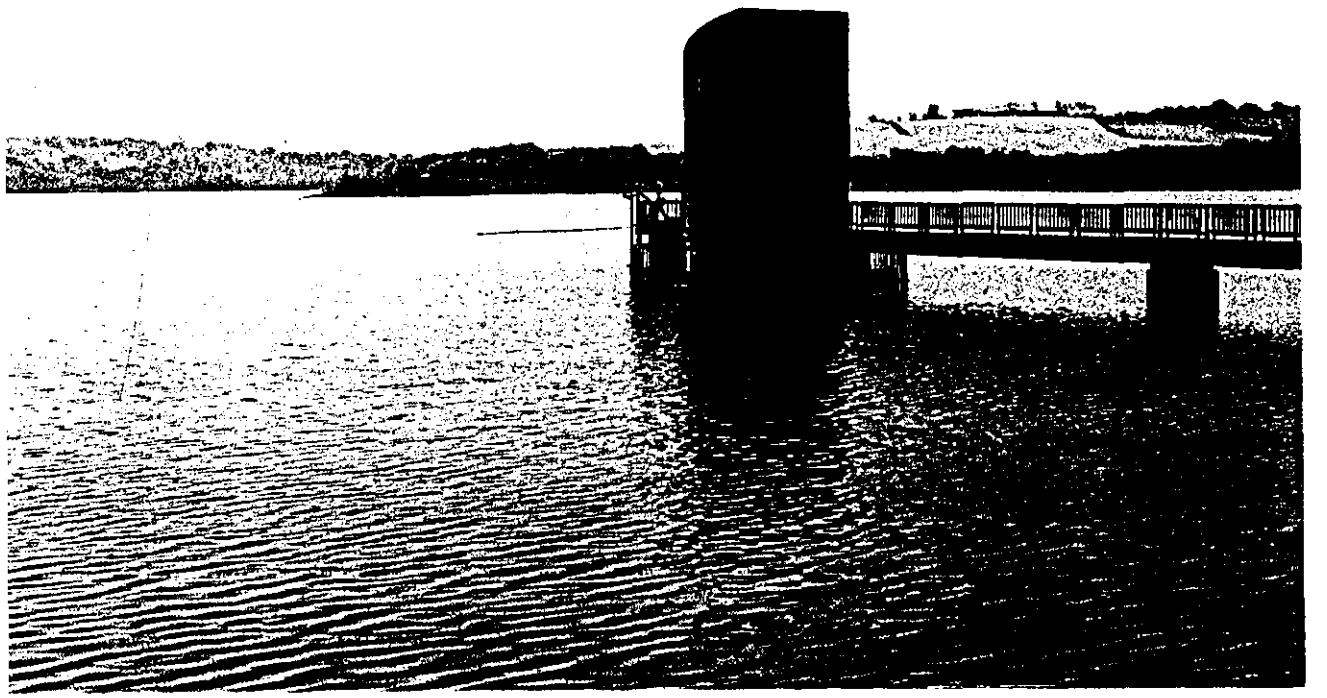

Figure 6.1: Foremark Reservoir.

6.3.1 DESCRIPTION OF THE EXPERIMENTAL SET-UP:

The new 40kHz 15 element array, together with a pan and tilt unit were fitted at the bottom of a 12m triangular tower and deployed in the water as shown in figure 6.2. The other end of the tower was fixed on the railings of the lower balcony of the control tower with a specially designed mount. In order to be able to pan and tilt the array without being fouled by the corners of the tower, a spacer was fitted between the pan and tilt unit and the tower.

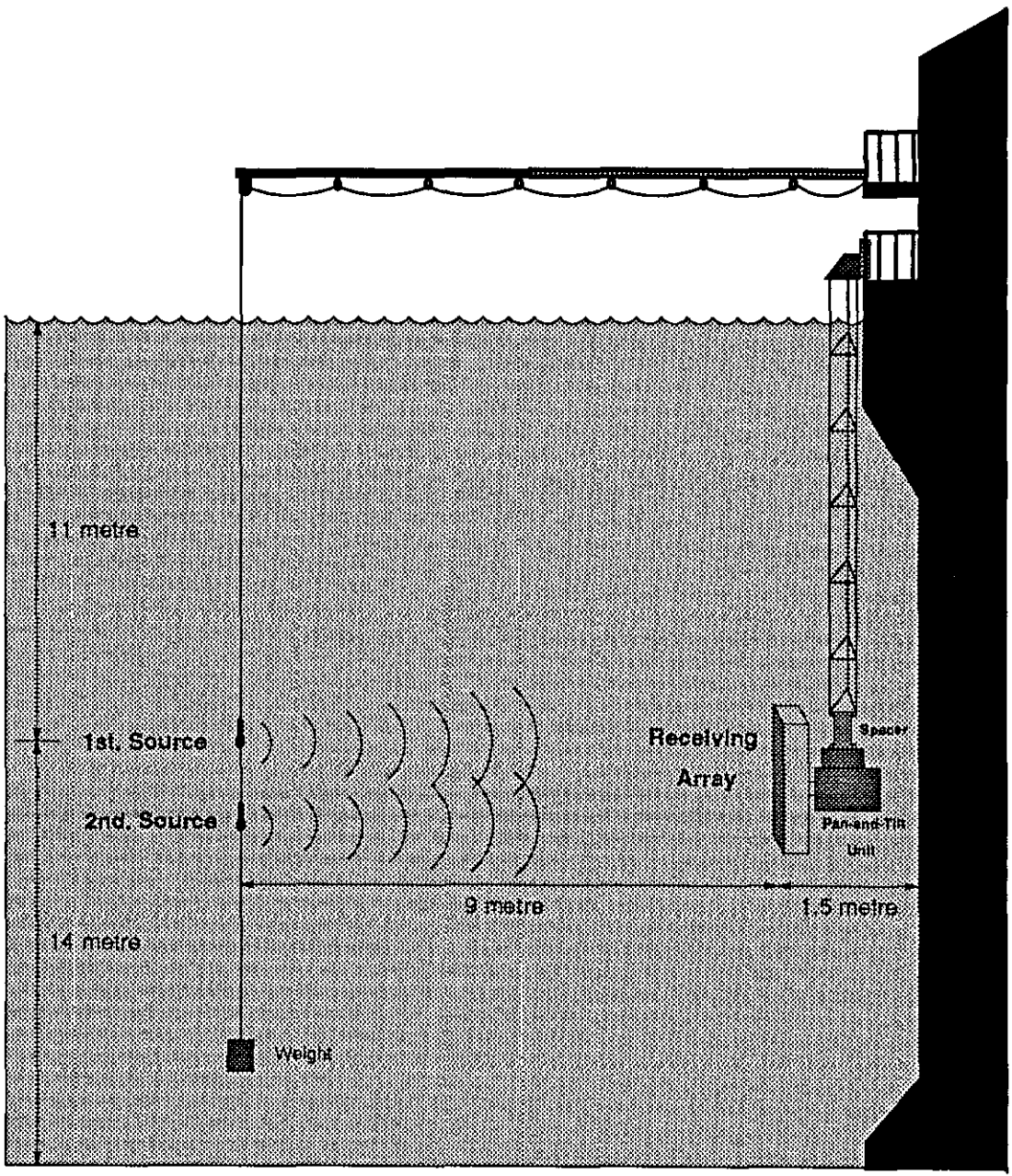

Figure 6.2: The Experimental Set-up.

It was decided to work in the vertical plane since it was easier to mount the sources/targets vertically rather than horizontally. The vertical alignment of the array was ensured by means of mechanical stops fitted to the pan and tilt head. Thus if the array was moved to the horizontal plane, it could be returned to the vertical without fear of misadjustment.

Initially, a ball hydrophone, supported below the end of a nine metre pole fixed to the upper balcony of the control tower, was deployed in the water at a depth of approximately 11 metres. A small weight was attached to the hydrophone to pull it down. This hydrophone was placed at the 0° direction (relative to the normal of the receiving array). This was adjusted by transmitting pulses continuously from it and monitoring the sum of the received signals from elements 1 and 10 of the receiving array. The zero position was the position which produced maximum output.
In the first experiment, the hydrophone was moved from the centre in steps of one metre in each direction across the sector and its position was detected by the DF system using the CBF algorithm. In the following experiments the first hydrophone was kept at the zero position and another hydrophone was placed above it. The distance between the two hydrophones was set to 100, 75 and 50cm which corresponds to 6.8, 5 and 3.5 degrees respectively.

The two hydrophones were fed from two separate power amplifiers. These amplifiers were driven by two pulse generator circuits working at slightly different frequencies around 40kHz. This difference in frequency was necessary to break the correlation between the two sources.

6.3.2 POSSIBLE SIGNAL MULTIPATHS:

Figure 6.3 shows the possible signal multipaths. It can be seen from this figure that the reflection from the tower is the first to arrive after the main pulse via the direct path (about 2msec later). This dictates that the length of the pulse used must not be longer than 2msec. However, because the cylindrical shape of the tower causes strong scattering, the reflected pulse is much weaker. Besides, this reflected pulse will hit the receiving array from the back which is less sensitive.

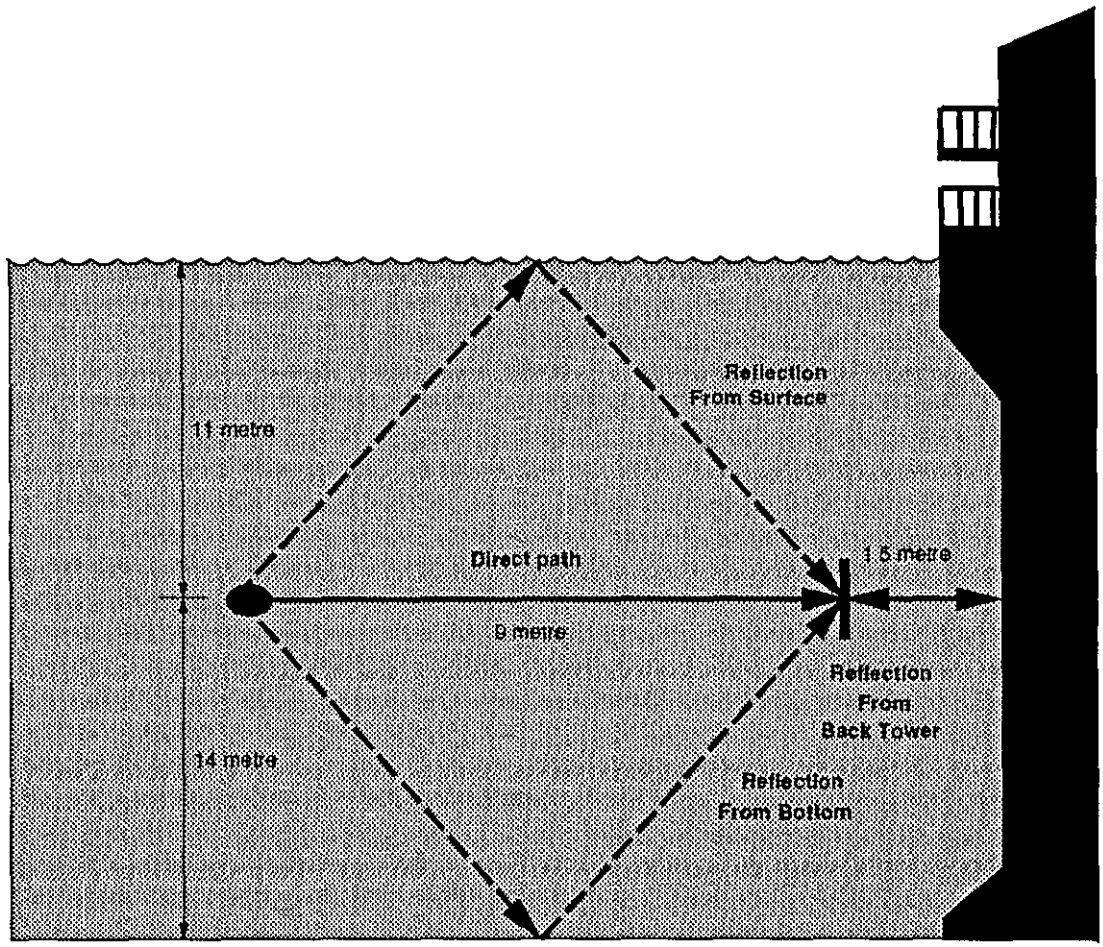

Figure 6.3: The Possible Signal Multipaths.

Figure 6.4 shows a photograph of the transmit and receive pulses. The pulse length used was 1.5msec.

The reflections from the surface and bottom will arrive much later (7.9 and 9.8 msec respectively).

Other possible reflections may be caused by a 4kHz array which is hung vertically about 2 metres to the right of the receiving array. Cables and strings are also possible sources of reflections although their effects are much less significant than the other sources mentioned earlier.

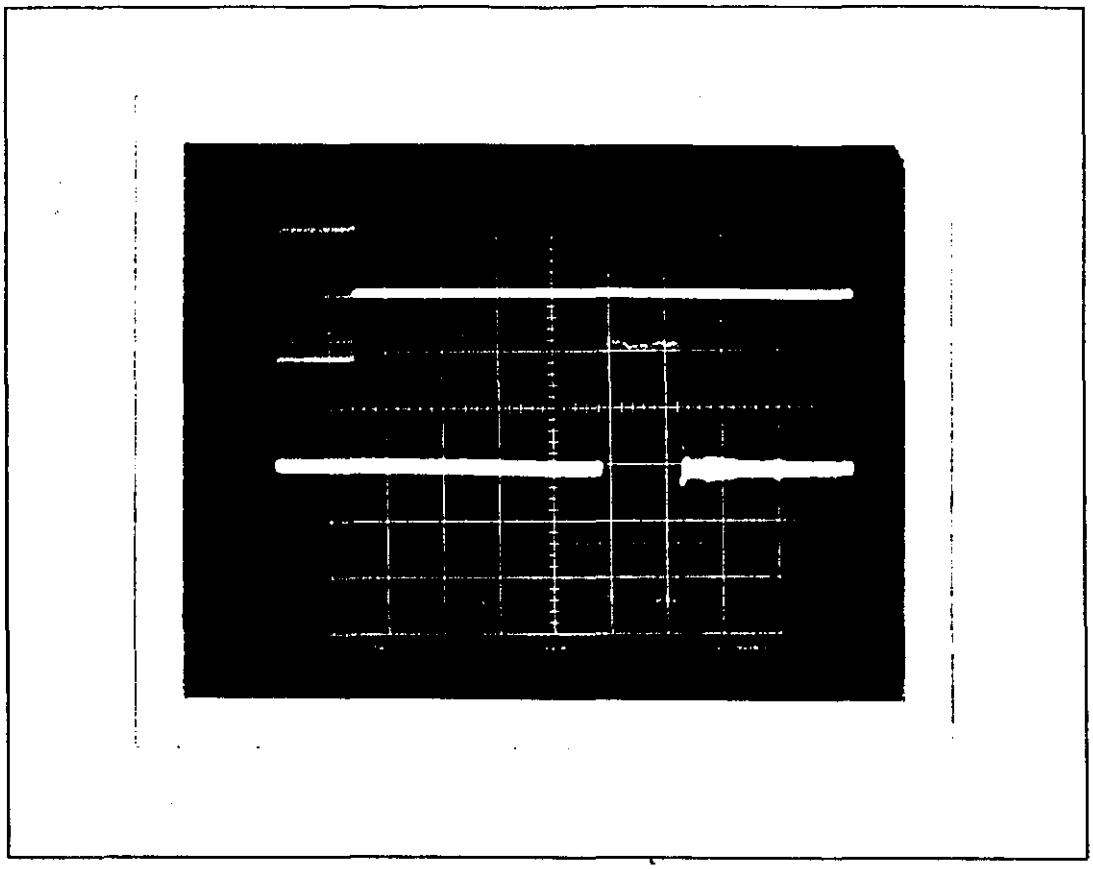

Figure 6.4: The Transmit and Receive Pulses.
Transmit 1V/Div. Receive 0.1V/Div Time 1msec/Div

6.3.3 SUMMARY OF THE EXPERIMENTS:

In the following, a summary of the experiments carried out at Foremark reservoir and their objectives is presented. The S/N ratio of the individual sources were measured by transmitting from the respective source and measure the ratio of the signal level to noise level (the level of noise when there is no signal) at the output of the first preamplifier stage on the receiver board.

EXPERIMENT No. 1: Moving single source vertically across the sector at intervals of 1metre and do the conventional beam former to detect its direction.

EXPERIMENT NO. 2: Resolving two sources one metre apart at a distance of 9m from the array.
S/N of both sources=20dB
No. of snapshots=15 and 30.
Algorithms: CBF, Capon, MUSIC and MNM.

EXPERIMENT NO. 3: Resolving two sources 0.75m apart at a distance of 9m from the array.
S/N of both sources=20dB.
No. of snapshots=15 and 30.
Algorithms: CBF, Capon, MUSIC and MNM.

EXPERIMENT NO. 4: Resolving two sources 0.5m apart at a distance of 9m from the array.
S/N of both sources=20dB.
No. of snapshots=15,30 and 50.
Algorithms: CBF, Capon, MUSIC and MNM.

EXPERIMENT NO. 5: Resolving two sources 0.75m apart at a distance of 9m from the array.
S/N of the first source=17dB.
S/N of the second source=8dB.
No. of snapshots=15,30 and 50.
Algorithms: CBF, Capon, MUSIC and MNM.

EXPERIMENT NO. 6: Resolving two sources 0.5m apart at a distance of 9m from the array.
S/N of the first source=8dB.
S/N of the second source=17dB.
No. of snapshots=15,30 and 50.
Algorithms: CBF, Capon, MUSIC and MNM.

EXPERIMENT NO. 7: Resolving two sources 0.75m apart at a distance of 9m from the array.
S/N of both sources=5dB.
No. of snapshots=15,30 and 50.
Algorithms: CBF, Capon, MUSIC and MNM.

EXPERIMENT NO. 8: Resolving two sources 0.5m apart at a distance of 9m from the array.
S/N of both sources=5dB
No. of snapshots=15,30 and 50.
Algorithms: CBF, Capon, MUSIC and MNM.

6.3.4 PRACTICAL RESULTS:

Figure 6.6 shows the results of experiment number 1 where a single hydrophone was moved across the sector in 1m steps. The results show agreement with the calculated positions.

In figures 6.7 to 6.13 a series of results are observed for two equal amplitude sources with different separations, different numbers of snapshots and different signal/noise ratios. Four algorithms are evaluated in each figure:

1. The Conventional Beamformer (CBF).
2. The Capon Estimator (CAPON).
3. The Music Algorithm (MUSIC).
4. Minimum Norm Method (MNM).

The array used had 15 elements spaced at one wavelength but only ten of these elements were used. Therefore the conventional beamwidth is approximately 5.6 degrees.

In figures 6.7 (a) and (b) the spacing of the two sources is 6.7 degrees and thus even the conventional beamformer is able to separate the sources. The other methods all perform considerably better however. The Capon estimator should estimate the level of the signals as well as the position but it should be noticed that for 15 snapshots there is a difference between the two estimates. In figure 6.7 (b) with 30 snapshots the estimates are much better.

In Figures 6.8 (a) and (b) the source separation is 5 degrees and the CBF now fails to separate them while all the high resolution methods separate them easily.

Figures 6.9 (a), (b) and (c) are for a source separation of 3.5 degrees and with 20dB S/N. All three high resolution methods are still separating the sources.

In figures 6.10 (a), (b) and (c) the source separation is 5 degrees but the power of the two sources is 8 and 17dB. All the three high resolution algorithms resolve the two sources while the CBF fails. It can be seen that Capons method estimation of the signal power is not very good for 15 snapshots but for 30 and 50 snapshots the power estimations are better.

The last tests were repeated for a source separation of 3.5 degrees. The results are presented in figure 6.11 (a), (b) and (c). Again all the high resolution algorithms resolve the two sources while the CBF fails.

In figures 6.12 (a), (b) and (c) the S/N ratio of the two sources are reduced to 5dB and the separation between the two sources is set to 5 degrees. All the high resolution algorithms resolve the two sources while the CBF fails.

However, in figure 6.13 (a) where the S/N was 5dB and the separation has been reduced to 3.5 degrees none of the methods are successful with only 15 snapshots. With 30 snapshots (figure 6.13 (b)), the MUSIC and MNM are able to separate the sources successfully, and with 50 snapshots the Capon method is managing to separate the sources.

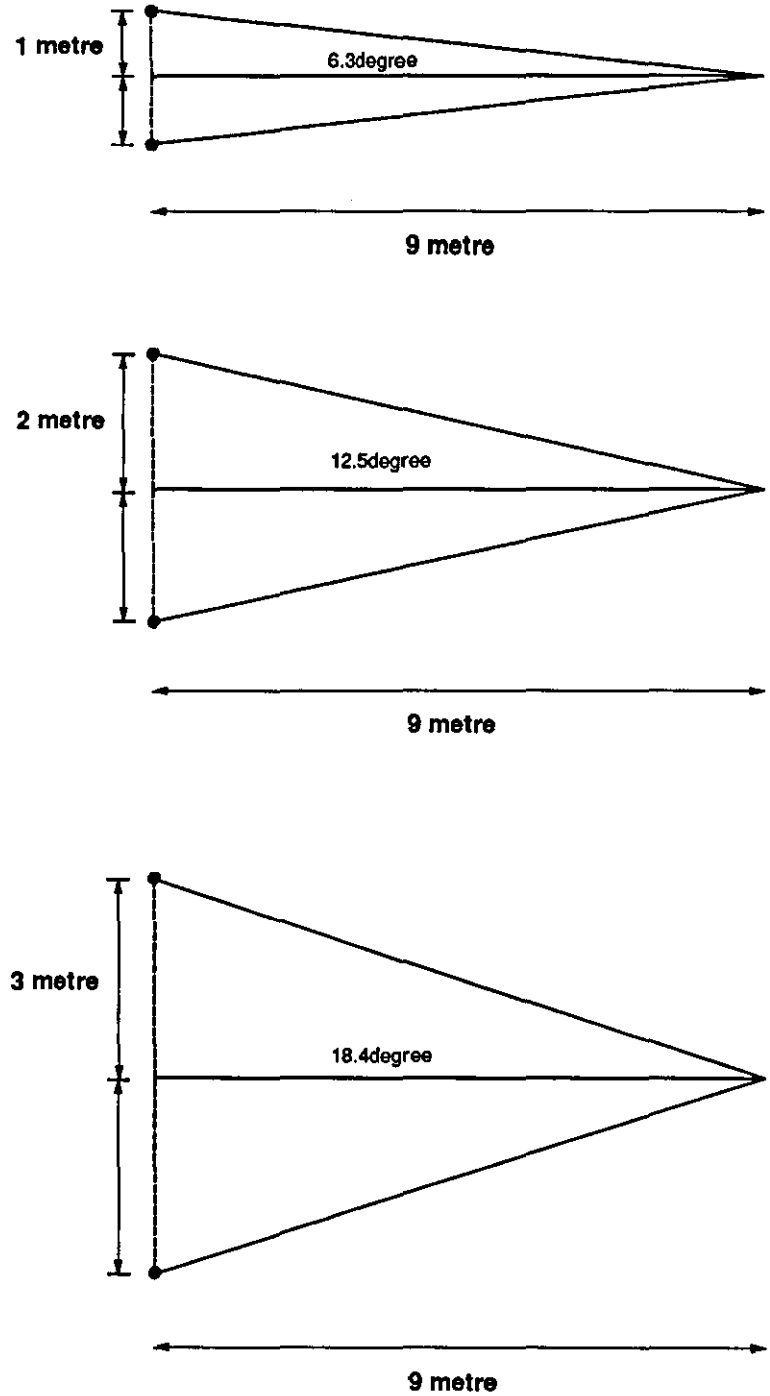

Figure 6.4: Moving One Source Across The Sector.

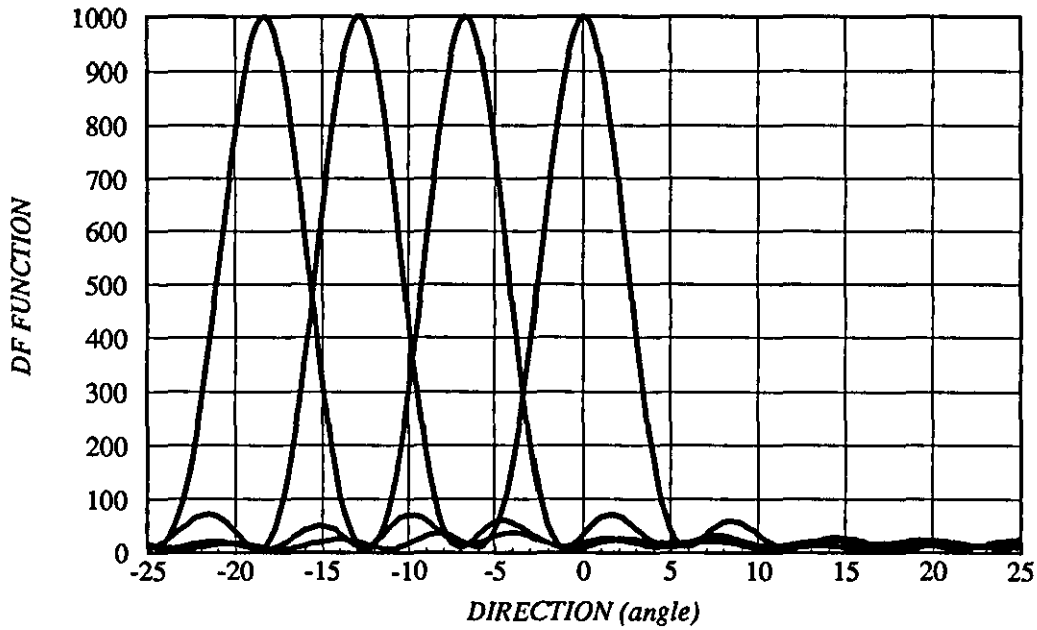

a. Moving The Source Down From The Centre.

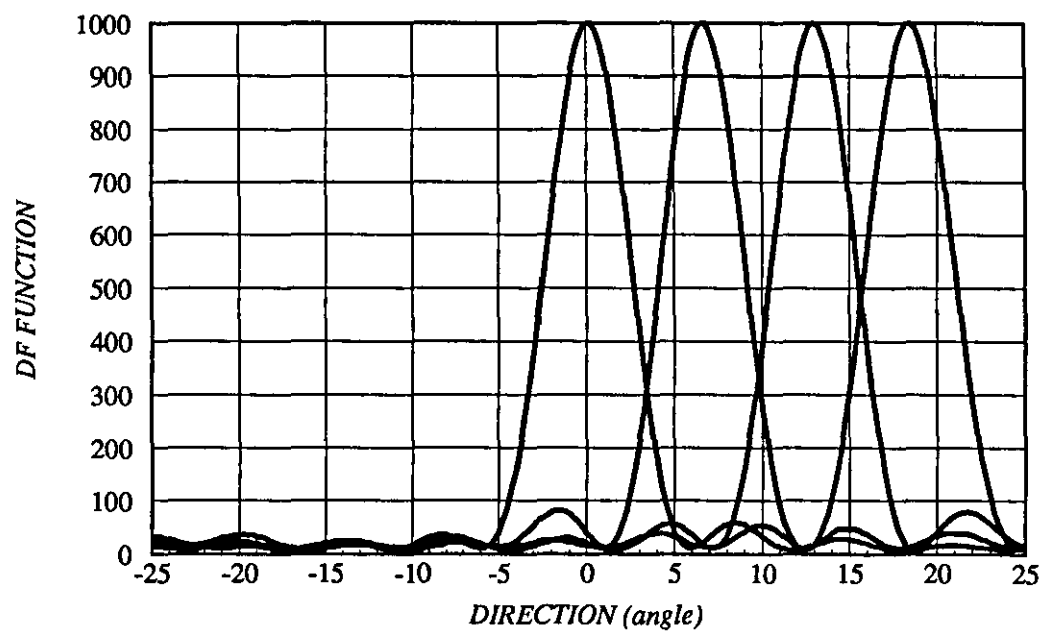

b. Moving The Source Up From The Centre.

Figure 6.6: Moving One Source Across the Sector at 1m Steps and Detect Its Position Using CBF.

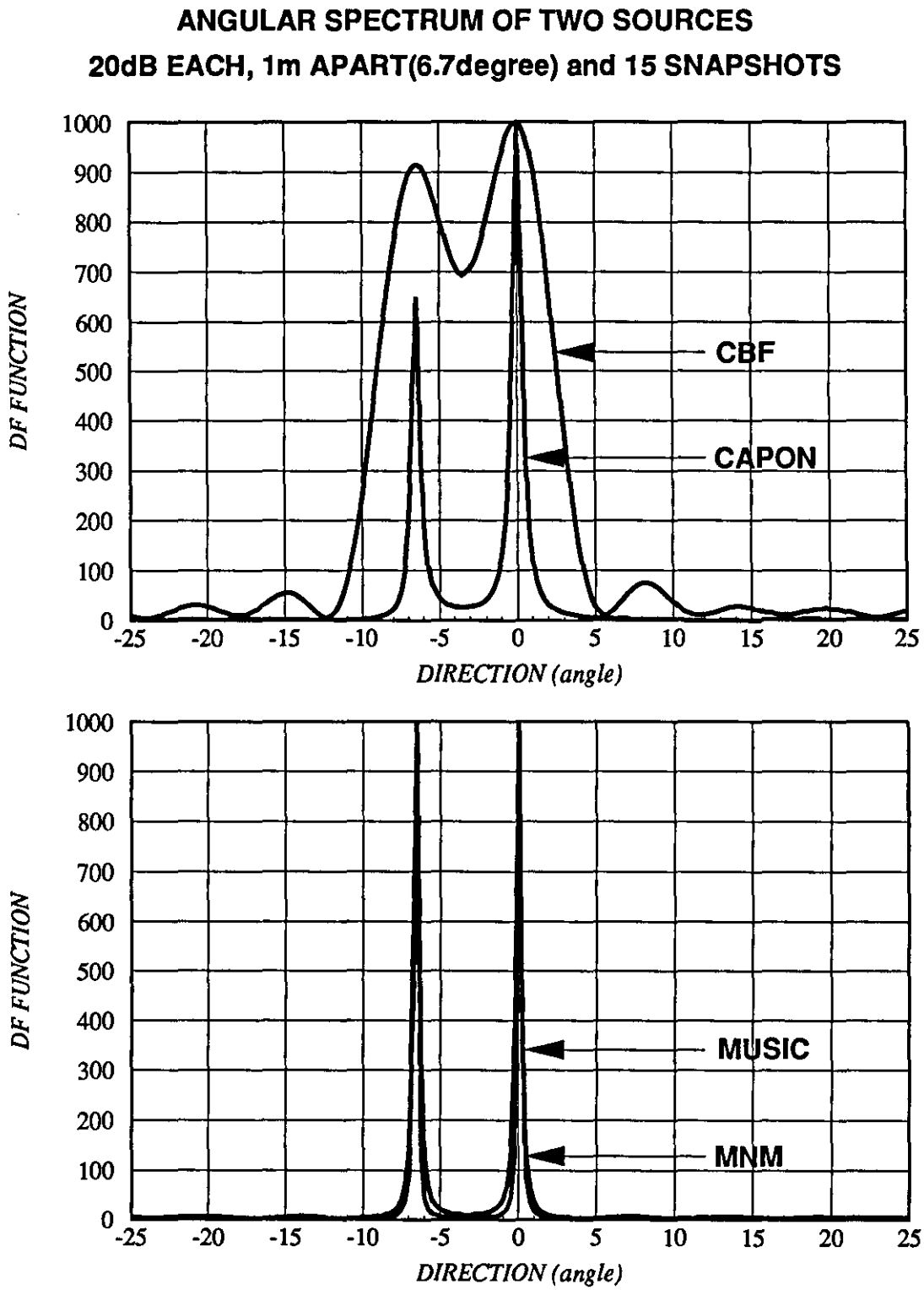
ANGULAR SPECTRUM OF TWO SOURCES
20dB EACH, 1m APART(6.7degree) and 15 SNAPSHOTS
DF FUNCTION
1000
900
800
700
600
500
400
300
200
100
0
-25
-20
-15
-10
-5
0
5
10
15
20
25
DIRECTION (angle)
CBF
CAPON
DF FUNCTION
DIRECTION (angle)
MUSIC
MNM

Figure 6.7a

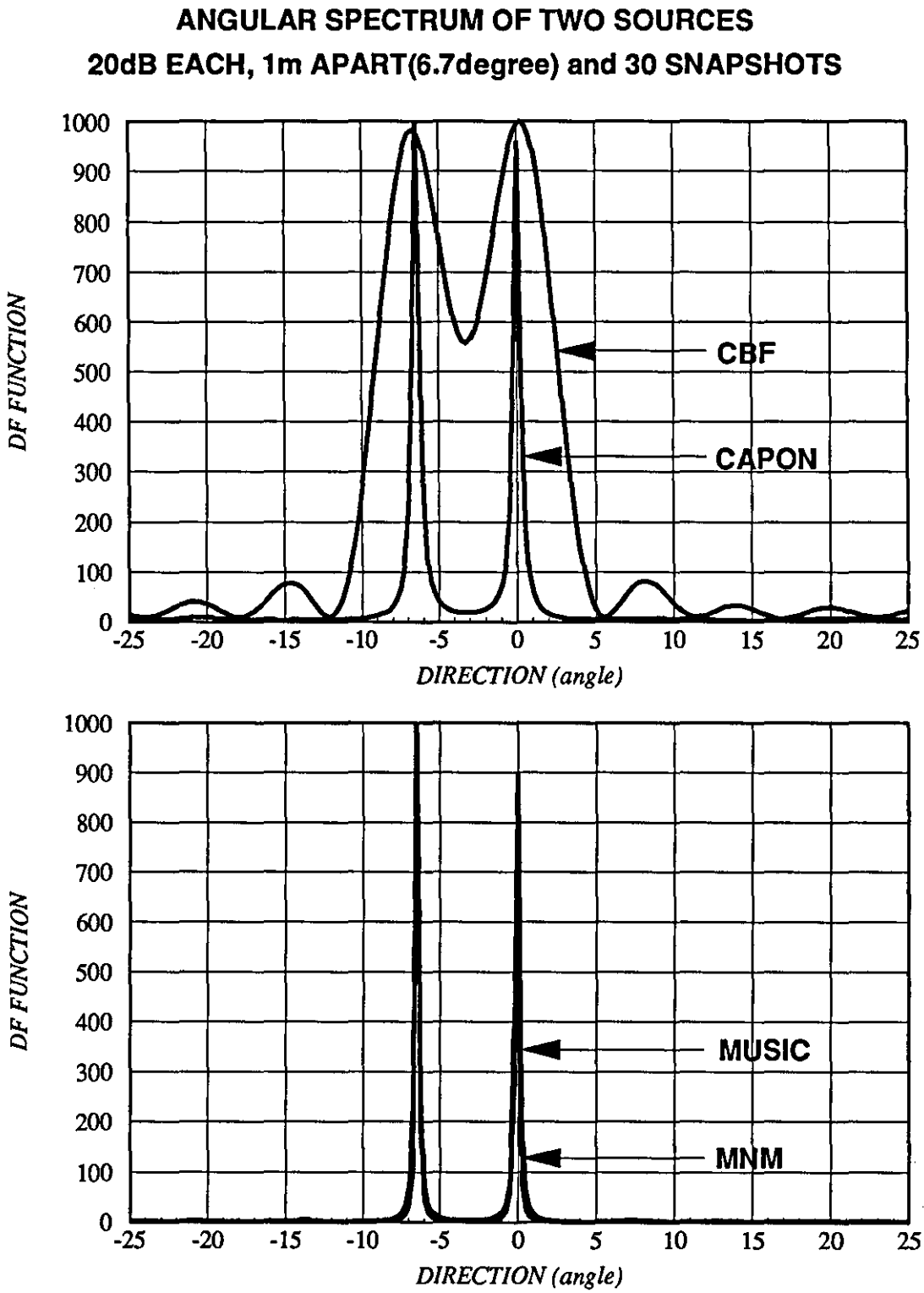
ANGULAR SPECTRUM OF TWO SOURCES
20dB EACH, 1m APART(6.7degree) and 30 SNAPSHOTS
DF FUNCTION
1000
900
800
700
600
500
400
300
200
100
0
-25
-20
-15
-10
-5
0
5
10
15
20
25
DIRECTION (angle)
CBF
CAPON
DF FUNCTION
DIRECTION (angle)
MUSIC
MNM

Figure 6.7b

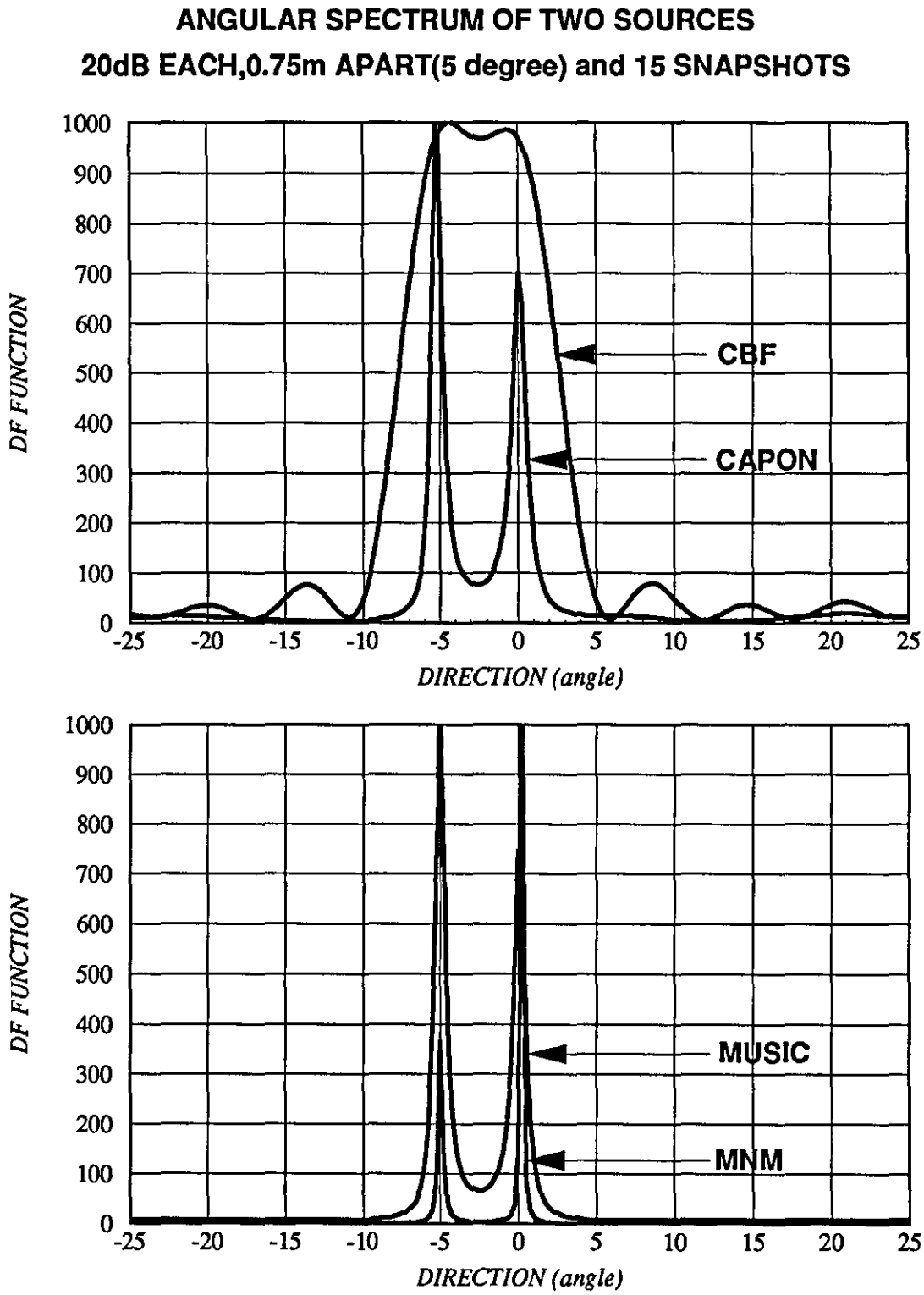
ANGULAR SPECTRUM OF TWO SOURCES
20dB EACH,0.75m APART(5 degree) and 15 SNAPSHOTS
DF FUNCTION
1000
900
800
700
600
500
400
300
200
100
0
-25
-20
-15
-10
-5
0
5
10
15
20
25
DIRECTION (angle)
CBF
CAPON
DF FUNCTION
DIRECTION (angle)
MUSIC
MNM

Figure 6.8a

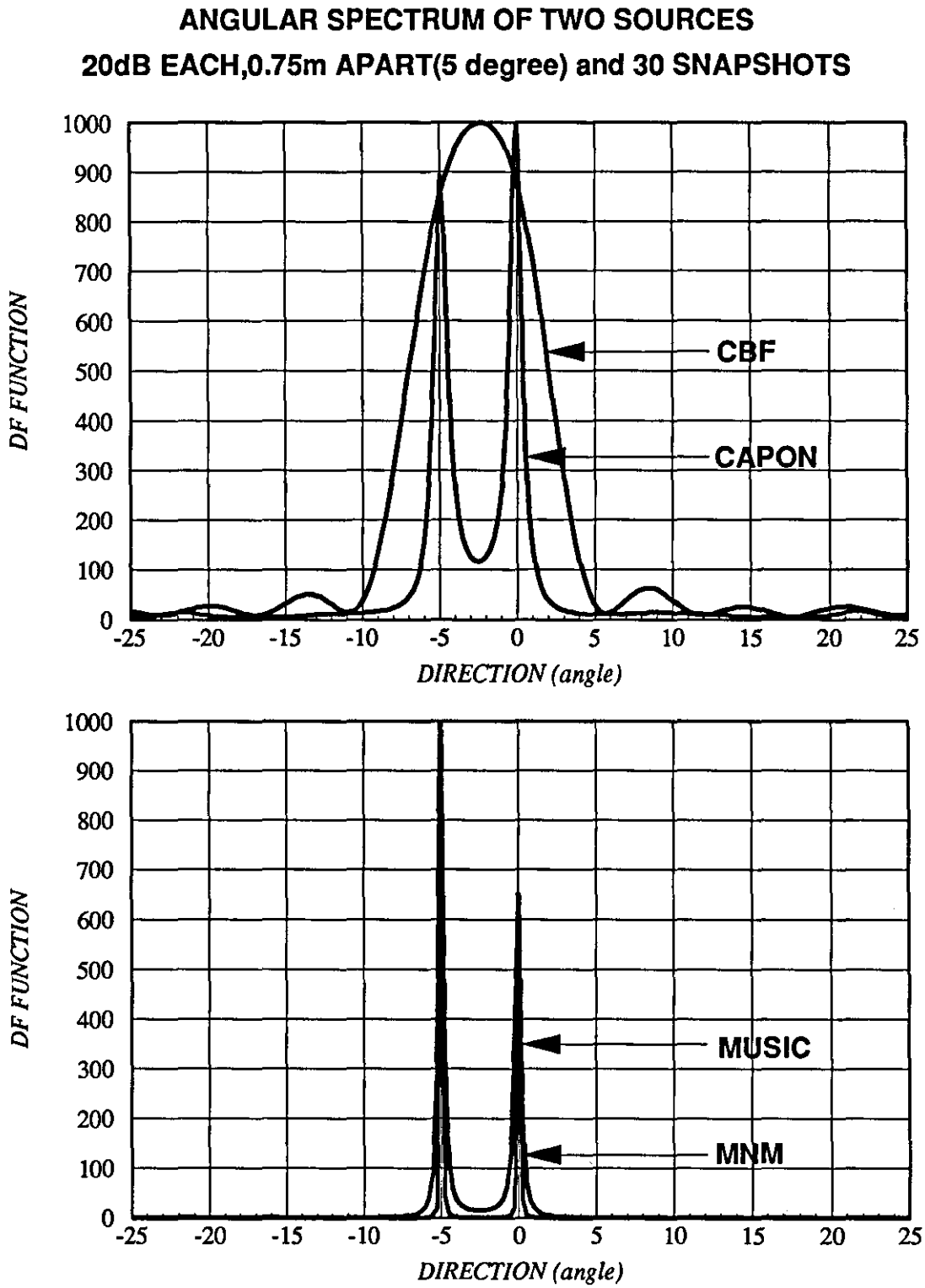
ANGULAR SPECTRUM OF TWO SOURCES
20dB EACH,0.75m APART(5 degree) and 30 SNAPSHOTS
DF FUNCTION
1000
900
800
700
600
500
400
300
200
100
0
-25
-20
-15
-10
-5
0
5
10
15
20
25
DIRECTION (angle)
CBF
CAPON
DF FUNCTION
DIRECTION (angle)
MUSIC
MNM

Figure 6.8b

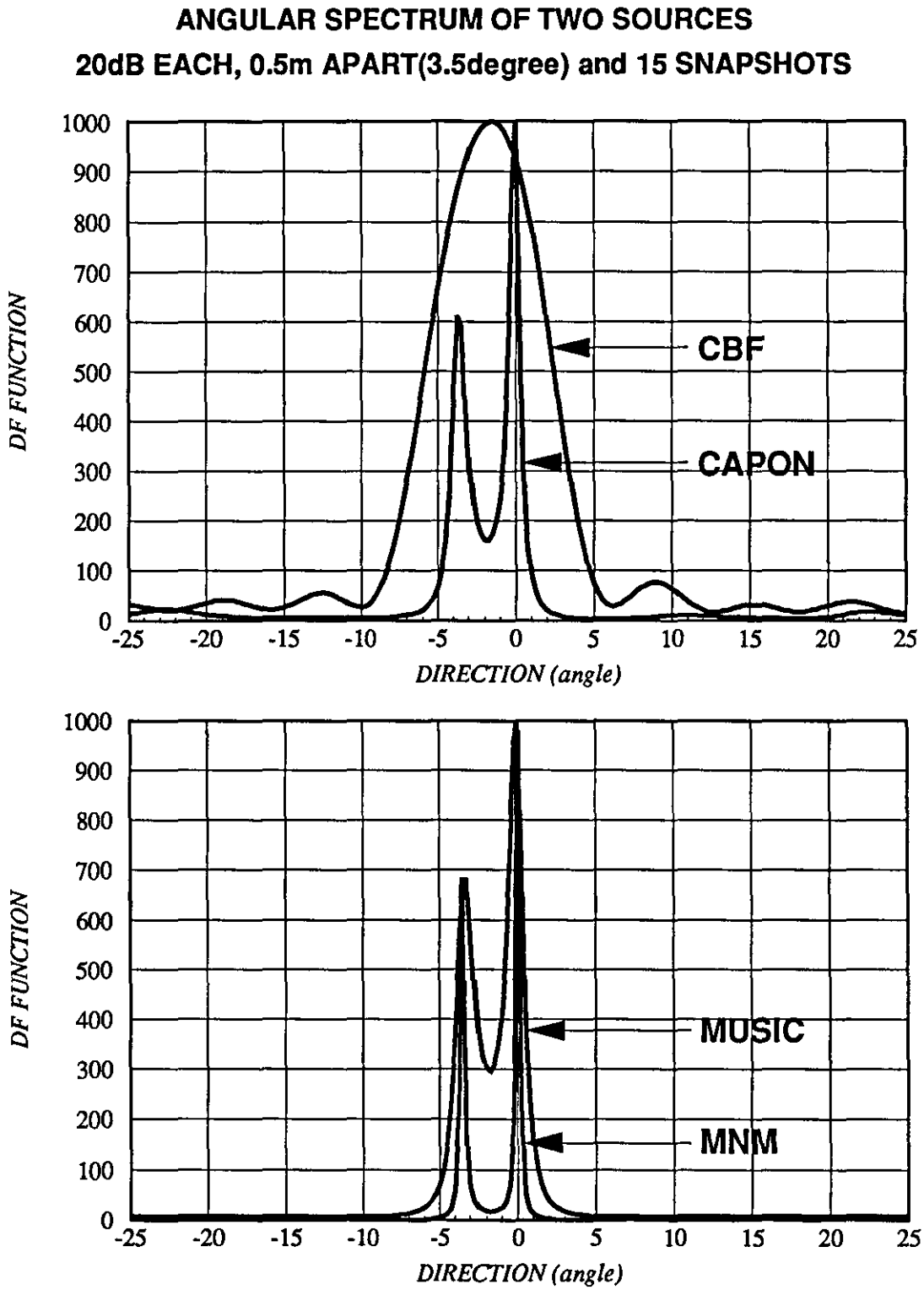
ANGULAR SPECTRUM OF TWO SOURCES
20dB EACH, 0.5m APART(3.5degree) and 15 SNAPSHOTS
DF FUNCTION
1000
900
800
700
600
500
400
300
200
100
0
-25
-20
-15
-10
-5
0
5
10
15
20
25
DIRECTION (angle)
CBF
CAPON
DF FUNCTION
DIRECTION (angle)
MUSIC
MNM

Figure 6.9a

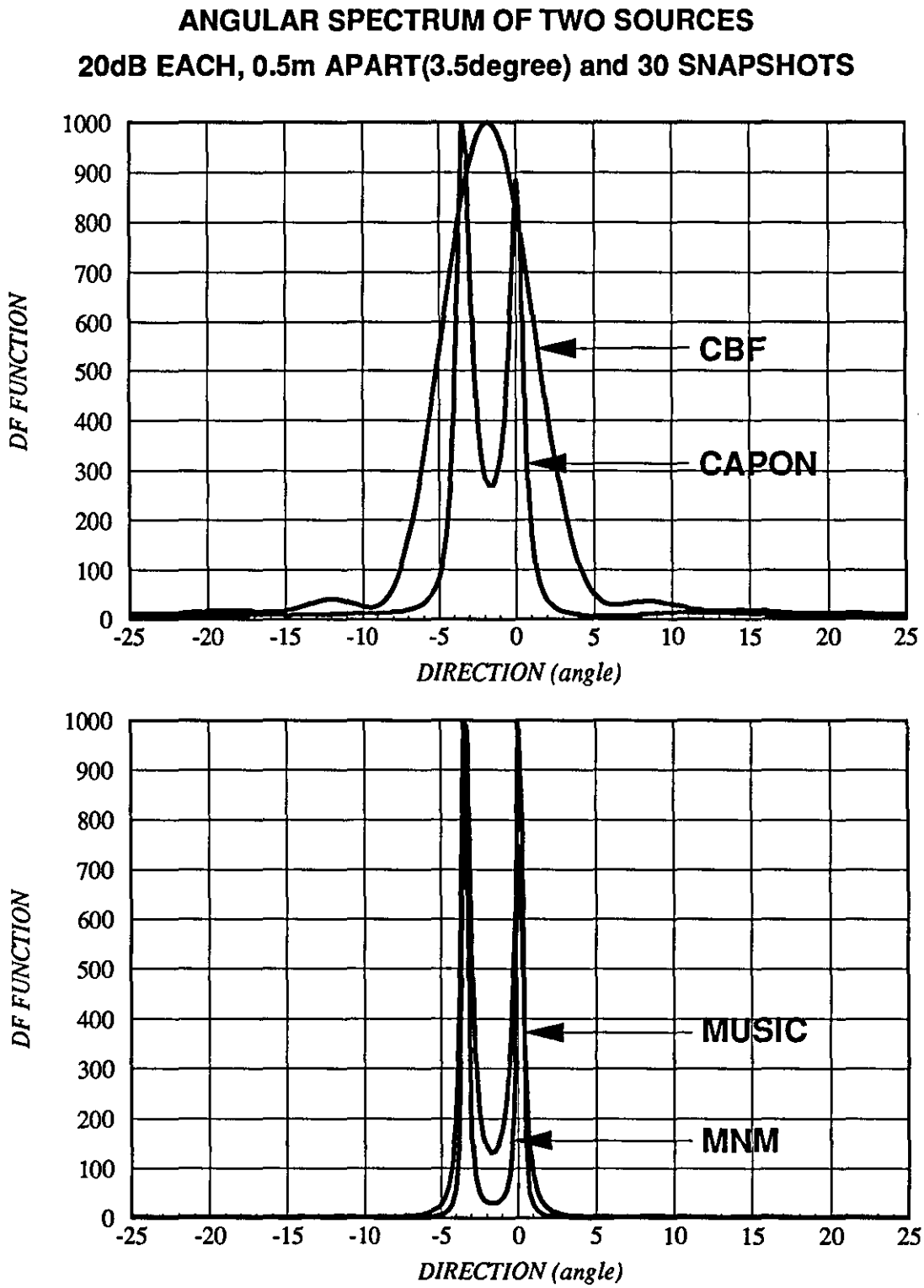
ANGULAR SPECTRUM OF TWO SOURCES
20dB EACH, 0.5m APART(3.5degree) and 30 SNAPSHOTS
DF FUNCTION
1000
900
800
700
600
500
400
300
200
100
0
-25
-20
-15
-10
-5
0
5
10
15
20
25
DIRECTION (angle)
CBF
CAPON
DF FUNCTION
DIRECTION (angle)
MUSIC
MNM

Figure 6.9b

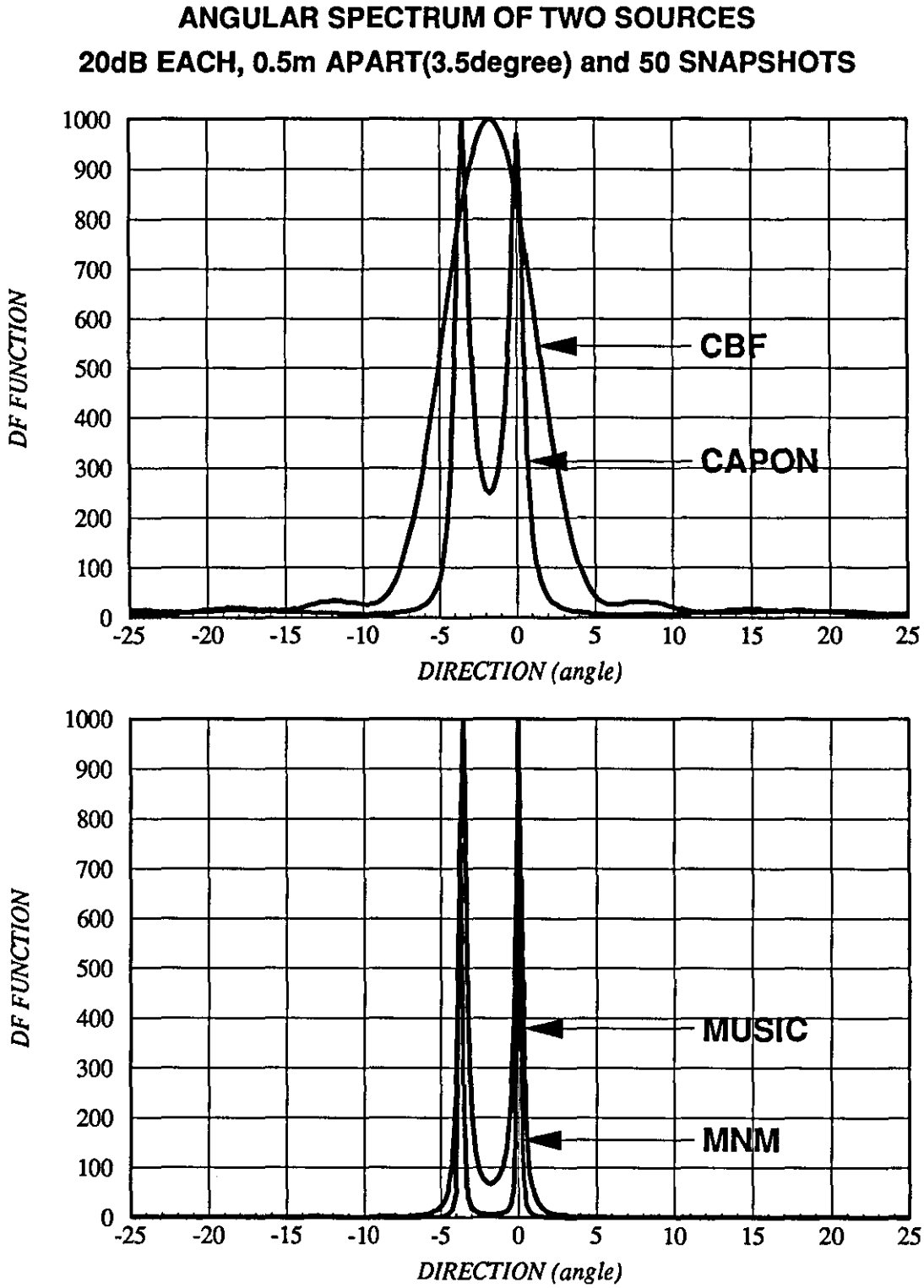
ANGULAR SPECTRUM OF TWO SOURCES
20dB EACH, 0.5m APART(3.5degree) and 50 SNAPSHOTS
DF FUNCTION
1000
900
800
700
600
500
400
300
200
100
0
-25
-20
-15
-10
-5
0
5
10
15
20
25
DIRECTION (angle)
CBF
CAPON
DF FUNCTION
DIRECTION (angle)
MUSIC
MNM

Figure 6.9c

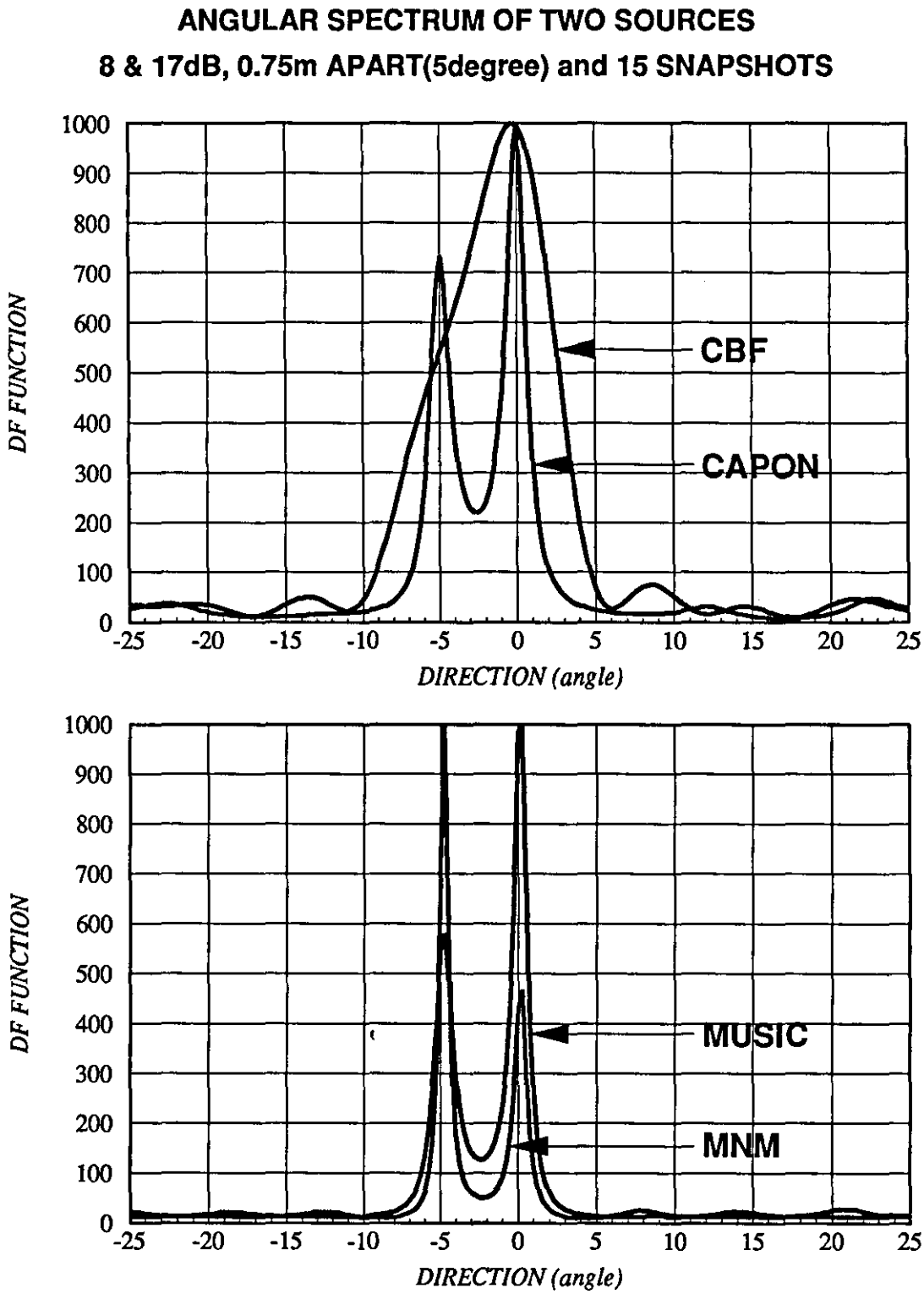
ANGULAR SPECTRUM OF TWO SOURCES
8 & 17dB, 0.75m APART(5degree) and 15 SNAPSHOTS
DF FUNCTION
1000
900
800
700
600
500
400
300
200
100
0
-25
-20
-15
-10
-5
0
5
10
15
20
25
DIRECTION (angle)
CBF
CAPON
DF FUNCTION
DIRECTION (angle)
MUSIC
MNM

Figure 6.10a

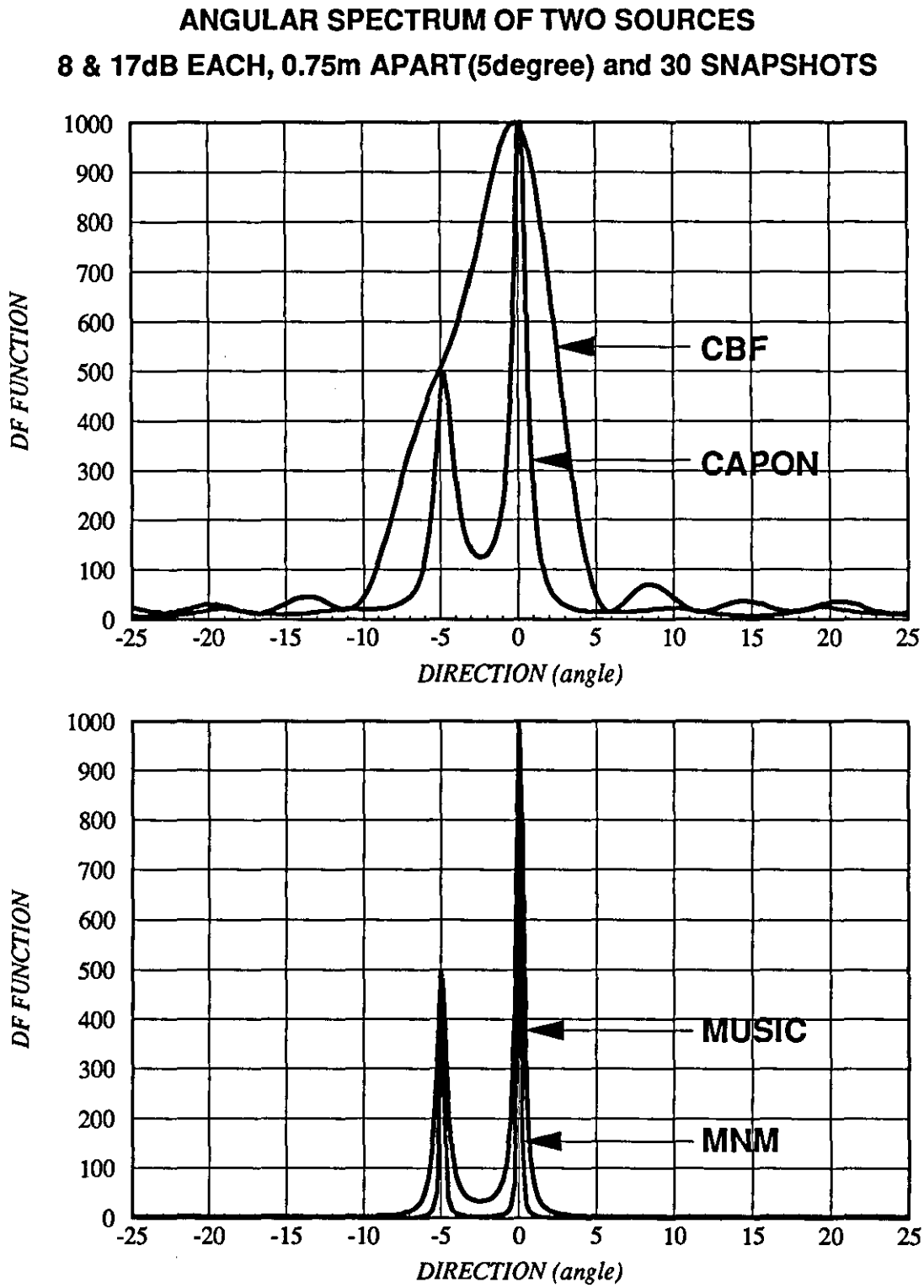
ANGULAR SPECTRUM OF TWO SOURCES
8 & 17dB EACH, 0.75m APART(5degree) and 30 SNAPSHOTS
DF FUNCTION
1000
900
800
700
600
500
400
300
200
100
0
-25
-20
-15
-10
-5
0
5
10
15
20
25
DIRECTION (angle)
CBF
CAPON
DF FUNCTION
DIRECTION (angle)
MUSIC
MNM

Figure 6.10b

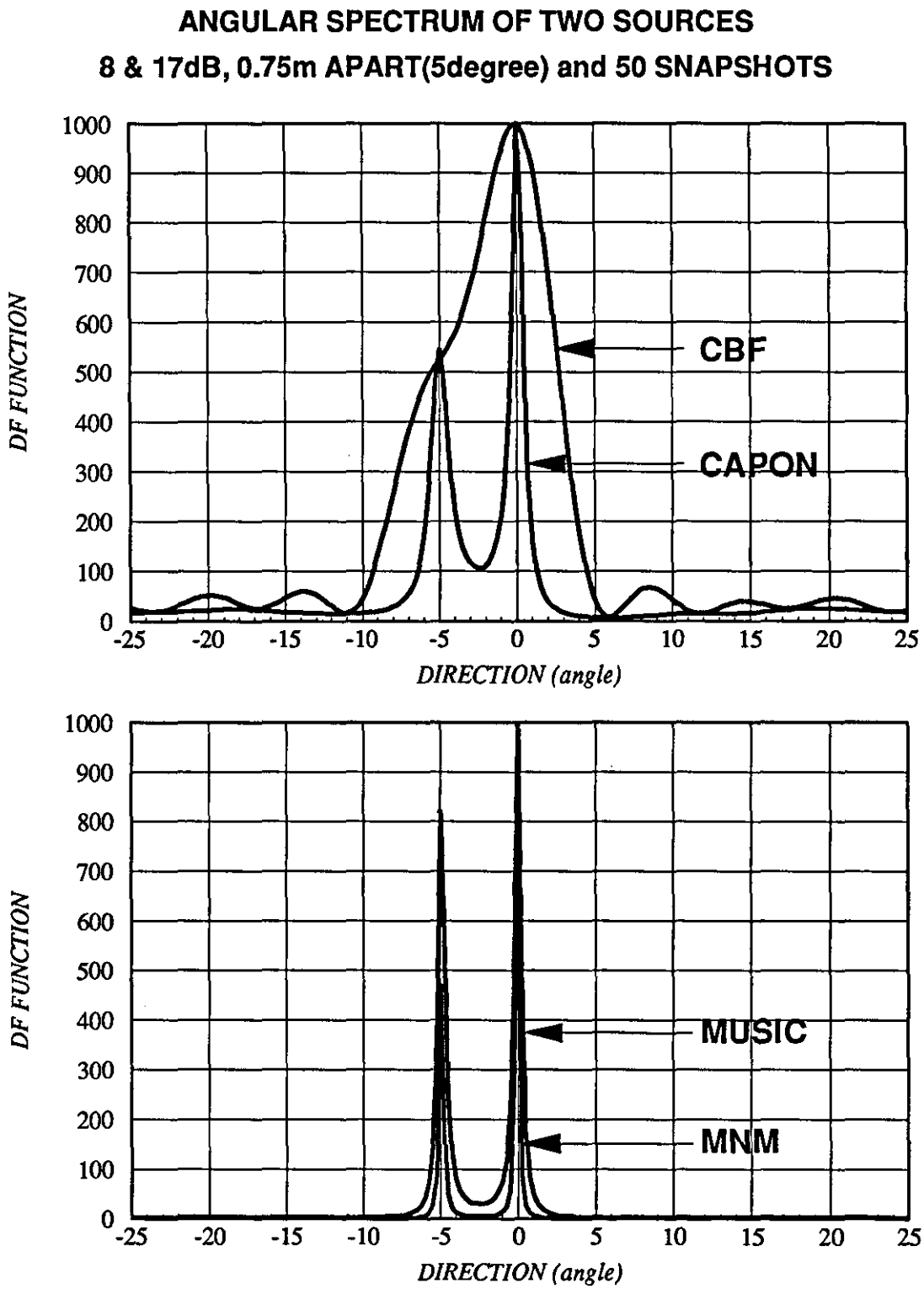
ANGULAR SPECTRUM OF TWO SOURCES
8 & 17dB, 0.75m APART(5degree) and 50 SNAPSHOTS
DF FUNCTION
1000
900
800
700
600
500
400
300
200
100
0
-25
-20
-15
-10
-5
0
5
10
15
20
25
DIRECTION (angle)
CBF
CAPON
DF FUNCTION
DIRECTION (angle)
MUSIC
MNM

Figure 6.10c

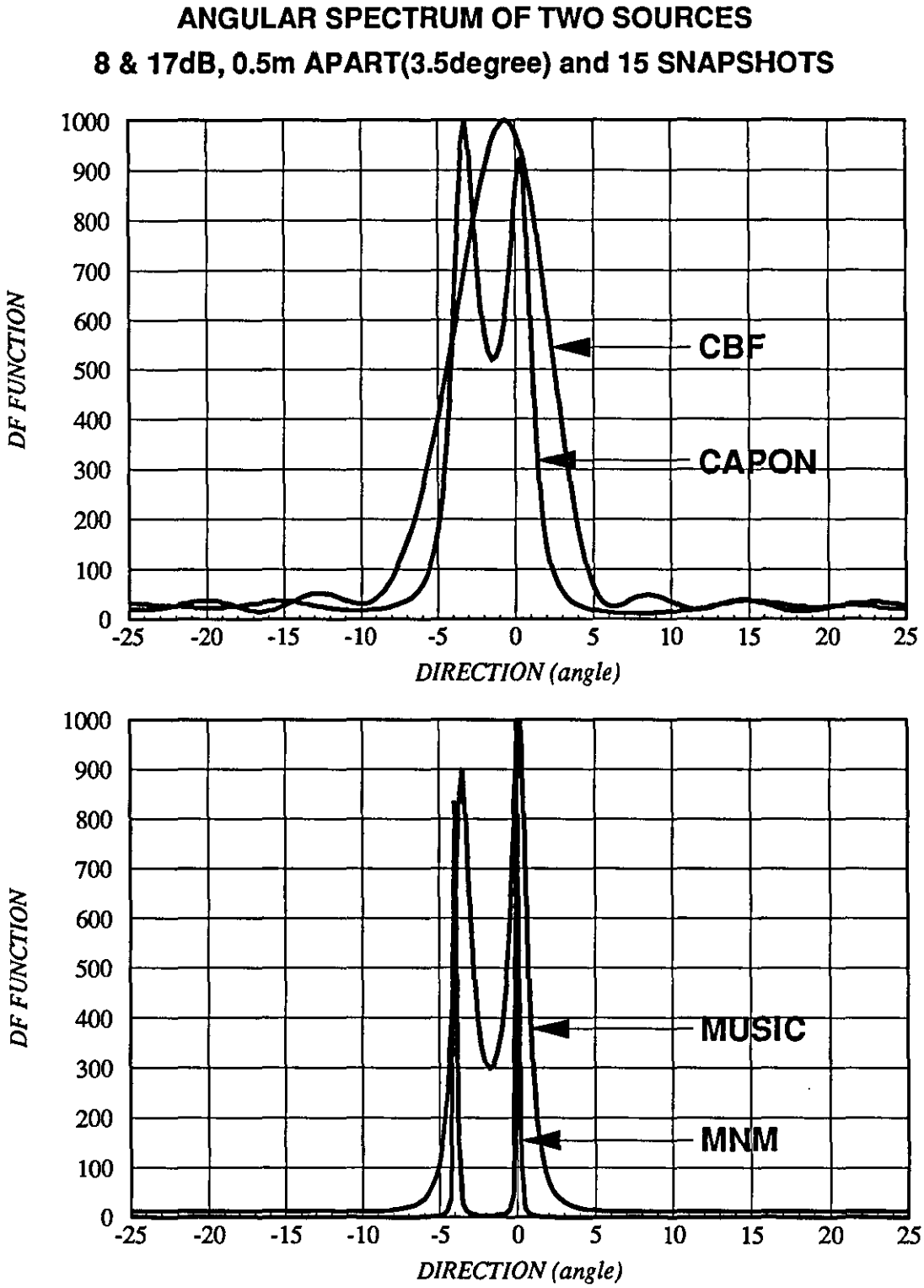
ANGULAR SPECTRUM OF TWO SOURCES
8 & 17dB, 0.5m APART(3.5degree) and 15 SNAPSHOTS
DF FUNCTION
1000
900
800
700
600
500
400
300
200
100
0
-25
-20
-15
-10
-5
0
5
10
15
20
25
DIRECTION (angle)
CBF
CAPON
DF FUNCTION
MUSIC
MNM
DIRECTION (angle)

Figure 6.11a

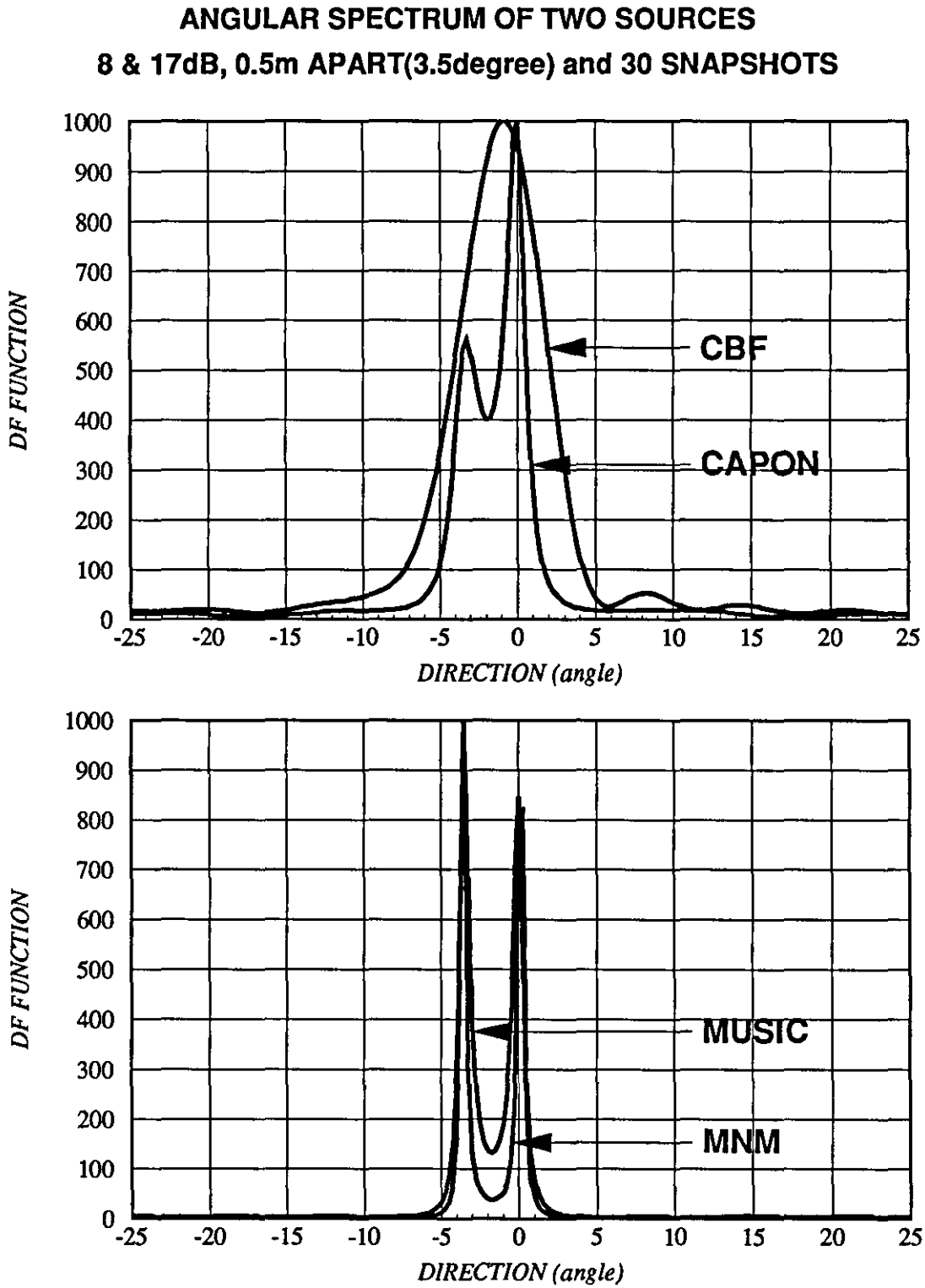
ANGULAR SPECTRUM OF TWO SOURCES
8 & 17dB, 0.5m APART(3.5degree) and 30 SNAPSHOTS
DF FUNCTION
1000
900
800
700
600
500
400
300
200
100
0
-25
-20
-15
-10
-5
0
5
10
15
20
25
DIRECTION (angle)
CBF
CAPON
DF FUNCTION
DIRECTION (angle)
MUSIC
MNM

Figure 6.11b

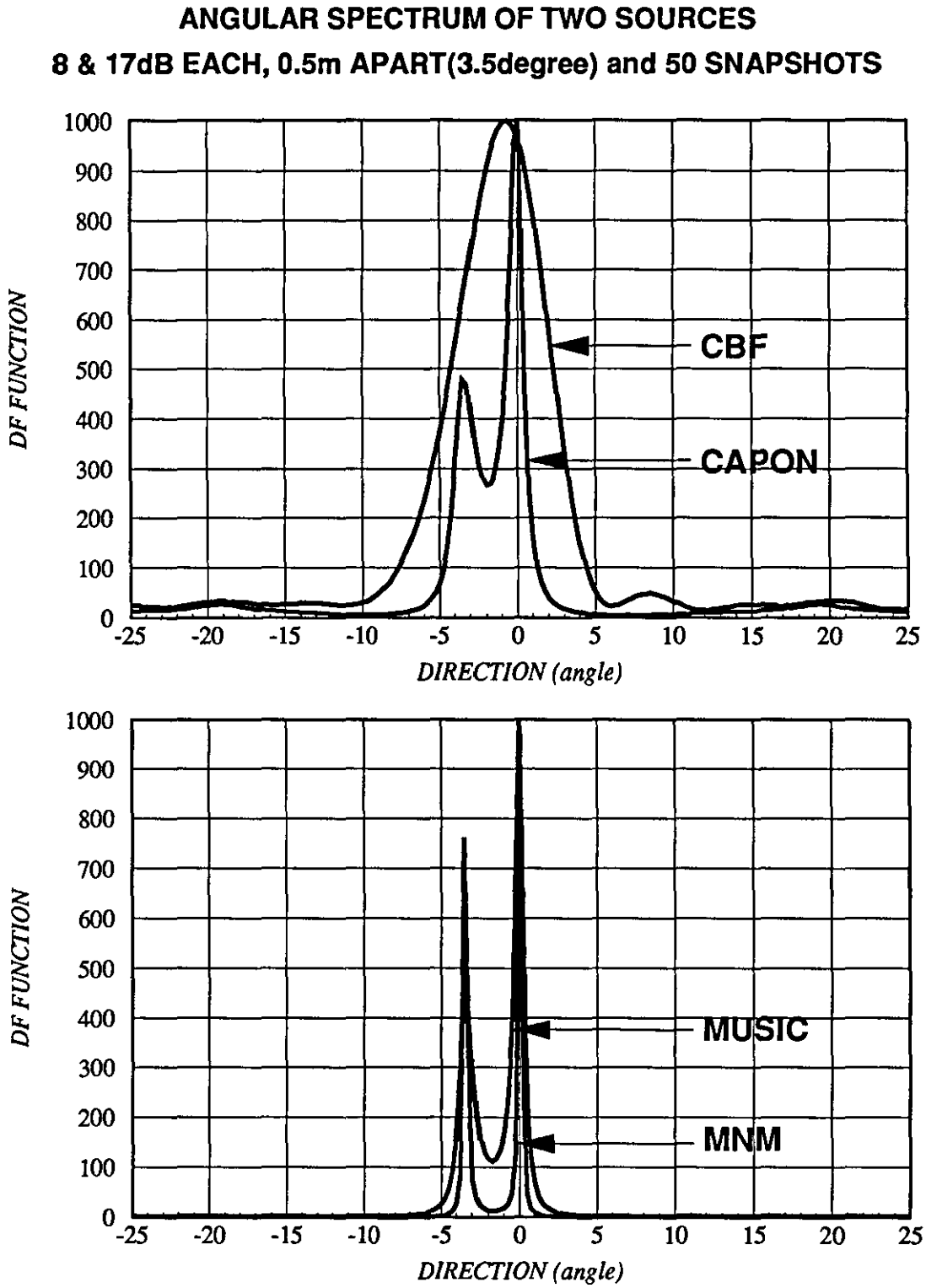
ANGULAR SPECTRUM OF TWO SOURCES
8 & 17dB EACH, 0.5m APART(3.5degree) and 50 SNAPSHOTS
DF FUNCTION
1000
900
800
700
600
500
400
300
200
100
0
-25
-20
-15
-10
-5
0
5
10
15
20
25
DIRECTION (angle)
CBF
CAPON
DF FUNCTION
DIRECTION (angle)
MUSIC
MNM

Figure 6.11c

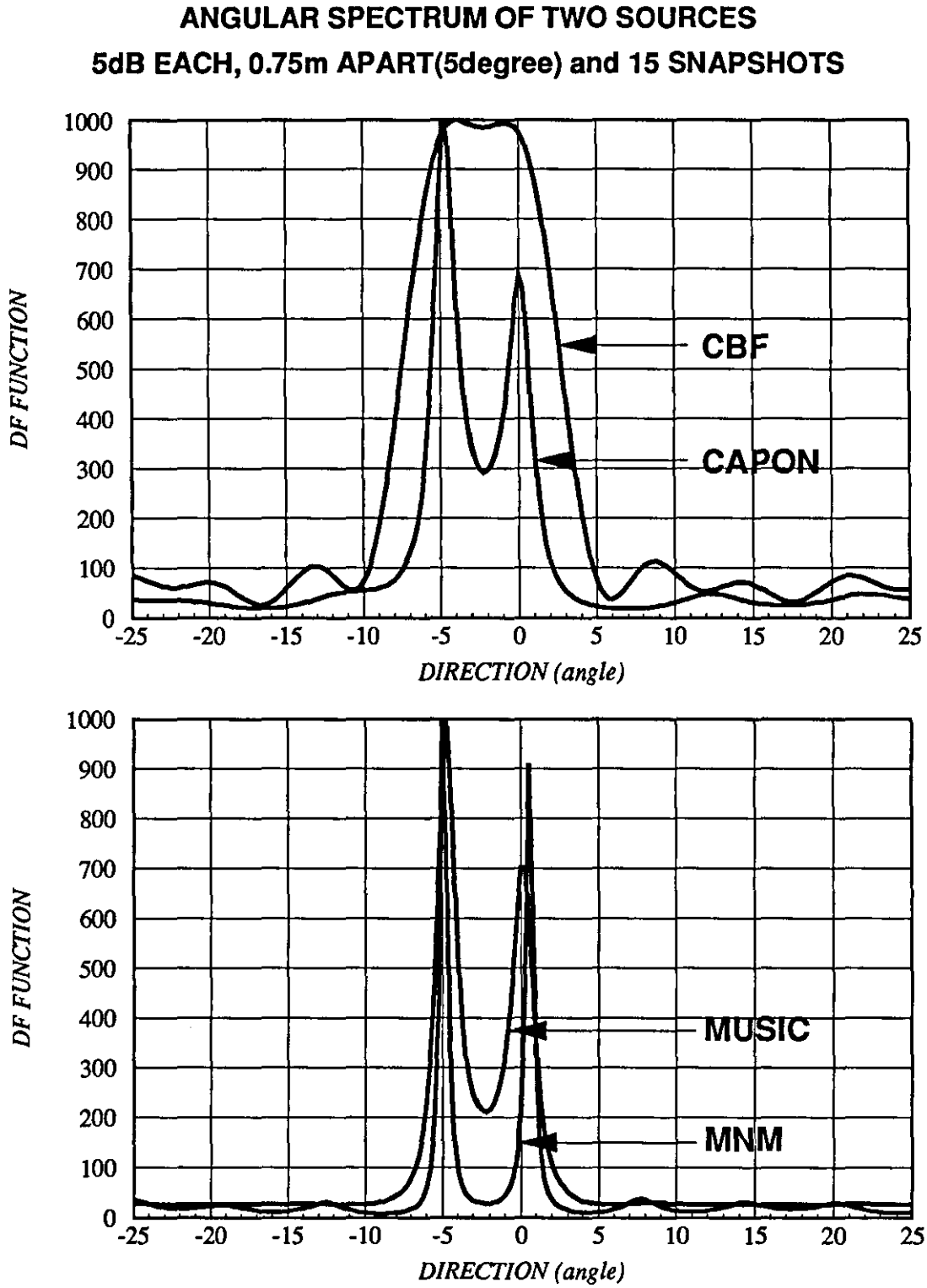
ANGULAR SPECTRUM OF TWO SOURCES
5dB EACH, 0.75m APART(5degree) and 15 SNAPSHOTS
DF FUNCTION
1000
900
800
700
600
500
400
300
200
100
0
-25
-20
-15
-10
-5
0
5
10
15
20
25
DIRECTION (angle)
CBF
CAPON
DF FUNCTION
DIRECTION (angle)
MUSIC
MNM

Figure 6.12a

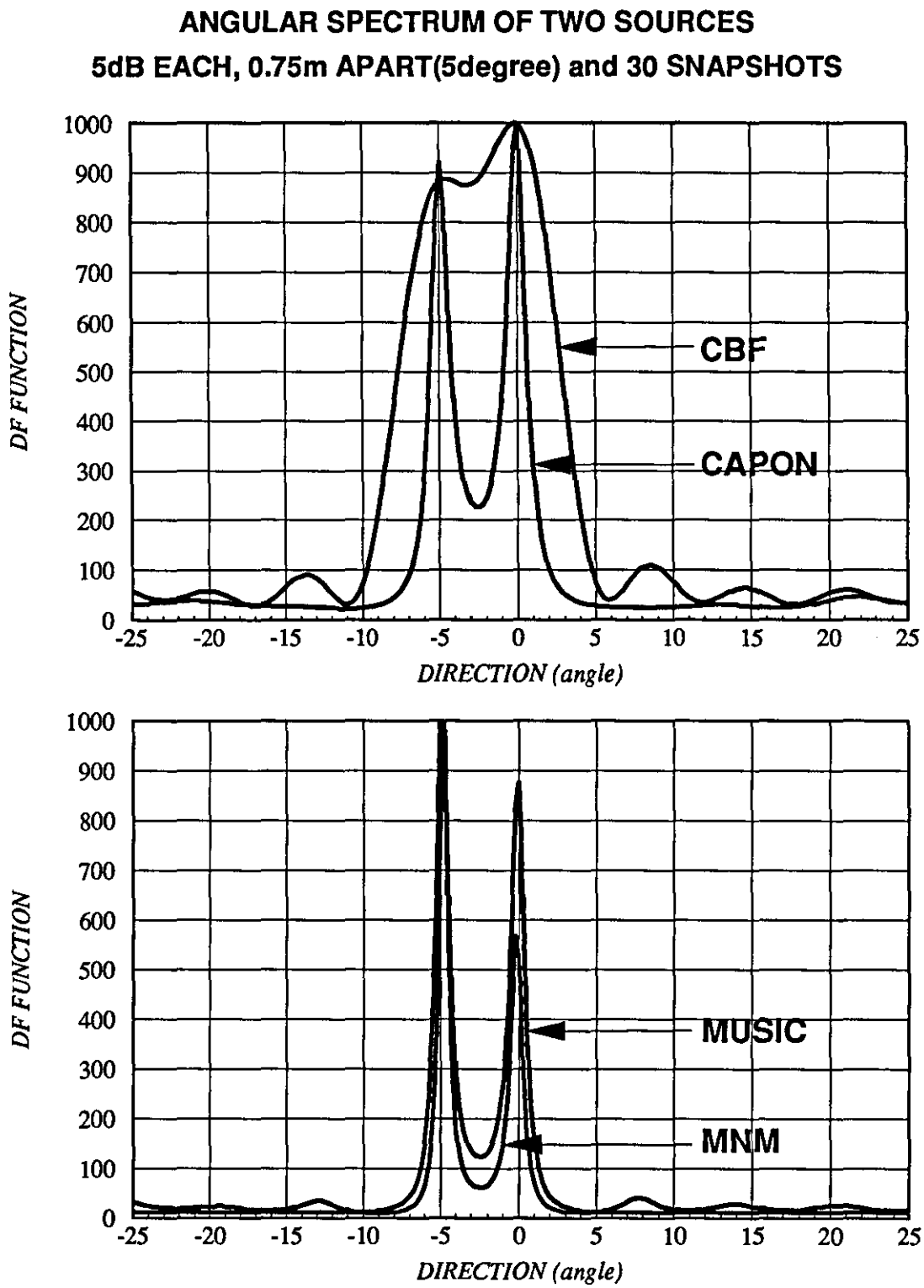
ANGULAR SPECTRUM OF TWO SOURCES
5dB EACH, 0.75m APART(5degree) and 30 SNAPSHOTS
DF FUNCTION
1000
900
800
700
600
500
400
300
200
100
0
-25
-20
-15
-10
-5
0
5
10
15
20
25
DIRECTION (angle)
CBF
CAPON
DF FUNCTION
DIRECTION (angle)
MUSIC
MNM

Figure 6.12b

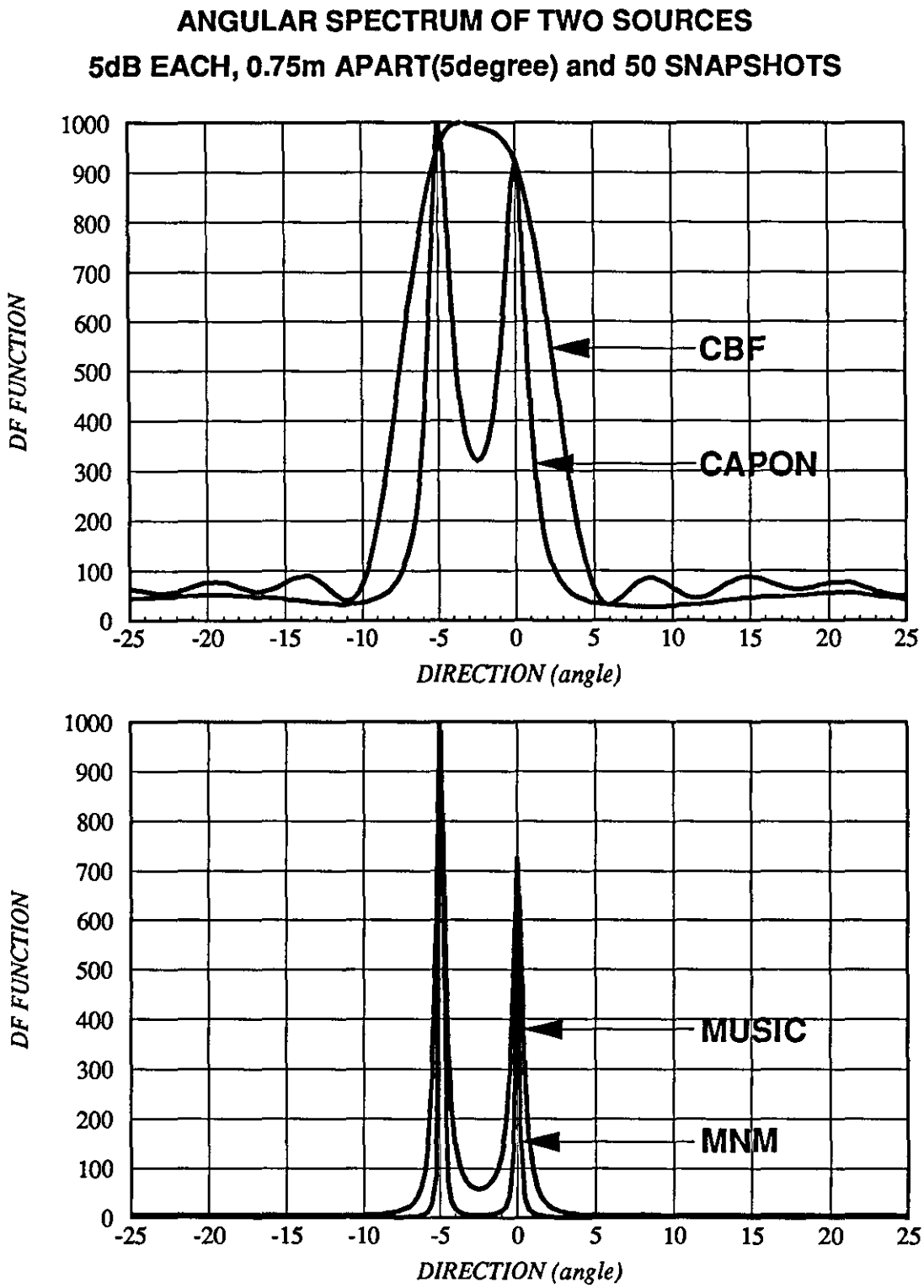
ANGULAR SPECTRUM OF TWO SOURCES
5dB EACH, 0.75m APART(5degree) and 50 SNAPSHOTS
DF FUNCTION
1000
900
800
700
600
500
400
300
200
100
0
-25
-20
-15
-10
-5
0
5
10
15
20
25
DIRECTION (angle)
CBF
CAPON
DF FUNCTION
DIRECTION (angle)
MUSIC
MNM

Figure 6.12c

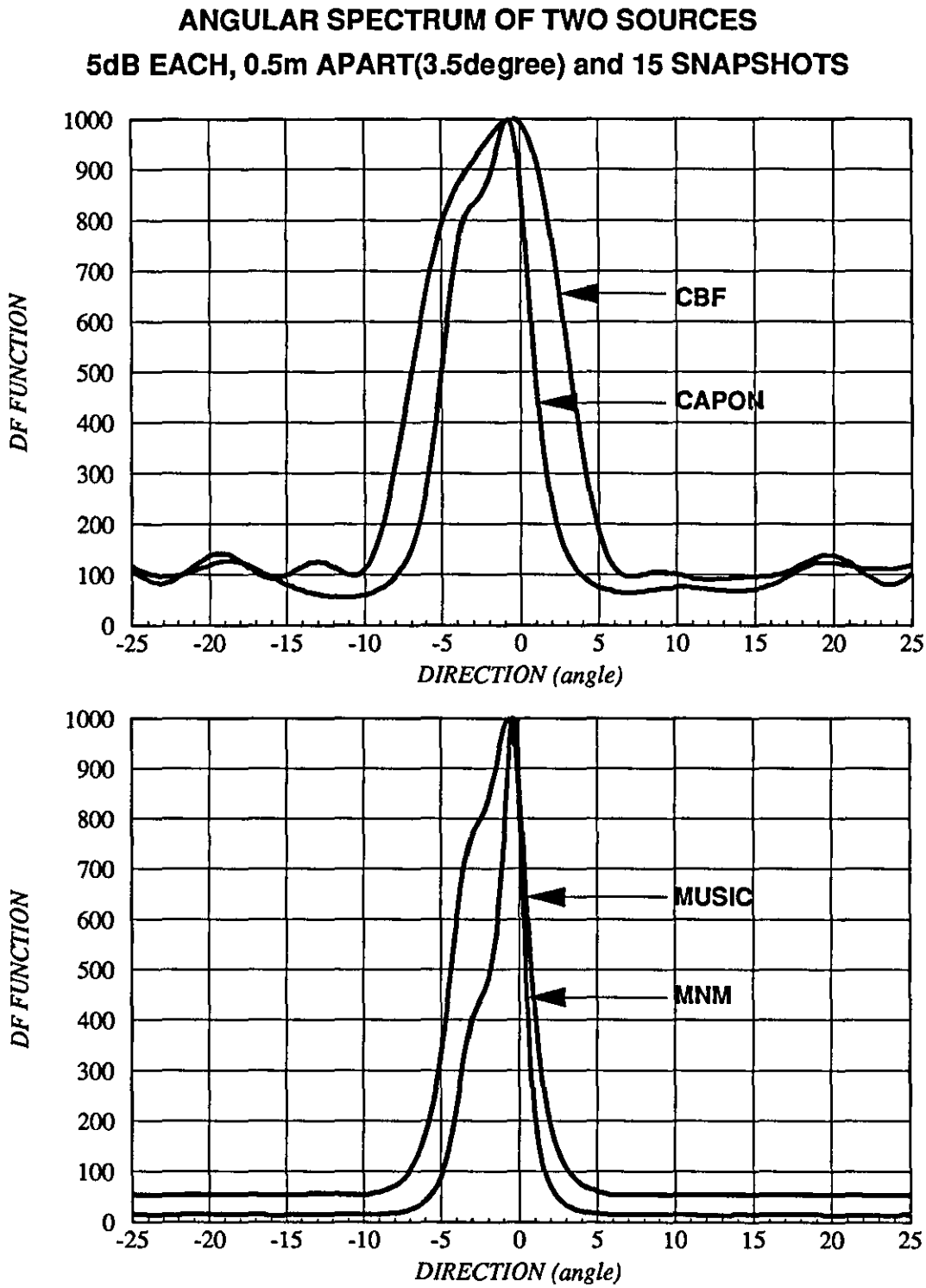
ANGULAR SPECTRUM OF TWO SOURCES
5dB EACH, 0.5m APART(3.5degree) and 15 SNAPSHOTS
DF FUNCTION
1000
900
800
700
600
500
400
300
200
100
0
-25
-20
-15
-10
-5
0
5
10
15
20
25
DIRECTION (angle)
CBF
CAPON
DF FUNCTION
DIRECTION (angle)
MUSIC
MNM

Figure 6.13a

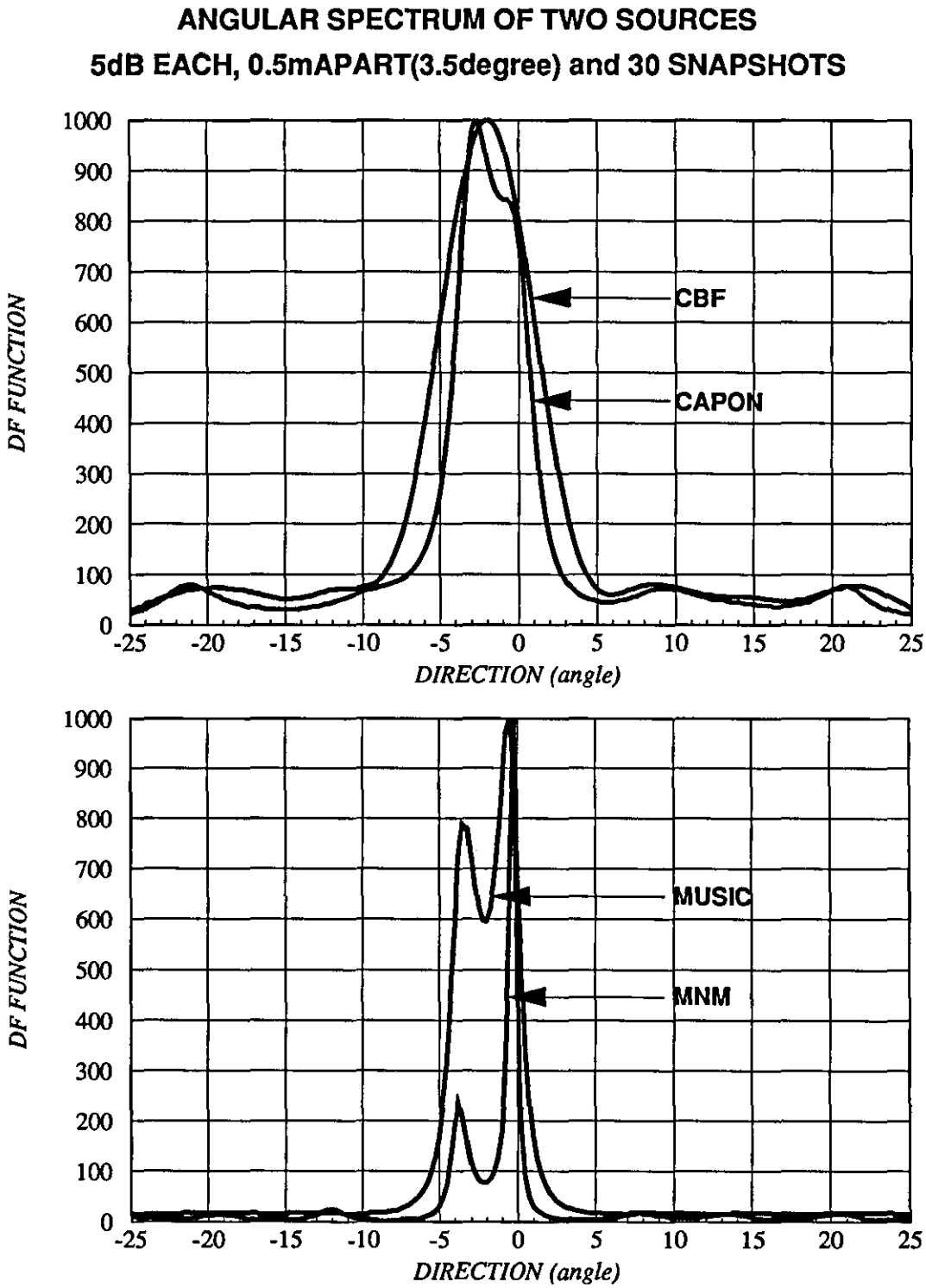
ANGULAR SPECTRUM OF TWO SOURCES
5dB EACH, 0.5mAPART(3.5degree) and 30 SNAPSHOTS
DF FUNCTION
1000
900
800
700
600
500
400
300
200
100
0
-25
-20
-15
-10
-5
0
5
10
15
20
25
DIRECTION (angle)
CBF
CAPON
DF FUNCTION
DIRECTION (angle)
MUSIC
MNM

Figure 6.13b

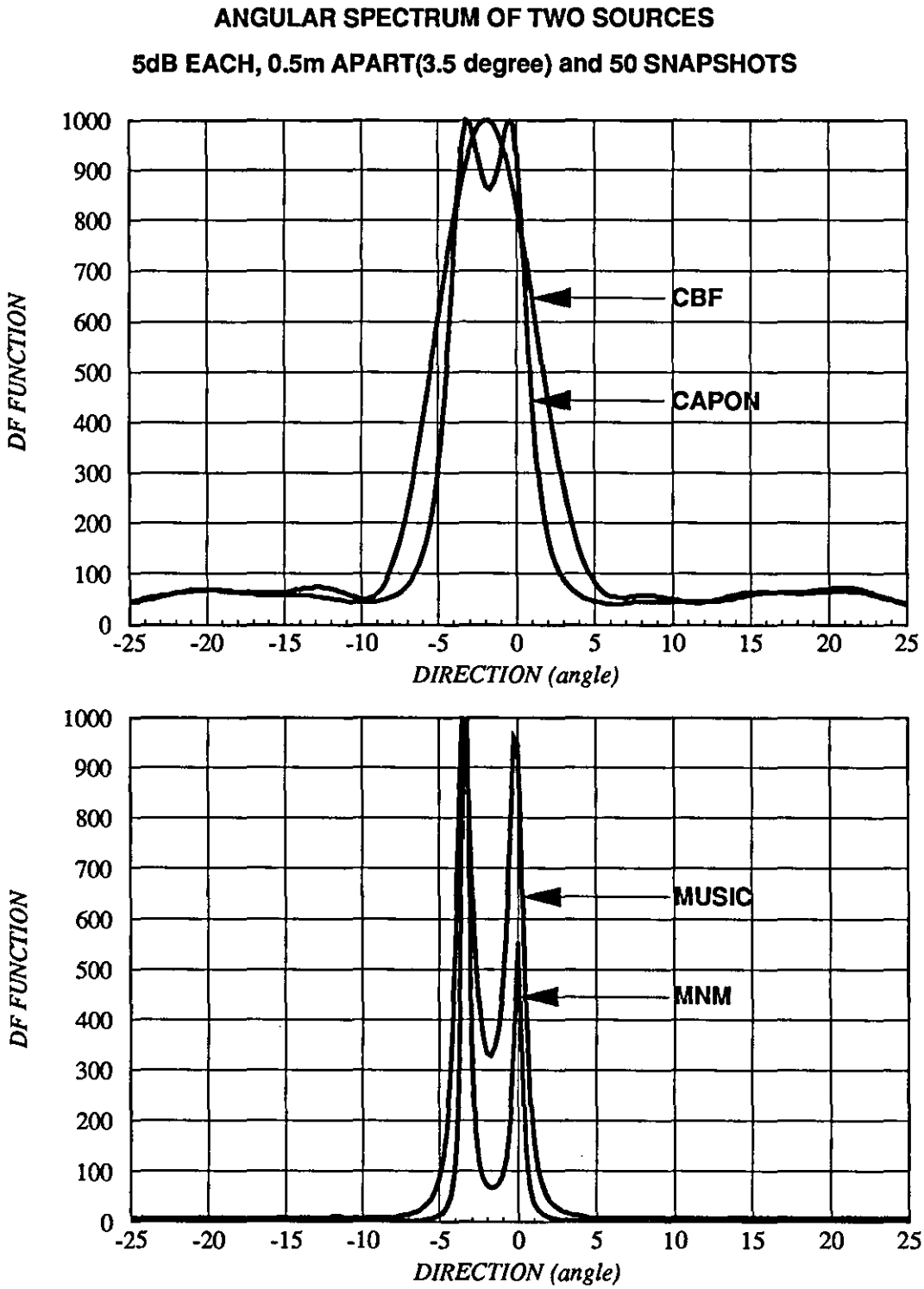
ANGULAR SPECTRUM OF TWO SOURCES
5dB EACH, 0.5m APART(3.5 degree) and 50 SNAPSHOTS
DF FUNCTION
1000
900
800
700
600
500
400
300
200
100
0
-25 -20 -15 -10 -5 0 5 10 15 20 25
DIRECTION (angle)
CBF
CAPON
DF FUNCTION
1000
900
800
700
600
500
400
300
200
100
0
-25 -20 -15 -10 -5 0 5 10 15 20 25
DIRECTION (angle)
MUSIC
MNM

Figure 6.13c

CHAPTER SEVEN

IMPLEMENTATION OF HIGH RESOLUTION ALGORITHMS IN AN AIR ACOUSTIC SYSTEM

7.1 INTRODUCTION:

The initial plan of this project was to do more experiments at Foremark reservoir using active sonar. A long time was spent on preparations for these tests including the mechanical system for mounting the targets, extending the system to 16 channel to increase the directivity, mounting a transmitting array next to the receiving array and carrying out extensive studies on reverberations. Unfortunately however, these tests were suspended due to the construction work at the tower of Foremark reservoir carried out by the Severn Trent.

Alternatively, we decided to move from underwater sonar to air acoustic and try to implement the high resolution DF algorithms to resolve two closely separated sources/targets in open air. One possible application for such a system is to use it as high resolution guiding for robotic vehicles [ref. 87].

This chapter describes the design, building and testing (including measuring the beam pattern) of a 15 element air acoustic array. It then presents the results of experiments carried out to resolve two sources/targets in open air using high resolution DF algorithms. The algorithms tested in this chapter were MUSIC, IMP and WSF besides the CBF. The IMP and WSF algorithms are relatively new algorithms that have been published recently. Their performance on simulated data shows very good results [ref.46 and 44].

Part of the results presented in this chapter have been published in ref.[85].

7.2. AIR ARRAY DESIGN

The Polaroid 7000 environmental electrostatic transducer was chosen to build a 15 element acoustic array. This transducer is specifically intended for operation in air at ultrasonic frequencies. The assembly comes complete with an integral protective cover. Figure 7.1 shows the physical dimensions of the transducer and table 7.1 summarizes its electro-acoustic characteristics [ref. 87].

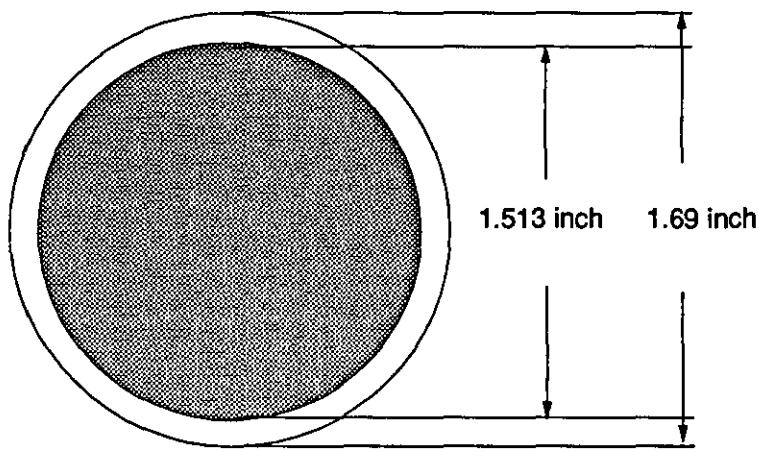

Figure 7.1: The physical dimensions of the Polaroid 7000 Electrostatic Transducer.

TABLE 7.1
ELECTRO-ACOUSTIC CHARACTERISTICS
OF
THE POLAROID 7000 ELECTROSTATIC TRANSDUCER

Usable Transmitting Frequency Range	20-100 kHz
Usable Receiving Frequency Range	30-100 kHz
Minimum Transmitting Sensitivity @ 50kHz 300 Vac P-P, 150 Vdc Bias (dB ref 20 μPa at 1metre)	106.9dB
Minimum Receiving Sensitivity @ 50kHz 150 Vdc Bias (dB ref 1V/Pa)	-43.4dB
Suggested DC Bias Voltage	150V

The transducer is a capacitive type and requires a dc bias voltage for operation. A suitable circuit was designed and built for use with this transducer containing a DC-DC convertor and diodes and is shown in figure 7.2.

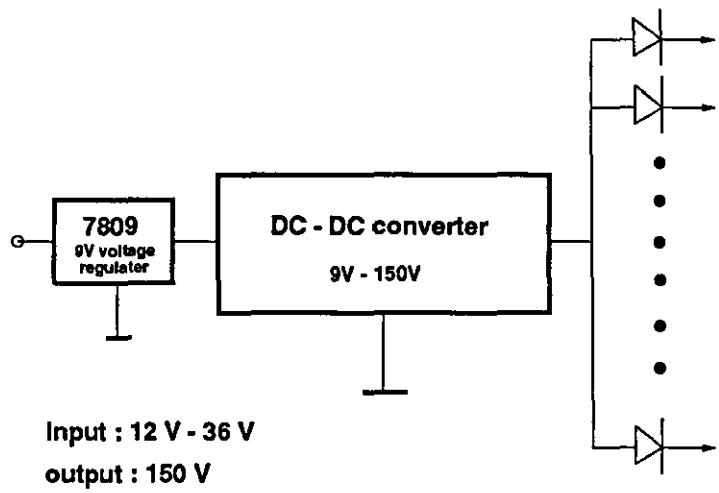

Figure 7.2 The DC bias supply circuit.

The elements of the array are about 5 wavelengths in diameter at the centre frequency of 50 kHz and, if a simple line array had been used, the resulting diffraction secondaries would have been unacceptable. Therefore it was decided to arrange the 15 elements in echelon with 8 elements in the upper row and 7 elements in the lower row as shown in figure 7.3.

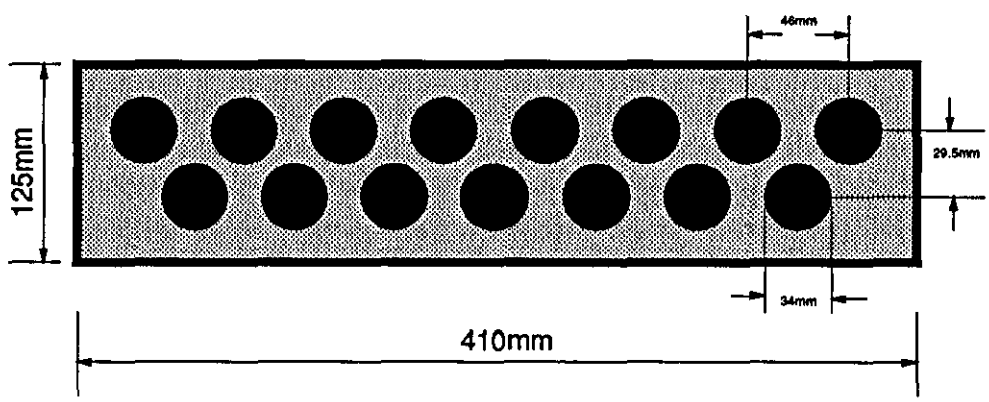

Figure 7.3: The 15 element air acoustic array.

By using this echelon formation the spacing of the elements is effectively halved although care has to be taken if the objects in the far field are off the horizontal plane containing the normal to the centre of the array. The operating frequency used in the experiments was 40 kHz which helped to reduce the spacing in terms of wavelength.

7.3 BEAM PATTERN CALCULATION

7.3.1 Beam pattern of one transducer

The elements of the array are circular plane transducers and the beam pattern of such a transducer can be calculated by:

$$S(\mu) = \frac{J_1(\pi\mu)}{\pi\mu} \tag{7.1}$$

where $[J_1(\pi\mu)]$ is the first-order Bessel function of $[\pi\mu]$, $[\mu = 2r\sin(\theta)/\lambda]$ and r is the radius of the circular plane (ref. [86]).

7.3.2 Beam pattern of the 15 element array

The air array is a two line echelon structure but in the far-field, if the sources are in the horizontal containing the normal to the centre of the array, then it can be assumed to be a linear array with an inter-element spacing of 23 mm. The wave length in air at the transmitting frequency of 40 kHz is 8.5 mm and so $d/\lambda = 2.7$.

The beam pattern of a line array of point sources can be shown to be [ref. 86]

$$D(\theta) = \frac{\sin(N \cdot \pi \cdot d \cdot \sin(\theta)/\lambda)}{N \cdot \sin(\pi \cdot d \cdot \sin(\theta)/\lambda)} \tag{7.2}$$

when $\pi d \sin(\theta) = 0, \pm 2\pi, \pm 4\pi \cdots$ the beam will have its maximum values. Using the parameters of this array : d = 23 mm, λ= 8.5 mm the beam pattern will have maximum values at $\theta = 0°, \pm 21.8°, \pm 47.8°$.

We need to modify this equation to take into account the directivity of the individual elements. According to the product theorem (ref. [88]), the beam pattern of the array of directional elements will be the product of the beam pattern of an identical array of nondirectional elements and the beam pattern of an individual element. Thus the beam pattern of the array will be given by:

$$P(\theta) = D(\theta) \times S(\theta) \qquad \ldots(7.3)$$

7.4 PRACTICAL MEASUREMENT OF THE BEAM PATTERN

The beampattern of a single transducer was measured by the LUT beamplotter [ref. 73 and 74]. A single Polaroid transducer was fixed on the pan-and-tilt unit and the whole assembly was mounted on a tripod. The transducer was used as a receiver and its output was connected through a 40dB preamplifier to the beamplotter. Another transducer, used as a transmitter, was placed at the same height and at a range of about one metre from the receiving transducer.

The beampattern for one element was calculated using equation 7.1. The result was compared to the measured beampattern as shown in figure 7.4. It can be seen that the theoretical result and the measured result of the beampattern of one element are very similar. The beam width of one element was found to be about 15 degrees at 40 kHz.

The beampattern of the whole array was measured by two methods. The first used the CBF (electronic steering) implemented on the high resolution DF system and the second used the LUT beamplotter. In both methods a source was used to transmit a pulsed signal of 40kHz towards the array and 40dB preamplifiers were used to amplify the received signals by the individual elements of the array.

In the first method, the outputs of the preamplifiers were fed to the high resolution DF system. The system then processed the data and produced the beampattern. In the second method, the outputs of the preamplifiers were summed and fed to the beamplotter.

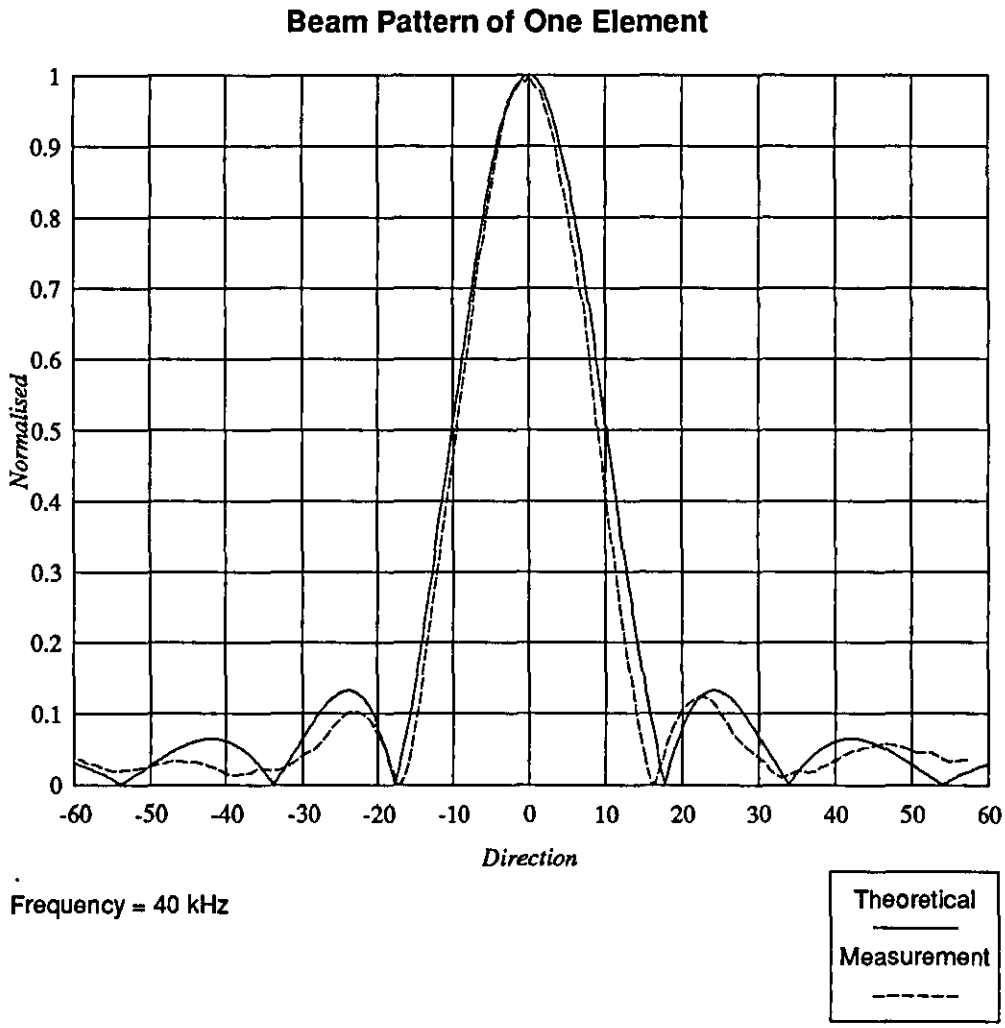

Figure 7.4: The theoretical and measured beampattern of one Polaroid electrostatic transducer.

Figure 7.5 shows the theoretical beampattern of the array and the one measured using the high resolution DF system. It can be seen that the two beampatterns are similar. The beamwidth was found to be 1.4 degree at 40kHz. It should be noticed that measuring the beam pattern by electronic steering produces diffraction secondaries since the beam pattern of the individual elements does not come into effect.

In figure 7.6, the theoretical result differs slightly from the result measured with the LUT beamplotter. There are two large sidelobes beside the mainlobe which are higher than the theoretical result. Some possible causes may be:

1. The 'Gate' signal was not set properly and that may allowed unwanted reflections to be mixed with the direct path signal.
2. Due to the noise within the A/D convertor of the BBC microcomputer.
3. The source was not at a sufficient distance to be in the far field of the array.

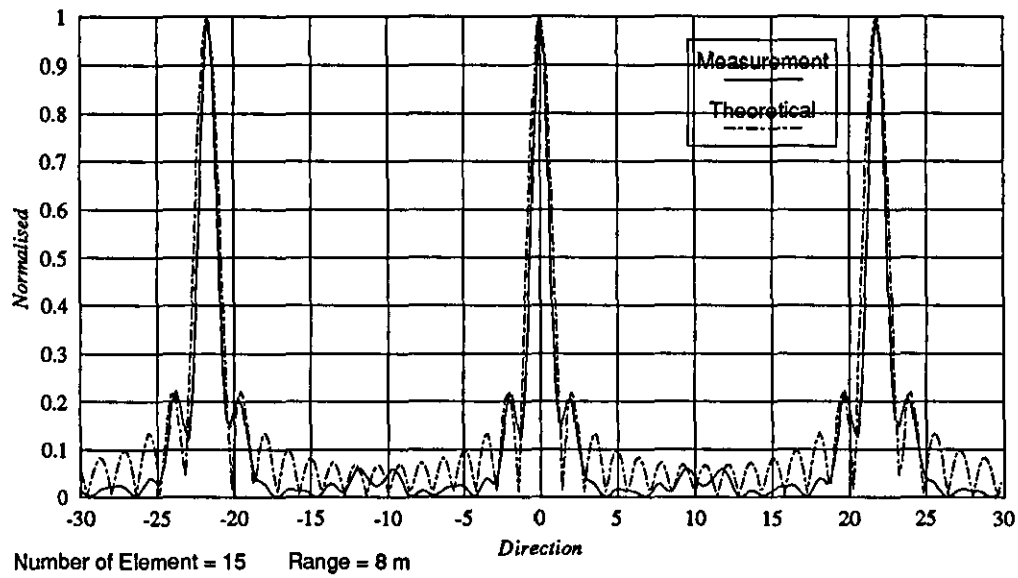

Number of Element = 15 Range = 8 m
Element Space = 2.7 Step = 0.2 degree
Frequency = 40 kHz

Figure 7.5: The theoretical and measured beampattern of the air acoustic array using the high resolution system.

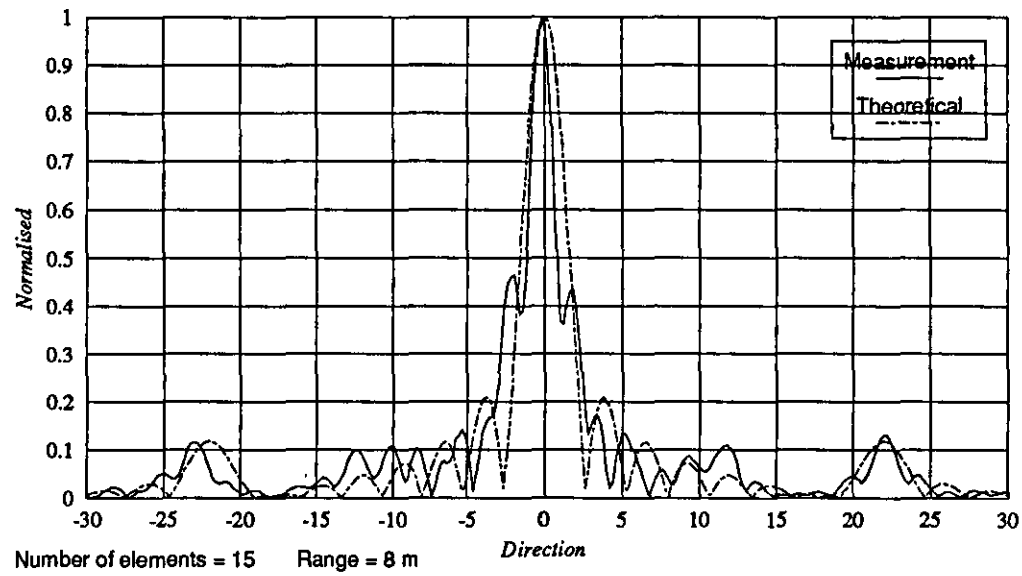

Number of elements = 15 Range = 8 m
Inter-element space = 23 mm Step = 0.2 degree
Frequency = 40 kHz

Figure 7.6: The theoretical and measured beampattern of the air acoustic array using the LUT Beam Plotter.

7.5 IMPLEMENTING HIGH RESOLUTION ALGORITHMS ON AIR ACOUSTIC SYSTEM

The implementation of high resolution DF algorithms involved two sets of experiments; one is passive and the other is active.

In the passive tests two sources, placed at a certain range, were used to transmit signals in the direction of the array. The angular separation between the two sources was varied and the estimated directions of the two sources were recorded using different high resolution algorithms. This test involved uncorrelated and correlated sources.

In the active tests two passive circular plates were placed at a certain range in front of the receiving array. They were illuminated by a pulse transmitted from a transducer placed on the top of the receiving array. The signals reflected from the targets were picked up by the receiving array and used to estimate the direction of the targets.

The algorithms tested in this chapter were MUSIC, IMP and WSF besides the CBF. In the following a detailed description of these tests is presented.

7.5.1 The Passive Tests

One advantage of starting the experiments with passive mode is that uncorrelated sources can be generated by feeding the two sources with slightly different frequencies. Some high resolution algorithms, including the most popular MUSIC method, can only applied to non-coherent sources.

Two types of passive tests were carried out; one with uncorrelated sources and the other with correlated sources.

In these tests, two sources (source #1 and source #2) were placed close to each other at about 7.5metre range from the receiving array. Figure 7.7 shows the experimental set up of the passive tests.

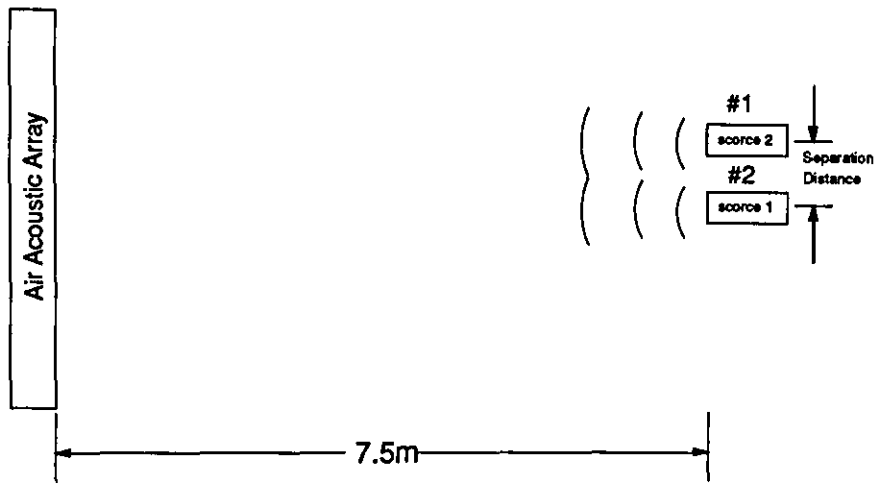

Figure 7.7: The experimental set-up for the passive test.

Source #1 was fixed at a direction 1.6° from the normal to the array. Its direction was measured by the CBF and the other algorithms when source #2 was switched off. Source #2 was moved to eleven different positions between 6.1° and 2.4°. The aim was to evaluate the algorithms ability to resolve the directions of the two sources.
In each position the actual direction of source #2 was verified by switching off source #1 and using the CBF and the high resolution methods to find the direction of source #2.

Since the IMP and the WSF algorithms do not produce angular spectrums, the results are presented in table form.

Table 7.2 shows the results of this test. In the first nine positions, the separations between the two sources were more than a beamwidth. Therefore the CBF was able to resolve the two sources. The high resolution algorithms also resolved the two sources in the first nine positions. In the tenth and eleventh positions the separation between the two sources was less than a beamwidth and the CBF failed to resolve the two sources. The high resolution methods resolved the two sources although there was some bias in the results.

Table 7.2
Results of Passive Test
For Two Uncorrelated Sources
(Range=7.5m No. of Snapshots=30
Fixed Source Position=1.6°)

Separation (mm)	Source State	Algorithms			
		CBF	MUSIC	IMP	WSF
600mm	#1 OFF #2 ON	6.2	6.2	6.2	6.2
	#1 ON #2 ON	1.6, 6.1	1.6, 6.1	1.6, 6.1	1.6, 6.1
550mm	#1 OFF #2 ON	5.8	5.8	5.8	5.8
	#1 ON #2 ON	1.6, 5.8	1.6, 5.8	1.7, 5.7	1.7, 5.7
500mm	#1 OFF #2 ON	5.3	5.3	5.3	5.3
	#1 ON #2 ON	1.6, 5.5	1.6, 5.5	1.6, 5.5	1.6, 5.5
450mm	#1 OFF #2 ON	5.0	5.0	5.0	5.0
	#1 ON #2 ON	1.6, 5.0	1.6, 5.0	1.6, 5.0	1.6, 5.0
400mm	#1 OFF #2 ON	4.6	4.6	4.6	4.6
	#1 ON #2 ON	1.5, 4.3	1.5, 4.3	1.5, 4.3	1.5, 4.4
350mm	#1 OFF #2 ON	4.3	4.3	4.3	4.3
	#1 ON #2 ON	1.4, 4.0	1.4, 4.0	1.4, 4.0	1.4, 4.0
300mm	#1 OFF #2 ON	3.9	3.9	3.9	3.9
	#1 ON #2 ON	1.7, 3.9	1.6, 3.9	1.5, 4.2	1.5, 4.2
250mm	#1 OFF #2 ON	3.5	3.5	3.5	3.5
	#1 ON #2 ON	1.4, 3.5	1.4, 3.7	1.4, 3.5	1.4, 3.5
200mm	#1 OFF #2 ON	3.1	3.1	3.1	3.1
	#1 ON #2 ON	1.3, 3.4	1.3, 3.5	1.3, 3.4	1.3, 3.4
150mm	#1 OFF #2 ON	2.8	2.8	2.8	2.8
	#1 ON #2 ON	2.2	1.8, 2.7	1.7, 3.1	1.7, 3.1
100mm	#1 OFF #2 ON	2.4	2.4	2.4	2.4
	#1 ON #2 ON	1.9	1.5, 2.7	1.6, 2.9	1.6, 2.9

A second set of experiments was carried out with correlated sources, where the two sources were fed from the same signal generator. The results of these experiments are tabulated in table 7.3. As was expected the MUSIC algorithm failed to resolve the two correlated sources when they became close to each other. The new algorithms, the IMP and the WSF, performed equally well in resolving the two sources.

Table 7.3
Results of Passive Test
For Two Correlated Sources
(Range=7.5m No. of Snapshots=30
Fixed Source Position=1.6°)

Separation (mm)	Source State	Algorithms			
		CBF	MUSIC	IMP	WSF
600mm	#1 OFF #2 ON	6.1	6.1	6.1	6.1
	#1 ON #2 ON	1.7, 6.0	1.7, 6.1	1.7, 6.1	1.7, 6.1
550mm	#1 OFF #2 ON	5.8	5.8	5.8	5.8
	#1 ON #2 ON	1.8, 5.8	1.7, 5.9	1.7, 5.9	1.7, 5.9
500mm	#1 OFF #2 ON	5.3	5.3	5.3	5.3
	#1 ON #2 ON	1.7, 5.3	1.7, 5.3	1.7, 5.3	1.7, 5.3
450mm	#1 OFF #2 ON	5.0	5.0	5.0	5.0
	#1 ON #2 ON	1.9, 4.8	1.6, 4.9	1.7, 4.9	1.7, 4.9
400mm	#1 OFF #2 ON	4.7	4.7	4.7	4.7
	#1 ON #2 ON	1.7, 4.8	1.5, 4.9	1.7, 4.8	1.7, 4.8
350mm	#1 OFF #2 ON	4.3	4.3	4.3	4.3
	#1 ON #2 ON	1.9, 4.5	1.7, 4.6	2.0, 4.4	2.0, 4.4
300mm	#1 OFF #2 ON	3.9	3.9	3.9	3.9
	#1 ON #2 ON	3.1	1.3, 3.0	1.4, 3.4	1.6, 3.5
250mm	#1 OFF #2 ON	3.4	3.4	3.4	3.4
	#1 ON #2 ON	2.9	2.9	1.6, 3.3	1.6, 3.3

7.5.2 The Active Tests

The experimental layout of the active tests is shown in figure 7.7. Two circular metal plates of diameter 8.5cm were fixed on special mounts and placed in front of the receiving array at a range of 5.6m. A transmitting transducer was used to illuminate the two targets and was placed on the top of the receiving array. One of the targets was placed in a fixed position at direction 0°. This was aligned by using CBF. The second target was placed at a known distance from the fixed target and its direction was calculated (knowing the range and the separation distance).

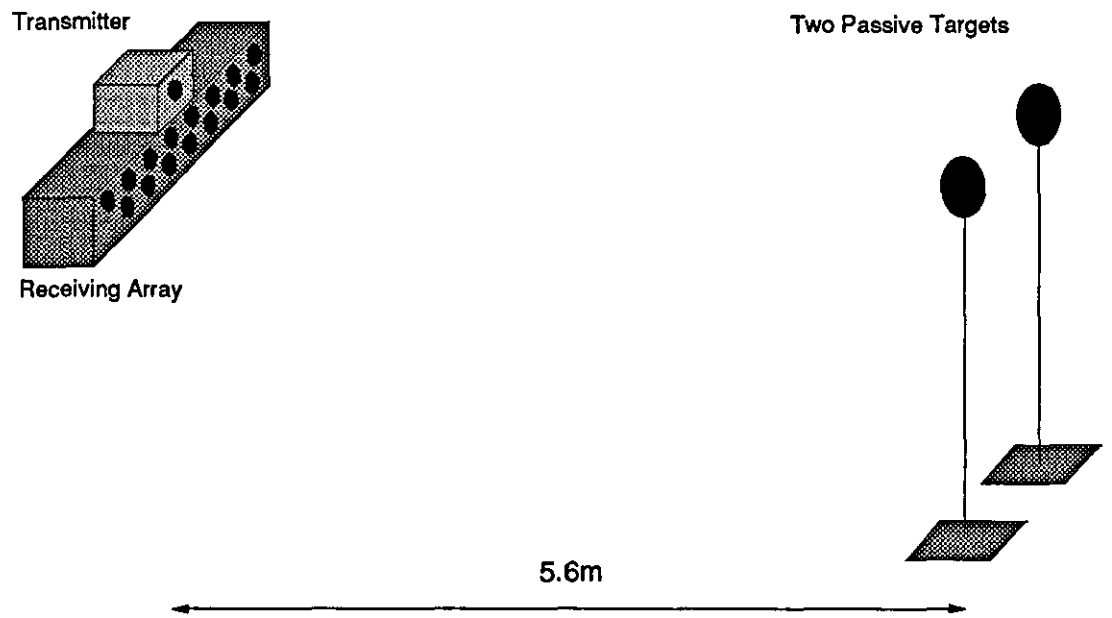

Figure 7.7: The experimental lay-out of the active tests (Range=5.6m No. of Snapshots=30)

The distance between the two targets was changed from 340cm to 100mm in 4 steps. In each position, the direction of the two targets were measured. Table 7.4 shows the results of these tests (the values parentheses represents the expected directions).

It must be noted that the reflected signals from the two targets are correlated and that explains why the MUSIC failed to resolve them at a separation distance of 100cm. The IMP and the WSF resolved the two targets but the estimated directions were biased. This is may be due to the relatively low number of snapshots used.

Table 7.4
Results of Active Test
(Range=5.6m No. of Snapshots=30)

Separation (mm)	Algorithms			
	CBF	MUSIC	IMP	WSF
340mm				
Calculated Positions	(-3.47, 0.0)			
Measured Positions	-3.0, 0.0	-3.1, 0.1	-3.0, 0.3	-3.0, 0.1
270mm				
Calculated Positions	(-2.76, 0.0)			
Measured Positions	-2.2, 0.0	-2.4, 0.2	-2.5, 0.2	-2.4, 0.2
200mm				
Calculated Positions	(-2.0, 0.0)			
Measured Positions	-1.9, -0.5	-2.1, -0.1	-2.1, -0.2	-2.0, -0.1
150mm				
Calculated Positions	(-1.53, 0.0)			
Measured Positions	-1.4, 0.1	-1.4, 0.2	-1.5, 0.1	-1.4, 0.2
100mm				
Calculated Positions	(-1.02, 0.0)			
Measured Positions	0.3	0.5	-1.1, 0.2	-1.1, 0.2

CHAPTER EIGHT

CONCLUSIONS AND SUGGESTIONS FOR FUTURE WORK

8.1 CONCLUSIONS:

The aim of the project was to carry out a study on the practical implementation of high resolution direction finding (DF) algorithms which provide resolution enhancement beyond that of the conventional beamformer (CBF).

The first stage of the project was to do a feasibility study of implementing high resolution DF algorithms in real time using the transputer as one of the most powerful computing devices available at that time. The study involved simulating some of the well known high resolution DF algorithms on a single transputer and measuring the time required to implement them. The study also investigated the distribution of the computation time among the main processes of these algorithms. The results of this study were quite encouraging especially for specific applications like sonar where the movement of underwater targets is relatively slow thus allowing more time to carry out the computations. In addition there were many possibilities for increasing the speed of computation by introducing concurrent processing especially with systolic arrays.

A 16 channel high resolution DF sonar system has been designed and built to implement some of the high resolution algorithms in a sonar environment. The system is based on transputers and because of its flexibility it can easily be

modified to include more transputers and/or other devices like modern Digital Signal Processors (DSP) or vector processors. The system can also be used as a general digital receiver to do other signal processing tasks.

The initial tests of the system were carried out in a large water tank at Loughborough University where the environment is relatively well controlled. The purpose of these tests was to resolve two sources/targets placed within the beamwidth of the receiving array using high resolution algorithms. The results of these tests were in agreement with the theoretical simulations.

A move to a more realistic and less controlled situation took place when the system was moved to Foremark Reservoir - Derbyshire to carry out a large number of experiments to resolve two closely separated sources. In these experiments the effects of signal power and source separation on the resolving capability of different algorithms were investigated.
The results of the tests again showed agreement with the simulations of these algorithms carried out by many researchers.

Finally the system was tested for its ability to resolve two sources/targets in open air using an air acoustic array which was designed and built for this purpose. In these tests, two of the latest high resolution direction finding algorithms, IMP (Incremental Multi-Parameter) and WSF (Weighted Subspace Fitting), were investigated and compared to the MUSIC algorithm.

The overall conclusions of this project is that the practical results agreed with the theoretical simulations.

8.2 SUGGESTIONS FOR FUTURE WORK:

The project was a significant step towards the full real time implementation of high resolution algorithms. However, some work still needs to be done to achieve this goal. In the following, some suggestions are presented for possible future research in this field:

1. In the last few years there have been more developments in semiconductors and computing technologies which have led to devices that are much faster than the one used in this project. Examples of these

are the T9000 transputer, i860 processor and many DSPs working in conjunction with transputers. These devices can speed up the computations tremendously.

2. There are great possibilities for introducing systolic arrays into the implementation of high resolution algorithms which can boost the speed by a great amount. These systolic arrays can easily be implemented on transputers.

3. One of the main problems we encountered during this project was the matching of the analogue multipliers of the different channels used to extract the I & Q components of the received signals. Now, as the cost of fast A/D chips is falling it might be better to sample the data directly rather than using the I & Q sampling.

4. In the present system one sample is taken from each pulse. This makes the time required to capture the data needed to form the data matrix quite long. A suggested solution to this is to use a longer pulse and take many snapshots from the same pulse. Another solution is to use adaptive techniques where, instead of starting from scratch each time we form a data matrix, we use the previous data matrix and just updated it with every pulse.

5. Correlated sources are one of the fundamental problems of high resolution DF algorithms. This problem has not been studied thoroughly in this project and it still needs more investigation.

6. The receiving array used in this project was a linear array and it might be worth investigating other forms of array, especially circular arrays.

REFERENCES:

Chapter 1

[1] Haykin S., " Array Signal Processing" Prentic Hall, 1985.

[2]. Kraus J.D. "Antennas", McGraw-Hill Book Company, 1988.

Chapter 2

[3] Jefferies D.J., " High Resolution Methods For Sonar" Ph.D. Thesis, University of Southampton, 1986.

[4] Sabbar, B.M., " High Resolution Array Signal Processing" Ph.D. Thesis, Loughborough University of Technology, 1987.

[5] Mather, John L., " Least Squares Solutions in Signal Processing Using The Singular Value Decomposition" RSRE Memorandum No. 3864, 1986.

[6] Starkey, P.G., " Direction-Finding With Linear Phased Arrays" Marconi Research Centre, Ref. 87/22, 1987.

[7] Hudson J.E. " Adaptive Signal Processing" Peter Peregrinus, 1981.

[8] Unnikrishna Pillai S., " Array Signal Processing" Springer-Verlag, NewYork, 1989.

[9] Childers G. D., " Modern Spectrum Analysis " IEEE press, 1978.

[10] Mardani R., " High Resolution Algorithms For Array Signal Processing " Ph.D. thesis, Southampton University, Jan. 1990.

[11] Nickel U., Dipl-Math and Dr rer nat " Angular Superresolution with Phased Array Radar: a Review of Algorithms and Operational Constraints " IEE Proc., Vol. 134, No. 1, Feb. 1987.

[12] Griffiths J.W.R., " Sensor Array Processing: a tutorial" Proc. of IOA Conf. on 'Acoustics 1991', Keele University, Keele, U.K, 1991.

[13] Griffiths J.W.R., " Adaptive Array Processing: a tutorial" IEE Proc., Vol. 130, No.1, 1983.

[14] Nielson R.O., " Sonar Signal Processing" Artech House, 1991.

[15] Capon J., " High Resolution Frequency Wave-Number Spectrum Analysis" Proc. IEEE, Vol. 57, pp. 1408-1418, August 1969.

[16] Burg J. P.," Maximum Entropy Spectral Analysis" Proc. of the 37th Meeting of the Society of Exploration Geophysicists, 1967.

[17] Lim J. S. and Oppenheim A.V., " Advanced Topics in Signal Processing" Prentice Hall, 1988.

[18] Pisarenko V.F. " The Retrieval of Harmonics From a Covariance Function " Geophs. J. R., Astr. Soc., 33, 1973.

[19] Schmidt R. O. " Multiple Emitter Location and Signal Parameter Estimation " Proc. RADC Spectral Estimation Workshop, 1979.

[20] Schmidt R. O. " A Signal Subspace Approach To Multiple Emitter Location and Spectral Estimation " Ph.D Thesis, Stanford University, 1981.

[21] Griffiths J.W.R., " Eigenvectors and High Resolution" Proc. IERE Conference on " Electronics for Ocean Technology", Edinburgh, March 1987.

[22] Johnson R.L., " Eigenvector Matrix Partition and Radio Direction Finding Performance" IEEE Trans. on Antennas and propagation, Vol. AP-34, No. 8, August 1986.

[23] Nickel U. " Algebraic Formulation of Kumaresan-Tufts Superresolution method, Showing Relation to ME and MUSIC Methods " IEE Proc., Vol. 135, No. 1, Feb. 1988.

[24] Swindlehurst A., Ottersten B. and Kailath T. " An Analysis of MUSIC and Root-MUSIC in the presence of Sensor Perturbations " ACSSC, MAPLE Press, 1989.

[25] Friedlander B. " A Sensitivity Analysis of the MUSIC Algorithm " IEEE Tran. ASSP, Vol. 38, No. 10,Oct. 1987.

[26] Yang J. and Kaveh M. " Adaptive Eigensubspace Algorithms for Direction or Frequency Estimation and Tracking " IEEE Tran. ASSP, Vol. 36, No. 2, Feb. 1988.

[27] Fuhrmann D. R. " Adaptive MUSIC " SPIE Vol. 826, Advanced Algorithms and Architectures for Signal Processing, 1987.

[28] Lee H. B. and Wengrovitz M. S. " Resolution Threshold of Beamspace MUSIC for Two Closely Spaced Emitters " IEEE Tran. ASSP, Vol. 38, No. 9, Sep. 1990.

[29] Haber F. and Zoltowski M. " Spatial Spectrum Estimation in a Coherent Signal Environment Using an Array in Motion " IEEE Tran. Antennas and Propagation, Vol. AP-34, No. 3, March 1986.

[30] Cadoz J.A. " Multiple Source Location: The Signal Subspace Approach " ACSSC, MAPLE Press, 1989.

[31] Bahaskar D. and Hari K.V.S. " MUSIC and Spatial Smoothing: A Statistical Performance Analysis " ACSSC, MAPLE Press, 1989.

[32] Mike K. " On Generalized Spatial Smoothing Method for Coherent Sources " ACSSC, MAPLE Press, 1989.

[33] Kwon B. and Unnikrishna Pillai S. " New Resolution Threshold Results in Three Source Scenes " ACSSC, MAPLE Press, 1989.

[34] Johnson D.H. and DeGraaf S.R., " Improving the Resolution of Bearing in Passive Sonar Arrays by Eigenvalue Analysis" IEEE Trans. on ASSP, Vol ASSP-30, No. 4, August 1982.

[35] Kumaresan R. and Tufts D.W., " Estimating the Angle of Arrival of Multiple Plane Waves" IEEE Trans. on Aerospace, and Electronic Systems, vol. AES-19, No. 1, January 1983.

[36] Byrne C.L., and Steel A.K., " Stable Non-Linear Methods for Sensor Array Processing " IEEE Vol. DE-10, No. 3, pp. 255-259, July 1985.

[37] Roy R., Paulraj A. and Kailath T. " Direction of Arrival Estimation by Subspace Rotation Method - ESPRIT" ICASP 86, Tokyo.

[38] Roy R. " Estimation of Signal Parameters via Rotational Invariance Techniques" Ph.D. Thesis, Stanford University, August 1987.

[39] Speiser J. M. " Some Observation Concerning the ESPRIT Direction Finding Method" SPIE vol 826, 1987.

[40] Ottersten B. and Kailath T. " Direction-of-Arrival Estimation for Wide-Band Signals Using the ESPRIT Algorithm " IEEE Tran. ASSP, Vol. 38, No. 2, Feb. 1990.

[41] Sun Chao " Simulation of ESPRIT in OCCAM " Sonar Group Internal Report No. 51, Loughborough University of Technology, July 1990.

[42] Roy R. " TSL-ESPRIT " RSRE Memorandum No. 4291, 1989.

[43] Viberg M. " Subspace Fitting Concepts in Sensor Array Processing ", Linkoping Studies in Science and Technology, Dissertation No. 217, Linkoping University, Sweden.

[44] Ottersten B. and Viberg M. " Analysis of Subspace Fitting Based Methods For Sensor Array Processing ", Proc. ICASP, Glasgow 1989.

[45] Buckley K. M. and Xu X.L." Spatial Spectrum Estimation in a Location Sector " IEEE Tran. ASSP, Vol. 38, No. 11, Nov. 1990.

[46] Mather J.L., " Characterisation of the Iterative Multi-Parameter (IMP) Algorithm " Proc. of IOA Conf. on 'Sonar Signal Processing', Loughborough University of Technology, Loughborough, U.K, 1989.

[47] Stoica P and Sharman K. C. " Novel Eigenanalysis Method for Direction Estimation " IEE Proc., Vol. 137, No. 1, Feb. 1990.

Chapter 3

[48] Rafik T.A and Griffiths J.W.R 'Feasibility Study of Implementing High Resolution DF Techniques In real Time Using Transputers' Proc. 'EUSIPCO88', 5-8 Sep. 1988, Grenoble, France.

[49] Rafik T.A and Griffiths J.W.R 'Simulation of High Resolution DF Algorithms on the T800 Transputer' IEE Coll. on 'Simulation Techniques Applied to Sonar', 19 May 1988.

[50] 'Transputer', INMOS, 1985.

[51] 'The Transputer Data Book ', INMOS, 1989.

[52] 'The 9000 Transputer ', SGS-Thomson Microelectronics, 1991.

[53] 'The Transputer Application Notebook, Architecture and Software', SGS-Thomson Microelectronics, 1989.

[54] 'The Transputer Application Notebook, Systems and Performance', SGS-Thomson Microelectronics, 1989.

[55] Pountain D. and May D. ' A Tutorial Introduction to Occam Programming', INMOS Limited, 1988.

[56] 'NAG - Fortran Library Manual' Mark 10, Vol. 4, F01-F03.

[57] Kung S.Y. 'VLSI Array Processors', Prentice-Hall, 1988.

[58] Wan C.R. 'Computational Loads and Hardware Requirments for Direction Finding Algorithms' Sonar Group Internal Report No. 64, Loughborough University, 1991.

[59] Wan C.R. ' Systolic Array Archetecture for Matrix Triangularisation' Sonar Group Internal Report No. 64, Loughborough University, 1990.

[60] McWhirter J.G. and Shepherd T.J. ' A Systolic Array for Linearly Constrained Least-Squares Problems', SPIE in Advanced Algorithms and Architectures for Signal Processing, Vol. 696, 1986.

[61] McWhirter J.G. and Shepherd T.J. ' Systolic Array for MVDR Beamforming', IEE Proc. Vol. 136, Pt. F, No. 2, April 1989.

Chapter 4

[62] Rafik T.A and Griffiths J.W.R 'An Experimental Sonar System Using Transputers' Proc. Underwater Acoustic Data Processing, NATO ASI series, Kluwer Academic Publishers, Canada 1988.

[63] Gida A.S 'Synthetic Aperture Sonar' Ph.D. Thesis, Loughborough University of Technology, Loughborough 1988.

[64] Kock W.E 'Radar, Sonar and Holography' Academic Press, 1973.

[65] Griffiths J.W.R and Rafik T.A 'A Multichannel Versatile Sonar Source' IEE Coll. on 'High Time-Bandwidth Product Waveforms in Radar and Sonar, 1 May 1991.

[66] Griffiths J.W.R and Rafik T.A 'A Versatile Sonar Transmitter Signal Generator' Proc. 'Transputer Applications 90' Southampton University, 11-13 July 1990.

[67] Lu Guogin 'Graphics and Video Communications Over an Integrated Services Network' Ph.D. thesis, Loughborough University, 1989.

[68] 'Analogue Multiplier RS1495', Data Sheet No. 5207 ,RS, 1988.

[69] Hilburn J.L. and Johnson D.E. ' Manual of Active Filter Design', McGraw-Hill, 1984.

[70] 'Data Conversion Products Data Book' Analog Devices, 1989/90.

[71] 'Hitachi IC Memory Data Book', Hitachi 1985.

[72] Bray A.C 'The Advanced User Guide For The BBC Microcomputer' The Cambridge Microcomputer Centre, 1983.

[73] Hill P. 'An Automatic Beam Plotting System', Proc. IOA, Vol. 8.3, Salford 1986.

[74] Wood W.J. 'Beamplotter Report', Sonar Group Internal Report No. 43, Loughborough University.

[75] Wood W.J 'The 40kHz Array' Sonar Group Internal Report , Loughborough University of Technology, 1988.

Chapter 5

[76] Rafik T.A and Griffiths J.W.R 'High Resolution Sonar DF System' Proc. of the IOA on 'Sonar Signal Processing', Loughborough University, 1989.

[77] Robert J.U.'Principles of Underwater Sound', Mcgraw-Hill Book Company, 1975.

[78] Coates R.F.W. 'Underwater Acoustic System', Macmillan Education Ltd., 1990.

[79] Griffiths J.W.R. ' Sonar Equations', Internal Notes for Sonar Research Group, Loughborough University.

[80] 'Application Equations for Underwater Sound Transducers', Manual of 'International Transducers Corporation', rev 2/90, 1984.

Chapter 6

[81] Rafik T.A and Griffiths J.W.R 'High Resolution Sonar DF System' IEE Coll. on 'Addaptive Antennas', 8 July 1990.

[82] Rafik T.A and Griffiths J.W.R 'Some Practical Results on a High Resolution Sonar System' Proc. of 'Acoustics 91', University of Keele, 15-18 April 1991.

[83] Goodson A.D. ' A Multi-Mode Sonar Transmitter ', a Master thesis, Loughborough University, 1989.

[84] Severn Trent Water Authority - South Derbyshire 'Reservoir at Foremark'.

Chapter 7

[85] Rafik T.A, LiBin and Griffiths J.W.R 'A High Resolution Air Acoustic DF System' Proc. of 'Sonar Signal Processing', Loughborough University, Dec. 1991.

[86] Robert S.E, 'Antenna Theory and Design', Prentic-Hall, 1981.

[87] Cox I.J. and Wilfong 'Autonomous Robot Vehicles', Springer-Verlag, 1990.

AUTHOR'S PUBLICATIONS

1. **'Measurment of phase shift for a wide range of frequencies'**, co-auther with Abu Al-Khail M.N., Int. J. of Electronics, Vol. 63, No. 1, 1987.
2. **'Comparison of some modern computing devices as a sinewave source'**, co-author with Prof J.W.R Griffiths, Seminar on 'The use of the TMS320 DSP Family in Teaching & Research in Universities/Polytechnics', Birmingham University, 19/20 April 1988.
3. **'Simulation of high resolution DF algorithms on the T800 Transputer'**, co-author with Prof J.W.R. Griffiths, IEE Coll. on 'Simulation Techniques Applied to Sonar', 19 May 1988.
4. **'An experimental sonar system using transputers'**, co-author with Prof J.W.R. Griffiths, NATO ASI on 'Underwater Acoustic Data Processing', 18-29 July 1988, Kingston, Canada.
5. **'Feasibility study of implementing high resolution DF techniques in real time using transputers'**, co-author with Prof J.W.R. Griffiths, 'EUSIPCO88', 5-8 September 1988, Grenoble, France.
6. **'High resolution sonar system'**, co-author with Prof J.W.R. Griffiths, Proc. I.O.A. Underwater Group Conference on 'Sonar Signal Processing', Loughborough University, December 1989.
7. **'High resolution sonar DF system'**, co-author with Prof J.W.R. Griffiths, IEE Coll. on 'Adaptive Antennas', 8 July 1990.
8. **'A versatile sonar transmitter signal generator'**, co-author with Prof J.W.R. Griffiths, D.B. Pyne and W.J. Wood, Proc. Conference 'Transputer Applications 90', Southampton University, 11-13 July 1990.
9. **'Some practical results on a high resolution sonar system'**, co-author with Prof J.W.R. Griffiths, 'Acoustics 91', University of Keele, 15-18 April 1991.

10. **'A multichannel Versatile signal source'**, co-author with Prof J.W.R. Griffiths, D.B. Payne and W.J. Wood, IEE Coll. on 'High Time-Bandwidth Product Waveforms in Radar and Sonar', 1 May 1991.

11. **'A high resolution air acoustic DF system'**, co-author with Prof J.W.R. Griffiths and LiBin, IOA Conf. Proc. on 'Sonar Signal Processing', Dec. 1991, Loughborough University.

12. **'Circular arrays for sonar beamforming applications'**, co-author with H.D. Griffiths, Prof J.W.R. Griffiths, R. Eiges, Prof D.E.N. Davies and T.E. Curtis, to be published in the 'European Conference on Underwater Acoustics', Sep. 1992, Luxembourg.

INTERNAL REPORTS

1. **'Feasibility study of implementing high resolution DF techniques in real time using transputers'**, Sonar Group Internal Report No. 3, Loughborough University, 1987.

2. **'Comparison of some modern computing devices as a sinewave source'**, Sonar Group Internal Report No. 4, Loughborough University, 1987.

3. **'Design proposal for High Resolution sonar system'**, Sonar Group Internal Report No. 13, Loughborough University, 1988.

4. **'Test of the Digital Receiver'**, Sonar Group Internal Report No. 21, Loughborough University, 1988.

5. **'Results of Testing the High Resolution Sonar System in Foremark Reservior'**, Sonar Group Internal Report No. 30, Loughborough University, 1989.

6. **'Transputer-Based Versatile Sonar Transmitter'**, Sonar Group Internal Report No. 31, Loughborough University, 1989.

7. **'Matched filter for FM pulse using the transputer'**, Sonar Group Internal Report No. 40, Loughborough University, 1989.

8. **'Transputer-BBC Interface'**, Sonar Group Internal Report No. 52, Loughborough University, 1990.

9. **'The UNIVERS Software'**, Sonar Group Internal Report No. 54, Loughborough University, 1990.

10. **'Automated Measurment of Equivalent Circuit Parameters of Sonar Transducers Using GPIB Interface'**, Sonar Group Internal Report No. 78, Loughborough University, 1991.

11. **'Test of the 7-Element Circular Array'**, Sonar Group Internal Report No. 79, Loughborough University, 1991.

12. **'Test of the 4-Element 20kHz Array'**, Sonar Group Internal Report No. 81, Loughborough University, 1991.

13. **'Test of the New 40kHz Array'**, Sonar Group Internal Report No. 83, Loughborough University, 1991.

14. **'A High Resolution Air Acoustic DF System'**, Sonar Group Internal Report No. 85, Loughborough University, 1991.